

Interactions cations - argiles : le cas du Fe(II). Application au contexte de stockage profond des déchets radioactifs

Christophe Tournassat

▶ **To cite this version:**

Christophe Tournassat. Interactions cations - argiles : le cas du Fe(II). Application au contexte de stockage profond des déchets radioactifs. Ingénierie de l'environnement. Université Joseph-Fourier - Grenoble I, 2003. Français. NNT : . tel-00710111

HAL Id: tel-00710111

https://theses.hal.science/tel-00710111

Submitted on 20 Jun 2012

HAL is a multi-disciplinary open access archive for the deposit and dissemination of scientific research documents, whether they are published or not. The documents may come from teaching and research institutions in France or abroad, or from public or private research centers.

L'archive ouverte pluridisciplinaire **HAL**, est destinée au dépôt et à la diffusion de documents scientifiques de niveau recherche, publiés ou non, émanant des établissements d'enseignement et de recherche français ou étrangers, des laboratoires publics ou privés.

OBSERVATOIRE DE GRENOBLE
et
LABORATOIRE DE GEOPHYSIQUE INTERNE ET TECTONOPHYSYQUE

THESE

présentée par

Christophe Tournassat

pour obtenir le titre de
Docteur de l'Université Joseph Fourier - Grenoble I

Spécialité : **Géochimie environnementale**

Interactions cations – argiles : le cas du Fe(II). Application au contexte de stockage profond des déchets radioactifs

Cations – clays interactions: the Fe(II) case. Application to the problematic of the French deep nuclear repository field concept

7 juillet 2003

Composition du jury :

Murray B. McBride	rapporteur	Pr, Cornell University, Ithaca, New York, USA
Kastriott Spahiu	rapporteur	Dr, Research Coordinator, SKB, Stockholm, Suède
Marc Fontecave	examinateur, président du jury	Pr, CEA Grenoble, France.
Eric Simoni	examinateur	Pr, Université Paris XI, Orsay, France
Nicolas Michau	examinateur, encadrant ANDRA	Dr, ANDRA, Châtenay-Malabry, France
Laurent Charlet	examinateur, directeur de thèse	Pr, Université Joseph Fourier Grenoble-I, France

REMERCIEMENTS

Voici chronologiquement le dernier chapitre de la thèse et peut-être le plus difficile à écrire. J'espère n'oublier personne.

La première personne que je tiens à remercier est tout naturellement mon directeur de thèse, Laurent Charlet. Merci Laurent donc, pour ces trois ans de travail commun. La liberté et la confiance que tu m'as accordées m'ont permis de réaliser cette thèse dans les meilleures conditions. Tu as toujours su m'aiguiller vers des directions de recherche fructueuses sans rien m'imposer : je ne compte plus le nombre de tes idées dont je me suis finalement accaparé. Malgré ton emploi du temps (sur)chargé, c'est toujours avec bonne humeur que tu m'as accueilli dans ton bureau même si souvent, tu savais que, quand je ressortirai, tu aurais les bras chargés d'un nouveau travail pour la nuit ou pour le week-end (Pardon Barbara, Alvaro et Anaïs, pour ce temps que je vous ai volé ces derniers mois).

Nicolas Michau m'a encadré au niveau de l'ANDRA tout au long de ces trois années. Merci Nicolas pour m'avoir accueilli et introduit au sein de l'agence, et pour ton soutien indéfectible quand il s'agissait de m'envoyer aux quatre coins de la France et de l'Europe. A travers toi, c'est également l'ANDRA que je remercie pour les très bonnes conditions de travail que l'agence m'a offertes.

Le Professeur Murray McBride a accepté d'être rapporteur de cette thèse. C'est un honneur et un immense plaisir personnel d'avoir été évalué par un grand nom de la géochimie environnementale. Thank you Murray for your corrections and pertinent remarks on this work. Dr Kastriot Spahiu a également accepté d'être rapporteur de cette thèse. J'ai beaucoup apprécié les corrections très détaillées sur le fond scientifique mais également sur la forme qu'il m'a fait parvenir. Je tiens également à le remercier pour le soutien qu'il a accordé à ce projet qui, peut-être, n'aurait pas vu le jour sans lui. Tack, Dr Kastriot Spahiu, för att du stött detta projekt och gått med på att vara opponent. Les Professeurs Marc Fontecave et Eric Simoni ont jugé ce travail en tant qu'examinateurs. Je les en remercie vivement.

Ce travail n'aurait pas été aussi riche sans les nombreuses collaborations dont il a bénéficié. Dirk Bosbach m'a toujours accueilli chaleureusement à l'INE Karlsruhe pour me faire profiter de son AFM et de la bière locale. Ses étudiants Heike et Felix ont grandement participé au bon déroulement de mes séjours. Dirk, Heike und Felix, Danke für die schöne Zeit bei euch. Tony Appelo m'a appris toutes les arcanes du logiciel Phreeqc et as toujours été là pour répondre chaleureusement à mes questions sur la modélisation. Bedankt voor jouw hulp, Tony. Au cours des derniers six mois de thèse, Jean-Marc Greneche s'est incroyablement impliqué dans ce travail. Merci Jean-Marc pour ta réactivité record et tes superbes spectres Mössbauer. Ces expériences au Mans n'auraient pas été possibles sans Jean-Pierre Jolivet. Je l'en remercie donc vivement. Frédéric Villiéras m'a fait connaître le Groupe Français des Argiles et m'a beaucoup aidé dans la

promotion de certains résultats. Merci, Frédéric pour ces échanges fructueux et toujours agréables. Yves Chapron m'a fait découvrir la dynamique moléculaire. Yves, je ne désespère pas de m'y impliquer un jour plus complètement. Outre la bonne humeur qu'il distille dans le labo, Eric Ferrage m'a initié aux joies de l'infrarouge et m'a permis ainsi d'éviter bien des écueils. Christiane Poinsignon a complété cette formation en m'apportant une touche de savoir-faire expérimental. Merci à vous deux. Enfin, je tiens à remercier Delphine Tisserand pour son sourire et son aide indéfectible sur mes problèmes analytiques.

D'autres personnes ont participé plus indirectement à ce travail. Merci donc à tous ceux qui m'ont ouvert leur porte au laboratoire pour discuter de science, Alain, Bruno, Lorenzo et Géraldine. Alain, je te remercie également tout particulièrement pour nos discussions non-scientifiques. Enfin le laboratoire ne pourrait fonctionner sans le travail consciencieux de Martine et Nicolas. Je les remercie vivement pour préserver nos conditions de travail. Merci également à Véronique Ensergueix, secrétaire à l'ANDRA, à France et à toute l'équipe du secrétariat du LGIT pour leur efficacité à résoudre mes problèmes administratifs.

Un laboratoire sans étudiant (ou assimilé) serait bien morne. Merci donc à Francis, Anne-Claire, Marie-Pierre, Alix, Virginie, Tanya et Ahmad, premiers compagnons de route ainsi qu'à ceux (et celles) qui ont suivi Gabriela, Sudipto, Ana, Tatiana et Frédéric pour avoir animé les locaux de géochimie du LGIT, mais aussi de nombreuses salles de bar et surtout de restaurants. Quand j'aurai quitté définitivement les lieux, j'espère d'ailleurs perdre quelques kilos. Antoine et Mariette prennent à présent le relais, soignez les bien.

Durant la thèse, il y a le travail mais surtout les à-côtés partagés avec la famille et les amis. Merci Maman, Papa, Thierry, Mémé, Pépé pour votre enthousiasme à suivre, envers et contre tout, mes travaux de thèse, Hélène, Marcel, Julie, Pierre, Jeanne, Joseph et tous les autres (vous vous reconnaîtrez, j'espère) pour votre accueil qui vous fait vraiment mériter le nom de « belle » famille. Merci à tous les amis avec qui j'ai partagé mes moments de détente. Je ne vous cite pas car j'ai peur d'en oublier. Une petite pensée pour ceux qui vont finir un peu plus tard : le dernier arrivé paye le coup à boire (pendant le pot de thèse par exemple).

Enfin je tiens à te remercier, Delphine, pour avoir tracé avec justesse les limites entre le travail et le reste, et pour m'avoir donné Estelle, une si bonne raison de rentrer plus tôt à la maison. Delphine, c'est en grande partie à toi que je dois mon équilibre pendant ces trois années.

RESUME

Les interactions entre du Fe(II) en solution et une montmorillonite sont étudiées dans des conditions anoxiques et à température ambiante, sur une échelle de temps variant de l'heure à la semaine.

Le Fe^{2+} s'adsorbe sur les sites d'échange cationique de l'argile avec la même affinité que le Ca^{2+} ; en présence de chlore, le Fe(II) forme des paires ioniques, $FeCl^{+}$, qui s'adsorbent avec une affinité comparable à celles de $CaCl^{+}$ et $MgCl^{+}$. Les simulations montrent qu'en fond anionique chloré concentré (comme l'eau de mer) les ions monovalents (Na^{+} et paires ioniques du type $CaCl^{+}$ et $MgCl^{+}$) sont majoritaires sur les sites d'échange cationique.

Le Fe^{2+} s'adsorbe sur les surfaces de bordure de la montmorillonite avec une affinité très forte. Cette adsorption spécifique peut être modélisée convenablement avec des modèles simples de complexation de surface. Le Fe^{2+} s'adsorbe sur l'argile avec une affinité d'environ 1000 fois plus forte que celle du Zn^{2+}. Des expériences couplées d'adsorption, de titrage, de dissolution et de spectroscopie Mössbauer montrent que l'adsorption spécifique du Fe^{2+} est due à plusieurs réactions distinctes :

- une adsorption compétitive avec remplacement de cations présents sur les surfaces de bordure ou dans la structure (ex : Mg^{2+}, Zn^{2+}) ;
- une adsorption coopérative avec H_4SiO_4, ce mécanisme étant compatible avec la précipitation de surface d'une phase Fe – Si ;
- un mécanisme d'adsorption suivi d'une oxydation du Fe^{2+} en Fe^{3+}, cette réaction libérant deux H^{+} en solution par Fe^{2+} adsorbé.

Ces phénomènes ne peuvent pas tous être pris en compte dans les modèles classiques de complexation de surface. Une approche nouvelle pour les argiles est donc développée pour modéliser les interactions solutés – argiles, basée sur une approche morphologique et structurale de l'argile. Les surfaces de la montmorillonite sont caractérisées par deux méthodes indépendantes, la microscopie à force atomique (AFM) et l'adsorption de gaz à très basse pression, qui donnent le même résultat pour les surfaces de bordure : 8,5 $m^2\ g^{-1}$. L'étude théorique de la structure de l'interface argiles – solutés montre qu'elle ne porte pas moins de 27 sites réactionnels différents pour les interactions argile – H^{+}. Le modèle MUSIC est utilisé pour prédire leur réactivité. L'excellent accord entre les données expérimentales de titrage potentiométrique et leur simulation nous encourage à poursuivre dans cette voie et à compléter le modèle pour prédire les interactions surface – cations métalliques.

ABSTRACT

Solute Fe(II) – montmorillonite interactions are studied in anoxic conditions and at room temperature for reaction times from hour to week.

Fe^{2+} is shown to be sorbed on cation exchange site with the same affinity than Ca^{2+}. In chloride anionic medium, Fe(II) form ionic pairs – $FeCl^+$ - which is sorbed with almost the same affinity than $CaCl^+$ and $MgCl^+$ are. The exchange thermodynamics constants derived from this study are used to simulate the change in the exchanger composition as clay river particles enter seawater. In high concentration chloride medium, as seawater, monovalent ions (Na^+ and $CaCl^+$, $MgCl^+$ ionic pairs) are shown to be the major species of the exchanger.

Fe^{2+} is sorbed specifically on the montmorillonite edge surfaces with a very high affinity. Simple complexation model are able to model the sorption data and show that the Fe^{2+} affinity for clay edge surfaces is ~1000 times higher than the Zn^{2+} one. Mössbauer experiments combined to sorption, titration and dissolution experiments show that the Fe^{2+} sorption is due to several different reactions:

- effective competitive sorption with replacement of previously sorbed or structural cations (Zn^{2+}, Mg^{2+});
- cooperative sorption together with H_4SiO_4, in agreement with a possible surface precipitation of a Fe – Si phase;
- a sorption mechanism followed by an oxidation reaction, with a release of two H^+ in solution per Fe(II) sorbed, and a product (Fe(III)) fitting better octahedral surface “sites”.

All these phenomena can not be taken into account in a classical surface complexation model. Hence, an innovative model is developed to model clay – solute interactions, based on a morphological and structural approach. Montmorillonite edge surface area was determined using two independent methods, AFM measurement and low-pressure gas adsorption, that give the same value for this area, i.e. 8.5 $m^2\ g^{-1}$. The clay – solute interface was found to be constituted by a mix of, at least, 27 reactive sites. Their reactivity towards H^+ was modeled with the MUSIC model. An excellent agreement is found between potentiometric measurement data and predicted curves. This model should be further developed to predict the clay surfaces – metallic cations interactions.

Note sur les publications issues de cette thèse

Cette thèse se présente majoritairement sous forme d'article dont la succession ne correspond pas forcement à la chronologie d'écriture. Ainsi, le lecteur pourra se trouver confronté à des renvois bibliographiques concernant des articles introduits plus loin dans la thèse. Les publications issues de cette thèse et en cours d'élaboration sont donc énumérées, ci-dessous, dans l'ordre chronologique d'écriture.

Articles soumis et en préparation

Auteurs, titre et journal	Outils analytiques
Tournassat, C., Neaman, A., Villiéras, F., Bosbach, D. and Charlet, L. Nanomorphology of montmorillonite particles: Estimation of the clay edge sorption site density by low-pressure gas adsorption and AFM observations, *American Mineralogist.*	AFM, Absorption de gaz à basse pression.
Tournassat, C. and Charlet, L. Competitive specific sorption of Fe(II) on clay minerals in anoxic waters, *Environmental Science and Technology.*	Chimie analytique, modélisation numérique thermodynamique.
Tournassat, C., Greneche, J. M., Tisserand, D. and Charlet, L. The titration of clay minerals. Part I. Discontinuous backtitration technique combined to CEC measurements, *Journal of Colloid and Interface Science.*	Chimie analytique, Mössbauer.
Tournassat, C., Ferrage, E., Poinsignon, C. and Charlet, L. The titration of clay minerals. Part II. Insights from infrared spectroscopy, and models using Bradbury and Baeyens or MUSIC approach. *Journal of Colloid and Interface Science.*	FTIR, modélisation structurale, modélisation numérique thermodynamique.
Charlet, L. and Tournassat, C. Fe(II)-Na(I)-Ca(II) cation exchange on montmorillonite in chloride medium; evidence for preferential clay adsorption of chloride – metal ion pairs in seawater. *Aquatic Geochemistry.*	Chimie analytique, Mössbauer, modélisation numérique.
Tournassat, C., Charlet, L. and Greneche, J. M. Sorption of Fe on montmorillonite in anoxic conditions: evidence for a new Fe-Si phase precipitation and for oxidation of Fe(II). *Geochimica et Cosmochimica Acta*.	Chimie analytique, Mössbauer.

Articles en projet

Thématiques et auteurs	Outils analytiques
Modélisation par dynamique moléculaire des phénomènes d'adsorption du Fe(II) sur les surfaces basales et de côté des argiles. Yves Chapron, Laurent Charlet, Christophe Tournassat.	Dynamique moléculaire, modélisation structurale.
Modélisation de la diffusion d'un panache de Fe(II) dans un aquifère anoxique. Tony Appelo, Christophe Tournassat, Laurent Charlet.	Modèle de transport réactif

SOMMAIRE

1. INTRODUCTION. 3

1.1. concept actuel du stockage en formation géologique profonde. 5

1.2. La réactivité du Fe(II) dans la barrière ouvragée. 7

1.3. Les propriétés de sorption des argiles 8

1.4. Moyens d'étude de la sorption à la surface des argiles 17

1.5. difficultés associées au système Fe(II) – argile 19

2. MÉTHODOLOGIE 21

2.1. Choix du matériau argileux 23

2.2. Stratégie des expériences de sorption 24

2.3. Représentation des données 25

2.4. Approches pour modéliser l'adsorption spécifique 32

2.5. Code de calcul et base de donnees thermodynamiques 33

3. LE FE(II) À LA SURFACE DE L'ARGILE, ADSORPTION ET PHÉNOMÈNES ASSOCIÉS 35

3.1. Adsorption du Fe(II) en position d'échange cationique ; importance des paires ioniques 37

FE(II)-NA(I)-CA(II) CATION EXCHANGE ON MONTMORILLONITE IN CHLORIDE MEDIUM; EVIDENCE FOR PREFERENTIAL CLAY ADSORPTION OF CHLORIDE – METAL ION PAIRS IN SEAWATER..... 41

3.2. Adsorption spécifique du Fe(II) sur les montmorillonites et phénomènes de compétition 60

COMPETITIVE SPECIFIC SORPTION OF FE(II) ON CLAY MINERALS IN ANOXIC WATERS 63

3.3. Evidences éxpérimentales de precipitation d'une phase Si-Fe et d'oxydation du Fe(II) à la surface des argiles 77

SORPTION OF FE(II) ON MONTMORILLONITE IN ANOXIC CONDITIONS: EVIDENCE FOR A NEW FE-SI SOLID PHASE PRECIPITATION AND FOR SURFACE OXIDATION OF FE(II). 79

4. MODÉLISATION MORPHOLOGICO - STRUCTURALE DE LA RÉACTIVITÉ DES ARGILES 103

4.1. Quantification des aires des différentes surfaces de l'argile 105

NANOMORPHOLOGY OF MONTMORILLONITE PARTICLES: ESTIMATION OF THE CLAY EDGE SORPTION SITE DENSITY BY LOW-PRESSURE GAS ADSORPTION AND AFM OBSERVATIONS. 107

4.2. Caractérisation des propriétés ACIDO-BASIQUES de l'argile et des sites d'adsorption 121

THE TITRATION OF CLAY MINERALS. PART I. DISCONTINUOUS BACKTITRATION TECHNIQUE COMBINED TO CEC MEASUREMENTS 123

THE TITRATION OF CLAY MINERALS. PART II. STRUCTURAL BASED MODEL AND IMPLICATIONS ON CLAY REACTIVITY. 143

5. CONCLUSION GÉNÉRALE 169

5.1. Démarche scientifique appliquée lors de ces trois années de recherche 171

5.2. Retour sur la problématique du stockage des déchets radioactifs en profondeur 172

5.3. Back to the problematic of the nuclear wastes deep repository field 173

5.4. Synopsis des résultats 175

5.5. Champs d'applications des résultats de cette thèse 179

5.6. Perspectives 180

6. ANNEXES 183

6.1. Préparation des argiles 185

6.2. Méthode de dosage du Fe(II) et du Fe(III) par spectrophotométrie d'absorption : méthode Ferrozine 188

6.3. Méthode pour limiter la quantité de O_2 présente dans les suspensions et les solutions 189

7. BIBLIOGRAPHIE GÉNÉRALE 191

1. INTRODUCTION.

N.B. : les textes de cette introduction sont, pour la plupart, issus de documents de référence de l'ANDRA. J'invite donc le lecteur, désireux d'obtenir plus de détails, à consulter les "référentiels ANDRA" (http://www.andra.fr).

Les travaux présentés dans cette thèse ont été initiés et financés par l'ANDRA dans le cadre de son programme sur le stockage géologique profond. Ce programme concerne les déchets les plus dangereux, qui présentent un niveau élevé de radioactivité et/ou une durée de vie très longue. Ces déchets, nommés HAVL (pour « Haute Activité Vie Longue ») nécessitent d'être confinés pendant des durées de l'ordre du million d'années, avant que leur radioactivité ne retombe au niveau de la radioactivité naturelle. Le stockage profond correspond à une des voies envisagées pour ce confinement.

Les résultats de cette thèse ne se limitent pas à cette application et leur extension à d'autres domaines (par exemple d'autres aspects de l'ingiénerie environnementale ou encore la chimie des océans) a toujours été recherchée.

1.1. CONCEPT ACTUEL DU STOCKAGE EN FORMATION GEOLOGIQUE PROFONDE.

A l'issue du rapport rendu par le médiateur, M. Christian Bataille, le Gouvernement a autorisé l'ANDRA, début janvier 1994, à engager des travaux de reconnaissance préliminaire, dans le cadre de la loi du 30 décembre 1991 relative à la gestion des déchets radioactifs à haute activité et à vie longue. Ces travaux de reconnaissance ont été effectués sur quatre départements : Gard, Haute-Marne, Meuse et Vienne. L'objectif de ces travaux était de s'assurer du caractère favorable des formations géologiques pour la réalisation de laboratoires de recherche souterrains. Les possibilités de stockage réversible ou irréversible des déchets radioactifs en formation géologique seront étudiées dans le laboratoire actuellement en voie de construction sur le site de Bure situé en Meuse et en Haute-Marne. L'architecture de ce laboratoire respectera l'architecture globale retenue actuellement dans le concept de stockage profond (Figure 1.1).

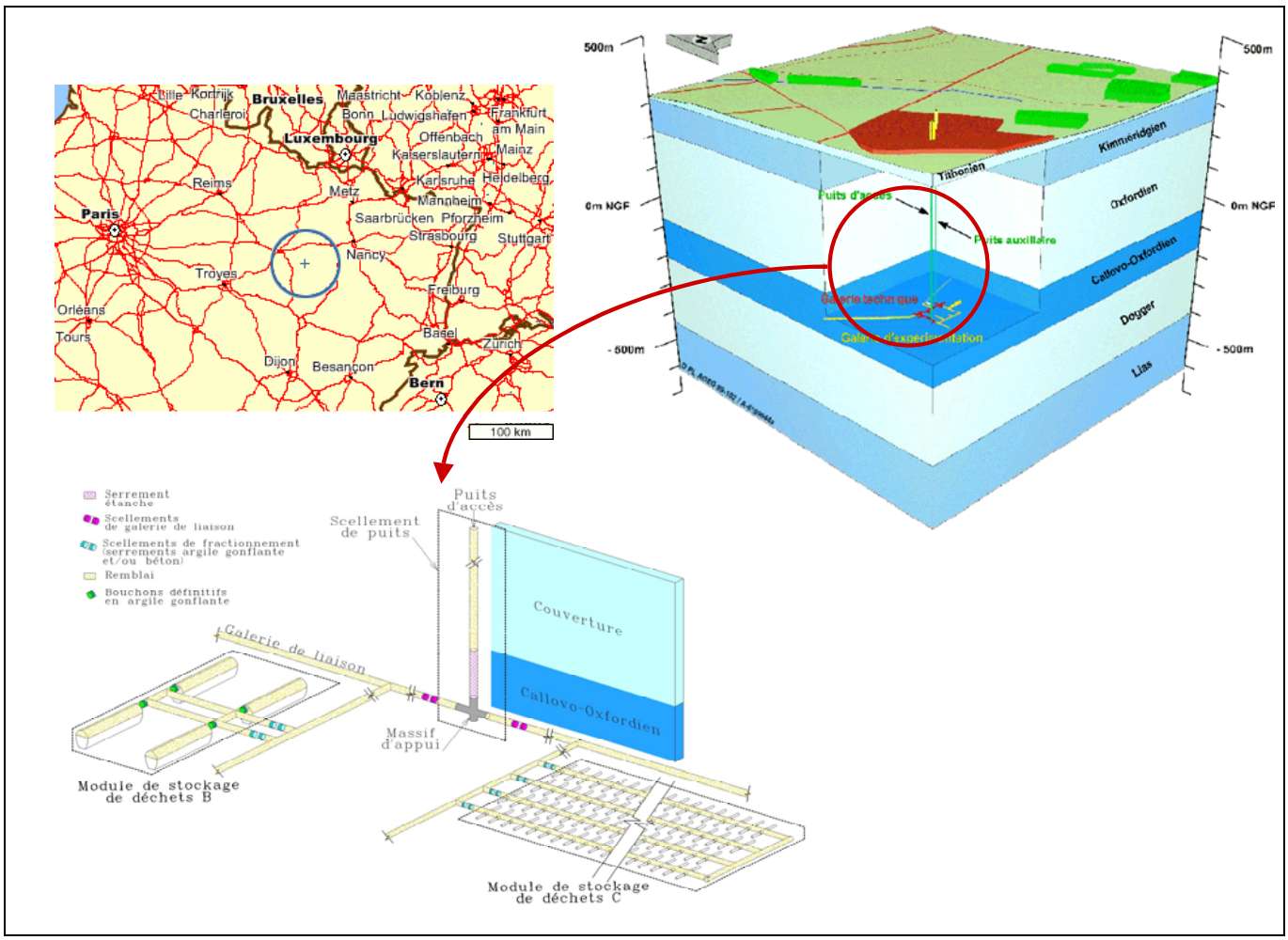


Figure 1.1 : Localisation du laboratoire souterrain de Meuse / Haute-Marne et architecture d'un site de stockage profond (concepts retenus par l'ANDRA en 2003)

Le concept actuel de stockage profond se base sur quelques grands principes, notamment que le stockage doit être constitué par une architecture dite « multibarrière » pour se prémunir des risques de défaillance d'une barrière particulière. Les barrières jouant un rôle de confinement sont : le colis de déchets avec les protections complémentaires qu'il peut

comporter (exemple : conteneur et surconteneur en acier), la barrière ouvragée – *i.e.* les matériaux placés entre le colis et la roche naturelle – et le milieu géologique (Figure 1.2). Dans le cas des déchets de type C vitrifiés (Tab. 1.1), le concept actuel repose sur un empaquetage du colis de déchet par un conteneur en acier noir ou en alliage passivable. Les argiles, sous forme de bentonite, sont de bons candidats pour la constitution de la barrière ouvragée, entre autres, pour leur forte capacité de rétention des cations, qui devrait permettre à la barrière d'immobiliser les radionucléides et empêcher leur migration vers la biosphère.

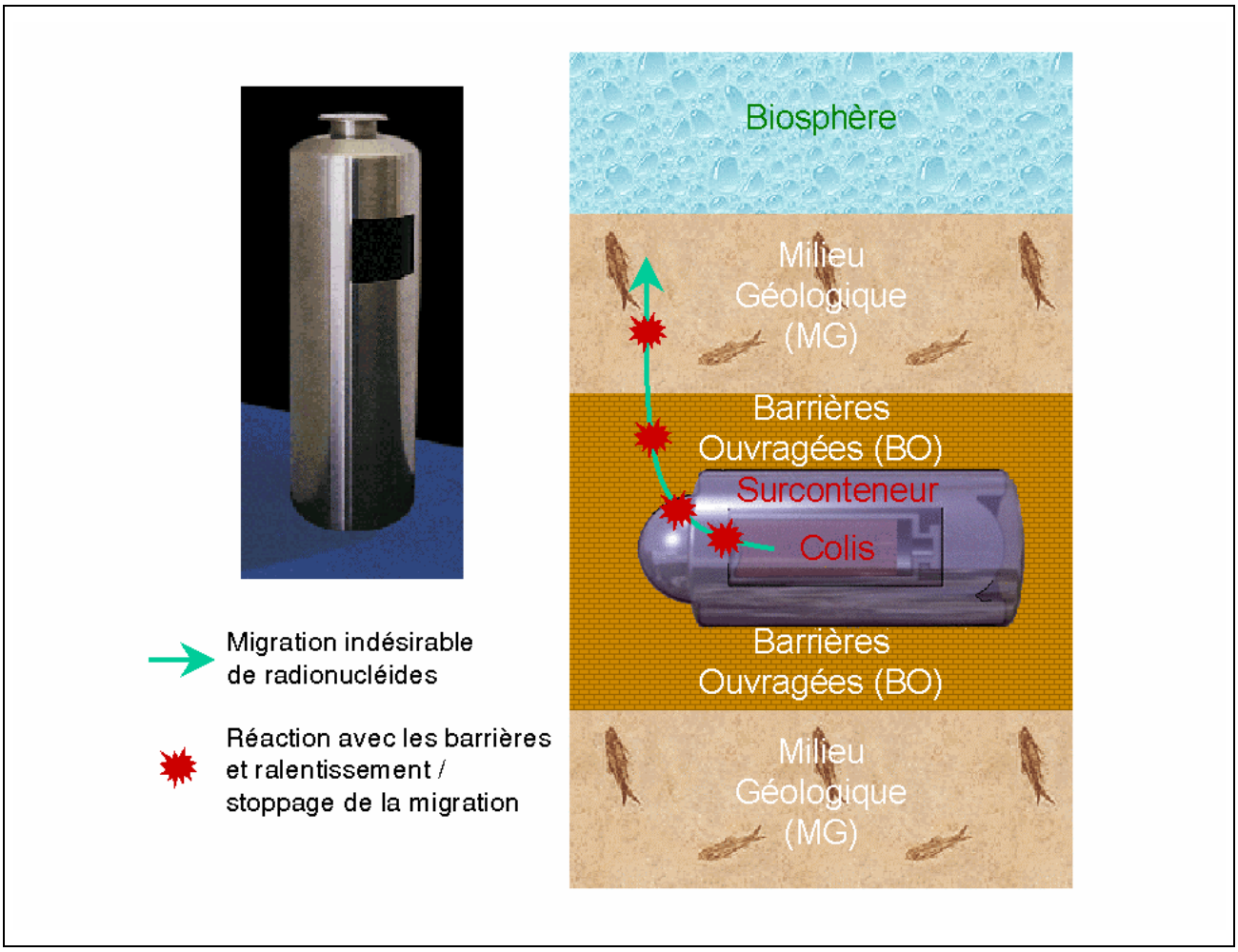


Figure 1.2 : A gauche : photo d'un conteneur en acier pour déchet de type C. A droite : principe de l'architecture "multibarrière".

Dénomination	Déchets A	Déchets B	Déchets C
Type de déchet	Déchets faiblement et moyennement radioactifs à vie courte	Déchets issus du retraitement des combustibles usés, du fonctionnement d'installation du CEA (recherche ou défense), ou du démantèlement des installations nucléaires.	Matière non valorisable de combustible usé
Type de stockage utilisé ou envisagé	Stockage de surface (opérationnel)	Stockage profond (en cours d'évaluation)	

Tab. 1.1 : Classification des déchets radioactifs selon leur provenance et le type de stockage envisagé.

1.2. LA REACTIVITE DU FE(II) DANS LA BARRIERE OUVRAGEE.

Cette thèse porte sur la réactivité des argiles vis-à-vis du Fe(II) en solution et s'inscrit dans la thématique de recherche de l'ANDRA sur le comportement des barrières ouvragées. Elle s'est déroulée au sein du service colis et matériaux (DS/CM), anciennement service matériaux (DS/MA). Les domaines d'activité couverts par ce service sont :

- la conception des barrières ouvragées ;
- la conception des scellements ;
- l'évaluation du comportement des colis de déchets ; et,
- l'évaluation du comportement des radionucléides au sein des différentes barrières de confinement.

Plus spécifiquement cette thèse a été suivie au sein du programme Fer – Argile. Ce programme se focalise sur les transformations de la barrière ouvragée induites par la libération de Fe(II) occasionnée par la dissolution des conteneurs en acier entourant les colis de déchets C et de combustible usé. Durant les travaux de réalisation, les ouvrages de stockage resteront ouverts pendant plusieurs dizaines d'années ce qui modifiera les conditions physico-chimiques locales par rapport aux conditions naturelles initiales. En particulier, sont attendues des modifications des contextes hydrologique (désaturation en eau), mécanique (création de fissures), thermique et géochimique (exemple : équilibre avec l'oxygène et les carbonates) et biologique (apparition de bactéries). Une fois refermé, le lieu du stockage redeviendra progressivement anoxique et saturé en eau. Dans ces conditions, le Fe(0) des containeurs en acier ne sera pas thermodynamiquement stable. La réaction d'oxydation du Fe(0) par l'eau devrait libérer des ions fer ferreux – Fe^{2+} – selon la réaction :

$$Fe^0 + 2\,H_2O \rightarrow Fe^{2+} + H_2\,(g) + 2\,OH^- \qquad \text{reaction 1.1}$$

Le fer ferreux – Fe(II), présent sous forme Fe^{2+}, $FeCl^{+}$ ou $FeHCO_3^{+}$ – libéré par le containeur interagira avec les argiles de confinement. Le but initial de cette thèse était donc de caractériser et de quantifier les interactions du Fe(II) avec une bentonite. Les principales interactions étudiées ont été les phénomènes d'adsorption.

1.3. LES PROPRIETES DE SORPTION DES ARGILES

Les mots « sorption » et « adsorption » désignent, dans toute cette thèse, l'ensemble des mécanismes permettant l'accumulation de matière sur une interface solide – solution. Classiquement, le mot adsorption est réservé aux phénomènes se déroulant sur une surface (2D) et absorption aux phénomènes faisant intervenir un volume (3D, exemple : précipitation) (Stumm and Morgan, 1996). La signification des mots « sorption » et « adsorption » englobe donc, dans cette thèse, des mécanismes parfois très distincts tels que l'échange cationique ou la précipitation de surface.

1.3.1. La sorption des métaux dans les milieux naturels

L'adsorption des cations métalliques sur les surfaces de minéraux est un processus naturel contrôlant les concentrations de la plupart des cations métalliques, considérés comme polluants ou non, dans les sols, sédiments et aquifères. Parmi les minéraux constituants des sols et des sédiments, les argiles et les oxydes jouent un rôle majeur. Leur petite taille en condition naturelle (inférieure à 1 µm) fait que ces minéraux développent de grandes surfaces spécifiques. Du fait de leur réactivité vis-à-vis des cations, ces minéraux sont considérés comme des « puits » naturels vis-à-vis des polluants métalliques.

1.3.2. La sorption sur les oxydes

Les oxydes dits « simples » sont les oxydes ne comportant qu'un seul type d'atome métallique dans leur formule structurale. Il s'agit par exemple des oxyhydroxydes de fer (magnétite, goethite, hématite, ferrihydrite …), de la silice (SiO_2) et de ses variétés cristallines polymorphes (ex : quartz, cristobalite), du rutile (oxyde de titane, TiO_2), des alumines (Al_2O_3)… A l'échelle macroscopique, les solides sont décrits comme des matériaux de charge neutre. Cependant à l'échelle nanoscopique, l'interface entre le solide et le milieu extérieur constitue une rupture du réseau cristallographique qui entraîne la création de charges en surface sur des sites fonctionnels de surface (Hiemstra et al., 1989a; Hiemstra et al., 1989b; Hiemstra et al., 1996). La charge ainsi créée peut être quantifiée à partir du modèle de Pauling sur les forces de liaison (Pauling, 1929). Dans un oxyde, chaque cation de valence V_M forme avec chacun des anions O^{2-} de son polyèdre de coordination une liaison électrostatique de force $f_{M\text{-}O} = V_M/n$, où n est le nombre d'anions du polyèdre de coordination. Au milieu de la structure, la valence $V_O = -2$ d'un oxygène est compensée par la somme des forces de liaisons établies avec ses m cations voisins :

$$\sum_m f_{M_m} = V_O = -2 \qquad \text{Eq. 1.1}$$

Sur les bordures des particules, certains oxygènes ne sont pas "entourés" complètement de cations métalliques mais sont en contact avec la solution. Ils sont alors dits insaturés et présentent des charges (Figure 1.3). Ces charges ne peuvent pas être neutralisées complètement au sein même du solide (Manceau and Gates, 1997), mais le sont au niveau de

l'interface par des interactions avec le milieu extérieur. La création de liaisons hydrogène avec l'eau environnante, l'adsorption d'un cation et la formation d'un complexe de surface font partie de ces interactions (e.g. Brown, 1976; Sposito, 1984; McBride, 1994; Hiemstra et al., 1996).

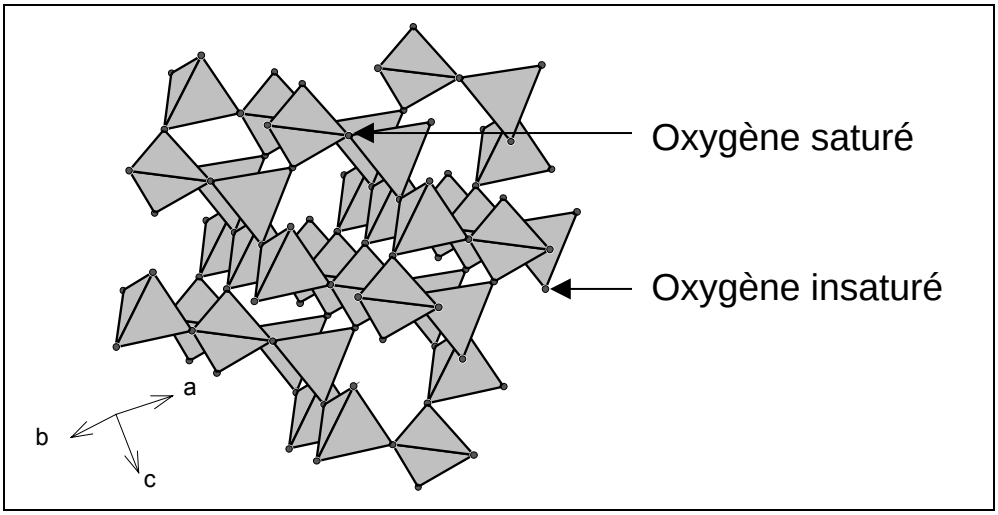
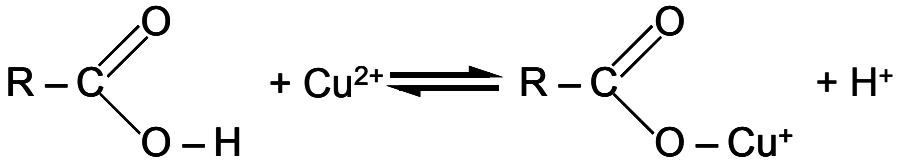


Figure 1.3 : Structure du quartz et présence d'oxygène insaturés en surface. La charge formelle de Si est +4, et est distribuée sur quatre atomes d'oxygène. La charge donnée à chaque atome d'oxygène est de donc de +1. Un atome d'oxygène n'est saturé que si il relie deux tétraèdres et qu'il reçoit ainsi la contribution de deux atomes de Si voisins.

Pour comprendre le phénomène de complexation de surface, une analogie avec la formation de complexes en solution peut être faite (Stumm and Morgan, 1996, p.520). Considérons un ligand en solution ayant une terminaison carboxylique (RCOOH). Cette terminaison peut réagir avec l'ion Cu^{2+} selon la réaction :



reaction 1.2

Remarque : *dans l'ensemble des réactions, la forme simplifiée de H_3O^+, marquée ici H^+, sera désignée sous le terme de « proton », bien que cette forme H^+ ne soit pas trouvée libre en solution et bien que proton désigne rigoureusement un constituant atomique portant une charge élémentaire positive.*

Les groupes fonctionnels de surface hydroxo (–OH), présents à la surface des oxydes, et désignés par le symbole générique >SOH, peuvent interagir avec l'ion Cu^{2+} selon une réaction analogue à la réaction 1.2 :



reaction 1.3

les ligands $>SO^-$ se comportant, de la même façon que $RCOO^-$, comme des bases de Lewis.

La quantification des phénomènes d'adsorption est souvent faite à l'aide d'isothermes d'adsorption. Ces isothermes sont en fait des courbes montrant la quantité de métal adsorbé en fonction d'un paramètre variable qualifiant la composition de la solution, les autres paramètres

étant fixés. Ce paramètre variable est souvent le pH, la concentration en métal libre de la solution ou sa fraction équivalente au sein du cortège de cations présents. Le choix de cette représentation se comprend parfaitement si l'on considère que d'après la réaction 1.3, le cation métallique entre en compétition avec les protons pour former un complexe avec le site fonctionnel de surface. Faire varier le pH (qui est en quelque sorte la mesure du nombre de protons libres en solution sur une échelle logarithmique) à concentration totale en cation métallique fixée ou faire varier la concentration du cation métallique à pH fixé, permet d'évaluer les affinités relatives de la surface vis-à-vis du cation et du proton (Figure 1.4).

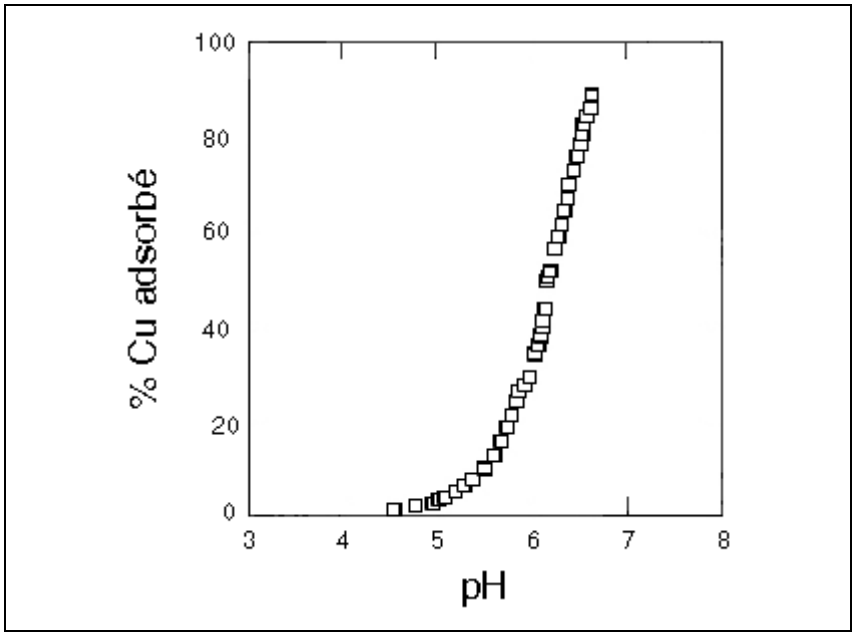


Figure 1.4 : Exemple d'isotherme de sorption. Adsorption de Cu^{2+} sur de la silice (SiO_2) en fonction du pH (Schindler et al., 1976).

Récemment un modèle a été proposé pour prédire, à l'aide d'informations structurales, l'affinité des sites fonctionnels de surface vis-à-vis des protons. Dans ce modèle – MUSIC (Hiemstra et al., 1996) –, l'affinité pour le proton est calculée à partir de la charge partielle portée par l'oxygène de surface et de la somme des valences de la liaison apportés par les cations entourant cet oxygène (Hiemstra et al., 1996; Venema et al., 1998) :

$$\log K = -A\left(\sum_j s_j + V\right) \qquad \text{Eq. 1.2}$$

où *A* est une constante égale à +19.8 (Hiemstra et al., 1996), *V* est la valence de l'oxygène (*V*= -2), et $\sum_j s_j$ est la somme des valences de liaison des cations entourant l'oxygène (métaux plus protons) :

$$\sum_j s_j = \sum_i s_{Me_i} + m \times s_H + n \times (1 - s_H). \qquad \text{Eq. 1.3}$$

où $\sum_i s_{Me_i}$ est la contribution des *i* cations structuraux Me_i ions, s_H la valence de liaison d'une liaison O-H (s_H = 0.8), et (1 - s_H) la valence de liaison d'une liaison hydrogène. *m* et *n* sont respectivement le nombre de protons complexés et le nombre de protons engagés dans une

liaison hydrogène. La contribution de chaque cation structural (s_{Me}) est calculée grâce à la formule de Brown et Altermatt (Brown and Altermatt, 1985) :

$$s_{Me} = e^{\frac{(R_0 - R)}{b}} \qquad \text{Eq. 1.4}$$

où R est la distance Me-O, R_0 est une distance spécifique de l'élément Me et tabulée par Brown et Altermatt (Brown and Altermatt, 1985) et b est une constante égale à 0.37 Å.

Par exemple, dans le cas de l'oxygène insaturé montré sur la Figure 1.3, on peut calculer les constantes de protonation pour les deux réactions suivantes :

$>SiO^- + H^+ \Leftrightarrow >SiOH$ $\log K_1$ reaction 1.4

$>SiOH + H^+ \Leftrightarrow >SiOH_2^+$ $\log K_2$ reaction 1.5

R = 1.621 Å, donné par les paramètres cristallographiques ;

R_0 = 1.624 Å, donné par la table de Brown et Altermatt (Brown and Altermatt, 1985) ;

S_{Si} = 1.008, donné par l'équation 1.4

$\sum_j s_j$ =1.008 + 3 $\times$ 0.2 = 1.608, en considérant que m + n = 3, pour la première protonation du site (réaction 1.4) et

$\sum_j s_j$ = 1.008 + 2 $\times$ 0.2 + 0.8 = 2.208 pour la deuxième protonation du site (réaction 1.5) et donc

$\log K_1 = -19.8 \times (1.608 - 2) = 7.8$

$\log K_2 = -19.8 \times (2.208 - 2) = -4.1$

On peut noter que la double protonation du site n'existe pas dans le domaine des pH usuels. D'autre part le pH pour lequel la charge globale de ces sites est nulle (PCN, point de charge nulle) est égal à (7.8 - 4.1) / 2 = 1.9 ce qui correspond effectivement au point de charge nulle mesurée pour la silice et le quartz (PCN = 2 $\pm$ 0.3, Sposito, 1984).

1.3.3. Structure des argiles et phénomènes de sorption associés

La structure particulière des argiles leur confère des propriétés de sorption différentes de celles des oxydes. Je me focaliserai ici sur le cas des montmorillonites ou smectites dioctaédriques, et en particulier sur la montmorillonite MX80. Les propriétés structurales présentées ci-dessous sont volontairement sommairement présentées. De plus amples précisions sont disponibles dans des ouvrages de références (référentiel ANDRA, 2001 et références incluses, C.RP.AMAT.01.060 Ind A).

1.3.3.1. Structure cristalline et surfaces développées

Les montmorillonites font parties des argiles T.O.T. Elles sont formées par un empilement de feuillets constitués d'une couche octaédrique (couche O) prise en sandwich par deux couches tétraédriques (couches T). Dans l'empilement, les feuillets sont séparés par un espace dit interfoliaire. Les couches tétraédriques sont constituées principalement d'ions Si^{4+}, dont les tétraèdres de coordination partagent uniquement des sommets. L'agencement des tétraèdres forme une structure en « nid d'abeille » dont les cavités sont appelées cavités siloxane ditrigonales (Figure 1.1). La couche octaédrique des feuillets est composée majoritairement de cations Al^{3+}, dont les octaèdres de coordination partagent uniquement des arêtes entre eux. Cet arrangement ménage, lui aussi, une structure en « nid d'abeille » avec la présence d'un site lacunaire sur 3 sites octaédriques (Figure 1.6). Chaque tétraèdre des couches T partage un coin avec la couche octaédrique. Les oxygènes de la couche octaédrique qui ne partagent pas une liaison avec les tétraèdres sont protonés (Figure 1.7). Cette structure particulière crée une grande diversité de surfaces en contact avec le milieu extérieur, surface de bordure de feuillet, surface interfoliaire et surface externe de la particule (Figure 1.8).

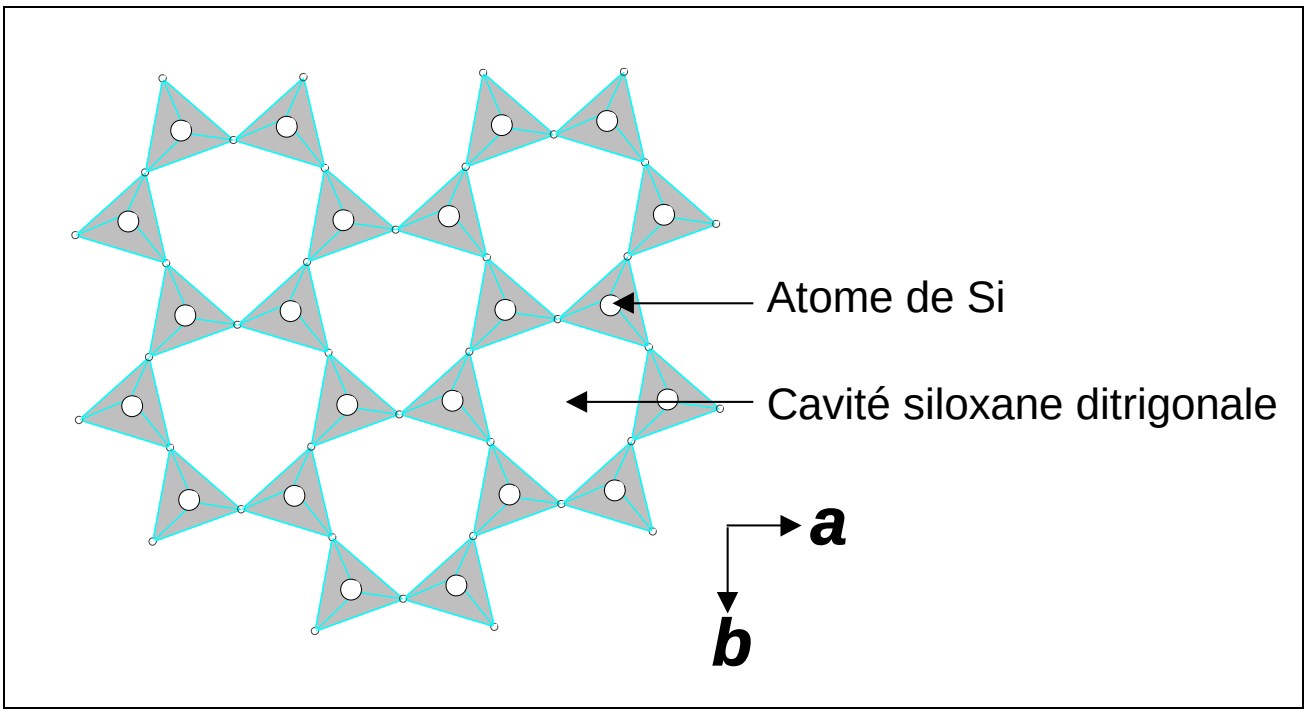


Figure 1.5 : Agencement des tétraèdres de Si et aménagement des cavités siloxane (vue selon l'axe cristallographique *c* et dans le plan *ab*).

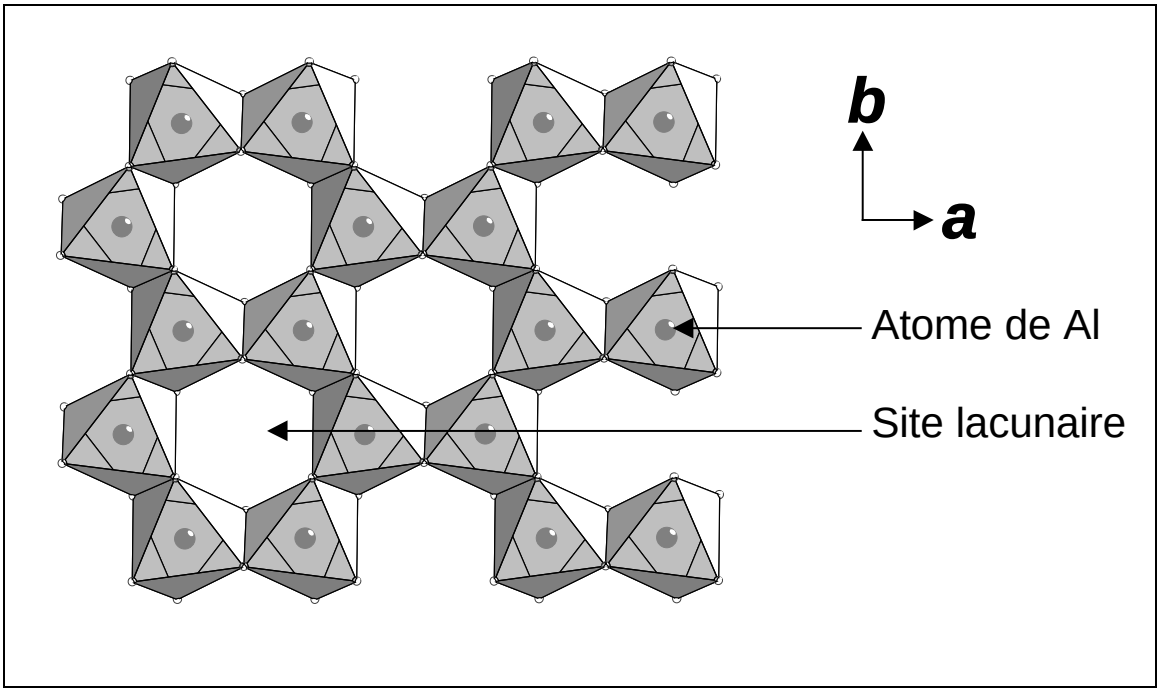


Figure 1.6 : Agencement des octaèdres d'Al dans le feuillet octaédrique et aménagement des sites lacunaires (vue selon l'axe cristallographique *c* et dans le plan *ab*).

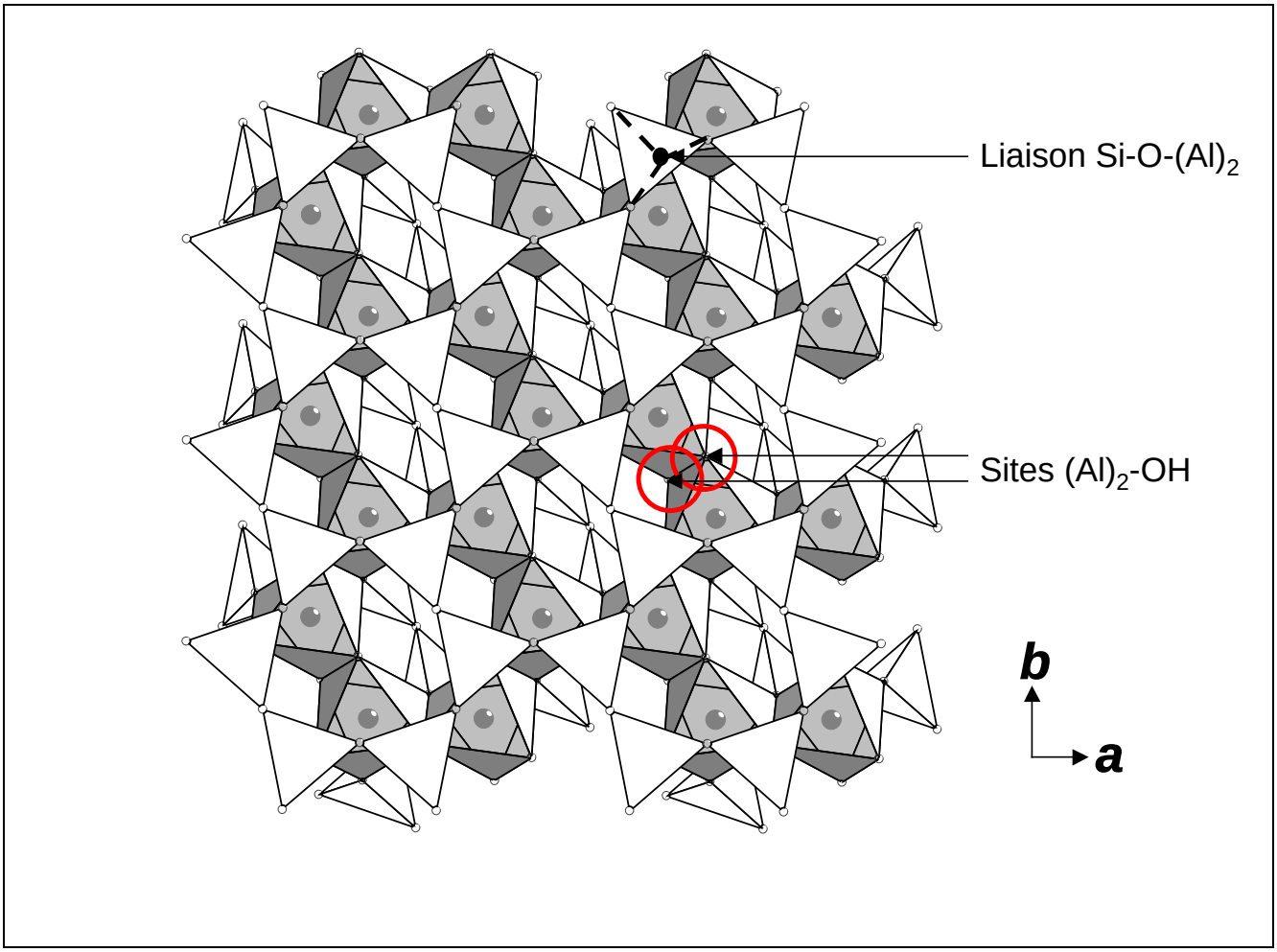


Figure 1.7 : Structure d'un feuillet TOT et position des sites protonés au centre des cavités siloxane (vue selon l'axe cristallographique *c* et dans le plan *ab*).

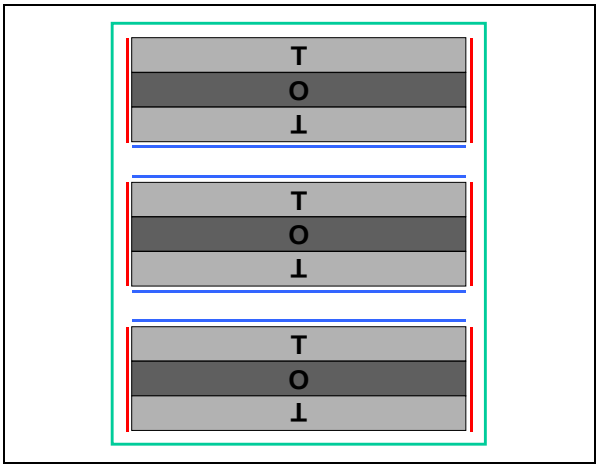


Figure 1.8 : Les différentes surfaces des particules argileuses constituées d'un empilement de feuillets TOT ; en rouge, les surfaces de bordures ; en bleu, les surfaces interfoliaires ; et, en vert la surface externe de la particule.

1.3.3.2. Formule structurale et échange cationique

Idéalement, la formule structurale d'une montmorillonite devrait s'écrire : $(Al^{III}_2)_{Oc}(Si^{IV}_4)_T O_{10}(OH)_2$. Cependant des substitutions ont lieu au sein des couches tétraédriques et octaédriques. En position octaédrique, un ion divalent (principalement Mg^{II} et Fe^{II}) ou un autre ion trivalent (Fe^{III}) peut remplacer un Al. Un ion trivalent (Al^{III} ou Fe^{III}) peut également se substituer à un Si^{IV} tétraédrique. Si le nombre de substitutions dans la couche octaédrique est supérieur au nombre de substitutions dans la couche tétraédrique, on a affaire à une smectite, et sinon à une vermiculite. Ces substitutions créent un déficit de charge qui est compensé par l'introduction d'un cation dans l'espace interfoliaire (Figure 1.9). La formule devient alors : $Cat^{z+}_{(x+y)/z}(Me^{III}_{2-x}Me^{II}_x)_{Oc}(Si^{IV}_{4-y}Me^{III}_y)_T O_{10}(OH)_2$ où Cat^{z+} représente un cation de charge *z* en position interfoliaire, Me^{III} représente un cation trivalent et Me^{II} un cation divalent. Les cations interfoliaires sont peu liés à la structure, à de rares exceptions près (exemple : Cs^+ et K^+). Ils forment en général des complexes de sphère externe, c'est à dire qu'ils gardent leur sphère d'hydratation. La plupart de ces cations s'échangent facilement avec d'autres cations présents dans le milieu extérieur, au cours d'un processus nommé échange cationique.

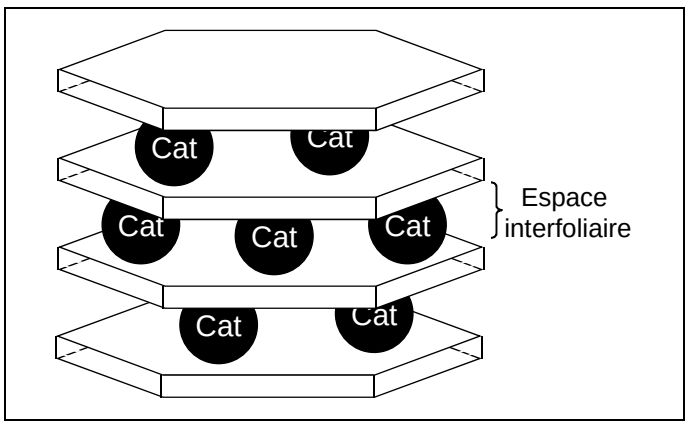


Figure 1.9 : Schéma d'une particule d'argile avec ses cations interfoliaires

1.3.3.3. Terminaison des feuillets et adsorption spécifique

A l'instar des oxydes, les feuillets des argiles ont des surfaces de bordure présentant des groupes hydroxo (Figure 1.10). Ces sites fonctionnels sont un deuxième lieu potentiel pour les phénomènes de sorption (Schlegel et al., 1999; Schlegel, 2000; Schlegel et al., 2001a; Dähn et al., 2003). Comme dans le cas des oxydes, la complexation de cation métallique à la surface de ces sites (Figure 1.11) est, entre autres, contrôlée par le pH (Figure 1.12) (Charlet et al., 1993; Stadler and Schindler, 1993; Zachara and Smith, 1994; Baeyens and Bradbury, 1997; Bradbury and Baeyens, 1997, 1998; Turner et al., 1998; Bradbury and Baeyens, 2002…).

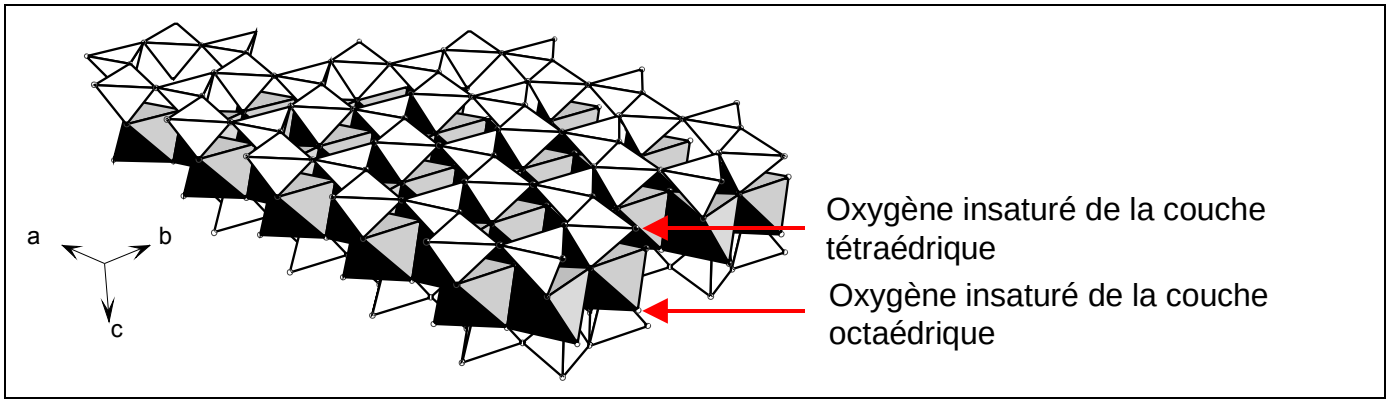


Figure 1.10 : Structure du feuillet TOT de l'argile et de ses terminaisons sur les bordures. Les oxygènes insaturés indiqués par les flèches sont à l'origine des phénomènes de sorption spécifique.

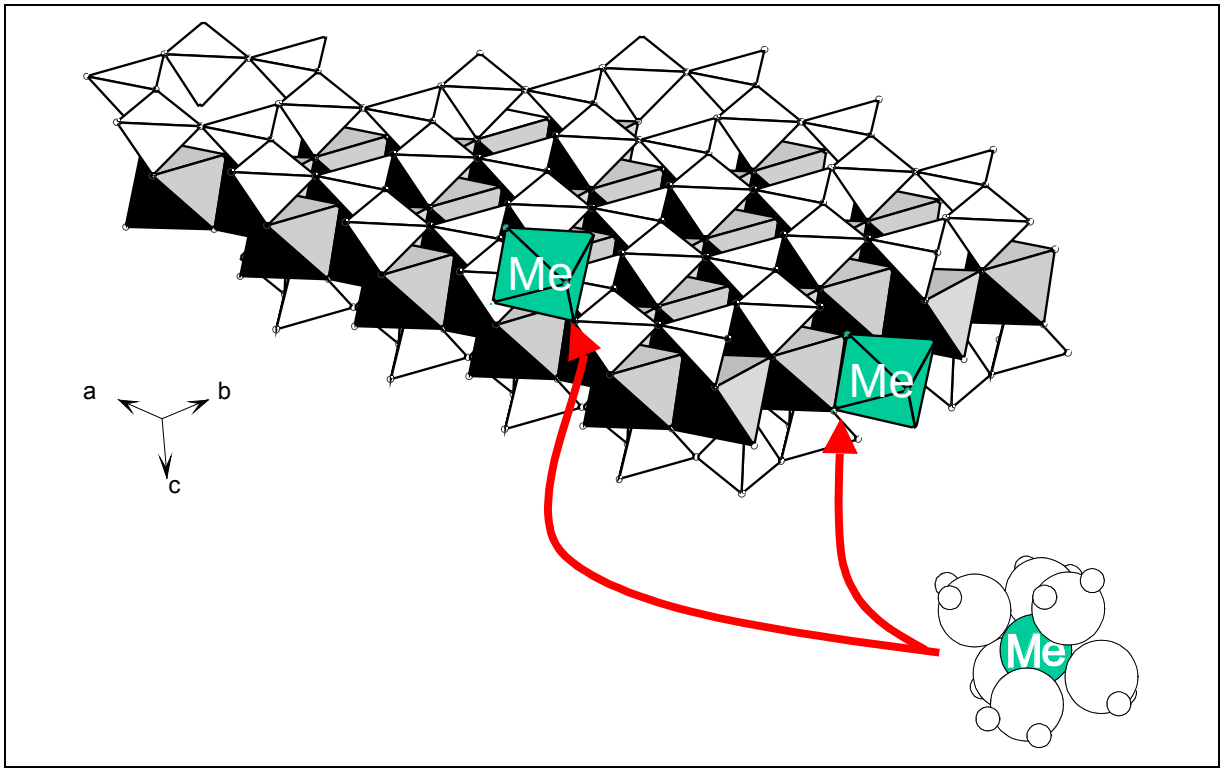


Figure 1.11 : Représentation schématique de deux types de sorption sur les bordures des feuillets. En bas à droite : cation métallique Me en solution avec sa sphère d'hydratation. En haut à gauche : sorption en complexe de sphère interne et liaison à la structure de l'argile par un sommet partagé avec un tétraèdre de bordure de l'argile. En haut à droite : sorption en

complexe de sphère interne et liaison à la structure de l'argile par une arête partagée avec un octaèdre de bordure de l'argile.

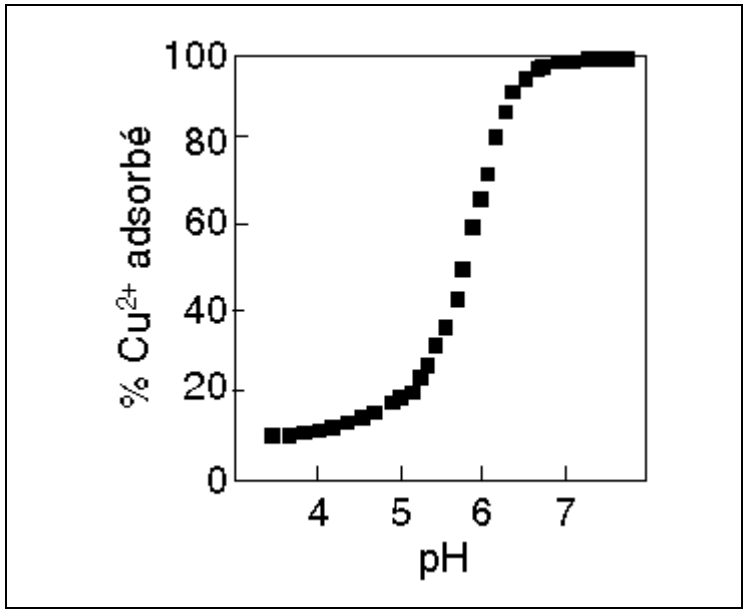


Figure 1.12 : Isotherme d'adsorption du Cu^{2+} sur une montmorillonite en fond ionique KCl (Stadler and Schindler, 1993). Cette courbe présente de grandes similitudes avec l'isotherme d'adsorption présentée sur la Figure 1.4.

A la différence des bordures des oxydes où les oxygènes sont souvent liés à un seul type de cation structural (Si^{4+}, Al^{3+}, Fe^{3+}…), les bordures des argiles présentent des oxygènes liés à un, deux, voir trois types de cations différents. A cette diversité chimique, s'ajoute une diversité structurale (Figure 1.13) qui vient renforcer la complexité de l'interface argile–solution.

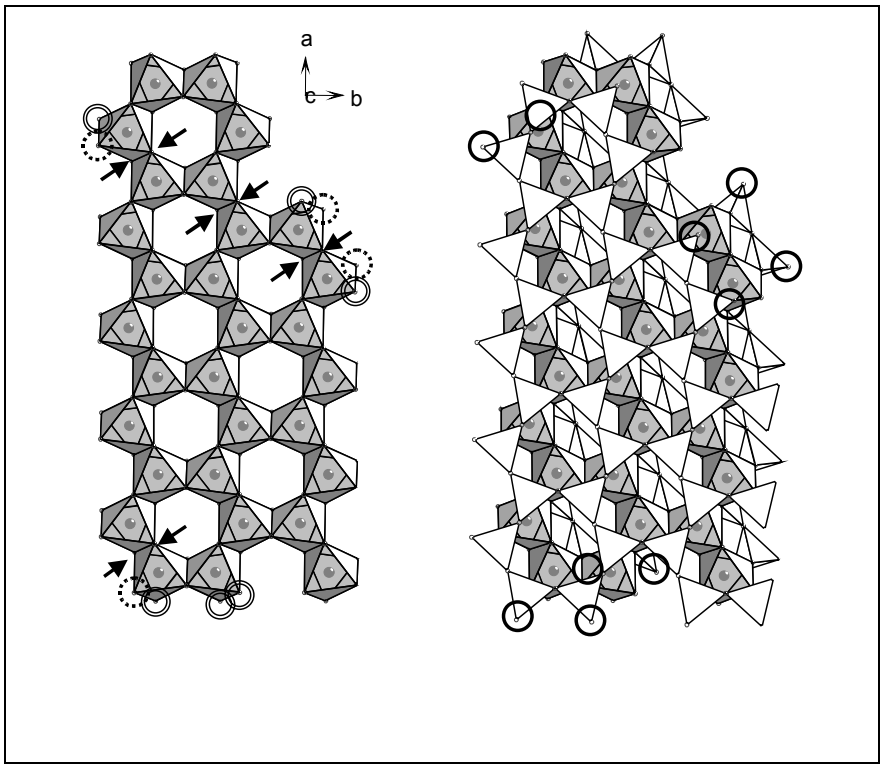


Figure 1.13 : Complexité des bordures d'un feuillet TOT d'argile. A gauche, le feuillet octaédrique et à droite le feuillet complet. Les cercles (un trait plein, deux traits pleins, et deux

traits tiretés) et les flèches indiquent des sites fonctionnels de surface différents structuralement.

1.4. MOYENS D'ETUDE DE LA SORPTION A LA SURFACE DES ARGILES

Le premier moyen d'étude des mécanismes de sorption à la surface des argiles est, bien sûr, la réalisation d'isothermes d'adsorption et l'analyse chimique de solutions en équilibre avec une phase argileuse. Les données issues de ces expériences sont des données dites macroscopiques, et aucun mécanisme à l'échelle microscopique ne peut en être déduit avec certitude. Les informations données par ces expériences permettent cependant de discerner les domaines de conditions chimiques propres à chaque type de phénomènes et de quantifier ces phénomènes, individuellement ou non. Les expériences de chimie analytique sont donc à la base de toute modélisation quantitative des phénomènes de sorption.

Les outils de spectroscopie, de diffractométrie et de simulation numérique forment le deuxième moyen d'investigation des phénomènes de surface, en les caractérisant jusqu'à l'échelle atomique. La spectroscopie d'absorption des rayons X (EXAFS) réunit des atouts considérables pour étudier les phénomènes de sorption spécifique, à la fois au niveau des conditions d'utilisation (possibilité de travailler à basse concentration et avec de nombreux espèces atomiques, dont tous les métaux) et au niveau des informations contenues dans les spectres (nature des atomes voisins, nombre moyen de voisins et distances moyennes jusqu'aux voisins entourant l'atome cible). Récemment, des travaux, utilisant au mieux la puissance de cet outil, ont permis de caractériser finement les interactions de cations tels que Co^{2+}, Zn^{2+} et Ni^{2+} avec des smectites dioctaédriques et trioctaédriques (Schlegel et al., 1999; Schlegel et al., 2001a; Schlegel et al., 2001b; Dähn et al., 2002b; Dähn et al., 2003). Ces travaux ont permis de montrer la réalité microscopique de deux phénomènes de sorption préalablement déduits des analyses chimiques : échange cationique et complexation de surface. Ils ont également mis en évidence la présence d'un phénomène supplémentaire : la nucléation de nouvelles phases argileuses contenant les cations métalliques Co^{2+}, Zn^{2+} et Ni^{2+} en position octaédrique. La spectroscopie par résonance paramagnétique électronique (RPE ou EPR en anglais) a également grandement contribué à la compréhension des phénomènes d'adsorption. Cette technique, dont la sonde est le moment magnétique d'un électron, n'est applicable qu'à certains éléments dans un état d'oxydation précis qui présentent un électron célibataire dans une orbitale m_l (ex : Cu^{2+}, Mn^{2+}, Fe^{3+}…). Cette technique permet de contraindre à la fois la position de l'élément étudié dans le solide (échange, adsorption, phase annexe…) et les changements structuraux induits par sa présence (pour exemple : McBride et al., 1975; McBride et al., 1984; Gehring et al., 1993; Gehring and Sposito, 1995; McBride, 1995; Hyun et al., 2000). Depuis peu, la spectroscopie de diffraction de neutrons, et les simulations numériques de type Monte-Carlo ou dynamique moléculaire permettent d'appréhender les mécanismes de sorption et leur influence sur la structure de l'eau liée à l'argile (pour exemple : Chang et al., 1995; Skipper et al., 1995a; Skipper et al., 1995b; Chang et al., 1998 ; Powell et al., 1998; Sposito et al., 1999; de Carvalho and Skipper, 2001; Pitteloud et al., *In press*). D'autres outils viennent compléter cette panoplie, comme la spectroscopie infrarouge (FTIR), qui permet de caractériser la nature des liaisons dans le solide, ou le Mössbauer, technique spécifiquement utilisée pour l'étude de l'environnement structural et l'état d'oxydation du fer.

Les outils microscopiques forment la dernière catégorie des moyens d'investigation. La petite taille des particules d'argile rend cet usage limité. Seuls le microscope électronique à transmission (MET) et le microscope à force atomique (AFM) permettent d'imager des particules d'argiles individuellement. Parmi ces deux outils, l'AFM fournit, dès à présent, des résultats prometteurs. Récemment, des phénomènes d'oxydation du Fe(II) à la surface d'une

phlogopite (mica de structure proche des montmorillonites mais formant des cristaux de grande taille) ont été observés par AFM et ont pu être localisés préférentiellement sur des terminaisons de feuillets (Figure 1.14). Les dissolutions de l'hectorite (une smectite trioactédrique magnésienne) et de l'illite (argile potassique) ont également été observées "en direct" à bas pH. Ces expériences ont permis de montrer que la dissolution est localisée sur les bordures des feuillets (Figure 1.15). Le développement de nouveaux dispositifs, permettant d'observer des particules d'argiles sous l'eau (*in situ*) et en boîte à gants, ouvre la voie à l'observation en direct de nucléations de phase et de réactions d'oxydo-réduction à la surface des argiles (Bosbach et al., 2002).

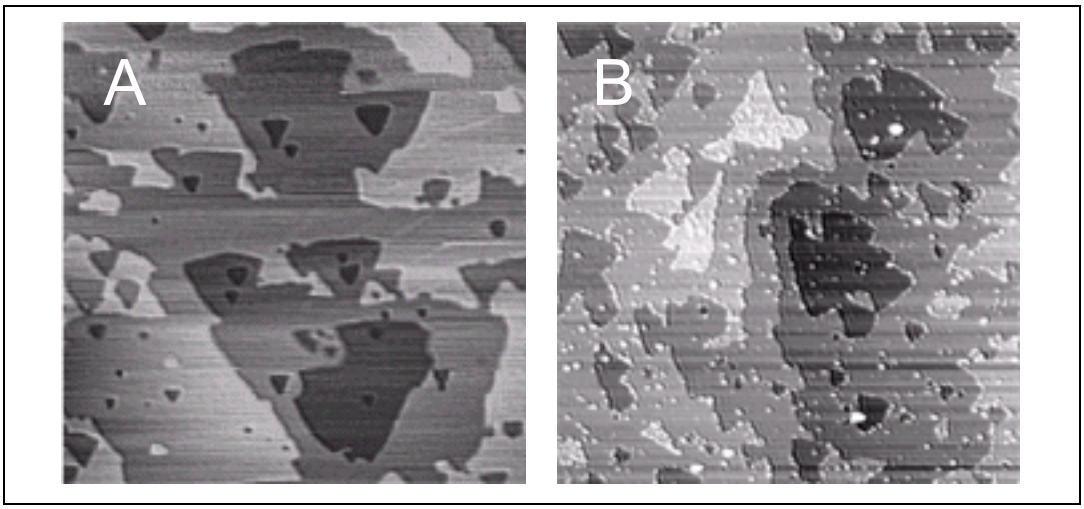


Figure 1.14 : A. Image AFM *in-situ* d'une surface fraîchement clivée de phlogopite. B. Image AFM *in-situ* d'une surface de phlogopite ayant réagi avec du Fe(II) et de l'As(V) sans fond ionique (temps de réaction : 2 h). D'après Charlet et al. (Charlet et al., 2002).

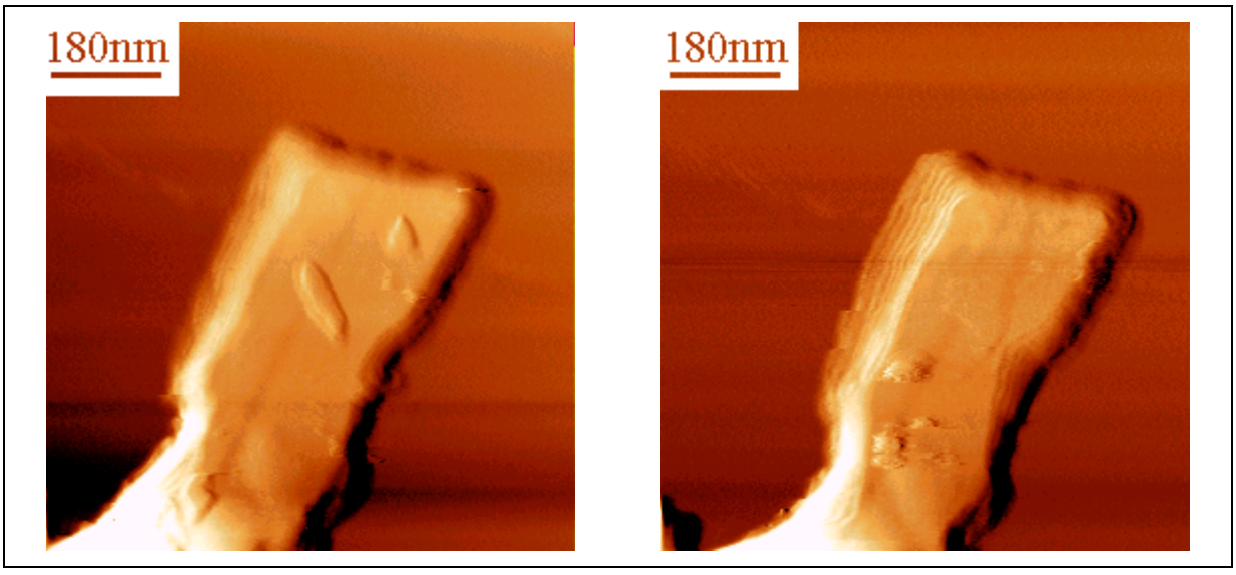


Figure 1.15 : Images AFM de la dissolution d'hectorite à bas pH 2 (Bosbach et al., 2000). A gauche : état initial. A droite, l'image de droite clairement l'apparition de marches sur les bords de la particule).

En résumé, les outils actuels peuvent être groupés en trois grandes catégories, ayant chacune leur fonction dans la compréhension des phénomènes à la surface de l'argile :

- chimie analytique des solutions : quantification, identification des phénomènes ;
- spectroscopie (ex : RPE, FTIR, Mössbauer, EXAFS, diffraction de neutrons) et modélisation numérique (dynamique moléculaire et simulation de type Monte Carlo) : caractérisation des phénomènes à l'échelle atomique ;
- microscopie (ex : AFM) : localisation des phénomènes.

1.5. DIFFICULTES ASSOCIEES AU SYSTEME FE(II) – ARGILE

Le système Fe(II) – argile présente deux types de difficultés. Le premier est lié à la nécessité de conserver le fer sous forme ferreuse pendant les expériences, ce qui est d'autant plus difficile que l'adsorption catalyse les réactions d'oxydation (Liger et al., 1999). Le deuxième est lié à la présence systématique de fer dans les systèmes naturels, et donc, dans les argiles.

La première difficulté m'a contraint à travailler en boîte à gants où des conditions d'anoxie stricte sont respectées (pO_2 < 10 ppm ou 0.5 ppm selon la boîte à gants utilisée). Les suspensions et solutions utilisées sont préalablement purifiées de leur O_2 dissous avant d'être rentrées dans l'enceinte de la boîte (protocole en 6.2). La plupart des solutions sont préparées à l'intérieur de la boîte en mélangeant de l'eau purifiée et des sels préalablement pesés à l'extérieur. Les véritables problèmes apparaissent quand il faut sortir les échantillons de la boîte à gants, comme, par exemple, pour effectuer des mesures spectroscopiques. Le moyen le plus efficace a été de sceller chaque échantillon dans des boîtes individuelles sous atmosphère anoxique, puis de les sortir de la boîte à gant et les mettre immédiatement dans une glacière contenant de la carboglace afin de bloquer au maximum les réactions d'oxydation du Fe(II). Une fois le transport terminé, les échantillons sont rapidement transférés dans l'azote liquide.

La deuxième difficulté m'a empêché d'utiliser certaines techniques, dont l'EXAFS au seuil du fer. En effet, l'EXAFS fournit une information moyenne sur tous les atomes cibles. Il n'est donc pas possible de distinguer le fer ajouté dans le système du fer déjà présent dans l'argile. Celui-ci excédant largement la quantité de fer ajoutée dans les expériences, des expériences EXAFS auraient caractérisé majoritairement le fer structural. Pour pallier à cet inconvénient, des expériences de chimie originales, bien que simples, et l'utilisation couplée d'outils tels que les spectroscopies Mössbauer et infrarouge (FTIR) ont été utilisées afin de contraindre au mieux les phénomènes et de les identifier aux phénomènes déjà caractérisés pour d'autres cations divalents (Zn^{2+}, Co^{2+}, Ni^{2+}…).

2. METHODOLOGIE

2.1. CHOIX DU MATERIAU ARGILEUX

Le concept de stockage des déchets nucléaires en formation profonde n'est pas un concept arrêté. En fonction des avancées technologiques et des connaissances sur les matériaux, ce concept évolue. L'ANDRA étudie actuellement le concept de stockage en milieu argileux avec une barrière ouvragée, elle aussi, argileuse. Le matériau argileux (bentonite), qui sera utilisé dans cette barrière, n'est pas encore choisi. Cependant, pour des besoins de comparaison entre études menées sur ce concept, il était nécessaire de travailler sur une base commune minimale. Ainsi, une bentonite, dite méthodologique, a été retenue par l'ANDRA pour les expériences menées par ses collaborateurs au sein du groupement de laboratoires Fer – Argile . Le choix de l'ANDRA s'est porté sur une bentonite commerciale, la MX80, après une étude comparative réalisée par le Laboratoire Environnement et Mineralurgie (LEM) et le Centre de Recherches sur la Géologie des Matières Premières Minérales et Energétiques (CREGU) (Sauzéat et al., 2001). Le tableau Tab. 2.1 résume la composition de la bentonite.

	% massique à T et P ambiante	% massique sans eau moléculaire à 105 °C
Montmorillonite	70.6 ± 2.7	79.2 ± 3.0
Phlogopite	2.7 ± 2.7	3.0 ± 3.0
Pyrite	0.5	0.6
Calcite	0.7 ± 0.5	0.8 ± 0.6
Ankérite	1.0 ± 0.3	1.1 ± 0.4
Anatase	0.1	0.1
Plagioclases	8.2 ± 2.7	9.2 ± 3.0
Feldspath K	1.8 ± 1.8	2.0 ± 2.0
Phosphate	0.6	0.6
Quartz ou cristobalite	2.5 ± 2.5	2.8 ± 2.8
Fe_2O_3	0.4 ± 0.3	0.5 ± 0.4
H_2O moléculaire	10.8	-
C organique	0.1	0.1
Total	100	100

Tab. 2.1 : Composition minéralogique de la MX-80 brute quartée, dans des conditions de pression et de température ambiantes, et à 105°C (Sauzéat et al., 2001).

La bentonite est constituée en majorité de montmorillonite. Cependant, des impuretés sont présentes en quantités non négligeables. La plupart des minéraux accessoires, présents dans cette bentonite, ainsi que la matière organique possèdent des propriétés de sorption vis-à-vis des cations métalliques. L'interprétation des données d'adsorption sur la bentonite est donc d'autant moins aisée que le nombre des composants actifs est grand. Par conséquent, la fraction argileuse de cette bentonite a été extraite afin d'étudier spécifiquement les interactions Fe(II) – argile et simplifier les interprétations. Le procédé d'extraction de la phase argileuse est présenté en annexe 2.

2.2. STRATEGIE DES EXPERIENCES DE SORPTION

2.2.1. Expériences d'adsorption spécifique sur les bordures des argiles

L'étendue de l'adsorption spécifique d'un métal sur les surfaces de bordure des argiles est principalement contrôlée par le pH, tandis que l'adsorption en position d'échange cationique est liée aux concentrations relatives des éléments dans la solution en équilibre avec l'argile. Pour ne "voir" que l'adsorption spécifique, il suffit donc d'augmenter la concentration du fond cationique jusqu'à ce que les phénomènes d'échange ne représente plus qu'une quantité inférieure à la barre d'erreur sur la quantité adsorbée totale. C'est pourquoi les expériences d'adsorption spécifiques ont été réalisées à haute concentration en NaCl ou $CaCl_2$, typiquement de 0.5 à 1 mol l^{-1} de NaCl et de 0.05 à 0.5 mol l^{-1} de $CaCl_2$. Les expériences consistaient en la mesure de l'adsorption du Fe(II) en fonction du pH, la concentration totale en Fe(II) et les autres conditions expérimentales (teneur en solide, force ionique…) étant maintenues constantes. Ces expériences ont été réalisées, soit dans des réacteurs chimiques (expériences en continu, à temps d'équilibre solide - solution court, de l'ordre de la demi-heure) soit dans des tubes (expériences discontinues ou en "batch", à temps d'équilibre long, de l'ordre du jour à la semaine).

2.2.2. Expériences d'échange cationique

Dans ces expériences, les phénomènes d'adsorption spécifique devaient être minimisés. L'adsorption spécifique étant plus importante à mesure que le pH augmente, les expériences d'échange cationique ont donc été réalisées à bas pH. Les premières expériences d'adsorption spécifique ont montré que le Fe(II) pouvait commencer à s'adsorber spécifiquement vers pH 2-3. Les expériences d'échange cationiques ont donc été réalisées dans cette fourchette de pH, où l'influence de l'adsorption spécifique était moins grande que les barres d'erreur sur la mesure du Fe(II) adsorbé en site d'échange cationique. Les expériences consistent à mesurer la variation des ions Na(I), Ca(II) et Fe(II) adsorbés en fonction des concentrations relatives de Na(I), Ca(II) et Fe(II) en solution. Des masses identiques d'argile sont mises à équilibrer dans des tubes avec des solutions contenant des concentrations relatives en Na(I), Ca(II) et Fe(II) différentes. La normalité totale (qui est égale à la concentration en ion Cl^-, dans notre cas) et le pH sont identiques dans chaque tube. Le temps d'équilibre varie d'une journée à une semaine selon les expériences.

2.2.3. Expériences de titration, de dissolution, de compétition…

Il est rapidement apparu que les deux types d'expériences décrites plus haut ne suffisait pas à comprendre entièrement les phénomènes d'échange et de sorption spécifique. Des expériences complémentaires de chimie ont été menées pour caractériser les sites d'adsorption (expériences de titration), la dissolution de l'argile à haut et bas pH, et enfin les phénomènes de compétition entre éléments pouvant s'adsorber sur l'argile. Ces expériences ont été réalisées

soit en "batch" soit en réacteur chimique. Leur description complète est disponible dans les articles qui constituent les parties 3 et 4 de cette thèse.

2.3. REPRESENTATION DES DONNEES

2.3.1. Echange cationique

2.3.1.1. Description thermodynamique de l'échange cationique

De nombreuses publications des années 1980 traitent de la description de l'échange cationique sur les surfaces des argiles (Sposito, 1981; McBride, 1994). Dans le court rappel qui suit je présente brièvement les paramètres de cette description en partant d'un exemple, le cas de l'échange Na^+ - Fe^{2+}, et en suivant les développements et les notations présentés par Sposito et McBride (Sposito, 1981; McBride, 1994).

L'échange binaire :

$2\ NaX + Fe^{2+} \Leftrightarrow FeX_2 + 2\ Na^+$ reaction 2.1

a pour constante thermodynamique d'échange :

$$K_{ex}^{Na/Fe} = \frac{f_{Fe}}{f_{Na}^2} \times \frac{N_{Fe}\left(Na^+\right)^2}{N_{Na}^2\left(Fe^{2+}\right)}$$ Eq. 2.1

où f_A est le coefficient d'activité de l'espèce adsorbée A, N_A est la fraction de l'échangeur occupée par l'espèce A, et (A) est l'activité en solution de l'espèce A. N_A s'exprime dans notre cas par les relations suivantes :

$$N_{Na} = \frac{[NaX]}{[NaX]+[FeX_2]} \text{ et } N_{Fe} = \frac{[FeX_2]}{[NaX]+[FeX_2]}$$ Eq. 2.2

Dans le cas d'un échange purement binaire, tous les termes de l'équation sont accessibles à la mesure sauf les coefficients d'activité. La constante thermodynamique de l'échange n'est donc pas mesurable directement. En revanche, il est possible de calculer une constante conditionnelle d'échange en posant des valeurs pour les coefficients d'activité *a priori*. Plusieurs conventions d'écriture, issus de modèles légèrement différent existent. Seul le modèle utilisé dans cette thèse, celui de Vanselow (Vanselow, 1932), est présenté. Dans ce modèle, les activités des espèces adsorbées sont considérées égales à 1 : $f_{Na} = f_{Fe} = 1$. La relation avec la constante thermodynamique d'échange est donnée par la relation :

$$K_{ex}^{Na/Fe} = \frac{f_{Fe}}{f_{Na}^2} K_v^{Na/Fe}$$ Eq. 2.3

où K_v est la constante conditionnelle d'échange de Vanselow. Toutes les grandeurs permettant le calcul de la constante de Vanselow sont accessibles à la mesure. De plus, dans un système

binaire, il est, théoriquement, possible d'obtenir la constante thermodynamique d'échange K_{ex} à partir des données de K_v obtenues en fonction des fractions équivalentes de l'échangeur occupées par les ions ainsi qu'une estimation des coefficients d'activité de chacune des espèces adsorbées (Sposito, 1981) :

$$\ln K_{ex}^{Na/Fe} = \int_0^1 \ln K_v^{Na/Fe} dE_{Fe} = -\frac{\Delta G_{ex}^{Na/Fe}}{RT} \qquad \text{Eq. 2.4}$$

$$2\ln f_{Na} = E_{Fe} \ln K_v^{Na/Fe} - \int_0^{E_{Fe}} \ln K_v^{Na/Fe} dE'_{Fe} \qquad \text{Eq. 2.5}$$

$$\ln f_{Fe} = -(1-E_{Fe}) \ln K_v^{Na/Fe} - \int_{E_{Fe}}^1 \ln K_v^{Na/Fe} dE'_{Fe} \qquad \text{Eq. 2.6}$$

où E_A est la fraction équivalente adsorbée de l'espèce A :

$$E_{Na} = \frac{[NaX]}{[NaX] + 2\times[FeX_2]} \text{ et } E_{Fe} = \frac{2\times[FeX_2]}{[NaX] + 2\times[FeX_2]} \qquad \text{Eq. 2.7}$$

Le nombre de points expérimentaux nécessaires et la précision requise sur ces points rendent la détermination des coefficients d'activité difficile, voir impossible. Toutefois, dans la plupart des systèmes binaires, les argiles se comportent comme des échangeurs idéaux, dans la limite des barres d'erreur expérimentales. Les coefficients d'activité sont alors égaux à 1 et le constante de Vanselow peut être considérée comme la constante thermodynamique de l'échange. C'est cette hypothèse qui sera faite tout au long de cette thèse.

2.3.1.2. Représentation des données

Dans l'échange cationique, la fraction adsorbée d'un cation est comparée à la fraction de ce même cation en solution. Il est donc logique de représenter les données de la même façon. Il est fréquent de représenter la fraction équivalente sur le solide de l'espèce A (E_A) en fonction de la fraction équivalente de l'espèce A en solution ($\widetilde{E}_A$) (Sposito, 1981; McBride, 1994). Dans le système binaire Fe^{2+} - Na^+, la réaction d'échange peut s'écrire :

$2\ NaX + Fe^{2+} \Leftrightarrow FeX_2 + 2\ Na^+$

où X^- représente un site de l'échangeur.

et $\widetilde{E}_A$ se calcule comme suit :

$$\widetilde{E}_{Na} = \frac{[Na^+]}{[Na^+] + 2\times[Fe^{2+}]} \text{ et } \widetilde{E}_{Fe} = \frac{2\times[Fe^{2+}]}{[Na^+] + 2\times[Fe^{2+}]} \qquad \text{Eq. 2.8}$$

En travaillant à normalité totale (T.N.) constante dans tous les tubes, le dénominateur $[Na^+] + 2 \times [Fe^{2+}]$ reste constant et égal à cette normalité. De même le dénominateur $[NaX] + 2 \times [FeX_2]$ reste constant et égal à la capacité d'échange cationique de l'argile. Nous verrons par la suite que certains phénomènes peuvent empêcher cette dernière égalité. Cette représentation a certains avantages. Par exemple, il est possible de directement comparer la position des points

expérimentaux avec l'isotherme de non-préférence qui est la courbe matérialisant une affinité de l'argile égale pour les deux cations. Dans le cas d'un échange homoionique (*i.e.* entre deux ions de même charge), cet isotherme est une droite de pente 1 passant par l'origine. Pour des échanges hétéroioniques (ex : Na(I) – Fe(II)), cet isotherme est une courbe de formule (Sposito, 1981) :

$$E_{Na} = \left[1 + \frac{2}{\Gamma \times TN} \left(\frac{1}{\widetilde{E}_{Na}^2} - \frac{1}{\widetilde{E}_{Na}} \right) \right]^{-1/2} \qquad \text{Eq. 2.9}$$

avec

$$\Gamma = \frac{\left[\gamma_{\pm}(NaCl) \right]^4}{\left[\gamma_{\pm}(FeCl_2) \right]^3} \qquad \text{Eq. 2.10}$$

$$\log\left(\gamma_{\pm}(NaCl) \right) = -A \left(\frac{\sqrt{I}}{\sqrt{I}+1} - 0{,}3I \right) \qquad \text{Eq. 2.11}$$

$$\log\left(\gamma_{\pm}(FeCl_2) \right) = -A \times 4 \times \left(\frac{\sqrt{I}}{\sqrt{I}+1} - 0{,}3I \right) \qquad \text{Eq. 2.12}$$

I étant la force ionique.

Si les points expérimentaux sont au-dessus de cette courbe, alors le cation représenté sur le graphique est préféré par l'argile à l'autre cation échangé (Figure 2.1).

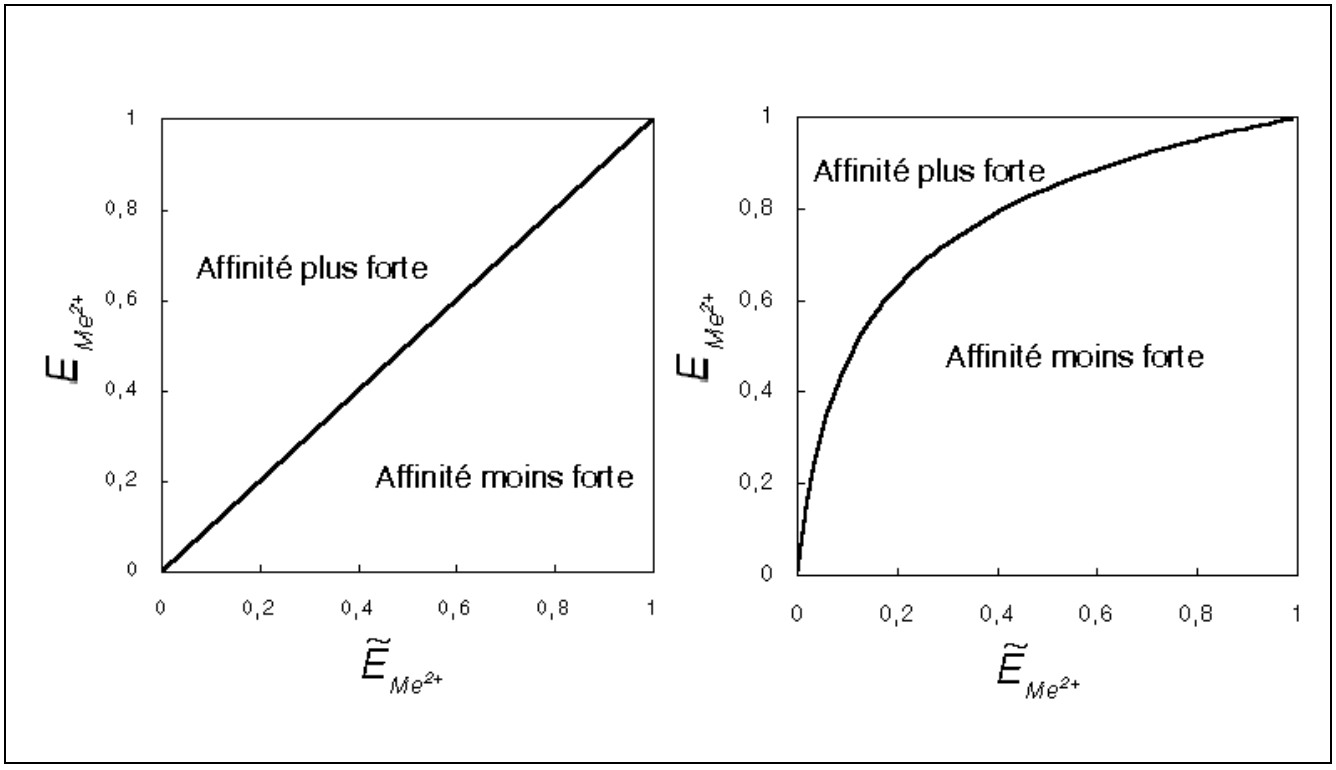


Figure 2.1 : Isothermes de non préférence dans un système binaire homovalent (à gauche, par exemple Fe^{2+} - Ca^{2+}) et dans un système binaire hétérovalent (à droite, par exemple Fe^{2+} - Na^{+}). Si Me^{2+} représente Fe^{2+}, alors, les domaines notés « Affinité plus forte » correspondent à

des domaines où les points expérimentaux dénote une affinité de l'argile plus forte pour Fe^{2+} que pour Ca^{2+} (figure de gauche) ou Na^{+} (figure de droite) (Sposito, 1981).

Toutefois, cette représentation a un inconvénient majeur : en ordonnée, deux données d'adsorption ([NaX] et [FeX_2] dans notre exemple) sont résumés en un seul point et des barres d'erreur, souvent importantes, s'ajoutent, ce qui cause inévitablement à une grande perte d'information. C'est pourquoi les données de cette thèse sont présentées en quantités équivalentes adsorbées (q_A pour l'espèce A, en eq kg^{-1}) en fonction de la fraction équivalente d'un des ions d'intérêt en solution. Les deux données d'adsorption ([NaX] et [FeX_2]) sont alors représentées par deux points et les barres d'erreur ne se cumulent pas. Il y a moins de perte d'information. Cette représentation permet également de représenter simplement des systèmes ternaires.

2.3.2. Adsorption spécifique

2.3.2.1. Description thermodynamique de l'adsorption spécifique

La complexation de bordure est habituellement décrite thermodynamiquement sous la forme :

$>SOH + Fe^{2+} \Leftrightarrow SOFe^{+} + H^{+}$ reaction 2.2

où >SOH représente un site de bordure. La constante de cet équilibre est :

$$K = \frac{(>SOFe^{+})(H^{+})}{(>SOH)(Fe^{2+})} \times e^{\frac{F\Psi}{RT}}$$ Eq. 2.13

où les termes entre parenthèse sont des activités. Le terme en exponentiel traduit l'influence des forces électrostatiques créées par la présence de sites chargés sur la surface. Dans la suite de cette thèse, il est montré que ce terme est négligeable dans le cas des argiles. Ce terme est donc ignoré dans un premier temps et la relation devient :

$$K = \frac{(>SOFe^{+})(H^{+})}{(>SOH)(Fe^{2+})}$$ Eq. 2.14

La définition de l'activité des espèces de surface est variable selon les modèles de calcul choisis. Dzombak et Morel (Dzombak and Morel, 1990) considèrent que l'activité d'un site $>SOH$ est égale à sa molarité [*>SOH*] en mol l^{-1}, et que le rapport des coefficients d'activité des espèces de surface est égal à 1. Les écarts à l'idéalité du sytème sont attribués à l'effet du potentiel moyen de surface. Dans ce cas l'équation de la constante d'équilibre devient :

$$K = \frac{[>SOFe^{+}](H^{+})}{[>SOH](Fe^{2+})}$$ Eq. 2.15

Dans la section précédente (2.3.1.1), il a été vu que l'activité d'un ion adsorbé sur une surface est égal à un coefficient d'activité f_{Me} multiplié par la fraction molaire de cet ion sur la surface, N_{Me}. Si les complexes monodentates, où l'ion complexant n'est lié qu'à un seul site

(Figure 2.2), sont les seuls pris en considération dans la modélisation, la convention de Dzombak et Morel décrit de façon adéquate le système car les termes au dénominateur des N_{Me} s'annulent dans le calcul (Parkhurst and Appelo, 1999). Cependant, dès que des complexes bidentates (Figure 2.2) ou plus compliqués (partage de plusieurs arêtes) sont utilisés, ces termes ne s'annulent plus et cette convention n'est plus applicable. Il faut alors considérer la fraction molaire de l'ion sur la surface (Parkhurst and Appelo, 1999).

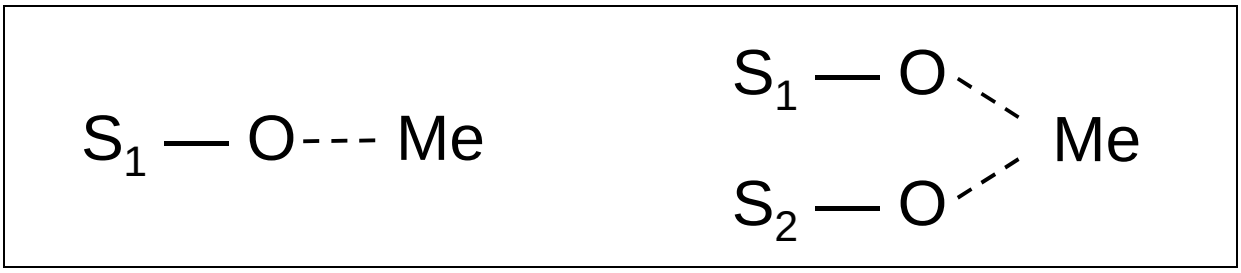


Figure 2.2 : Schématisation d'un complexe monodentate sur un site S_1 (à gauche) et d'un complexe bidentate sur deux sites S_1 et S_2 (à droite). Me représente l'ion complexé. Ces deux complexes peuvent être vus comme l'interprétation macroscopique des phénomènes microscopiques présentés sur la Figure 1.11.

2.3.2.2. Représentation des données

2.3.2.2.1. Différentes représentations possibles

Les données d'isotherme d'adsorption d'un élément en fonction du pH sont en général représentées

- soit sous la forme : pourcentage de l'ion adsorbé en fonction du pH ;
- soit sous la forme : quantité adsorbé en mol kg^{-1} en fonction du pH ;
- soit sous la forme log du coefficient de partition solide / liquide – Rd – (en l kg^{-1}) en fonction du pH (par exemple dans Baeyens and Bradbury, 1997) :

$$Rd = \frac{[Fe^{2+}]_{tot} - [Fe^{2+}]_{eq}}{[Fe^{2+}]_{eq}} \times \frac{L}{S} \qquad \text{Eq. 2.16}$$

où $[Fe^{2+}]_{tot}$ représente la concentration totale de Fe^{2+} (*i.e.* en solution plus adsorbée), $[Fe^{2+}]_{aq}$ la concentration à l'équilibre et $\frac{L}{S}$ le rapport volume du solvant (l'eau) sur masse du solide.

La représentation en pourcentage est pauvre en information, mais elle est facilement interprétable par tout type de public. Elle a donc un rôle pédagogique pour montrer, par exemple, que l'adsorption d'un métal se fait très bien sur une surface ou pas du tout. La représentation en mol kg^{-1} est plus riche en information que la représentation en pourcentage car elle contient en plus une quantification de l'adsorption par masse de solide qui peut-être utile pour faire des calculs d'ordre de grandeur de l'adsorption en milieu naturel. Une fois connue la surface spécifique, elle permet d'estimer l'adsorption par nm^2 qui est riche en

informations de type structural. La représentation en Rd a des avantages et des inconvénients. Elle est appréciée du monde des radioisotopes, car elle permet de caractériser des systèmes où presque 100% de l'isotope est adsorbé mais où des traces présentes en solution présentent un danger. Pour les autres systèmes, elle présente un avantage de représentation expliqué dans les paragraphes suivants.

2.3.2.2.2. Représentation en Rd et adsorption sur un seul site

On ne considère ici que des sites monodentates et on peut donc utiliser la convention de Dzombak et Morel (Dzombak and Morel, 1990) pour les activités des espèces surfaciques. Soit un site $>S_1OH$, la constante d'équilibre qui lui est associée est :

$$K_1 = \frac{[>S_1OFe^+](H^+)}{[>S_1OH](Fe^{2+})} \qquad \text{Eq. 2.17}$$

en incorporant Rd dans cette équation, K_1 devient :

$$K_1 = \frac{Rd\,(H^+)}{[>S_1OH]\gamma_{Fe^{2+}}} \times \frac{S}{L} \qquad \text{Eq. 2.18}$$

où $\gamma_{Fe^{2+}}$ est le coefficient d'activité de l'ion Fe^{2+} en solution. En considérant que :

$$[>S_1OH] = [>S_1O]_{tot} - [>S_1OFe^+] \qquad \text{Eq. 2.19}$$

et en posant :

$$\begin{aligned} q_{S_1} &= [>S_1O]_{tot} \times \frac{L}{S} \\ q_{S_1}^{H} &= [>S_1OH] \times \frac{L}{S} \\ q_{S_1}^{Fe^{2+}} &= [>S_1OFe^+] \times \frac{L}{S} \end{aligned} \qquad \text{Eq. 2.20}$$

où q_{S_1} est la quantité de site 1 par kg d'argile, $q_{S_1}^{H}$ est la quantité de site 1 protonée par kg d'argile, et $q_{S_1}^{Fe^{2+}}$ est la quantité de site 1 complexée par Fe^{2+} par kg d'argile, la relation devient alors

$$K_1 = \frac{Rd \times (H^+)}{(q_{S_1} - q_{S_1}^{Fe^{2+}})\gamma_{Fe^{2+}}} \qquad \text{Eq. 2.21}$$

et donc si $q_{S_1} >> q_{S_1}^{Fe^{2+}}$, alors :

$$\log(Rd) = pH + Constante \qquad \text{Eq. 2.22}$$

Cette condition sur l'occupation des sites n'est vérifiée que pour une concentration totale en Fe^{2+} très inférieure à la concentration totale de sites. Dans ce cas il est intéressant de tracer $\log(Rd)$ en fonction du pH. Si la pente obtenue est de 1, alors la sorption se fait vraisemblablement sur un seul site.

2.3.2.2.3. Cas de l'adsorption sur deux sites

Soit deux sites $>S_1O$ et $>S_2O$, les constantes d'équilibre qui leur sont associée sont :

$$K_1 = \frac{[>S_1OFe^+](H^+)}{[>S_1OH](Fe^{2+})} \quad K_2 = \frac{[>S_2OFe^+](H^+)}{[>S_2OH](Fe^{2+})} \qquad \text{Eq. 2.23}$$

Plusieurs cas de figure peuvent se présenter :

- aucun des deux sites n'est saturé ;
- un site est saturé ;
- les deux sites sont saturés.

Le dernier cas ne présente aucun intérêt pour le calcul car l'équilibre thermodynamique n'est pas respecté. Choisissons le deuxième cas de figure et supposons que le site 1 soit saturé ($q_{S_1} = q_{S_1}^{Fe^{2+}}$). Posons $q_{tot} = q_{S_1} + q_{S_2}$ avec les mêmes significations que précédemment.

$$K_2 = \frac{q_{S_2}^{Fe^{2+}} \times (H^+)}{q_{S_2}^{H} \times (Fe^{2+})} = \frac{(q_{Stot}^{Fe^{2+}} - q_{S_1}) \times (H^+)}{(q_{S_2} - q_{Stot}^{Fe^{2+}} + q_{S_1}) \times (Fe^{2+})} \qquad \text{Eq. 2.24}$$

et

$$Rd = \frac{q_{Stot}^{Fe^{2+}}}{[Fe^{2+}]} = \frac{q_{S_2}^{Fe^{2+}} + q_{S_1}}{[Fe^{2+}]} \qquad \text{Eq. 2.25}$$

donc

$$K_2 = \frac{Rd \times (H^+)}{\gamma_{Fe^{2+}} \times (q_{S_2} - q_{Stot}^{Fe^{2+}} + q_{S_1})} - \frac{q_{S_1} \times (H^+)}{(q_{S_2} - q_{Stot}^{Fe^{2+}} + q_{S_1}) \times (Fe^{2+})} \qquad \text{Eq. 2.26}$$

Dans ce cas, même si $q_{S_2} >> q_{Stot}^{Fe^{2+}}$ log(*Rd*) ne peut pas être relié simplement au pH car le système a trois composantes indépendantes : $Rd, (Fe^{2+})$ et (H^+). *A fortiori*, si cette relation de dominance du nombre de sites total par rapport au nombre de sites occupés par le Fe^{2+} n'est plus vraie ce système de représentation n'est plus valide. Il convient alors de représenter le système en trois dimensions dont les vecteurs principaux sont $q_{Stot}^{Fe^{2+}}$, (Fe^{2+}) et (H^+), tous les autres paramètres étant constants.

Enfin dans le dernier cas de figure, à savoir quand aucun site n'est saturé, le système se résume à :

$$\frac{K_2}{K_1} = \frac{(q_{Stot}^{Fe^{2+}} - q_{S_1}^{Fe^{2+}})(q_{S_1} - q_{S_1}^{Fe^{2+}})}{q_{s_1}^{Fe^{2+}} \times (q_{S_2} - q_{Stot}^{Fe^{2+}} - q_{S_1}^{Fe^{2+}})}$$

avec Eq. 2.27

$$q_{S_1}^{Fe^{2+}} = \frac{K_1(Fe^{2+})(q_{S_1} - q_{S_1}^{Fe^{2+}})}{(H^+)} = \frac{K_1(Fe^{2+})q_{S_1}}{(H^+) + K_1(Fe^{2+})}$$

Le système peut alors encore être décrit avec les trois vecteurs indépendants cités précédemment.

Des études précédentes ont montré que les phénomènes d'adsorption spécifique sur les argiles ne pouvaient pas être décrits avec un seul type de site (ex. : Wanner et al., 1994; Zachara and Smith, 1994; Bradbury and Baeyens, 1997; Avena, 2002) et que les adsorptions ne se font pas forcément par le biais de complexes monodentates (ex. : Schlegel et al., 1999; Schlegel, 2000; Schlegel et al., 2001a; Dähn et al., 2003). La représentation en Rd a donc peu d'intérêt dans notre cas particulier. Elle ne sera donc pas utilisée dans cette thèse.

2.4. APPROCHES POUR MODELISER L'ADSORPTION SPECIFIQUE

2.4.1. Utiliser des modèles déjà existants : les limites des modèles empiriques

La modélisation de la complexation de surface sur les argiles est un domaine de recherche encore jeune mais de multiples modèles sont déjà disponibles. Ils sont souvent issus des modèles développés sur les oxydes (Charlet et al., 1993; Stadler and Schindler, 1993; Zachara and Smith, 1994; Bradbury and Baeyens, 1997; Turner et al., 1998) et sont construits de manière empirique, c'est-à-dire, que le modèle est conçu en fonction des points expérimentaux à ajuster. Il est donc logique qu'il existe presque autant de modèles que d'études, chacun ayant leurs constantes de complexation et leur description de l'interface solide – liquide. La multiplicité des modèles est un problème, car les constantes de complexation ne sont pas transposables d'un modèle à l'autre.

Il m'a semblé préférable de ne pas développer un nouveau modèle empirique pour ajuster mes données. Celles-ci sont modélisées avec la même approche que celle de Bradbury et Baeyens (Bradbury and Baeyens, 1997, 1998, 2002), afin de pouvoir comparer les constantes de complexation du Fe(II) avec celles disponibles pour d'autres ions (Ni^{2+}, Zn^{2+}, Eu^{3+}). Pouvant modéliser un grand nombre de données d'adsorption, ce modèle a l'avantage de la simplicité. Il en a aussi les inconvénients, à savoir une grande rigidité et donc l'impossibilité de prendre en compte tous les phénomènes mesurés et observés lors des expériences.

2.4.2. Développer un modèle morphologico-structural de sorption

Les travaux de Hiemstra et Van Riemsdijk sur les phénomènes de sorption à la surface des oxydes « simples » a ouvert la voie à une nouvelle forme de modélisation des phénomènes de complexation de surface (Hiemstra et al., 1989a; Hiemstra et al., 1989b; Hiemstra et al., 1996). Ce type de modèle s'appuie sur des données morphologiques et structurales pour obtenir les types de sites réactionnels en surface, leur quantité massique et leur réactivité (voir

section 1.3.2). C'est ce type d'approche qui a été tenté dans cette thèse pour modéliser certaines des interactions argiles – solutés.

2.5. CODE DE CALCUL ET BASE DE DONNEES THERMODYNAMIQUES

Le code de calcul Phreeqc2 (Parkhurst and Appelo, 1999) a été choisi pour sa grande souplesse d'utilisation. Un module intégré est spécialement conçu pour la modélisation de la complexation de surface. L'activité des espèces en surface y est égale à leur fraction molaire sur la surface (N_{Me}). Il est donc possible, en utilisant ce module, de modéliser l'échange cationique en utilisant la convention de Vanselow.

La base de données thermodynamiques utilisée est la base Llnl.dat, du Lawrence Livermore National Laboratory. Elle est fournie avec la dernière version de Phreeqc2 (Parkhurst and Appelo, 1999).

3. LE FE(II) A LA SURFACE DE L'ARGILE, ADSORPTION ET PHENOMENES ASSOCIES

3.1. ADSORPTION DU FE(II) EN POSITION D'ECHANGE CATIONIQUE ; IMPORTANCE DES PAIRES IONIQUES

L'affinité du Fe(II) pour les sites d'échange cationique a été mesurée grâce à des expériences d'échange dans les systèmes Na(I)-Fe(II), Ca(II)-Fe(II) et Na(I)-Ca(II)-Fe(II) en fond ionique chloré. Des expériences préliminaires d'adsorption spécifique ayant montré que le Fe(II) pouvait s'adsorber sur l'argile à bas pH, les expériences d'échange ont été réalisées à pH 2-3.

Cette étude montre que le Fe(II) s'adsorbe avec la même affinité que le Ca(II) sur les sites d'échange (Figure 3.1), confirmant la relative homogénéité des ions divalents vis-à-vis de l'échange cationique (Fletcher and Sposito, 1989).

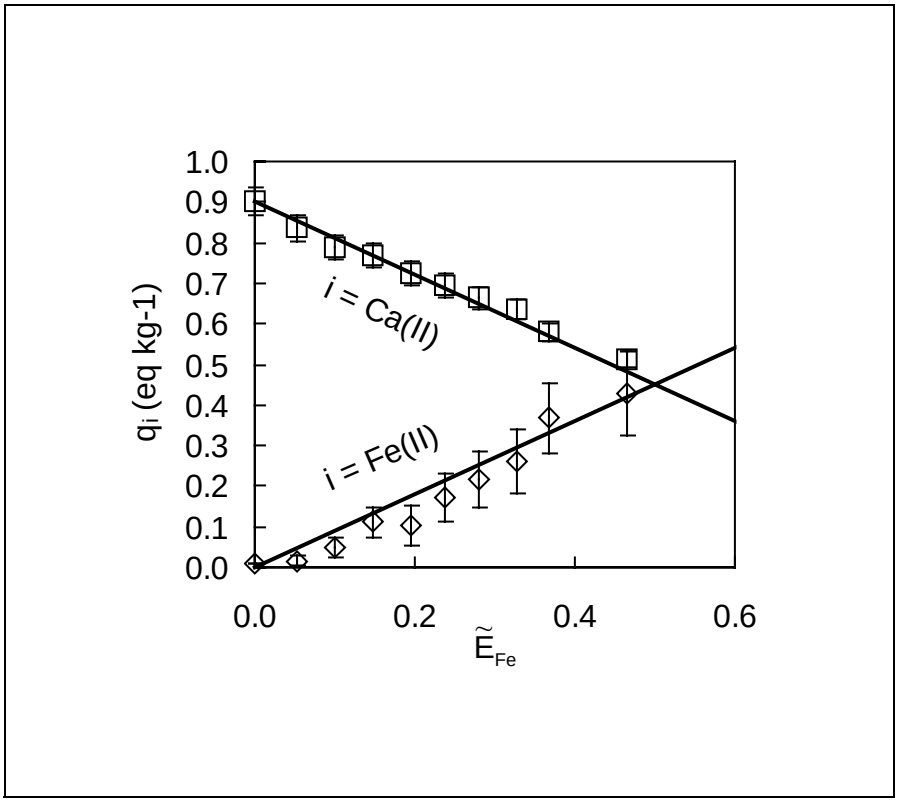


Figure 3.1 : Quantités de Ca(II) et de Fe(II) adsorbé sur les sites d'échange cationique (en eq kg^{-1}) en fonction du rapport équivalent de Fe(II) en solution (sans unité). Les lignes indiquent une relation de non-préférence de l'argile vis-à-vis des deux cations.

Il est également montré, par les données de chimie et de spectroscopie Mössbauer, que les paires d'ions $FeCl^+$ s'adsorbent avec une grande affinité. Ce comportement confirme ce qui a déjà été observé pour les ions $CaCl^+$ et $MgCl^+$ (Sposito et al., 1983a; Sposito et al., 1983b). Les affinités des sites d'échange de la montmorillonite pour H^+, Na^+, K^+, Ca^{2+}, $CaCl^+$, $CaOH^+$, Mg^{2+}, $MgCl^+$, Fe^{2+} et $FeCl^+$ ont été calculées à partir de données issues de cette thèse, ou de la littérature et sont présentées sur le tableau Tab. 3.1.

Réactions d'échange	Log K_v	Source des données expérimentales
$\equiv XNa + H^+ \Leftrightarrow \equiv XH + Na^+$	0.0	Cette thèse
$\equiv XNa + K^+ \Leftrightarrow \equiv XK + Na^+$	0.6	Jensen, 1973
$\equiv XNa + CaCl^+ \Leftrightarrow \equiv XCaCl + Na^+$	2.5	Sposito et al., 1983a
$\equiv XNa + CaOH^+ \Leftrightarrow \equiv XCaOH + Na^+$	2.5	Cette thèse
$\equiv XNa + MgCl^+ \Leftrightarrow \equiv XMgCl + Na^+$	1.9	Sposito et al., 1983a
$\equiv XNa + FeCl^+ \Leftrightarrow \equiv XFeCl + Na^+$	2.3	Cette thèse
$2 \equiv XNa + Ca^{2+} \Leftrightarrow \equiv X_2Ca + 2 Na^+$	0.5	Cette thèse
$2 \equiv XNa + Mg^{2+} \Leftrightarrow \equiv X_2Mg + 2 Na^+$	0.5	Sposito et al., 1983a
$2 \equiv XNa + Fe^{2+} \Leftrightarrow \equiv X_2Fe + 2 Na^+$	0.4	Cette thèse

Tab. 3.1 : Réactions d'échange à la surface de la montmorillonite et coefficients de sélectivité (convention de Vanselow)

La simulation de données de terrain trouvées dans la littérature ont permis de valider ces résultats de laboratoire sur les milieux naturels. La grande affinité des paires ioniques chlorées pour les surfaces argileuses a des implications sur la chimie des particules argileuses des rivières et des océans. Par le calcul, on montre ainsi que les particules argileuses océaniques portent presque uniquement des cations monovalents (simples ou paires ioniques) sur leur site d'échange, alors que les particules d'argile des rivières portent surtout des divalents. Les cations monovalents ayant moins tendance à faire floculer les particules que les cations divalents, la vitesse de floculation des argiles à l'embouchure des deltas et estuaires, et donc la distance de transport des particules, doivent être controlées, en partie, par ce phénomène d'adsorption de paires ioniques (Figure 3.2).

Une autre implication de ce résultat est que les surfaces des argiles en milieu alcalin et chloré devraient être couvertes en partie par des paires d'ions $CaCl^+$ et $CaOH^+$. Ces cations monovalents ont beaucoup moins tendance à générer des aggrégats de particules que les cations divalents (Sposito, 1984). Ils devraient donc théoriquement créer des conditions de faible conductivité hydraulique, la circulation d'eau étant défavorisée par l'absence des aggrégats qui structurent normalement les sols et les sédiments.

Cations	Quantités équivalente adsorbée (Saylest and Mangelsdorf, 1979)	Quantités équivalentes adsorbées modélisées sans les paires ioniques	Quantités équivalentes adsorbées modélisées avec les paires ioniques
Na(I)	~ 38 %	72 %	29 %
Mg(II)	~ 38 %	18 %	57 %
Ca(II)	~ 15 %	4 %	11.5 %
K(I)	~ 9 %	6 %	2.5 %

Tab. 3.2 : Comparaison mesure / simulations des proportions d'ions échangés sur une argile équilibrée avec de l'eau de mer. Le modèle qui ne considère pas les paires ioniques ne permet pas de reproduire les données expérimentales, contrairement au modèle avec paires ioniques.



Figure 3.2 : Image prise d'un satellite montrant l'embouchure de l'Amazone sur l'océan Atlantique. Le panache de particules en suspension, s'étendant sur plusieurs centaines de km, est visible sur la droite de l'image (Source : NASA).

Fe(II)-Na(I)-Ca(II) cation exchange on montmorillonite in chloride medium; evidence for preferential clay adsorption of chloride – metal ion pairs in seawater.

Laurent Charlet[1], Christophe Tournassat[1,2]

[1] LGIT - CNRS/UJF, Université Joseph Fourier (Grenoble), P.O. Box 53, F 38041 Grenoble, France

[2] ANDRA, Parc de la Croix Blanche, 1/7 rue Jean Monnet, F-92298 Châtenay-Malabry CEDEX, France

ABSTRACT

Fe(II)-Ca(II), Fe(II)-Na(I), and Fe(II)-Ca(II)-Na(I) exchange experiments on montmorillonite were performed in chloride background. These experiments show the possible sorption of Fe^{2+} and $FeCl^{+}$ ions pair in exchange site position. This result was confirmed with 77 K ^{57}Fe Mössbauer experiments. The results were modeled and the cation exchange selectivity for Fe(II) is found to be nearly equal to this of Ca(II). The Vanselow activity coefficients, for Na-Fe^{2+} and Na-$FeCl^{+}$ reactions respectively, were found to be equal to 0.4 (0.5 for Ca^{2+}) and 2.3 (2.5 for $CaCl^{+}$). The sorption of chloride ions pairs with high affinity on montmorillonite seems to be a common mechanism as first stated by Sposito et al. (Sposito et al., 1983a), and should have implications on the chemistry of seawater sediments. Exchange selectivity coefficients derived from this study and others were used to model experimental data on river water and seawater equilibrated particles. The agreement between simulations and experimental data is very good. The simulation shows the predominance of monovalent ion sorption (Na^{+} and chloride ionic pairs) on clay particles in seawater. This sorption of monovalent ion contribute to the dispersion of particles in seawater and to the extension of particles “plumes” away from the delta of rivers like Amazon River. Besides, the high clay exchanger affinity for $FeCl^{+}$ might have lead to a significant contribution of clay sedimentation in the Banded Iron Formation (BIF) at the proterozoic era.

INTRODUCTION

Aqueous ferrous iron is a major cation and an important reductant in a variety of natural anoxic environments (eutrophic lakes, ocean and swamp sediments, hydromorphic soils, anoxic groundwaters, fjords and ocean trenches). The fate of this cation depends on its uptake – or sorption – at the surface of natural particles, such as organic matter, oxides and phyllosilicates. Sorption mechanisms vary from uptake by hydrophobic forces to uptake leading to the formation of covalent bonds. On phyllosilicate surfaces, according to chemical analyses and spectroscopic studies, cations are sorbed by two distinct mechanisms: cation exchange in the interlayer planes of the clay particles, and specific sorption at the edges of the platelets (e.g. Fletcher and Sposito, 1989; Charlet et al., 1993; Zachara and Smith, 1994; Bradbury and Baeyens, 1997, 1998; Schlegel et al., 2001b; Bradbury and Baeyens, 2002). The clay sorption capacity has been well established for a wide range of potential pollutants in Na^+ and Ca^{2+} background cationic media. The influence of background anionic media such as Cl(-I) is poorly documented and data on sorption of Fe(II), a species which had a great importance in seawater in the proterozoic era and is still important in anoxic surface water, does not exist. The aim of this study is the investigation of the Fe(II) sorption in cation exchange site positions in chloride medium. The results are discussed in terms of Ca(II), Mg(II) and Fe(II) partitioning in chloride rich media, and the change of partitioning as particles move through an estuary.

MATERIALS AND METHODS

Chemicals

All solutions and suspensions were prepared in a glove box with boiled, argon-degassed Millipore Milli-Q 18 MΩ water. NaOH and HCl stock solutions were made from Titrisol ampoules. $FeCl_2$, NaCl, and $CaCl_2$ solutions were prepared from analytical grade salts.

Clay material preparation and characterization

MX80 clay sample (commercial Wyoming bentonite, reference BF100, CETCO France) material was obtained after an homogenization treatment from ANDRA (the French National Radioactive Waste Management Agency) and was dispersed in deionized water. The fine fraction (< 2 µm) was isolated by sedimentation. After saturating the suspension with NaCl (0.5 M), it was successively treated with a 0.1 M acetic acid, 0.5 M NaCl solution to remove carbonates, then with a dithionate-citrate-bicarbonate solution (DCB + 0.5 M NaCl), and finally with 3% H_2O_2, 0.5 M NaCl to remove mineral impurities and organic matter (Schlegel, 2000). The final suspensions were washed with either 0.5 M NaCl or 0.05 M $CaCl_2$ solutions and then argon-degassed.

The fine fraction of the MX80 montmorillonite has the following structural formula (Tournassat et al., submitted-c):

$(Si_{3.98}Al_{0.02})(Al_{1.61}Fe^{3+}_{0.13}Fe^{2+}_{0.02}Mg_{0.24})O_{10}(OH)_2Na_{0.28}$ for the Na-saturated form and $(Si_{3.98}Al_{0.02})(Al_{1.61}Fe^{3+}_{0.13}Fe^{2+}_{0.02}Mg_{0.24})O_{10}(OH)_2Ca_{0.14}$ for the Ca-saturated form.

Its cation exchange capacity corresponds to its structural charge, *i.e.* is equal to about 0.76 eq kg^{-1} (Tournassat et al., submitted-b).

Fe(II) – Na(I), Fe(II) – Ca(II) and Fe(II) – Ca(II) – Na(I) Exchange experiments

Tournassat and Charlet have shown that Fe(II) sorbs specifically onto clay minerals in acidic conditions (Tournassat and Charlet, submitted). Hence, to avoid specific sorption of Fe(II), the following exchange experiments were conducted at low pH (pH value between 2.1

and 3.6 depending on the experiment). We used the experiment procedure designed by Sposito et al. for exchange experiments (Sposito et al., 1981; Sposito et al., 1983a; Sposito et al., 1983b). All experiments were conducted in a N_2/H_2 atmosphere glove box in which the pO_2 was monitored continuously by a Jacomex O_2 sensor. The O_2 content never exceeded 10 ppm in the glove box atmosphere. Centrifugation tubes were numbered and precisely weighed (m_{tube} in g) with a Mettler Toledo AG285 balance. All volumes were added with a calibrated micropipette. A known volume of clay suspension was added in each 17-ml centrifuge tube (V_{susp}, clay content ρ). Adequate volumes of acidified NaCl, $CaCl_2$ and $FeCl_2$ were then added (V_{NaCl}, V_{CaCl2} and V_{FeCl2}, concentrations C_{NaCl}, C_{CaCl2} and C_{FeCl2}). In each experiment, the concentrations of NaCl, $CaCl_2$ and $FeCl_2$ solutions were chosen to obtain a constant total normality of the final suspension. Total normalities and clay contents are shown in Tab. 3.3 for each experiment. The tubes were shaken for one week, then centrifuged and filtrated . The pH was measured with a microelectrode (Mettler Toledo, inlab 423). An aliquot of supernatant was filtrated and diluted for Na, Ca and Fe measurement. Na and Ca were measured on a Perkin-Elmer Optima 3300 DV inductively coupled plasma atomic emission spectrometer (ICP-AES). Fe(II) was measured in the glove box on a HACH DR/2010 spectrophotometer using the O-phenantrolin method (Rodier, 1996). The centrifuged reaction tubes, containing the clay slurry, were weighed ($m_{centrif}$) and 10 ml of 1 M ammonium acetate were added to each tube. They were shaken for one week. The supernatant was then filtrated and diluted, and the concentration of Na and Ca were measured (Na_{Amm}^{Na} and Ca_{Amm}^{Na} respectively) by ICP-AES. Exchanged Na(I) and Ca(II) in eq kg^{-1} were then calculated according to:

$$q_{Na} = \frac{C_{Amm}^{Na} \times 10 \times d - C_{sol}^{Na} \times \left(m_{centrif} - m_{tube} - \left(V_{susp} \times \rho \times d\right)\right)}{\left(V_{susp} \times \rho\right)} \quad \text{in eq kg}^{-1} \quad \text{Eq. 3.1}$$

$$q_{Ca} = 2 \times \frac{C_{Amm}^{Ca} \times 10 \times d - C_{sol}^{Ca} \times \left(m_{centrif} - m_{tube} - \left(V_{susp} \times \rho \times d\right)\right)}{\left(V_{susp} \times \rho\right)} \quad \text{in eq kg}^{-1} \quad \text{Eq. 3.2}$$

where volumes are given in ml, concentration in mol l^{-1}, clay content in g l^{-1} and masses in g. The density d of all solutions is taken equal to 1.0. The exchanged Fe(II) (q_{Fe}) was determined by subtracting the Fe(II) measured in the supernatant (C_{meas}^{Fe}) from total Fe(II) added in the tube (C_{added}^{Fe}):

$$q_{Fe} = 2 \times \frac{C_{added}^{Fe} - C_{meas}^{Fe}}{\left(V_{susp} \times \rho\right)} \quad \text{in eq kg}^{-1} \quad \text{Eq. 3.3}$$

The total Fe(II) corresponds to the Fe(II) added concentration plus the Fe(II) originated from the dissolution of the clay material. This value was approximated using dissolution experiments at low pH and high Ca concentration to avoid re-adsorption of dissolved Fe(II) in exchange site position. The error bars were calculated using a 2% standard error on the concentration measurements for Na, Ca and 3% for Fe(II).

	Experiment A	Experiment B	Experiment C	Experiment D	Experiment E	Experiment F
pH	3.37 ± 0.05	3.23 ± 0.02	2.17 ± 0.03	2.22 ± 0.09	3.59 ± 0.10	3.40 ± 0.08
Clay content (g l^{-1})	5.85	3.90	8.25	8.25 and 5.50 *	5.85	3.90
Cations	Ca(II) – Fe(II)	Ca(II) – Fe(II)	Na(I) – Fe(II)	Na(I) – Fe(II)	Na(I) – Ca(II) – Fe(II)	Na(I) – Ca(II) – Fe(II)
T.N. (meq l^{-1}) = [Cl^-]	49 ± 1	49 ± 3	132 ± 3	127 ± 8	50 ± 3 †	50 ± 3 ‡

* 8.25 g l^{-1} for the first four experimental points and 5.50 g l^{-1} for the other experimental points

† [Ca(II)] = 13.1 mmol l^{-1} ± 0.5

‡ [Ca(II)] = 9.1 mmol l^{-1} ± 0.3

Tab. 3.3 : Cation exchange experimental conditions

Mössbauer Experiments

The preparation of the samples was conducted in a Jacomex N_2 atmosphere glove box in which the pO_2 was monitored continuously by a Jacomex O_2 sensor. For this experiment, The O_2 content never exceeded 1 ppm in the glove box atmosphere. 100 mg of $^{57}Fe(0)$ were dissolved in concentrated HCl (0.1 mol l^{-1}) at ~100°C. Then, the dissolved iron was put in the glove box and diluted in deionized water to a final volume of 100 ml, to obtain a ~1000 ppm $^{57}Fe(II)$ stock solution. The acidic conditions prevented the oxidation of the suspension prior to its transfer in the glove box. Several cycles of centrifugation and washing with deionized water were conducted to decrease the NaCl concentration in the Na-conditioned clay stock suspension outside of the glove box. This washing of the clay facilitates the sorption of Fe(II) in cation exchange site position by mass action phenomenon: the less Na^+ in solution, the less competitive Na^+ in exchange site position. This new Na-conditioned clay stock suspension was degassed with a stream of N_2 during one night, put in the glove box and allowed to equilibrate with the free O_2 atmosphere during one day. Then, the suspension and the $^{57}Fe(II)$ stock solution were mixed to obtain a $^{57}Fe(II)$ exchanged clay. After three days reaction time, the sample was centrifuged, the supernatant was removed and the clay slurry was frozen before being transported to the Mössbauer facility. The Mössbauer spectrum of the Na-conditioned smectite was recorded at 77 K using a constant acceleration spectrometer and a ^{57}Co source diffused into a rhodium matrix. Velocity calibrations were made using α-Fe foil at 300 K. The hyperfine parameters were refined using a least-squared fitting procedure (program MOSFIT, Teillet and Varret).

RESULTS

Exchange experiments

In many cation exchange studies (e.g. Sposito, 1981; McBride, 1994), the equivalent fraction of one cation in solution ($\widetilde{E}_{Cat}$, where Cat is a cation species) is plotted as a function of the equivalent fraction of the cation on the exchanger phase (E_{Cat}). For Fe(II) in a Na(I) – Ca(II) – Fe(II) system, these equivalent fractions are calculated according to the following formulas:

$$\widetilde{E}_{Fe} = \frac{2 \times [Fe(II)]}{2 \times [Fe(II)] + 2 \times [Ca(II)] + [Na(I)]} \quad \text{Eq. 3.4}$$

$$E_{Fe} = \frac{q_{Fe}}{q_{Fe} + q_{Ca} + q_{Na}} \quad \text{Eq. 3.5}$$

where [*Fe(II)*], [*Ca(II)*] and [*Na(I)*] are the solution concentration of Fe(II), Ca(II) and Na(I) (in mol l^{-1}) respectively . Due to the large error bar on the measurement of sorbed Fe(II) in our experiments, the error on the E_{Fe} is large and no quantitative information can be obtained from E_{Fe}. Thus, we decided to plot q_i (in eq kg^{-1}), the amount of sorbed cation species *i*, as a function of the equivalent fraction of Fe(II) in solution ($\widetilde{E}_{Fe}$). Figure 3.3 shows the results of the exchange experiments. As first stated by Sposito et al. (Sposito et al., 1983a; Sposito et al., 1983b) and re-demonstrated by Tournassat et al. (Tournassat et al., submitted-b; Tournassat et al., submitted-c), the sorbed amount of divalent species in Cl^- anionic background is an apparent quantity, since ionic pairs (e.g. $CaCl^+$, $CaOH^+$…) are also adsorbed in cation exchange positions. Thus, the apparent CEC, which is equal to the sum of all q_i, varies from one experiment to another (figure 1). For example, q_{Ca} in the first point of experiment A (*i.e.* in case of a pure Ca – exchanged clay) is greater than q_{Na} in the first point of experiment C (*i.e.* in case of a pure Na-exchanged clay). This difference is due to the sorption of $CaCl^+$ ionic pairs, which are taken twice into account in Eq. 3.2 (Sposito et al., 1983a; Sposito et al., 1983b; Tournassat et al., submitted-c). If $FeCl^+$ sorbed like $CaCl^+$ on the clay exchanger phase, then one would expect the apparent CEC to increase as a function of $\widetilde{E}_{Fe}$ in the Na(I)-Fe(II) exchange experiment. The trend of the results shown on Figure 3.3 confirms this point but the error bars associated to q_{Fe} are too large to prove the sorption of $FeCl^+$. Nevertheless, Fe(II) and Ca(II) seem to have the same overall behavior towards the clay exchanger phase. The Fe(II) – Ca(II) exchange is a homoionic exchange. Then, the non – preference isotherm is very easy to build since each desorbed Ca(II) corresponds to one adsorbed Fe(II). The experimental results of experiment A, plotted together with a non-preference isotherm, show that this non-preference isotherm fit perfectly the data. Then, we can conclude that $FeCl^+$ sorb on the clay exchanger phase exactly in the way $CaCl^+$ does.

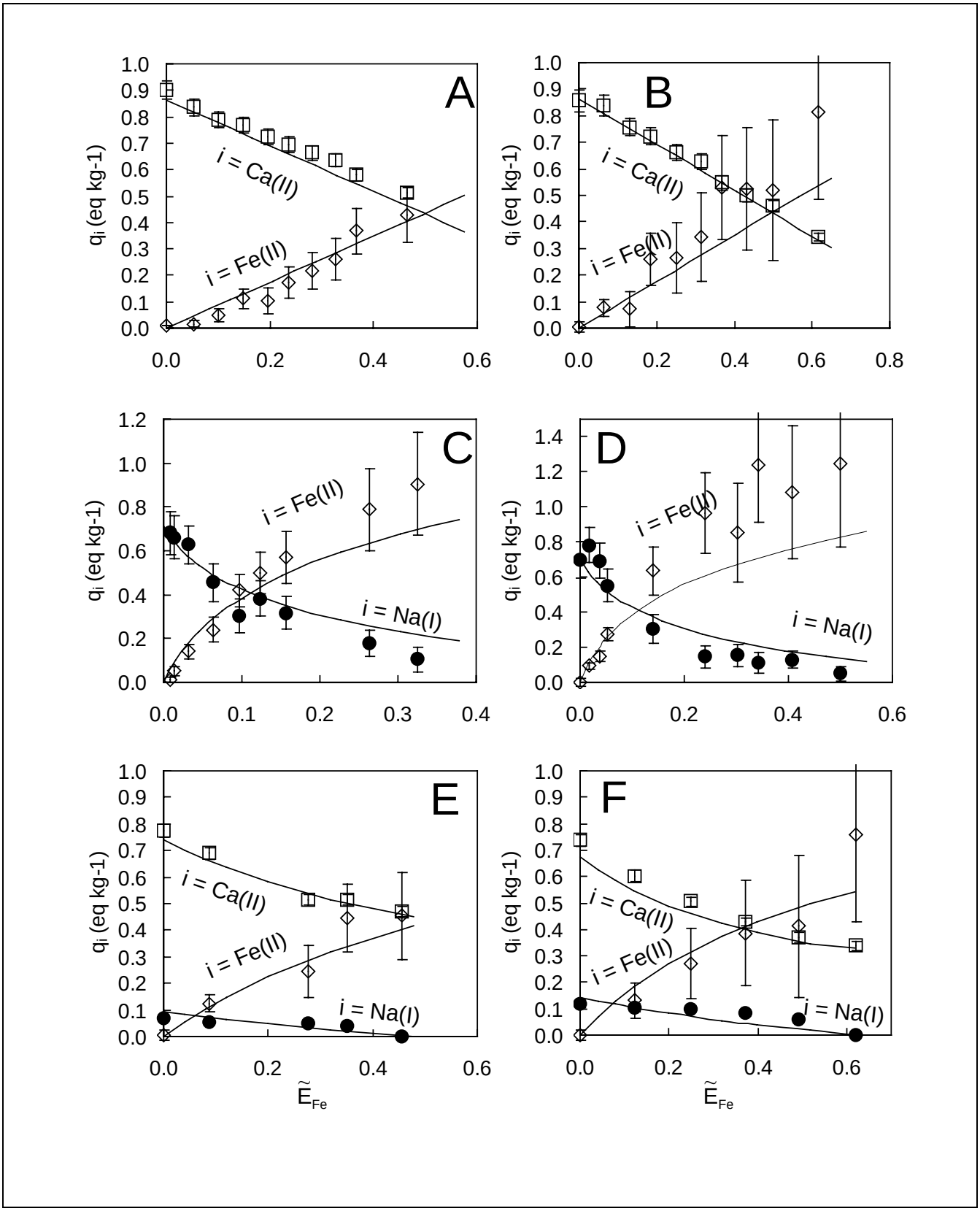


Figure 3.3 : Fe(II) – Na(I) and Fe(II) – Ca(II) exchange data plotted as equivalent sorbed amount of ion i (q_i, eq kg^{-1}), together with simulations whose parameters are given in Tab. 3.4. Experimental conditions are given in Tab. 3.3.

Model

The Vanselow convention (Vanselow, 1932; Sposito, 1981) was used to model the data. The Phreeqc2 code (Parkhurst and Appelo, 1999) is used as this versatile computer code is

amenable to the various conventions used to describe cation exchange and surface complexation. The Llnl.dat database is used for the calculation of speciation in solution together with the structural CEC of the MX80 montmorillonite and the cation exchange selectivity coefficients for H^+, Na^+, Ca^{2+} and $CaCl^+$, obtained from Tournassat et al. (Tournassat et al., submitted-b), allowing only two parameters to be refined: the cation exchange selectivity coefficients for Fe^{2+} and $FeCl^+$. The refined values are shown in Tab. 3.4. We need to slightly adjust the previously obtained Ca^{2+} exchange selectivity coefficient to obtain a better fit of the data, but this adjustment lies in the error bar of the given parameter (Tournassat et al., submitted-b). Figure 3.3 shows the goodness of the fit. According to the goodness of fit reported in Figure 3.3, one has to emphasize that binary systems – Na(I)-Fe(II) or Ca(II)-Fe(II) –, as well as ternary systems – Na(I)-Ca(II)-Fe(II) – are described in the limits of the error bars. It was not possible to fit the data reasonably well without introducing a cation exchange selectivity coefficient for $FeCl^+$. Fe^{2+} and Ca^{2+} have similar exchange selectivity coefficients (log K_v = 0.4 and 0.5 in respect with Na^+, respectively). $CaCl^+$ has a greater exchange selectivity coefficient than that of $FeCl^+$ (log K_v = 2.5 and 2.3 in respect with Na^+, respectively), but the association constant of reaction (Llnl.dat database, given with the Phreeqc2 new version)

$Ca^{2+} + Cl^- \Leftrightarrow CaCl^+$ log K_a = -0.696

is weaker than the association constant of reaction

$Fe^{2+} + Cl^- \Leftrightarrow FeCl^+$ log K_a = -0.167

Thus, $CaCl^+$ is slightly preferred over $FeCl^+$ on the exchanger phase, but $FeCl^+$ forms in greater amount than $CaCl^+$, at equal solution total normality. Consequently, the two ion pairs are sorbed in comparable amounts and, as a result, the clay exchanger appears not to have any preference for Fe(II) or Ca(II): Figure 3.3A looks the same as Figure 3.4. For comparison, Sposito et al. (Sposito et al., 1983a) had demonstrated the high affinity of clay surface for $MgCl^+$ ion pairs, Ca(II) and Mg(II) behaving similarly towards exchange on clay in chloride ionic background. Their experimental Mg(II)-Na(I) exchange data in ClO_4^- and Cl^- ionic media were fitted (Figure 3.5), together with Ca(II)-K(I) exchange data from Jensen (Jensen, 1973) (Figure 3.6). The results of the fitting procedure (Tab. 3.4) indicate that:

the Mg^{2+} - Na^+ and Ca^{2+} - Na^+ exchange reactions have close cation exchange selectivity coefficients (log K_v = 0.4 and 0.5, respectively);

the $MgCl^+$ - Na^+ exchange selectivity coefficient (log K_v = 1.9) corresponds to the difference between the association reaction constants for $CaCl^+$ (log K_a = -0.6956) and $MgCl^+$ (log K_a = -0.1349) ionic pairs formation plus the $CaCl^+$ - Na^+ exchange selectivity coefficient (log K_v = 2.5) and then, at equal solution total normality, $MgCl^+$ and $CaCl^+$ have the same apparent affinity for clay exchange sites;

the $MgCl^+$ - Na^+, $CaCl^+$ - Na^+, and $FeCl^+$ - Na^+ exchange selectivity coefficients are significantly larger than the K^+-Na^+ and H^+-Na^+ exchange selectivity coefficient.

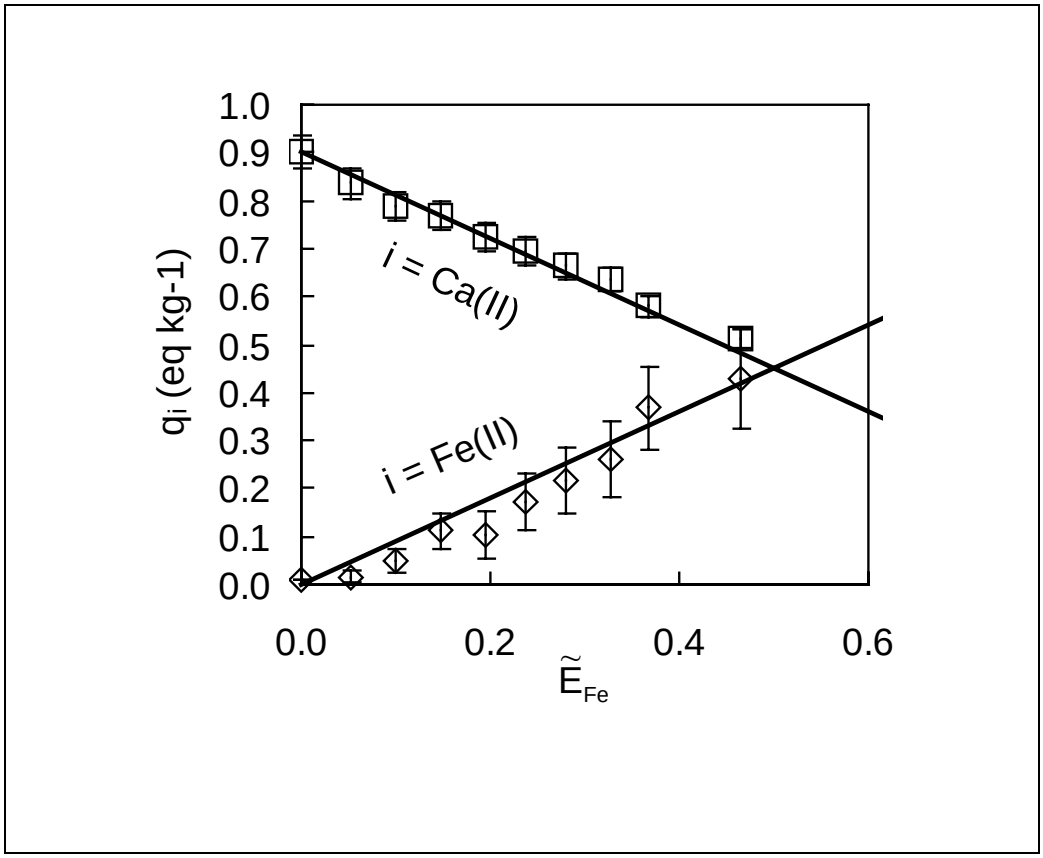


Figure 3.4 : Comparison of Fe(II) – Ca(II) exchange data with a non-preference isotherm (see text for details).

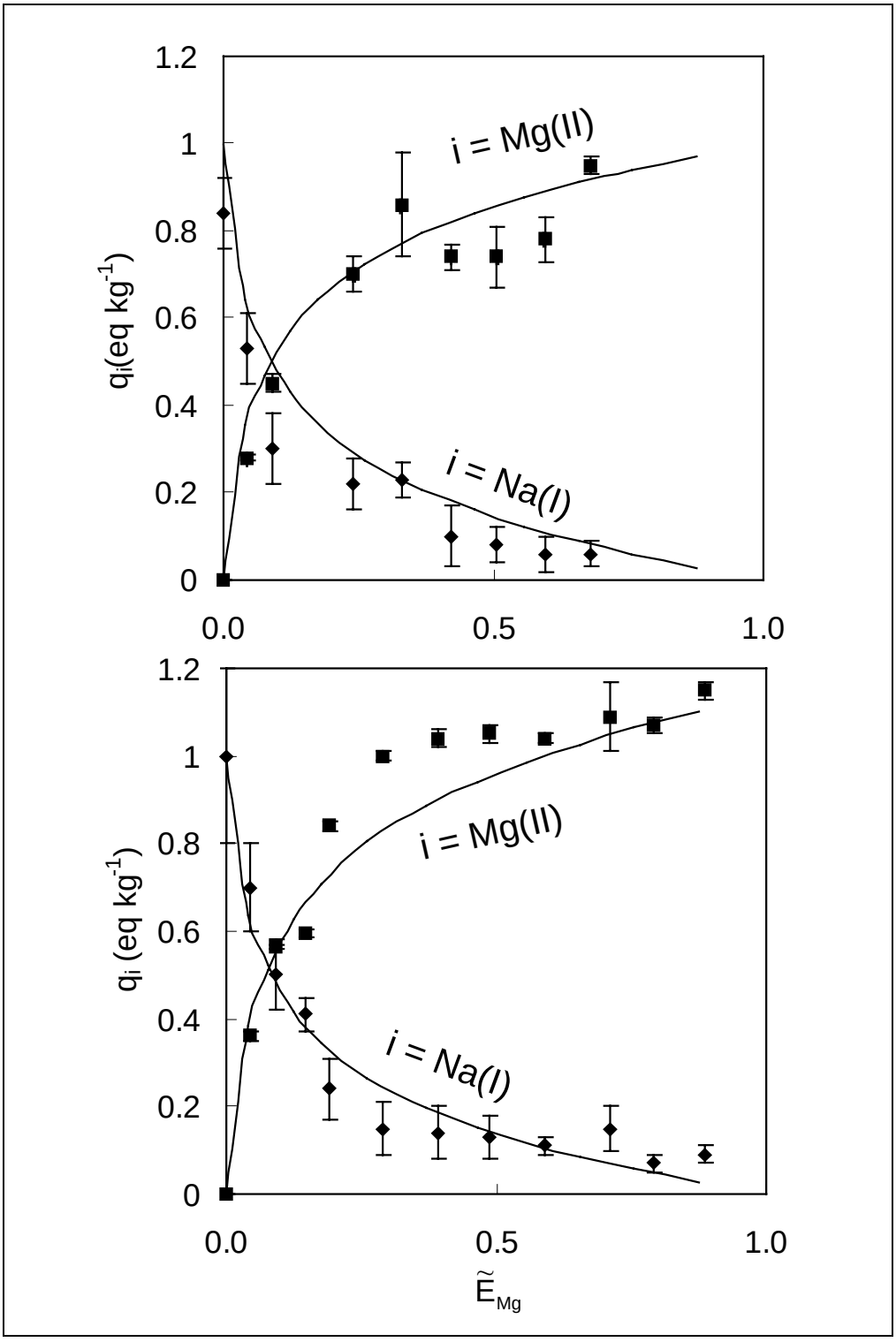


Figure 3.5 : Mg(II) – Na(I) exchange isotherm. Experimental data are from Sposito et al. (Sposito et al., 1983a). Model curves were computed with the parameters given in Tab. 3.4. Top: experiment in ClO_4^- anionic background medium. Bottom: experiment in Cl^- anionic background medium

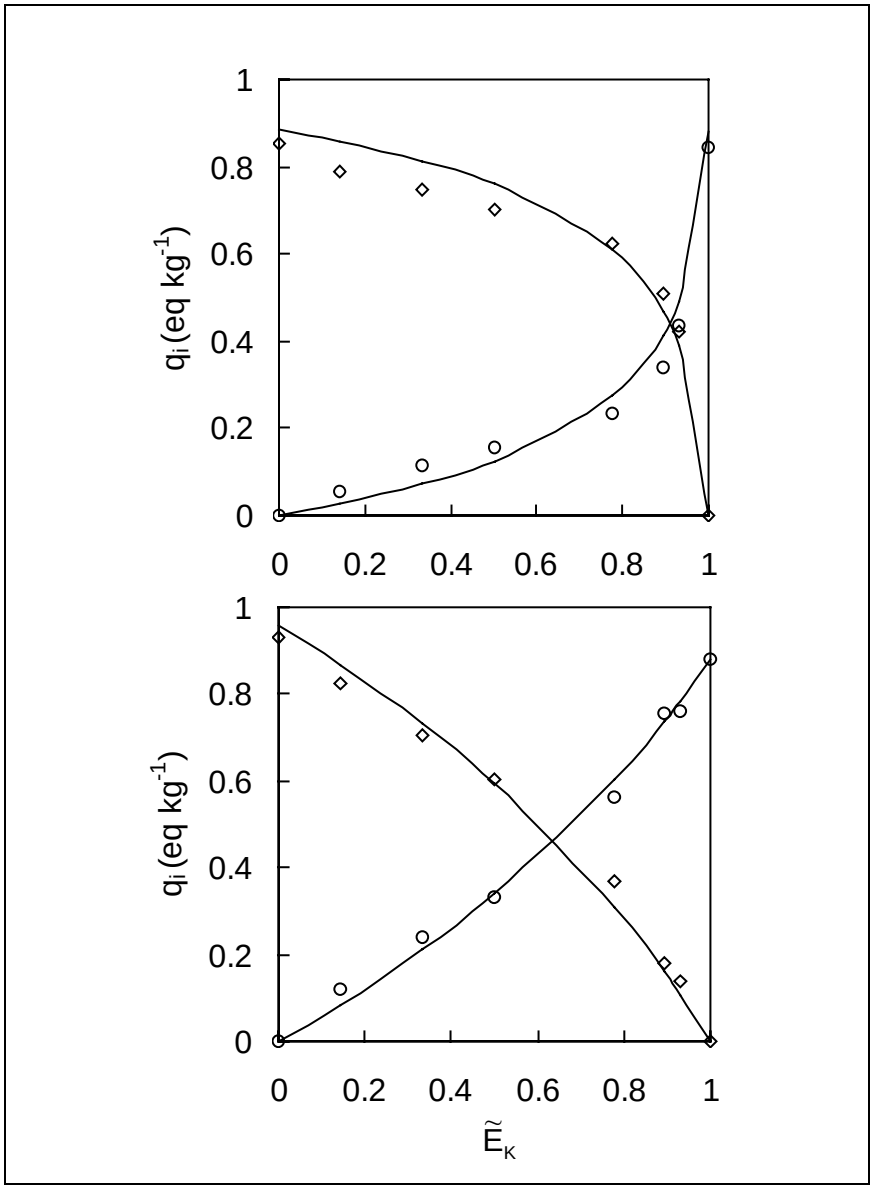


Figure 3.6 : Ca(II) – K(I) exchange isotherm dependence on the ionic strength (Chloride medium). Data are from Jensen (Jensen, 1973) and simulated curves were computed with the selectivity coefficients given in Tab. 3.4. The data are plotted as apparent equivalent sorbed amounts (q_i where i denotes K^+, circles, or Ca(II), diamonds) as a function of equivalent K^+ fraction in solution. Ionic strength: I = 0.005 mol l^{-1} (top), and 0.05 mol l^{-1} (bottom). Error bars were not available from reference publication.

Exchange reaction	Log K_v	Reference
$\equiv XNa + H^+ \Leftrightarrow \equiv XH + Na^+$	0.0	Fletcher and Sposito, 1989; Tournassat et al., submitted-b
$\equiv XNa + K^+ \Leftrightarrow \equiv XK + Na^+$	0.6	This study (data from Jensen, 1973)
$\equiv XNa + CaCl^+ \Leftrightarrow \equiv XCaCl + Na^+$	2.5	Fletcher and Sposito, 1989; Tournassat et al., submitted-b
$\equiv XNa + MgCl^+ \Leftrightarrow \equiv XMgCl + Na^+$	1.9	This study (data from Sposito et al., 1983a)
$\equiv XNa + FeCl^+ \Leftrightarrow \equiv XFeCl + Na^+$	2.3	This study
$2 \equiv XNa + Ca^{2+} \Leftrightarrow \equiv X_2Ca + 2\ Na^+$	0.5	Fletcher and Sposito, 1989; Tournassat et al., submitted-b
$2 \equiv XNa + Fe^{2+} \Leftrightarrow \equiv X_2Fe + 2\ Na^+$	0.4	This study
$2 \equiv XNa + Mg^{2+} \Leftrightarrow \equiv X_2Mg + 2\ Na^+$	0.4	This study (data from Sposito et al., 1983a)

Tab. 3.4 : List of cation exchange reactions and selectivity coefficients (Vanselow convention) for the Fe(II) – Na(I) – Ca(II) exchange experiments of this study, and for Na(I) – Mg(II) and K(I) – Ca(II) exchange experiments of published studies.

Mössbauer experiment

Mössbauer results are shown in Figure 3.7, and the associated hyperfine parameters are shown in Tab. 3.5. The fitting model, of both frozen ^{57}Fe stock solution and ^{57}Fe exchanged clay, consists in two main quadrupolar doublets (A and B) attributed to two different Fe(II) surface species. The quadrupolar doublet due to the presence of Fe(III) in MX80 clay octahedral layer (Tournassat et al., submitted-c) is almost non detected. It is clear that other fitting models can be proposed, *e.g.* with additional quadrupolar components to be attributed to iron species with other environments. However, the presence of, at least, two species is in good agreement with the presence of Fe^{2+} and $FeCl^+$ both in solution and in cation exchange site position. Solution and exchange speciation computation, with experimental conditions, indicates that Fe^{2+} is the main iron species in the solution, whereas $FeCl^+$ is the main iron species in the Fe(II) exchanged clay. By considering that part of Mössbauer contribution A could be attributed to $FeCl^+$ species, the increase of the extent of contribution A, in the Fe(II) exchanged clay sample, is in agreement with these computations. Furthermore, the differences in quadrupolar splitting values of mean Fe(II) contributions denote the effect of the clay structure on Fe(II) in cation exchange site position. Hence, the Mössbauer experiment confirms the sorption of $FeCl^+$ and Fe^{2+} in cation exchange site position on clay minerals.

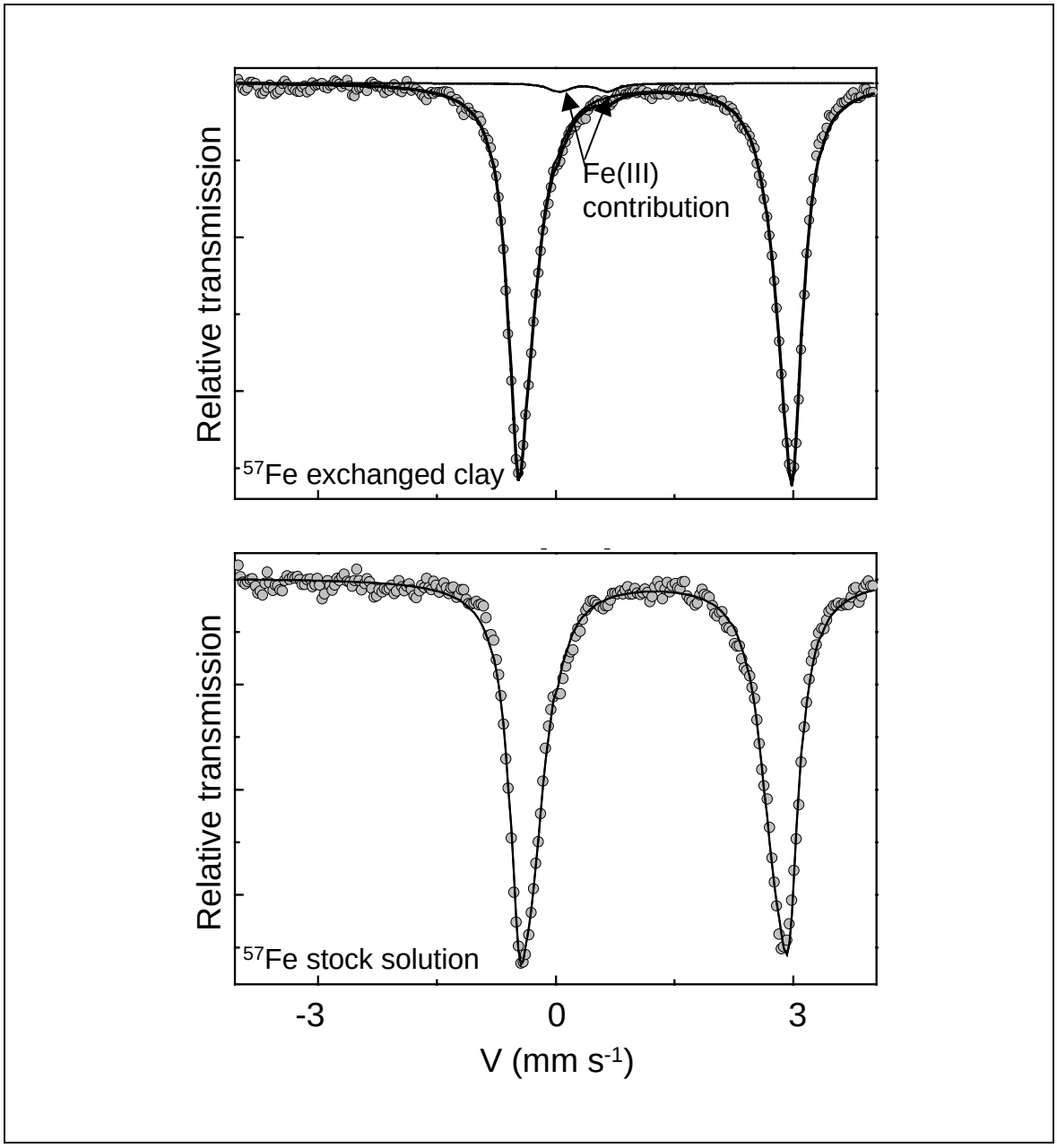


Figure 3.7 : Dots: 77 K Mössbauer spectrum of ^{57}Fe exchanged clay (top) and frozen ^{57}Fe stock solution (bottom). Thin lines: sum of all the contributions of the decomposition. The parameters of the decomposition are given in Tab. 3.5. Contributions of Fe(II) A and Fe(II) B are summed up. Arrows indicate the contribution of Fe(III).

		I.S. mm s^{-1}	Γ mm s^{-1}	Q.S. mm s^{-1}	%
Frozen ^{57}Fe stock solution	Fe(II) A	1.37 (0.01)	0.29 (0.04)	3.37 (0.05)	40 (5)
	Fe(II) B	1.36 (0.01)	0.47 (0.04)	3.02 (0.05)	60 (5)
	Mean A+B	1.36 (0.02)		3.13 (0.05)	100
^{57}Fe exchanged clay	Fe(II) A	1.38 (0.01)	0.30 (0.04)	3.43 (0.05)	63 (5)
	Fe(II) B	1.40 (0.01)	0.49 (0.04)	3.10 (0.05)	37 (5)
	Mean A+B	1.39 (0.02)		3.31 (0.05)	100

I.S. = isomer shift value quoted to that of α-Fe at 300 K; Γ = linewidth; Q.S. = quadrupolar splitting value ; % = ratio of each component.

Tab. 3.5 : Mössbauer parameters of the ^{57}Fe-exchanged smectite and of the HCl acidified ^{57}Fe frozen solution. Error bars are indicated in parenthesis.

DISCUSSION

The clay high affinity for chloride-bivalent cation ion pairs should have important implications in the modifications in exchanger composition of river suspended particles as they enter seawater. This change is modelled based on the cation exchange selectivity coefficients given in Tab. 3.4.

The Saylest and Mangelsdorf's study on Amazon River particles (Saylest and Mangelsdorf, 1979) was taken as a reference experimental study, as the Amazon River carries a large amount of clay particles. Indeed the < 2 µm fraction of Amazon River suspended particles represents 54 % of the CEC. In this study, the authors measured the composition of the river particle exchanger, together with the cation composition of the river water. Afterwards, they equilibrated their particles with seawater and analysed the composition of the exchanger. Since no data on anionic composition is given, concentrations of HCO_3^- and Cl^- were chosen so that (i) $[HCO_3^-] + [Cl^-]$ is equal to the total equivalent concentration of cations in solution and (ii) $[Cl^-]$ is equal to 0.13 mmol l^{-1} (= mean Cl^- concentration in South America river water: Holland, 1978). We considered a simplified composition of ocean water, shown in Tab. 3.6, to calculate the clay exchanger composition in seawater.

Figure 3.8 and Figure 3.9 show the good agreement between experimental and modeled equivalent sorbed fraction (X_{Me}) on the particles in equilibrium with Amazon River. Therefore a model based on montmorillonite surface chemistry is able to simulate these river sediments although the < 2 µm fraction of these sediments represents only 54 % of the total CEC and although kaolinite is quite widely reported in Amazonian environment. This may account for the underestimation of K^+ sorption (Figure 3.9). By analyzing more precisely the results of the simulation, we note that the major cations on the exchanger are Ca^{2+} and Mg^{2+}. $CaCl^+$ and $MgCl^+$ do not sorbed in any significant amount on the particles, since the river water is a dilute system ($I_{mean} \approx 0.6$ mmol l^{-1}) and Cl^- is not the predominant anion.

ions	Concentrations (mmol kg^{-1})
Sodium	481
Magnesium	55
Calcium	11
Potassium	11
Chloride	564
Sulfate	29
Bicarbonate	2

Tab. 3.6 : Simplified composition of ocean water. Salinity = 36 ‰ (after Holland, 1978).

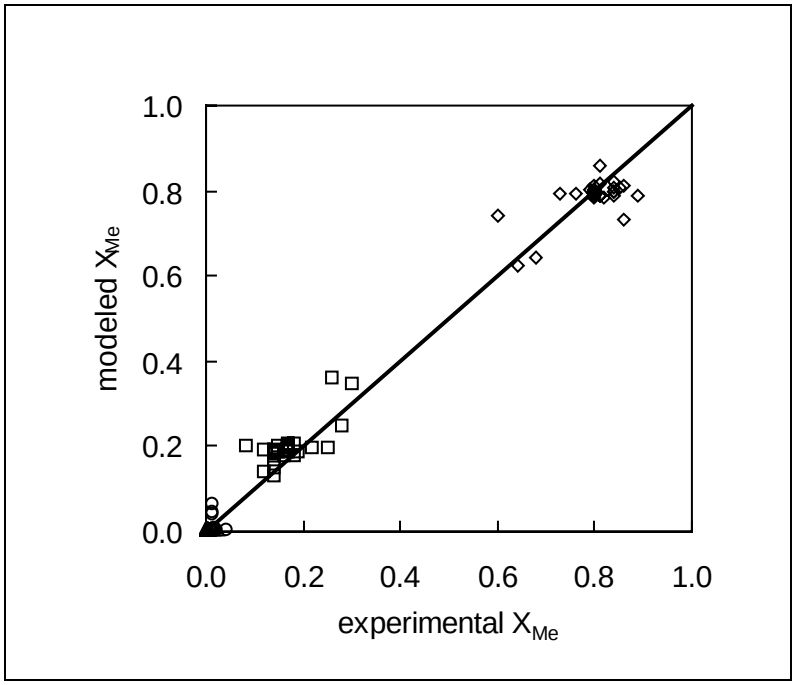


Figure 3.8 : Cation exchange composition of particles suspended in the Amazon River. Comparison between experimental (Saylest and Mangelsdorf, 1979) and modeled apparent sorbed equivalent fractions (X_{Me}) of Na(I) (triangles), K(I) (circles), Mg (II) (squares) and Ca(II) (diamonds). The straight line depict a 1:1 relationship, *i.e.* the perfect conformity of the model with the experimental points. Error bars were not available from reference publication.

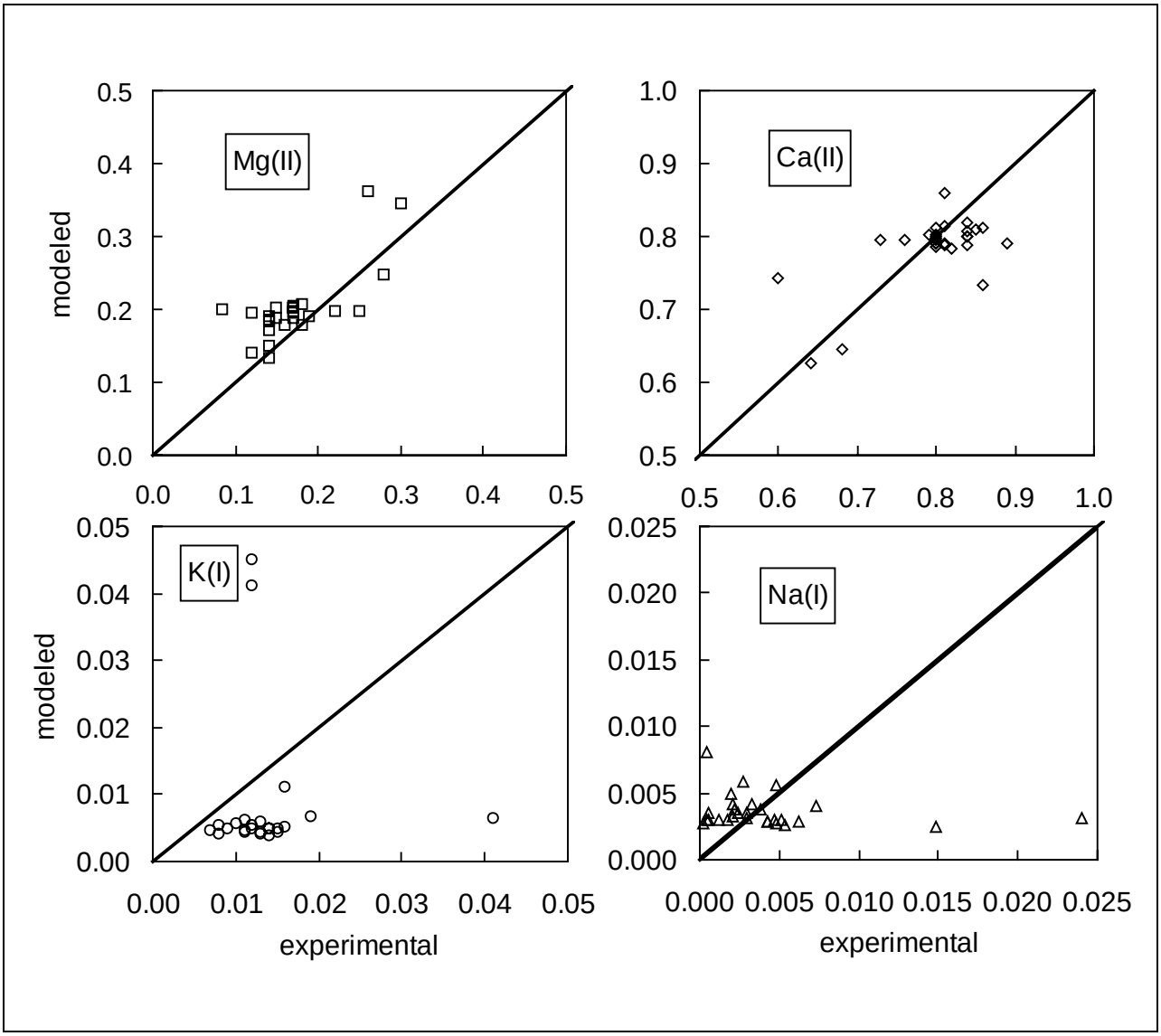


Figure 3.9 : Details of Figure 3.7. Cation exchange composition of particles suspended in the Amazon River. Comparison between experimental (Saylest and Mangelsdorf, 1979) and modeled apparent sorbed equivalent fractions (X_{Me}) of Na(I) (triangles), K(I) (circles), Mg (II) (squares) and Ca(II) (diamonds). The straight line depict a 1:1 relationship, *i.e.* the perfect conformity of the model with the experimental points. Error bars were not available from reference publication.

Saylest and Mangelsdorf (Saylest and Mangelsdorf, 1979) have equilibrated their particles with seawater and analysed the changes in exchanger composition. As already stated, their experimental measurement method leads to an apparent overestimation of metal equivalent fraction, as they did take twice into account the amount of $CaCl^+$ and $MgCl^+$ sorbed onto the solid. The mean values for Na(I), Mg(II), Ca(II), and K(I) experimental sorbed equivalent fractions are shown in Tab. 3.7, for particles equilibrated with seawater, together with the equivalent fractions calculated with the exchange selectivity coefficients for montmorillonite taking account free species cation exchange listed in Tab. 3.4. As shown in Tab. 3.7 in third column, Amazon particles suspended in seawater show an exchanged composition at variance with that predicted, based on cation exchange of free species only, *i.e.* not of ionic pairs. On the contrary, the simulation including ionic pairs adsorption, while underestimating slightly the sorbed Na(I) and Ca(II) fraction, and overestimating slightly the Mg(II) sorbed fraction, gives altogether a much better account of the experimental exchanger composition. The < 2 µm clay contribution to the CEC of sediment collected in Saylest and Mangelsdorf's study is

approximately 50%. Then, the difference between the simulated and the experimental results for K^+ might originate from the presence of illite or kaolinite whose cation exchange selectivity coefficients are greater than in case of montmorillonite particles (Jensen, 1973). The activity coefficient of ionic species can also lead to some inaccuracy, since one may only use, with Phreeqc2, the Davies or Debye-Hückel activity coefficient relations, which are not appropriate conventions for concentrated systems. However, in general, the whole tendency of sorption is respected and the sorption of ionic pairs ($CaCl^+$ and $MgCl^+$) are obviously taking place in marine environment, due to high Ca(II), Mg(II) and Cl(-I) concentrations. Then, as particle move in the estuary, the surface of Amazonian clay particles becomes increasingly saturated with $MgCl^+$, Na^+, and $CaCl^+$ species, *i.e.* with monovalent species. The critical coagulation concentration for these species is two orders of magnitude higher for monovalent than for divalent species (e.g. Sposito, 1984) and thus, the particles will tend not to flocculate, *i.e.* to remain monodispersed, against what could be expected from the double layer thickness contraction observed as ionic strength increases. This clearly contributes to the formation of the particles “plume” which is observed several hundred km away from the Amazon River delta, e.g. along the Guyana coasts.

Cation	Experimental sorbed equivalent fraction (Saylest and Mangelsdorf, 1979)	modeled sorbed equivalent fraction (model without ionic pairs)	modeled sorbed equivalent fraction (model with ionic pairs)
Na(I)	~ 38 %	72 %	29 %
Mg(II)	~ 38 %	18 %	57 %
Ca(II)	~ 15 %	4 %	11.5 %
K(I)	~ 9 %	6 %	2.5 %

Tab. 3.7 : Comparison of measured and simulated equivalent fraction of main cations sorbed on Amazon River suspended particles equilibrated with seawater . Simulation parameters are given in Tab. 3.4.

In Figure 3.10A, the sorbed equivalent fraction of major cations on a montmorillonite clay is computed, in seawater, as a function of possible Fe(II) concentrations in solution, showing the high affinity of the clay exchanger for $FeCl^+$. Figure 3.10B shows the repartition of Fe(II) species on the exchanger phase: almost all surface ferrous iron is present as $FeCl^+$. In the Proterozoic era global ocean, as well as yet in the Black Sea or in the Carioca Trench, seawater was or is rich in dissolved ferrous iron (Holland, 1978; Millero, 2002). Since sedimentation of clay particles could remove a high amount of $FeCl^+$ present as cation exchange species, clay sedimentation might have played a significant role in the Banded Iron Formation (BIF) at the Proterozoic era.

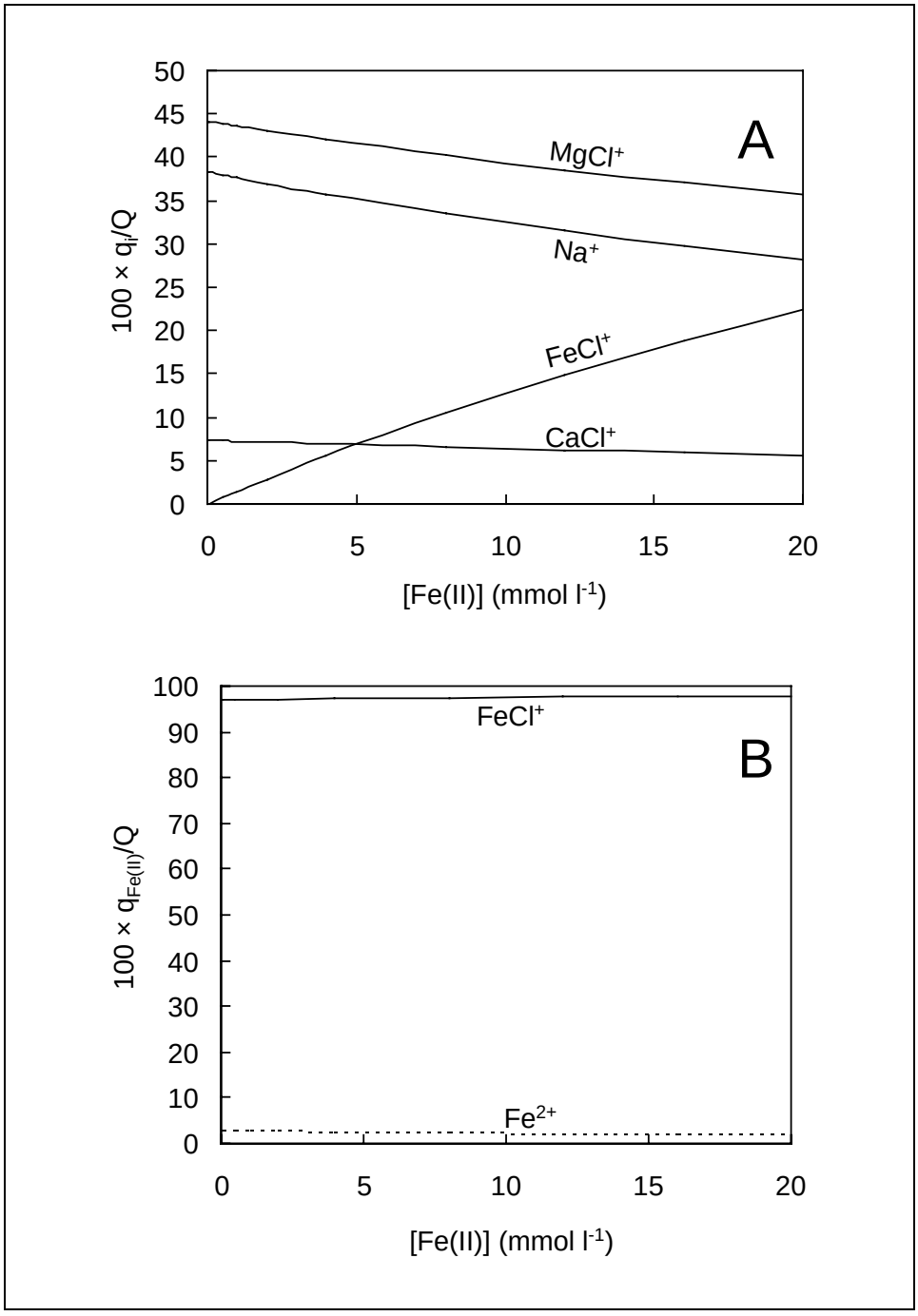


Figure 3.10 : A. Simulation of a montmorillonitic exchanger phase composition at equilibrium with seawater as a function of a hypothetical Fe(II) content in paleo - seawaters. Monovalent species (Na^+ or Cl^- - divalent cation ion pairs) are the main components of sorbed species. B. Partitioning of Fe(II) species on the exchanger phase as a function of Fe(II) concentration in seawater.

ACKNOWLEDGEMENTS

This research was partially funded by the French National radioactive waste management agency (ANDRA), and by the CNRS “Geomex” grant. Mössbauer facilities at the “Laboratoire de Physique de l'Etat Condensé” in the University of Maine (Le Mans, France) were used. Special thanks to J.M. Greneche for his help with the Mössbauer.

3.2. ADSORPTION SPECIFIQUE DU FE(II) SUR LES MONTMORILLONITES ET PHENOMENES DE COMPETITION

Des expériences d'adsorption du Fe(II) sur l'argile montrent la très forte affinité de cet élément pour les bordures des argiles (Figure 3.11).

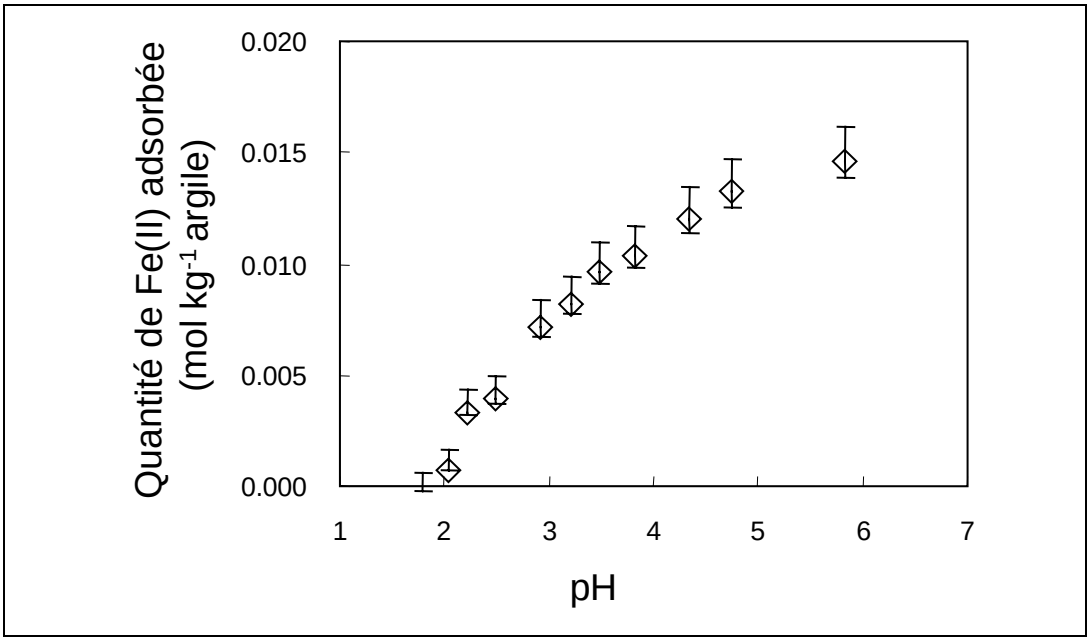


Figure 3.11 : isotherme d'adsorption du Fe(II) en fonction du pH. Conditions expérimentales : 1.7 g d'argile l^{-1}, $[Fe(II)]_{totale}$ =26 µM, fond ionique 1 mol l^{-1} NaCl.

Après modélisation des résultats, grâce à un modèle déjà disponible dans la littérature (Bradbury and Baeyens, 1997), il est apparu que l'affinité du Fe(II) pour les bordures de l'argile était au moins 1000 fois plus importante que celle d'autres cations divalents pourtant similaires (Zn^{2+} et Ni^{2+}). Un grand nombre de polluants (métaux lourds par exemple) peut être fixé par les argiles des aquifères et des sols. La présence de Fe(II) en grande concentration pourrait limiter cette action « nettoyante » des argiles en libérant les polluants déjà présents (effet compétitif, Figure 3.12) ou en empêchant de nouveaux polluants de se fixer (effet de saturation des sites, Figure 3.12). Dans l'article qui suit, l'effet compétitif est prouvé dans le système Fe(II) – Zn(II) sur un type de site de sorption spécifique.

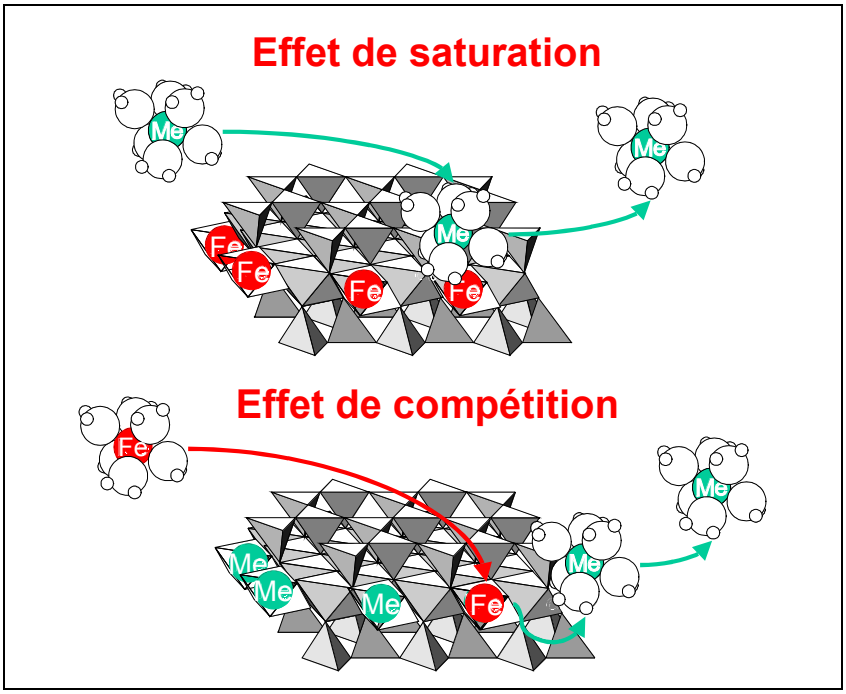


Figure 3.12. Illustration des principes de l'effet de saturation et de l'effet compétitif. Me représente un cation métallique pouvant s'adsorber sur les mêmes sites que le Fe(II).

COMPETITIVE SPECIFIC SORPTION OF FE(II) ON CLAY MINERALS IN ANOXIC WATERS

Christophe Tournassat[1, 2], Laurent Charlet[1]

[1] LGIT - CNRS/UJF, Université Joseph Fourier (Grenoble), P.O. Box 53, F 38041 Grenoble, France

[2] ANDRA, Parc de la Croix Blanche, 1/7 rue Jean Monnet, F-92298 Châtenay-Malabry CEDEX, France

ABSTRACT

Clay minerals are among the most efficient natural materials for immobilizing pollutants in natural and engineered systems. Although clay affinity has been well established for a wide range of pollutants in Na^+ and Ca^{2+} salt backgrounds, clay sorption capacity in iron-containing waters is poorly documented. In this study, we show that Fe(II) can strongly sorb to smectite particles. Complexation constants for Fe(II) specific sorption on clay edge reactive sites are much higher than those published for other divalent cations, such as Zn(II) and Ni(II). Thus, based on thermodynamic models, sorption of Fe(II) on clay particles may potentially have a strong impact on the clay immobilization capacity towards a variety of inorganic pollutants in anoxic environments. Fe(II) – Zn(II) competitive sorption experiments clearly show that Fe(II) displaces Zn(II) on clay edge sites. This competition could lead to a weakening of clay immobilization capacity towards heavy metals and radionuclides in natural iron-rich ground- and pore-waters, and in engineered systems such as zero-valent iron permeable reactive barriers and deep radioactive waste depository sites.

INTRODUCTION

Aqueous ferrous iron is a major cation and an important reductant in a variety of natural anoxic environments (eutrophic lakes, ocean and swamp sediments, hydromorphic soils, anoxic groundwaters and ocean basins), as well as in engineered systems (zero-valent iron permeable reactive barriers, or PRBs, and radioactive waste repository sites). At radioactive waste disposal sites, vitrified waste should be placed in steel containers and overpacks, which are encased in exogenous materials (near-field engineered barrier) and buried in a clay-rich or granite geological formation (far-field engineered barrier). Under anoxic conditions, steel from containers, concrete structural elements, and iron granules may react with water and release large amounts of Fe(II):

$Fe^0 + 2\ H_2O \rightarrow Fe^{2+} + H_2 + 2\ OH^-$. reaction 3.1

Dissolved Fe(II) is controlled by siderite ($FeCO_{3(s)}$) and Fe-rich calcite in sulphide-poor, carbonate-rich surficial environments, and by FeS_x (with $1<x<2$; pyrite for $x = 2$) in sulphide-rich environments (Berner, 1971). In the former case, Fe(II) concentrations range from 10^{-4} to $10^{-2.5}$ M, depending on pH and P_{CO2} (Emerson, 1976; Postma, 1982; Criaud and Fouillac, 1986a, b); while in the later case, Fe(II) concentrations are often in the 10^{-4} to 10^{-3} M range (Emerson et al., 1980; Balzer, 1982; Davison et al., 1999; Bott, 2002). In low P_{CO2}, low P_{H2S} environments, Fe(II) solubility is controlled by precipitation of $Fe(OH)_{2(s)}$, Fe_3O_4 (magnetite), or $Fe_3PO_{4(s)}$. In granular, zero-valent iron PRBs and their outflows, Fe(II) concentrations typically lie between 10^{-6} and $3\cdot10^{-4}$ M (Naftz et al., 2000). The migration of Fe(II) ions in aqueous environments is, like for most divalent cations, retarded by sorption on minerals with a large surface area and specific sorption properties (Drever, 1971; Liger et al., 1999). Among these minerals, phyllosilicates play a significant role. According to chemical analyses and spectroscopic studies, cations are sorbed on phyllosilicate surfaces by two mechanisms: cation exchange in the interlayer planes of the clay particles and specific sorption at the edges of the platelets (Fletcher and Sposito, 1989; Charlet et al., 1993; Zachara and Smith, 1994; Bradbury and Baeyens, 1997, 1998; Schlegel et al., 2001b; Bradbury and Baeyens, 2002). The clay sorption capacity has been well established for a wide range of potential pollutants in Na^+ and Ca^{2+} background ionic media (Fletcher and Sposito, 1989; Charlet et al., 1993; Zachara et al., 1993; Zachara and Smith, 1994; Baeyens and Bradbury, 1997; Bradbury and Baeyens, 1997; Akcay, 1998; Bradbury and Baeyens, 1998; Turner et al., 1998; Bradbury and Baeyens, 2002). However, the influence of other background ionic media such as Fe(II)-containing waters is poorly documented. The aim of this study is to investigate the Fe(II) specific sorption on clay minerals and to discuss the results in terms of clay immobilization capacity towards inorganic pollutants in Fe(II)-rich waters.

MATERIALS AND METHODS

Chemicals.

All solutions and suspensions were prepared in a glove box with boiled, argon-degassed Millipore Milli-Q 18 MΩ water. NaOH and HCl stock solutions were made from Titrisol ampoules. $FeCl_2$, $ZnCl_2$, NaCl, and $CaCl_2$ solutions were prepared from analytical grade salts.

Clay material preparation and characterization.

MX80 sample material was obtained from ANDRA (the French National Radioactive Waste Management Agency) and was dispersed in deionized water. The fine fraction (< 2 μm) was isolated by sedimentation. All treatments were performed in 0.5 M NaCl. After saturating the suspension with NaCl, it was treated with 0.1 M acetic acid to remove carbonates, then with

dithionate-citrate-bicarbonate (DCB), and finally with 3% H_2O_2 to remove mineral impurities and organic matter. The final suspensions were washed with either 0.5 M NaCl or 0.05 M $CaCl_2$ solutions.

The fine fraction of the MX80 montmorillonite has the following structural formula in the Na-saturated form (Sauzéat et al., 2001):

$(Si_{3.98}Al_{0.02})(Al_{1.55}Fe^{3+}_{0.09}Fe^{2+}_{0.08}Mg_{0.28})O_{10}(OH)_2Na_{0.38}$

and the following formula in the Ca-saturated form:

$(Si_{3.98}Al_{0.02})(Al_{1.55}Fe^{3+}_{0.09}Fe^{2+}_{0.08}Mg_{0.28})O_{10}(OH)_2Ca_{0.19}$

The X ray diffraction patterns were found to be in agreement with Na- and Ca-saturated smectites and showed that few impurities (mostly quartz and cristobalite) were present after preparation.

Fe(II) specific sorption experiments.

All experiments were conducted in a N_2/H_2 atmosphere glove box in which the pO_2 was monitored continuously by a Jacomex O_2 sensor. The O_2 content never exceeded 10 ppm in the glove box atmosphere. For sorption experiments a constant flux of purified N_2 gas ensured that the suspensions were under O_2- and CO_2-free conditions in the reactor. N_2 gas was purified by bubbling it through acidic (H_2SO_4, 10%) and basic (NaOH, 10%) solutions to remove impurities, including possible traces of CO_2, and then through a solution of the ionic medium (NaCl or $CaCl_2$) to saturate the gas with water. After 1 – 2 hours of purging, pyrogallol powder was added to the NaOH solution to reduce any remaining O_2. The redox potential of the suspension was monitored with a Pt combined redox electrode.

Cation exchange between Fe(II) ions and the clay surface was minimized by using a concentrated salt background solution, which limits cation exchange by mass effect (Fletcher and Sposito, 1989). The total normality of the suspensions was fixed between 0.5 and 1 M in a NaCl ionic background or 0.05 and 1 M in a $CaCl_2$ ionic background, depending on the total Fe(II) added to the system.

Experiments were carried out in 350-mL glass reactors in which an aliquot of clay stock suspension was added to a NaCl or $CaCl_2$ ionic background solution. The suspension was acidified with HCl to a pH between 1 and 2 and then allowed to reach a quasi-equilibrium overnight (approximately 16 hrs), upon which $FeCl_2$ solution was added. The total Fe(II) concentration and clay content varied from one experiment to another and are indicated in the legend of figures 1 and 2. Sorption experiments proceeded by increasing the pH incrementally with successive additions of NaOH until all Fe(II) was sorbed. After each addition of NaOH, a 10 ml sample of suspension was filtered through a 0.22 µm pore size membrane and analyzed for dissolved Fe(II) using two spectrophotometric methods: the Ferrozin method (Viollier et al., 2000) and the O-phenantrolin method (Rodier, 1996). The Ferrozin method was used to measure separately Fe(II) and Fe(III) concentrations up to 30 µM, and to check that no Fe(II) to Fe(III) oxidation occurred in solution. The O-phenantrolin method was used to measure Fe (II) concentrations up to 200 µM, before dilution.

Equilibrium was assumed when either the Fe(II) concentration or the pH were constant (*i.e.* no change in the Fe(II) concentration within the precision of the analytical method (~ ± 2%), or no variation in the pH greater than 0.02 pH units for more than 15 minutes). These criteria are operational as the clay particles dissolve at pH<4, and hence true equilibrium cannot be attained. Preliminary experiments showed that Fe(II) sorbs onto clay mineral surfaces at very

low pH (down to pH 2). Hence, some Fe(II) could have already been sorbed on the clay prior to the experiments. In order to desorb this iron, clay suspensions were "equilibrated" at pH 1.5 – 2 before each experiment . The sorbed Fe(II) was determined as the difference between the initial dissolved Fe(II) – *i.e.* the sum of initial Fe(II) and the added Fe(II) – and the dissolved Fe(II) after each addition of NaOH. At the end of each experiment, the pH was dropped to below pH 2 and all the Fe(II) was allowed to desorb back into solution. Preliminary experiments confirmed that desorption of Fe(II) is much slower (~ 1 day) than sorption (~ 1 hour, depending on the pH). The final dissolved Fe(II) in solution was compared to the initial total dissolved Fe(II) to confirm that sorption was fully reversible and that no reactions, besides sorption, had occurred.

Zn – Fe(II) competition experiment.

In a separate competition experiment, a clay suspension was prepared and allowed equilibrating overnight at pH 5.82. In order to minimize any influence of a pH change, the suspension was pH buffered with a 0.1 M HEPPS buffer (4-(2-Hydroxyethyl)-piperazine-1-propane-sulfonic acid) and remained at a pH of 5.82 $\pm$ 0.02 throughout the experiment. Sorption via cation exchange was minimized using a 0.05 M $CaCl_2$ background solution. Zn(II) was added to the suspension and allowed to sorb specifically on strong sites. After 73 hrs, Fe(II) was added to the suspension and the subsequent desorption of Zn was monitored. For this experiment, the O_2 content of the confined atmosphere never exceeded 0.5 ppm. Other experimental conditions were chosen on the basis of calculated Zn sorption edges after Bradbury and Baeyens data and models (Bradbury and Baeyens, 1998). The clay content in the suspension was 3.5 g/L. The added dissolved Zn was 3.6×10^{-6} mol L^{-1}, i.e. ~0.83 mmol of Zn per kg of clay. After 73 hours, 0.63 mmol of Zn per kg of clay was sorbed and Fe(II) was added to the suspension; the added Fe(II) concenetration in the suspension was ~69×10^{-6} mol L^{-1}. Zn(II) concentrations were measured using a Perkin-Elmer Optima 3300 DV inductively coupled plasma atomic emission spectrometer (ICP-AES).

RESULTS AND DISCUSSION

Figure 3.13 presents the results of the specific sorption experiments. Results of experiments during which $Fe(OH)_3$ could have precipitated, based on thermodynamic calculations made using Phreeqc2 (Parkhurst and Appelo, 1999), were excluded. The sorption isotherms are represented as the percentage of sorbed iron as a function of pH and shows how efficiently Fe(II) sorbs onto clay particles. Figure 3.13A corresponds to an experiment where no Fe(II) was added to the suspension at the start of the experiment, and thus represents the sorption curve of the initially desorbed Fe(II). Figure 3.13B corresponds to a sorption experiment conducted with the same suspension after decreasing the pH down to pH = 1.7 and adding a small amount of Fe(II). Between pH 2 and 4, the amount of sorbed Fe(II) is higher in Figure 3.13B than in Figure 3.13A.

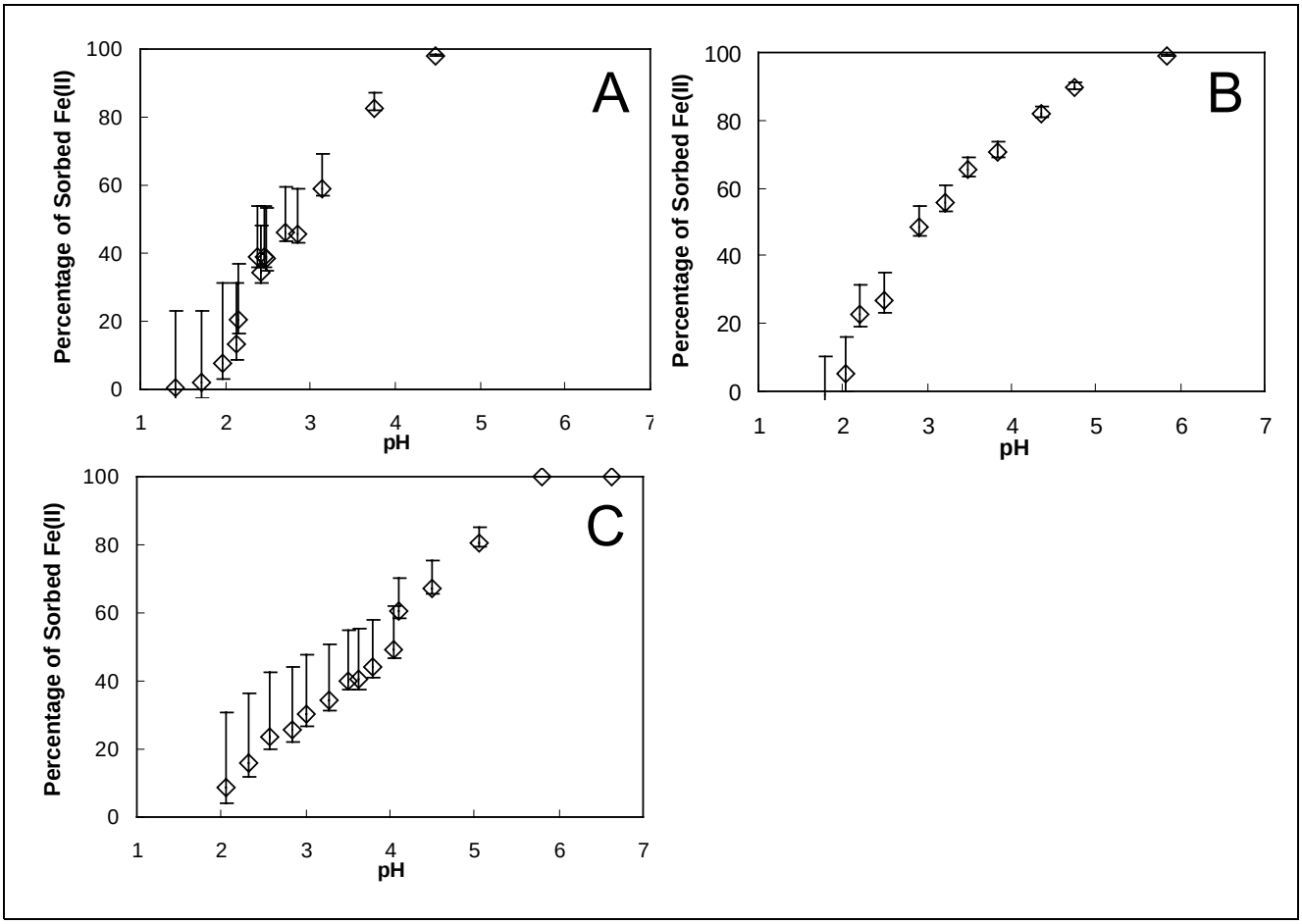


Figure 3.13 : Fe(II) specific sorption experiments at high ionic strengths, and various $[Fe(II)]_{tot}$ to [solid] ratio. A. 2.3 g clay/L, 10 µM Fe(II), 1 M NaCl. B. 1.7 g clay/L 26 µM Fe(II), 1 M NaCl. C. 1.4 g clay/L, 15 µM Fe(II), 1 M $CaCl_2$. For the asymmetry of the error bars, see Results and Discussion.

Figure 3.14 presents the same experimental results with the model results (discussed below) in a different way: the sorption isotherms are plotted as the amount of sorbed Fe(II) per kilogram of clay as a function of pH. This representation allows us to directly compare the results of experiments conducted under different experimental conditions and shows the plateaus and edges which are characteristic of the different sorption sites. The sorption isotherms are relatively complex with at least two different domains: the first increase occurs between pH 2 and pH 3 – 4, and the second one above pH 4.

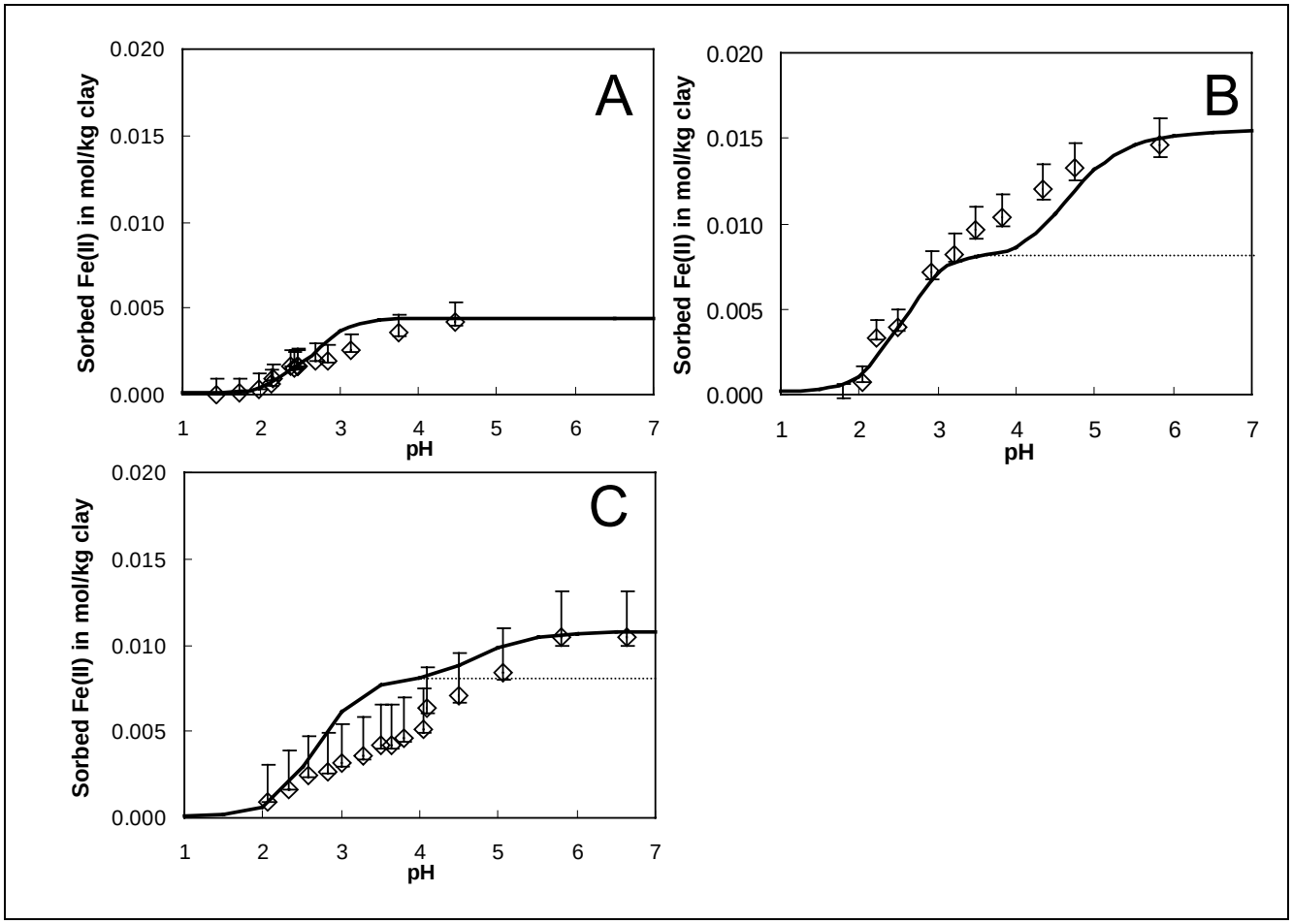


Figure 3.14 : Sorption of Fe(II) on high and low energy sites of clay edges. Solid line: total Fe(II) sorption model curve. Dotted line: high-energy site Fe(II) sorption. A. 2.3 g clay/L, 10 µM Fe(II), 1 M NaCl. B. 1.7 g clay/L 26 µM Fe(II), 1 M NaCl. C. 1.4 g clay/L, 15 µM Fe(II), 1 M CaCl2. For the asymmetry of the error bars, see Results and Discussion.

The experimental method introduces some uncertainties to the results since we cannot be sure that all the Fe(II) desorbs over one night, and it is difficult to estimate the Fe(II) released from the dissolution of the clay material. We must also take into account the uncertainties in the total added Fe(II) and the dissolved Fe(II) measurements. Error bars are plotted with results in Figure 3.13 and Figure 3.14. The positive error bar is calculated on the basis of a standard error of 20 % on the initial Fe(II) amount, *i.e.* the total amount in solution and previously sorbed on the clay surface before any addition of Fe(II), plus a standard error of 5% for the measurement of dissolved Fe(II). The negative error bar includes only the 5% standard error for the measurement of dissolved Fe(II).

The reactive sites corresponding to the sorption behavior at low pH (2 – 4) can be considered as a unique type of site, the so-called “strong sites”. A comparison between Figure 3.13A and Figure 3.13C shows that there is little difference between Fe(II) sorption at these sites when experiments were performed either in a Ca^{2+} or in a Na^{+} salt background. The density of strong sites is not easily measurable by sorption isotherms. Indeed, if enough Fe(II) is available, a second sorption edge occurs at pH 4 (Figure 3.14B) limiting the accuracy of the plateau site density. Besides, as explained previously, the initial amount of sorbed iron is not an absolute, reliable value. Therefore as a rough estimate, the strong sites density is estimated to be between 0.005 and 0.015 mole sites per kilogram of clay.

The sites responsible for the second sorption edge are called the “weak sites”. It was not possible to evaluate the exact density of these sites, as experiments conducted to attain a

second plateau region by increasing both the equilibrium pH and the total Fe(II) content in the solution failed to point to a single value. In other words, it was never possible to “sorb” all Fe(II) by increasing the pH (data not shown). The oxidation of Fe(II) to Fe(III) by oxygen present in the solution could have lead to the precipitation of amorphous iron oxyhydroxides and thus to an overestimated and unlimited apparent sorption capacity. However, every precaution was taken to minimize the presence of oxygen in solution. Besides, the rate of Fe(II) oxidation would have been negligible under these experimental conditions. Fe(II) oxidation in solution occurs very slowly at pH<4, but increases at higher pH (Stumm and Lee, 1961). For example, considering the oxygen partial pressure between 5 and 10 ppm in the glove box, the concentration of O_2 in the suspension was about 6.3×10^{-9} M. The following formula gives the oxidation rate of Fe(II) in solution (Stumm and Morgan, 1996):

$$d[Fe(III)]/dt = (k_0 \times [Fe^{2+}] + k_1 \times [FeOH^{+}] + k_2 \times [Fe(OH)_2]) \times [O_2] \qquad \text{Eq. 3.6}$$

where $k_0 = 10^{-5.1}\ mol^{-1}\ s^{-1}$, $k_1 = 10^{1.4}\ mol^{-1}\ s^{-1}$, $k_2 = 10^{6.9}\ mol^{-1}\ s^{-1}$. Speciation of 100 µM Fe(II) in solution was calculated as a function of pH with Phreeqc2 (Figure 3.15). At pH 8 (the maximum experimental pH), the oxidation rate did not exceed 10^{-1} µM h^{-1}. This rate is negligible compared to the lowest total Fe(II) concentration value used in our experiments (10 µM) and the duration of one experiment (less than one day). Therefore the oxidation of Fe(II) in solution cannot be considered as a major sink for Fe(II) in the sorption experiments. However, redox reactions are enhanced on mineral surfaces (Liger et al., 1999; Charlet et al., 2002) and thus the oxidation rate could have been much faster in our system. Nevertheless, as explained in the materials and methods, the desorption test and the full recovery of the iron in the Fe(II) form indicated little or no oxidation.

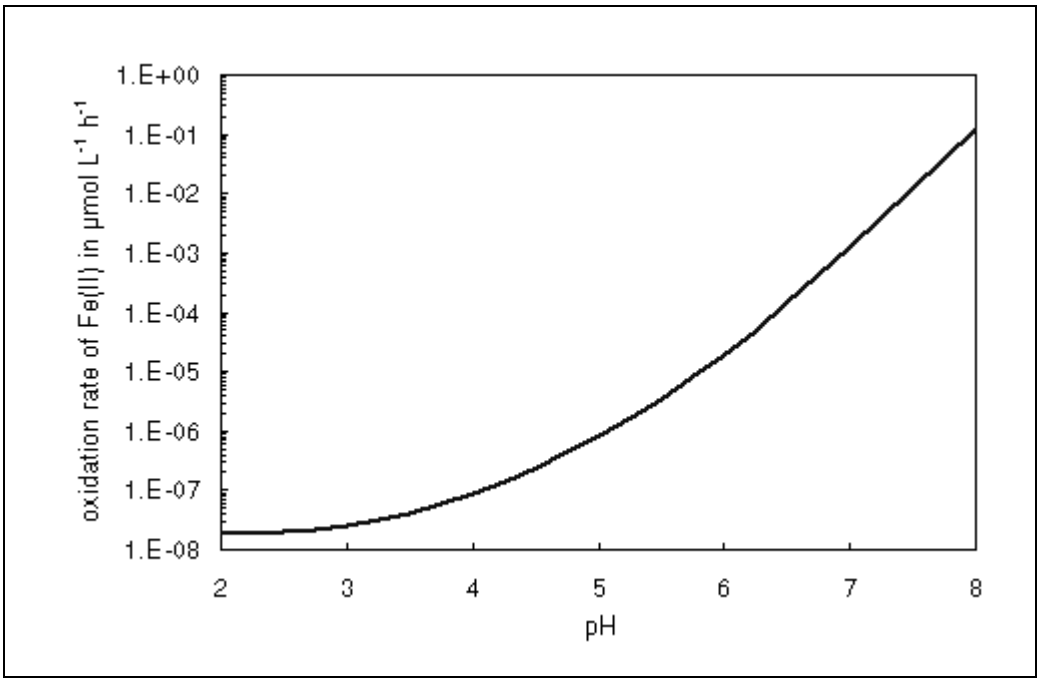


Figure 3.15 : Dissolved Fe(II) oxidation rate as a function of pH. Conditions of the simulation are: pO_2 = 5 ppm, $[Fe(II)]_{tot}$ = 100 µM.

Another secondary reaction which may have lead to an overestimation of the apparent Fe(II) sorption capacity, far in excess of the edge surface site concentration, is the precipitation of Fe(II) with dissolved silicic acid, produced by the dissolution of quartz or smectite, as an iron-silica phase. Such heterogeneous precipitation has already been demonstrated in systems such as Co-Quartz (Manceau et al., 1999), Zn-hectorite (Schlegel et al., 2001b), and Ni-smectite (Dähn et al., 2002b). However, these precipitation reactions are usually very slow with smectite

(Dähn et al., 2002b) and such precipitates cannot be dissolved in the short time scale used to recover all the iron in form of Fe(II) by decreasing the pH. Future spectroscopic studies will certainly help us to understand these results.

Experimental data on Fe(II) sorption on the montmorillonite strong surface sites were modeled in order to compare the thermodynamic complexation constant derived for Fe(II) to similar constants obtained with other divalent metal ions. No attempt was made to find a perfect fit to the data. The Baeyens and Bradbury model (Bradbury and Baeyens, 1997, 1998) was chosen among the variety of models currently being used to describe the sorption of cations on clay particle edges (Fletcher and Sposito, 1989; Charlet et al., 1993; Zachara and Smith, 1994; Bradbury and Baeyens, 1997). The Baeyens and Bradbury model was selected since it can easily model sorption data using Phreeqc2, a versatile computer code amenable to the various conventions used to describe cation exchange and surface complexation. In addition, thermodynamic constants for the sorption of Ni(II), Zn(II) and Eu(III) have already been published by these authors (Bradbury and Baeyens, 1997, 1998, 2002). The parameters of the model are shown in Tab. 3.8 and Tab. 3.9 and the model results depicted in Figure 3.14. The density of strong sites was calculated based on the results mentioned above, rather than estimated on the basis of Zn sorption results as done in the original work (Bradbury and Baeyens, 1997). Indeed, according to Baeyens and Bradbury, their value is not well constrained; furthermore, some Fe(II), or even Al(III), with a high affinity constant for edge sites (Charlet et al., 1993) could have occupied part of the sites. The intrinsic constants for the complexation of Fe(II) with both weak and strong montmorillonite edge sites are given in Tab. 3.9. The high value for the intrinsic constant for Fe(II) specific sorption on strong sites (log K_{int} = 5) is representative of the high affinity of Fe(II) for clay surfaces. This high affinity should result in competitive sorption of Fe(II) on clay minerals with pollutants like heavy metals.

Site types	Site capacities
$S^{S}OH$ ‡	0.008 mol kg^{-1} †
$S^{W1}OH$ ‡	0.04 mol kg^{-1} ‡
$S^{W2}OH$ ‡	0.04 mol kg^{-1} ‡

S^{s} = strong surface sites; S^{w1} and S^{w2} = weak surface sites
‡ after Bradbury and Baeyens (Bradbury and Baeyens, 1997)
† fixed (see discussion in text)

Tab. 3.8 : List of surface sites and their respective capacities.

Reactions	Log K_{int}
$S^SOH + H^+ = S^SOH_2^+$	4.5 ‡
$S^SOH = S^SO^- + H^+$	-7.9 ‡
$S^{W1}OH + H^+ = S^{W1}OH_2^+$	4.5 ‡
$S^{W1}OH = S^{W1}O^- + H^+$	-7.9 ‡
$S^{W2}OH + H^+ = S^{W2}OH_2^+$	6.0 ‡
$S^{W2}OH = S^{W2}O^- + H^+$	-10.5 ‡
$S^SOH + Fe^{2+} = S^SOFe^+ + H^+$	5.0 *
$S^{W1}OH + Fe^{2+} = S^{W1}OFe^+ + H^+$	0.5 **

S^s = strong surface sites; S^{w1} and S^{w2} = weak surface sites
‡ after Bradbury and Baeyens (Bradbury and Baeyens, 1997)
* adjusted value
** The log K value for weak sites -S^{W1}OH- is given as an indicative value and may be overestimated due to high uncertainty associated with the amount of strong sites and the position of the second sorption edge.

Tab. 3.9 : List of reactions with known and estimated intrinsic constants.

Figure 3.16 presents the results of the Zn – Fe(II) competition experiment at pH ~5.8. The initial Zn(II) concentration was calculated based on the dilution of the Zn(II) stock solution concentration in the clay suspension. The error bar of the first point represents a standard error of 2% on the concentration measurement, plus an error of 2% for the dilution. The error bars of the other points include only the 2% standard error for the measurement of dissolved Zn(II). After 73 hours, 0.5 mmol of Zn per kg of clay was sorbed on the clay particles. More than 250 hours after the Fe(II) addition in the suspension, the dissolved Zn(II) increased to 100% of its original concentration of 3.4 µM (within the confidence limit of the error bars). Clearly, the addition of Fe(II) is responsible for the desorption of all the sorbed Zn.

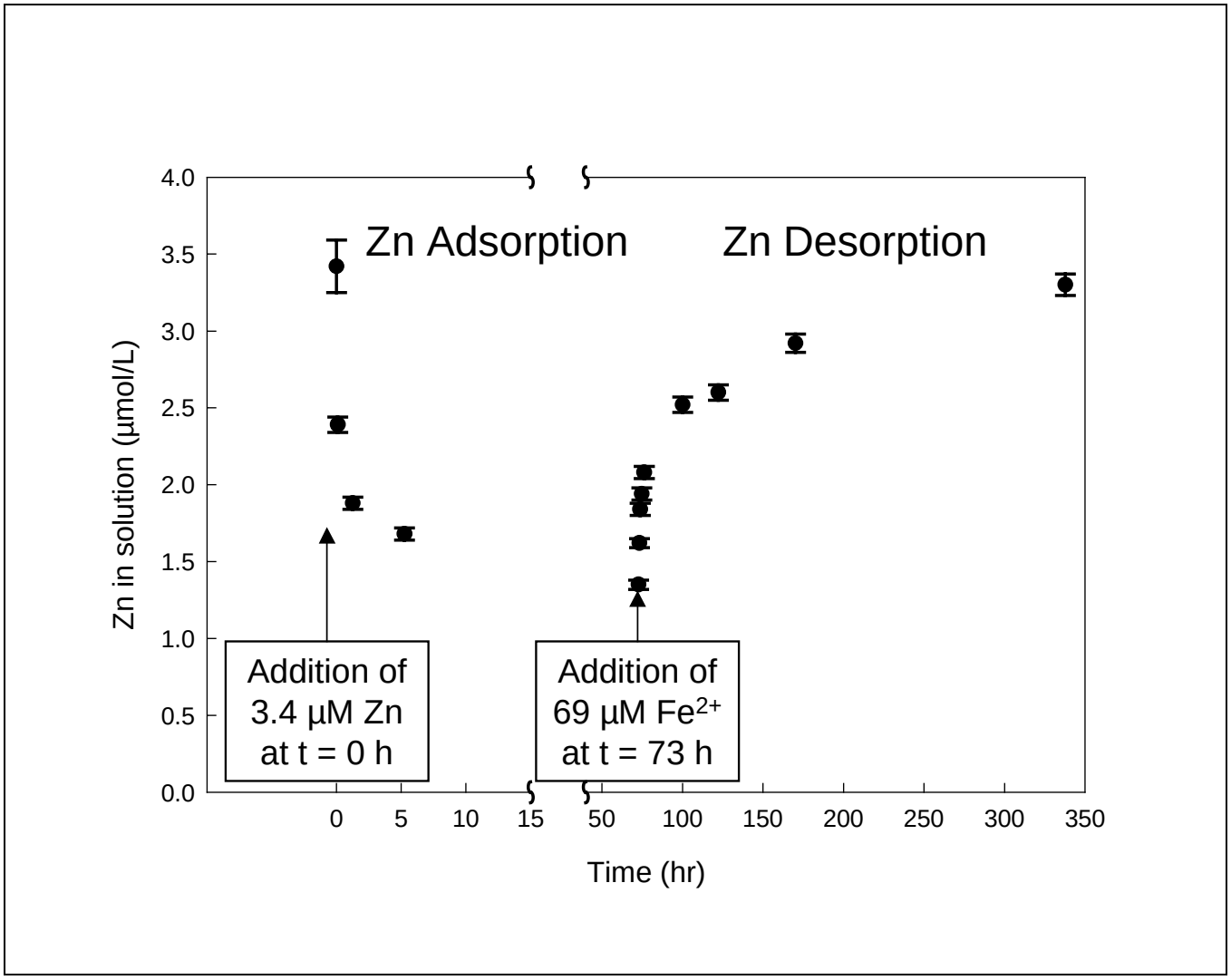


Figure 3.16 : Zn(II) sorption and desorption at pH 5.82, by successive additions of 3.4 µM Zn(II) at t = 0 hrs and 69 µM Fe(II) at t = 73 hrs to a 4.35 g L^{-1} and 0.05 M $CaCl_2$ clay suspension.

In Tab. 3.10, the log K_{int} value obtained in the present study for Fe(II) is compared with those obtained in previous studies for Zn(II), Ni(II) (Bradbury and Baeyens, 1997, 1998), Eu(III) (Bradbury and Baeyens, 2002) and U(VI) (log K_{int} value adjusted with the present model after the results of Pabalan et al. (Pabalan et al., 1994) presented by Turner (Turner, 1995)). The log K_{int} value for Fe(II) sorption is more than three orders of magnitude larger than the values reported for Zn(II), Ni(II), Eu(III) or U(VI) (Tab. 3.9). In other words, the affinity of the montmorillonitic clay is 10^3 times larger for Fe(II). Hence, in the presence of a high amount of dissolved Fe(II), nearly all the strong sites will be saturated by sorbed Fe(II). This will decrease the clay's ability to sorb any other cation in such anoxic environments. This effect is illustrated by the simulation results presented in Figure 3.17. The sorption edges of Zn(II), Ni(II), Eu(III) and U(VI) are shifted towards high pH as Fe(II) is introduced into the system. Considering a pH of 7 representative for groundwaters, the presence of Fe(II) in solution leads to the decrease of pollutant sorption on clay minerals from 100 %, 93 %, 100% and 95.6% to 38%, 18 %, 87%, and 0% for Zn(II), Ni(II), Eu(III) and U(VI), respectively. Moreover, the Zn – Fe(II) competition experiment clearly demonstrates that a previously sorbed pollutant such as Zn(II) can be displaced when aqueous Fe(II) is present in solution.

Reactions	Log K_{int}
$S^SOH + Fe^{2+} = S^SOFe^+ + H^+$	5.0 *
$S^SOH + Zn^{2+} = S^SOZn^+ + H^+$	1.6 ‡
$S^SOH + Ni^{2+} = S^SONi^+ + H^+$	-0.1 ‡
$S^SOH + Eu^{3+} = S^SOEu^{2+} + H^+$	0.8 ‡
$S^SOH + UO_2^{2+} = S^SOUO_2^+ + H^+$	1.7 **

S^s = strong surface sites; S^{w1} and S^{w2} = weak surface sites
‡ after Bradbury and Baeyens (Bradbury and Baeyens, 1997, 1998, 2002)
* adjusted value after the present study data
** adjusted value after Turner data (Turner, 1995)

Tab. 3.10 : Comparison of strong sites Log K_{int} for Fe(II), Zn(II), Ni(II), Eu(III) and U(VI)

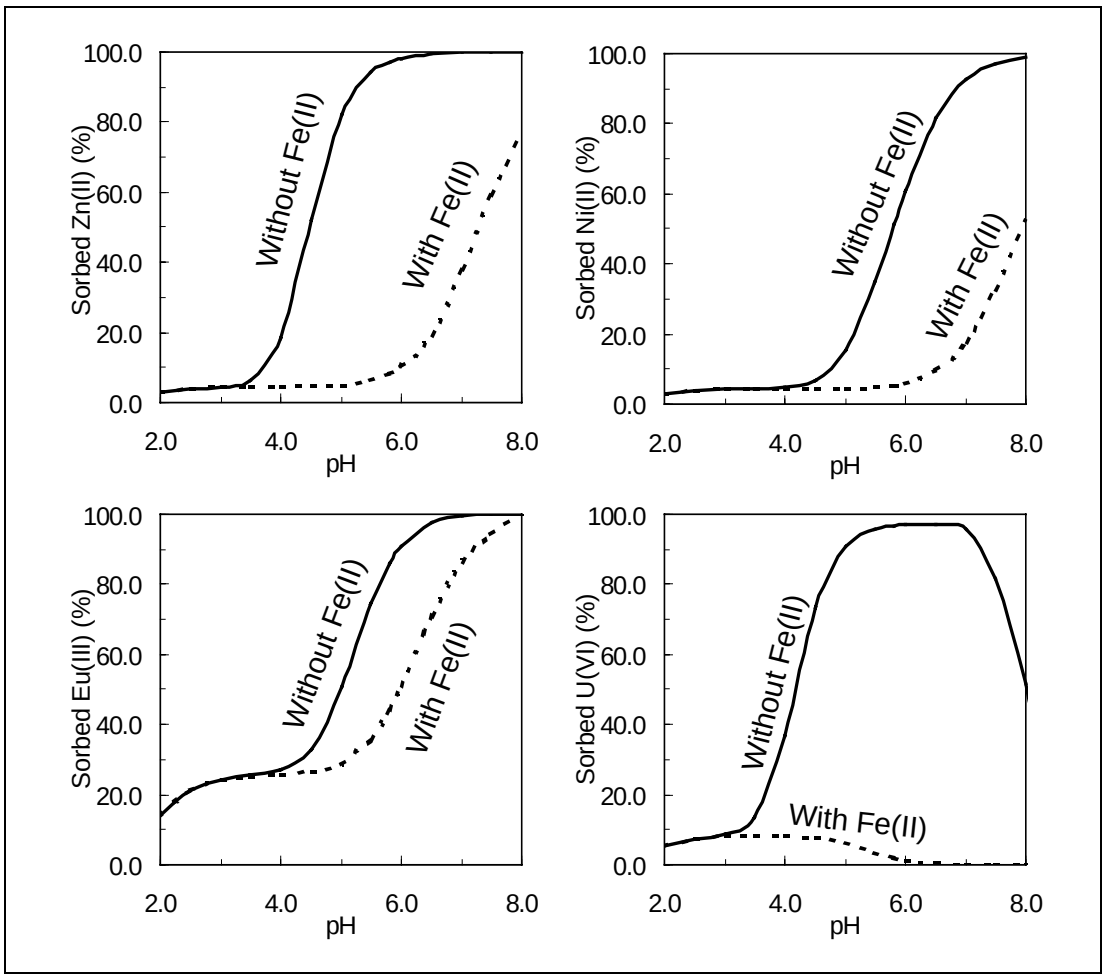


Figure 3.17 : Simulation of the competitive effect of Fe(II) on the Zn(II), Ni(II), Eu(III) and U(VI) sorption on a 4.35 g L^{-1} 0.04 M $CaCl_2$ clay suspension . The parameters of the simulation are given in Tab. 3.8, Tab. 3.9 and Tab. 3.10. Solid line: 3.6 µM pollutant sorption isotherm in absence of added Fe(II) (*i.e.* only with 0.005 mol kg^{-1} of preliminary sorbed Fe(II)). Dotted line: 3.6 µM pollutant sorption isotherm in presence of 69 µM Fe(II).

If this behavior also applies to other cations and to the clay weak sorption sites in a compacted bentonite system, this could lead to a weakening of clay immobilization capacity towards heavy metals and radionuclides in natural iron-rich ground- and pore-waters, and in engineered systems such as zero-valent iron PRBs and deep radioactive waste depository sites. In particular, the presence of a zero-valent PRB upstream from a polluted area could lead to the release of a secondary pollution downstream from the barrier due to the replacement of sorbed heavy metals by Fe(II).

ACKNOWLEDGEMENTS

This research was funded by the French National radioactive waste management agency (ANDRA).

3.3. EVIDENCES EXPERIMENTALES DE PRECIPITATION D'UNE PHASE SI-FE ET D'OXYDATION DU FE(II) A LA SURFACE DES ARGILES

Les deux articles précédents ont quantifié deux phénomènes d'adsorption du Fe(II) à la surface de l'argile : l'échange cationique et une adsorption spécifique sur des sites permettant des effets de compétition entre cations. Ces types de sorption sont modélisés avec succès avec des modèles disponibles dans la littérature.

L'article qui suit montre que ces deux phénomènes de sorption ne sont pas les seuls à rendre compte des quantités de Fe(II) fixées par l'argile. Il est ainsi montré que la sorption du Fe(II) est due à haut pH à la précipitation d'un composé au rapport Si/Fe compris entre 1 et 2. A bas pH, la grande affinité du Fe(II) pour les sites de côtés de l'argile est confirmée. La fixation du Fe(II) par l'argile est alors due à plusieurs phénomènes qui se superposent (Figure 3.18):

- un remplacement du Mg(II) octaédrique par le Fe(II) ;
- une sorption du Fe(II) sur les bordures suivie d'une oxydation. L'oxydant est, ici, supposé être le Fe(III) structural de l'argile ;
- une sorption coopérative avec H_4SiO_4, à l'origine d'une précipitation de surface.

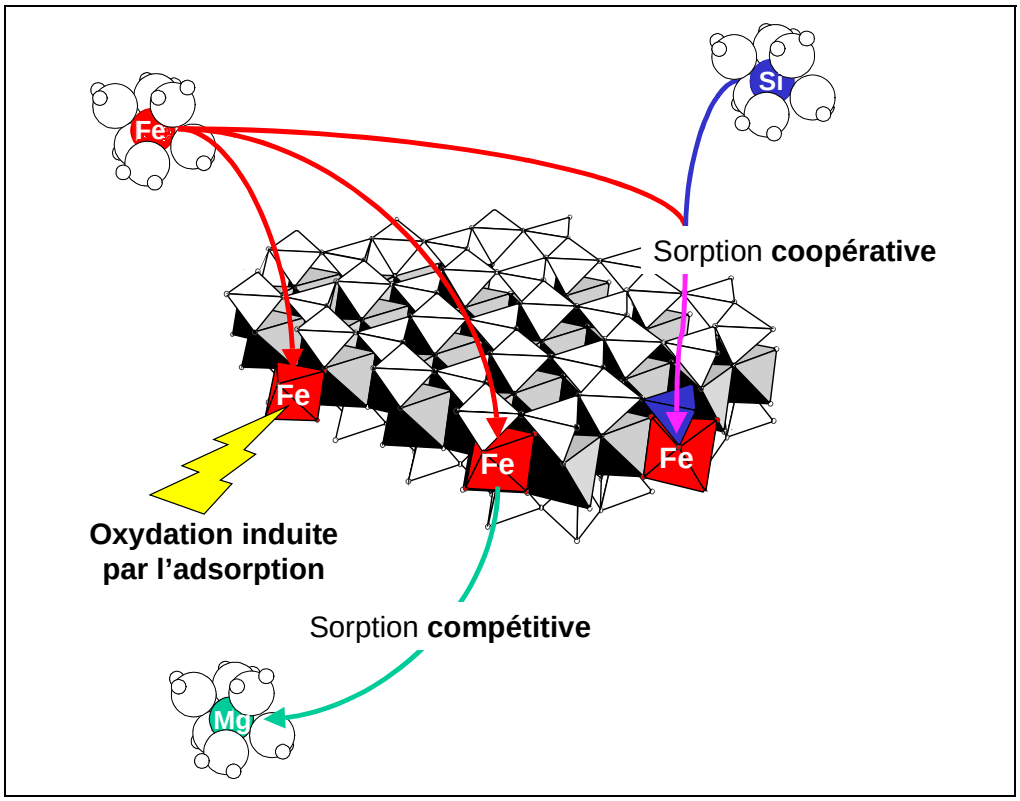


Figure 3.18 : Schématisation des différents mécanismes à l'origine de la sorption du Fe(II) par la montmorillonite à bas pH.

SORPTION OF FE(II) ON MONTMORILLONITE IN ANOXIC CONDITIONS: EVIDENCE FOR A NEW FE-SI SOLID PHASE PRECIPITATION AND FOR SURFACE OXIDATION OF FE(II).

Christophe Tournassat[1,2], Laurent Charlet[1], Jean-Marc Greneche[3]

[1] LGIT - CNRS/UJF, University of Grenoble-I, P.O. Box 53, F 38041 Grenoble, France

[2] ANDRA, Parc de la Croix Blanche, 1/7 rue Jean Monnet, F-92298 Châtenay-Malabry CEDEX, France

[3] Laboratoire de physique des états condensés UMR CNRS 6087, University of Maine, F 72085 Le Mans, Cedex 9, France

ABSTRACT

The mechanisms of Fe(II) sorption on montmorillonite in anoxic conditions is investigated through Mössbauer spectroscopy and original analytical chemistry experiments. The whole sorption of Fe(II) is found to be caused by several mechanisms taking place at the same time on the montmorillonite edge surfaces. The relative importance of these mechanisms is dependent on the pH. In the alkaline pH range, a Si-Fe precipitate forms from pH equal to ~9.5, with Si/Fe ratio comprising between 1 and 2. In the acid pH range, we confirm the high affinity of clay surfaces for Fe^{2+} sorption. This sorption is mainly due to a two steps mechanism including a sorption step followed by an oxidation step. This mechanism is responsible for the net release of 2 H^+ per Fe^{2+} adsorbed. The oxidation of Fe^{2+} into Fe^{3+}, likely due to the clay structure, should explain the high affinity of clay for Fe^{2+} sorption, through the structural fit between the montmorillonite octahedral layer and Fe^{3+}. Fe^{2+} oxidized or not into Fe^{3+} is also shown to replace Mg^{2+} on the clay edges, as it has been shown for Zn^{2+} (Tournassat and Charlet, submitted). Finally, if a sufficient concentration of H_4SiO_4 towards clay dissolution equilibrium is available, Fe^{2+} and H_4SiO_4 can be sorbed together (cooperative sorption), leading to the formation of a surface precipitate.

INTRODUCTION

Sorption mechanisms on clay surfaces have been studied for decades and one distinguishes: (i) inorganic cation exchange in the interlayer and on basal plane surfaces (*e.g.* Sposito, 1981) and (ii) specific pH dependent sorption of cations and anions on the edges (*e.g.* Sposito, 1984). Edge sorption mechanism is related to the acido-basic properties of the clay edges (Fletcher and Sposito, 1989; Charlet et al., 1993; Stadler and Schindler, 1993; Zachara and Smith, 1994; Bradbury and Baeyens, 1997; Avena, 2002 and others) whereas cation exchange on basal planes is related to the permanent charge generated by the clay structure (Sposito, 1981). The former mechanism is a pH dependant specific sorption on the clay edges. It has already been well established that the proton surface charge density (σ_H) on the clay edges depends on physico-chemical solution parameters (pH, ionic strength) that control the protonation state of the surface (Fletcher and Sposito, 1989; Charlet et al., 1993; Zachara et al., 1993; Wanner et al., 1994; Baeyens and Bradbury, 1997; Bradbury and Baeyens, 1997; Avena, 2002 and others). At variance, the cation exchange mechanism originates from the presence of a permanent negative structural charge in the alumino-silicate layer created by isomorphic substitutions in the lattice. The density of exchange sites (σ_o) can be derived from structural formula, and is electrically balanced by “exchangeable cations”, which generally form outer sphere complexes with siloxane cavities (Sposito, 1981, 1984). The modeling of both of these mechanisms should permit to predict the extent of metallic cation uptake by clay minerals. Nevertheless, some authors showed that other mechanisms must be involved as precipitation of new clay-like phases (Charlet and Manceau, 1994; Schlegel et al., 2001b; Dähn et al., 2002b), or dehydration of some cations in exchangeable positions (*e.g.* Chang et al., 1998).

Previous studies of Fe(II) sorption processes on montmorillonite have shown (i) that Fe(II) can sorb onto clay minerals in cation exchange position with a similar clay affinity for Fe(II) and Ca(II) (Tournassat et al., submitted-a) and (ii), Fe(II) can compete with other metals for sorption on edge sites (Tournassat and Charlet, submitted). These behaviors can be modeled with already published models (*e.g.* Bradbury and Baeyens, 1997). However, other uptake mechanisms, like the possible precipitation of Fe(II)-rich new phases, must not be discarded. In the present study, we propose new chemical and spectroscopic experiments to characterize the different mechanisms of Fe(II) “specific sorption” on montmorillonite.

MATERIAL AND METHOD

Chemicals

All solutions and suspensions were prepared with boiled, argon-degassed Millipore Milli-Q 18 MΩ water. NaOH and HCl stock solutions were made from Titrisol ampoules. NaCl, $CaCl_2$, $FeCl_2$, and $FeCl_3$ solutions were prepared from analytical grade salts. All experiments were conducted in a O_2 "free" atmosphere glove box (Jacomex, pO_2 < 0.5 ppm), except for experiment E, conducted in air.

Clay material preparation

MX80 (commercial Wyoming bentonite, reference BF100, CETCO France) clay sample material was obtained after homogenization from ANDRA (the French National Radioactive Waste Management Agency). STx-1 Texas montmorillonite sample was obtained from Source Clay repository (Missouri, USA). The clay samples were dispersed in deionized water. The fine fractions (< 2 μm) were isolated by sedimentation. After saturation with NaCl (0.5 M), the suspensions were successively treated with a 0.1 M acetic acid, 0.5 M NaCl solution (to remove the carbonates), then with a dithionate-citrate-bicarbonate solution (DCB + 0.5 M NaCl, to remove Fe and Mn oxides impurities), and finally with 3% H_2O_2, 0.5 M NaCl (to remove organic matter, Schlegel, 2000). The final suspensions were washed with either 0.5 M NaCl or 0.05 M $CaCl_2$ solutions and then argon-degassed.

Clay material characterization

The Na- and Ca- conditioned MX80 clay characterization is available from Tournassat et al. (Tournassat et al., submitted-c). The Na- and Ca- conditioned MX80 clay samples still contain some impurities, mostly as silica phase (quartz and cristobalite) and iron remaining oxides. The MX80 structural formula are:

$(Si_{3.98}Al_{0.02})(Al_{1.61}Fe^{3+}_{0.13}Fe^{2+}_{0.02}Mg_{0.24})O_{10}(OH)_2Na_{0.28}$ for the Na-saturated form and

$(Si_{3.98}Al_{0.02})(Al_{1.61}Fe^{3+}_{0.13}Fe^{2+}_{0.02}Mg_{0.24})O_{10}(OH)_2Ca_{0.14}$ for the Ca-saturated form.

The structural CEC was found to be equal to 0.76 eq kg^{-1}. Due to large amounts of silica impurities in the STx-1 clay sample (Mermut and Cano, 2001), we do not give any structural formula for this clay. Its mean structural CEC was estimated to be equal to 0.86 eq kg^{-1} (Mermut and Lagaly, 2001). The method used to measure the clay suspension content is available from Tournassat et al. (Tournassat et al., submitted-c).

Experimental procedures

Experiments A (MX80) and B (STx-1). Comparative potentiometric titrations

In this experiment the level of H^+ desorption from montmorillonite was studied as a function of pH and compared for Fe(II)-free and Fe(II)-rich clay suspension. The experimental titration procedure is fully described in details in Tournassat et al. (Tournassat et al., submitted-c) and only summarized here. Centrifugation tubes were numbered and precisely weighed (m_{tube} in g) with a Mettler Toledo AG285 balance. A known volume of clay suspension was added in each 17-ml centrifuge tube with a calibrated micropipette (V_{susp}, clay particle

concentration ρ). Volumes of NaOH and HCl were then added (V_b and V_a, concentration C_b and C_a). Volumes of NaCl or $CaCl_2$ solutions (V_c, $[H^+] = C_c$) solution were used to complete at 15 ml (V_{tot}). Mean measured concentration of $CaCl_2$, added $FeCl_2$ concentration, and clay contents are shown in Tab. 3.11. Care was taken to minimize the variations of salt ionic background concentrations from one tube to another in a given experiment. The tubes were shaken for one week. The two experiments (with and without Fe(II)) were conducted in a O_2-free atmosphere glove box (Jacomex, $pO_2 < 0.5$ ppm). After one week the tubes were centrifuged. An aliquot of each supernatant tube was filtered and used for backtitration (V_{back}). The backtitrations were performed with a dosimeter (Metrohm 665 Dosimat, volume resolution = 0.005 mL) with pH 7 chosen as the titration end point. The pH was measured with a microelectrode (Mettler Toledo, inlab 423). One other aliquot was filtered for Si, Al, Mg and Fe measurement by ICP-AES. Control Fe(II) measurement were done with the O-phenantrolin method (Rodier, 1996) in order to check that the iron concentration measured by ICP was in the Fe(II) form. The Si, Al, Mg, Fe concentrations of a third supernatant aliquot was measured without filtration to obtain an estimated mass of particles still present in the supernatant ($m_{correction}$, see Tournassat et al. (Tournassat et al., submitted-c)). The centrifuged reaction tubes, containing the clay slurry, were weighed ($m_{centrif}$) and 10 ml of 1 M ammonium acetate were added to each. They were shaken for one week. Na- and Ca-CEC were then measured as described by Sposito et al. (Sposito et al., 1983a). The relative proton surface charge $\Delta[H^+]$ is given by (Tournassat et al., submitted-c):

$$\Delta\left[H^+\right] = \frac{1}{a}\left[\left(V_A C_A - V_B C_B\right) + \left(V_{BT_A} C_{BT_A} - V_{BT_B} C_{BT_B}\right)\frac{V_{tot}}{V_{back}}\right] \qquad [1]$$

where

a = the clay content of the suspension in kg l^{-1};

V_{tot} = the whole volume of solution in one tube in l;

V_{back} = the volume of filtrated suspension used in the backtitration in l;

V_A = the volume of acid solution added to the clay suspension in l;

V_B = the volume of alkali solution added to the clay suspension in l;

C_A = the concentration of the acid solution in mol l^{-1};

C_B = the concentration of the acid solution in mol l^{-1};

V_{BT_A} = the volume of acid solution used in backtitration in l;

V_{BT_B} = the volume of alkali solution used in backtitration in l;

C_{BT_A} = the concentration of acid solution used in backtitration in mol l^{-1};

C_{BT_B} = the concentration of alkali solution used in backtitration in mol l^{-1}.

The Ca-CEC, in eq kg^{-1}, is given by:

$$Ca-CEC = 2\times\frac{C_{Amm}^{Ca}\times 10 - C_{sol}^{Ca}\times\left(m_{centrif} - m_{tube} - \left(V_{susp}\times\rho\right)\right)}{\left(V_{susp}\times\rho\right) - m_{correction}} \qquad [2]$$

where volumes are given in ml, concentration in mol l^{-1}, clay content in g l^{-1} and masses in g. The density of all solutions is taken equal to 1.0. The ionic background was set to $CaCl_2$ = 0.05 mol l^{-1}. This ionic background ensures us that no exchange reaction occurs with Fe(II) and that Fe(II) sorbs only on specific sorption site (Tournassat et al., submitted-a).

	Titration experiment A	Titration experiment B
Clay sample	MX80	STx-1
Ionic background	$CaCl_2$ 0.05 mol l^{-1}	$CaCl_2$ 0.05 mol l^{-1}
Clay content	1.41 g l^{-1}	2.03 g l^{-1}

Tab. 3.11 : Experimental conditions of the two comparative potentiometric titration experiments

Experiment C. Dissolution and readsorption

Tournassat and Charlet (Tournassat and Charlet, submitted) showed that Fe(II) can sorb onto clay edge sites at low pH (i.e. at pH values as low as pH 2). In their experiments they decreased the pH below pH 2 to desorb (or dissolve) Fe(II) from the clay and then increased the pH, step by step, and measured Fe(II) present in solution within the reactor vessel. They also showed that Fe(II) can compete for sorption with Zn(II) at pH 5.8, while Charlet et al. (Charlet et al., 1993) demonstrated that Al^{3+} can also sorb at low pH (between pH 3 and 4). At even lower pH values, soluble H_4SiO_4 and Al^{3+} can originate from the clay particle dissolution. Then, experiment C was designed to measure the influence of Fe(II) on both the Al^{3+} readsorption and the change of Si solution concentration, as a function of increasing pH, after a clay dissolution step. The Ca- conditioned MX80 clay sample was selected for this experiment. A 3.6 g clay l^{-1}, 0.05 mol l^{-1} $CaCl_2$, O_2 free suspension was allowed to dissolve at a pH value of 2.1 in a magnetic stirred reactor, within the glove box. Since this clay material contains iron oxides impurities (Tournassat et al., submitted-c), 1.5 mmol l^{-1} sodium dithionite was added to remove them partially and to increase the Fe(II) amount in solution. This adding should ensure us reductive experimental conditions. The clay was allowed to dissolve during 23 days. During this time, samples were collected and analyzed for Si, Al, Fe and Mg by ICP-AES. Afterwards, two groups of centrifugation tubes were filled with 5 ml of clay suspension with 5 ml of solutions, so that pH values varied between 2.2 and 10.7. The ionic background was 0.05 mol l^{-1} $CaCl_2$ in each tube. 1 ml of Fe(II) solution was added in the tubes of one group. The added Fe(II) corresponded to 110 mmol kg^{-1} clay. Final clay content were 1.75 g l^{-1} for tubes without added Fe(II) and 1.52 g l^{-1} for tubes containing added Fe(II). The suspensions were allowed to further equilibrate for 24-hrs.

Experiment D. ^{57}Fe Mössbauer spectroscopy

The clay obtained after the dissolution step of experiment C was used in this experiment. ^{57}Fe(II) stock solution was prepared with the method developed in Tournassat et al. (Tournassat et al., submitted-a). Aliquots of clay suspension were mixed with ^{57}Fe(II) stock solution in tubes and equilibrated for 24-hrs at a given pH and in presence or absence of sodium dithionite, in the

O_2 free glove box. Full experimental conditions are given in Tab. 3.12 and as close as possible to the experimental conditions of sorption experiments. Then, the suspensions were filtrated (0.02 µm), deposited on Mössbauer sample holders and these holders were put in small carefully capped plastic boxes. The filtrated solutions were analyzed for Fe(II) by ICP-AES to quantify the ^{57}Fe sorption. The samples were then taken out of the glove box and immediately frozen in dryice, before being transported to Mössbauer facilities. There, samples were stored in liquid N_2. The smectite Mössbauer spectra were recorded at 77 K using a constant acceleration spectrometer and a ^{57}Co source diffused into a rhodium matrix. Velocity calibrations were made using α-Fe foil at 300 K. The hyperfine parameters were refined using a least-squared fitting procedure (program MOSFIT, Teillet and Varret).

Name of the sample	Equilibrium pH	Clay content ($g.l^{-1}$)	^{57}Fe sorbed amount ($mmol\ kg^{-1}$)	Added sodium dithionite
MX80_2.2	2.2	3.5	0	No
MX80_4.4	4.4	3.4	5.4	No
MX80_5.9+Dit	5.9	2.5	30.7	Yes 0.01 mol l^{-1}

Tab. 3.12 : Experimental conditions of Mössbauer samples preparation.

Experiment E. Fe(III) and Fe(II) sorption isotherms comparison

One iron sorption experiment was conducted in oxic condition to compare the Fe(III) and Fe(II) behaviors. Aliquots of Ca- conditioned MX80 stock suspension were mixed with $FeCl_3$ acidified solution in centrifugation tubes. The pH was adjusted with HCl and NaOH solutions in each tube. The experimental conditions were 0.95 $g_{clay}\ l^{-1}$, $CaCl_2$ = 0.05 mol l^{-1}, and $[Fe(III)]_{added}$ = 46 mmol kg^{-1}_{clay} = 44 µmol l^{-1}. The suspensions were allowed to equilibrate for 24-hrs and then, were centrifuged. The supernatants were filtered. Fe(III) concentrations were measured by ICP-AES and the final pH measured with a microelectrode.

RESULTS AND DISCUSSION

Surface complexation of Fe(II) on montmorillonite

Potentiometric titration of STx-1 and MX80 clay samples and solute Fe(II) concentration measured as a function of pH are presented in Figure 3.19 (experiments A and B). In each subfigure, data obtained in absence or presence of added Fe(II) are compared. Potentiometric titration data are presented as $\Delta\Delta[H^+]$ as a function of pH (Tournassat et al., submitted-c). As $\Delta\Delta[H^+]$ is a relative value and not an absolute one, the pH of the reference point where $\Delta\Delta[H^+]$ = 0 was set equal to pH ~2.5 (see Tournassat et al., submitted-b; Tournassat et al., submitted-c).

Both, Fe(II) solute concentration and potentiometric titration data are normalized to the amount of clay present in suspension, so that the results are expressed in mmol kg^{-1} clay.

As a first result, both types of clay sorb Fe(II) in the pH range from 3.5 to 7 and they depict a negative Fe(II) surface excess below pH 3.5 which may originate both from desorption or from dissolution. MX80 clay sample desorb (or dissolve) more Fe(II) than the STx-1 clay sample does. This can be related to the higher amount of Fe(II), in the MX80 structure or to the impurities more present in this clay material, than in the STx-1 clay (Mermut and Cano, 2001; Tournassat et al., submitted-c). The presence of added Fe(II) causes a discrepancy in the potentiometric titration curves, by decreasing the $\Delta\Delta[H^+]$ values while Fe(II) sorbs onto clay. This discrepancy corresponds to 2 or 3 times the amount of Fe(II) sorbed onto the clay. Thus each Fe(II) adsorbed lead to a release of 2 to 3 protons. The arrows in Figure 3.19 shows how to restore the potentiometric titration curves without added Fe(II) by subtracting the amount of sorbed Fe(II) from the $\Delta\Delta[H^+]$ value given in the potentiometric titration curve with Fe(II). Figure 3.20 exhibits the potentiometric curves without added Fe(II) together with the rebuilt potentiometric titration curves. For experiment A (MX80), the restoration is better by adding twice the amount of sorbed Fe(II), whereas for experiment B (STx-1), the restoration is better by adding three times the amount of sorbed Fe(II). Then, the sorption of one mole of Fe(II) leads to the desorption of two moles of H^+ for MX80. Hence, the clay edge charge is unaffected by sorption of Fe(II). This conclusion is also supported by results presented in Figure 3.21, where the Ca-CEC, plotted as a function of pH, is found not to be influenced by the presence of Fe(II). Then, as expected by the $[Ca^{2+}]/[Fe^{2+}]$ ratio previously in solution, Fe(II) must not sorb in exchange site position and the change of $\Delta\Delta[H^+]$ has no effect on this curve. However, we must note that the error bars extents are greater than the charge difference observed in Figure 3.19.

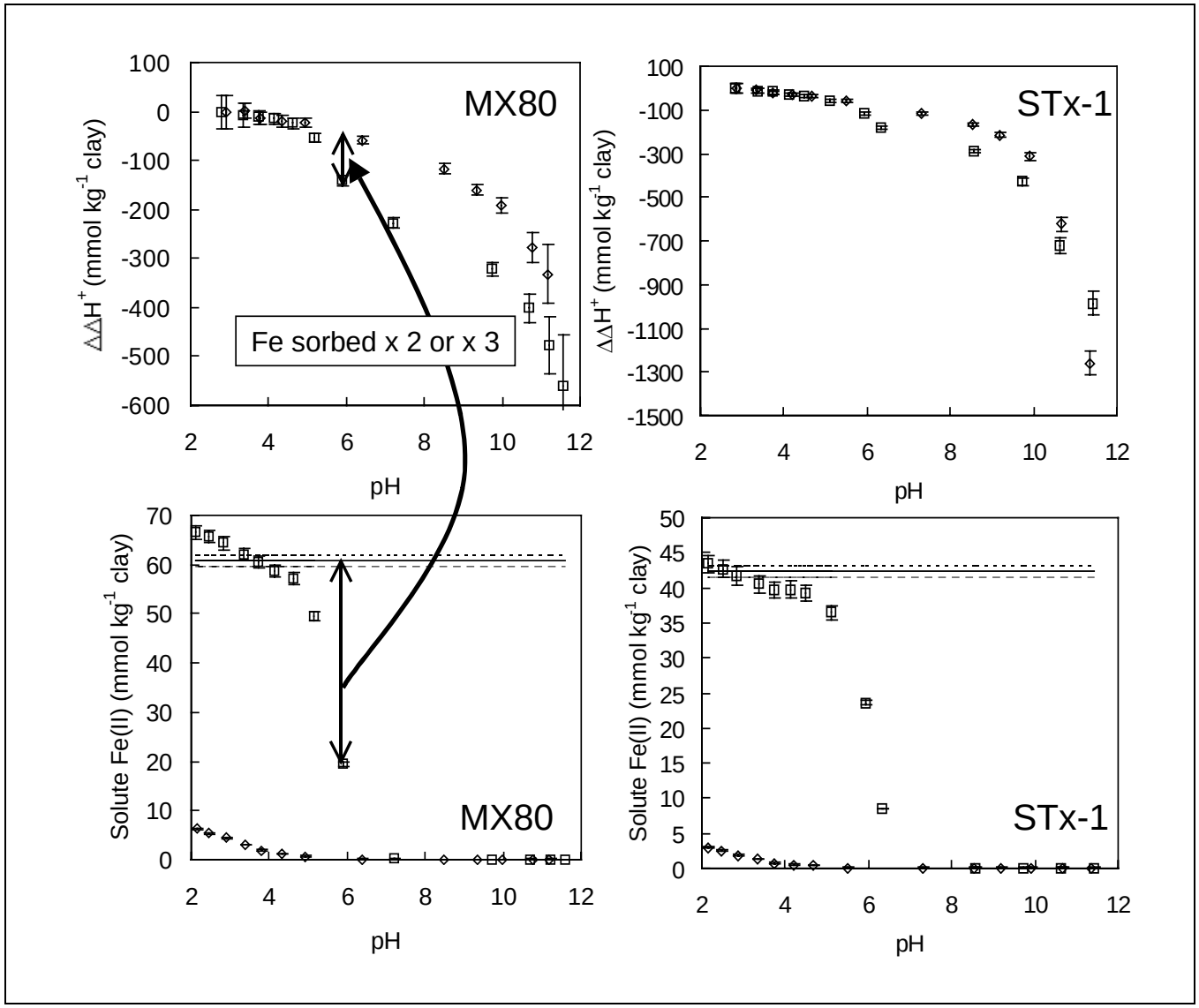


Figure 3.19 : Comparison of clay potentiometric backtitration experiments, with and without Fe(II) added in solution. $\Delta\Delta[H^+]$, the relative amount of H^+ adsorbed on the surface, is plotted as a function of pH. Left: experiment A, 1.41 g l^{-1} MX80, 0.05 mol l^{-1} $CaCl_2$. Right: experiment B, 2.03 g l^{-1} STx-1, 0.05 mol l^{-1} $CaCl_2$, added [Fe(II)] = 86 µmol l^{-1}. Top: Comparative backtitration results. Diamonds: experiments without added Fe(II). Squares: experiments with added Fe(II). Bottom: Fe(II) sorption/desorption data. Diamonds: experiments without added Fe(II). The continuous lines represent the amount of Fe(II) added. Dotted lines represent the error bar on this value. The arrows on the left part indicate how the potentiometric titration curve without added Fe(II) can be rebuild with the Fe(II) sorption curve (bottom part) and the potentiometric titration curve with added Fe(II).

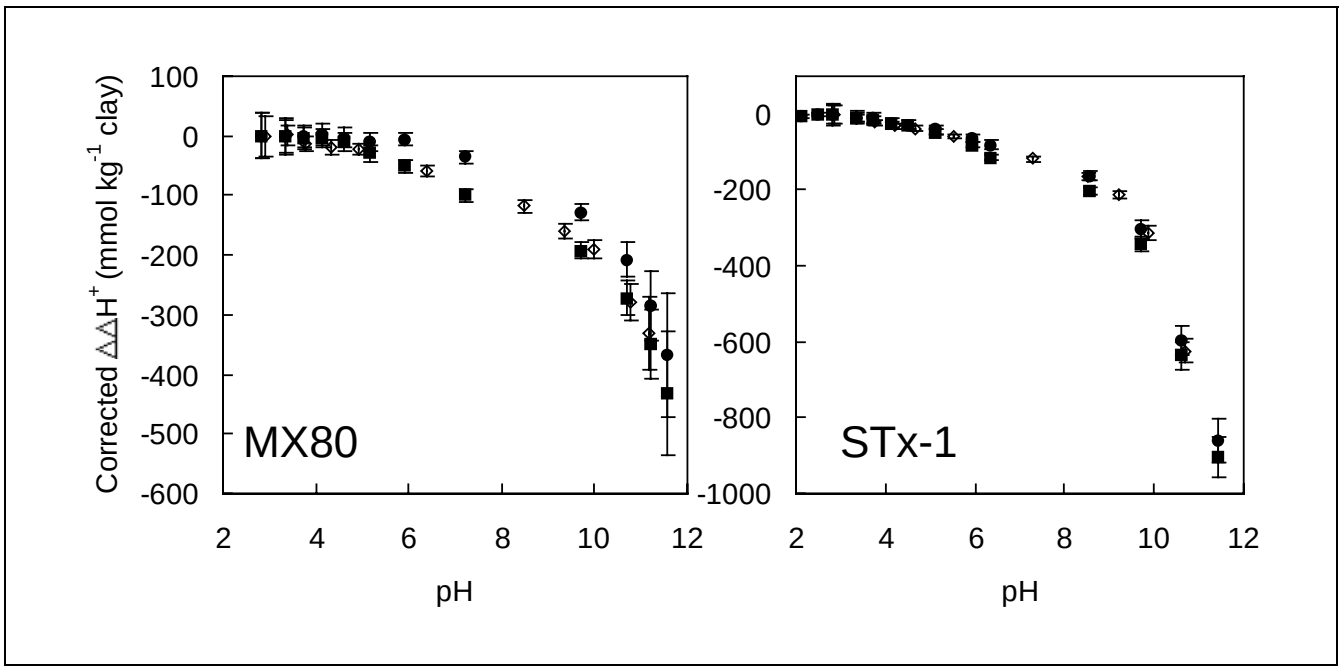


Figure 3.20 : Comparison of clay potentiometric backtitration data without Fe(II) added in solution (open diamonds), together with the curves rebuild with the method explained in figure 1. The corrections correspond to the addition of twice the amount of Fe(II) adsorbed (black squares) or three times this amount (black diamonds).

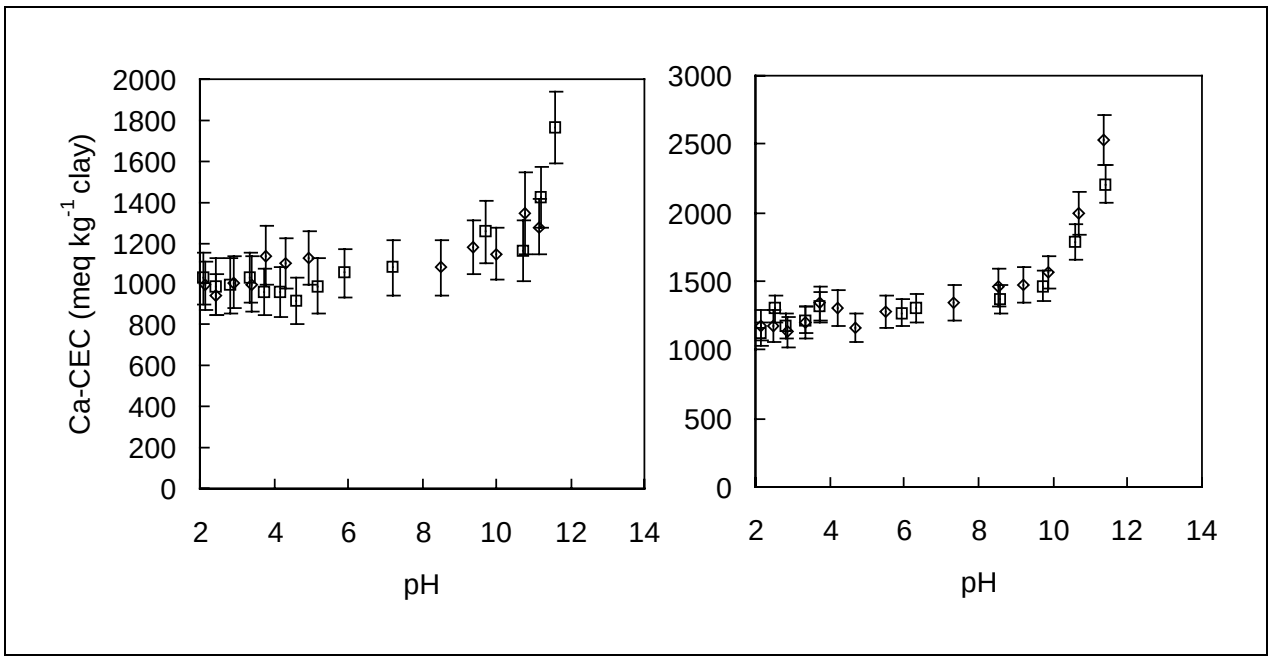


Figure 3.21 : Comparison of the Ca- CEC plotted as a function of pH, in experiments with (squares) and without (diamonds) addition of Fe(II). Left: experiment A, 1.41 g l^{-1} MX80, 0.05 mol l^{-1} $CaCl_2$. Right: experiment B, 2.03 g l^{-1} STx-1, 0.05 mol l^{-1} $CaCl_2$, added [Fe(II)] = 86 µmol l^{-1}.

Several Fe(II) edge sorption mechanisms can be proposed in agreement with the observed stoichiometry (Figure 3.22). Analytical chemistry studies give macroscopic results. Therefore we can not deduce from our results mechanisms at the atomic level. Several combinations of reactions 1 to 6 (Figure 3.21) could account for the experimental chemical result. However, the two moles of protons released by mole of Fe(II) adsorbed shows that the amount of proton sorption site should not be equivalent to the amount of metal sorption sites in the thermodynamic clay sorption model, *i.e.* pure monodentate complexes should be avoided in such models. This result is in agreement with spectroscopic results that show metal sorption on montmorillonite STx-1 to occur via double corner sharing linkage (Th sorption, Dähn et al., 2002a) or via edge sharing linkage with Al octahedrons plus corner sharing linkage with Si tetrahedron sorption (Ni(II), Dähn et al., 2002b). Figure 3.23 shows the great impact of monodentate (reaction 1 in Figure 3.22), vs. hydroxo- monodentate (reaction 2 in Figure 3.22), or bidentate (reaction 3 in Figure 3.22) complexes on the slope of the predicted adsorption edge. Then, we think that sorption model should not consider only monodentate complexes as done previously (e.g. Zachara and Smith, 1994; Bradbury and Baeyens, 1997) and that the net sorbed metal / released H^+ mole ratio should be measured together with metal sorption data to constrain the model.

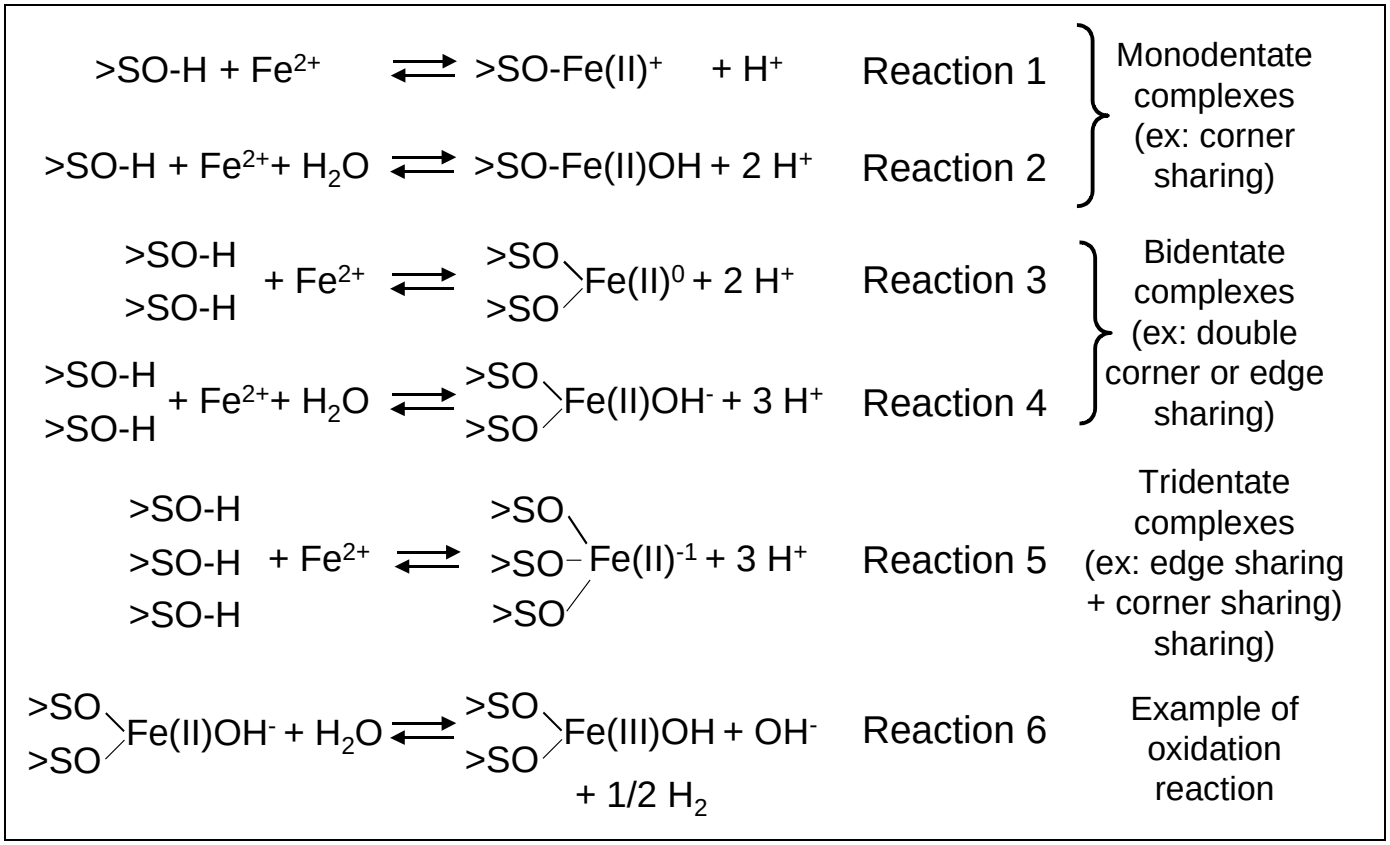


Figure 3.22 : Comparison of some possible quantitative sorption mechanisms and their H^+ stoichiometry.

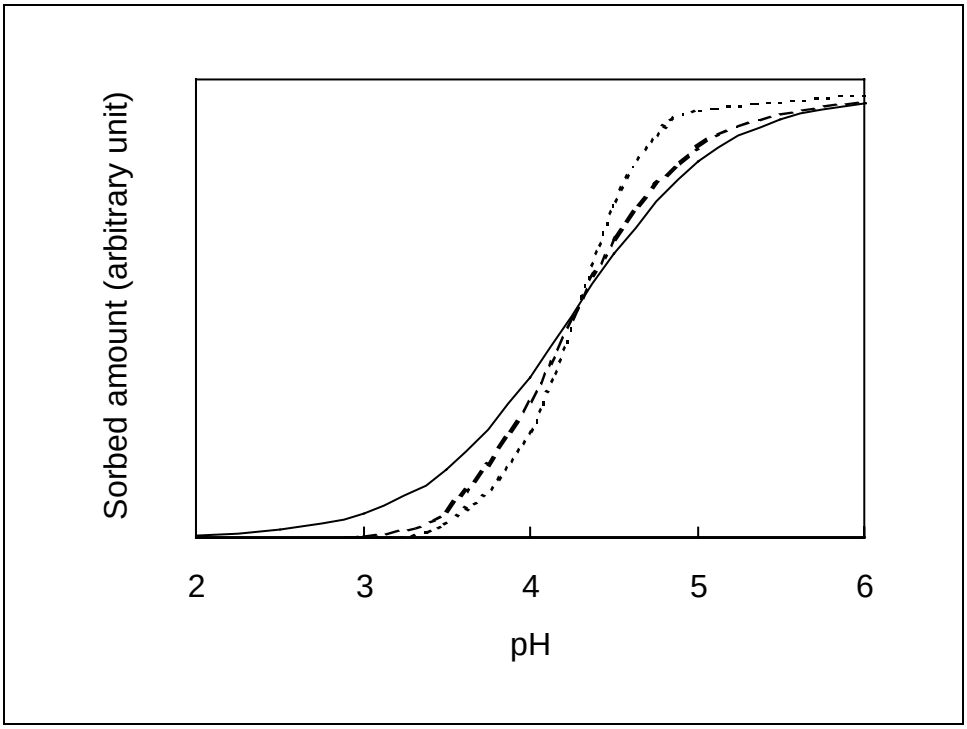


Figure 3.23 : Effect of the complex considered in a sorption model on a hypothetical sorption simulation. Full line: monodentate complex (reaction 1 in Figure 3.22). Dotted line: monodentate hydroxo- complex (reaction 2 in Figure 3.22). Dashed line: bidentate complex (reaction 3 in Figure 3.22)

Whatever the model used to simulate the Fe(II) sorption data, it shows that Fe(II) has a very high affinity for clay edge surfaces (log $K_{Fe(II)}$ = 5.0 , to be compared to log $K_{Zn(II)}$ = 1.6, Tournassat and Charlet, submitted) since sorption start, at least, at pH 4 in these experiments. One should question the origin of this high affinity.

Causes of montmorillonite high affinity for Fe^{2+}

Structural fit

Figure 3.24 shows clearly that Fe(II) is able to replace Mg(II) and not only previously sorbed Zn(II) in the competition experiment designed by Tournassat and Charlet (Tournassat and Charlet, submitted). Hence, the high affinity of montmorillonite for Fe^{2+} (more than three orders of magnitude larger than for Zn(II) or Ni(II), Tournassat and Charlet, submitted) could originate from a structural fit of Fe(II) in Mg(II) edge sites. However, in octahedral environment, the effective ionic radius of Fe^{2+},0.780 Å, is larger than the effective ionic radius of Mg^{2+}, 0.720 Å (Shannon, 1976). For comparison the effective ionic radii of Al^{3+} and Fe^{3+} are equal to 0.535 Å and 0.645 Å respectively (Shannon, 1976) in octahedral environment. Then, Fe^{2+} should misfit the structure more than Mg^{2+} does, unless it were oxidized.

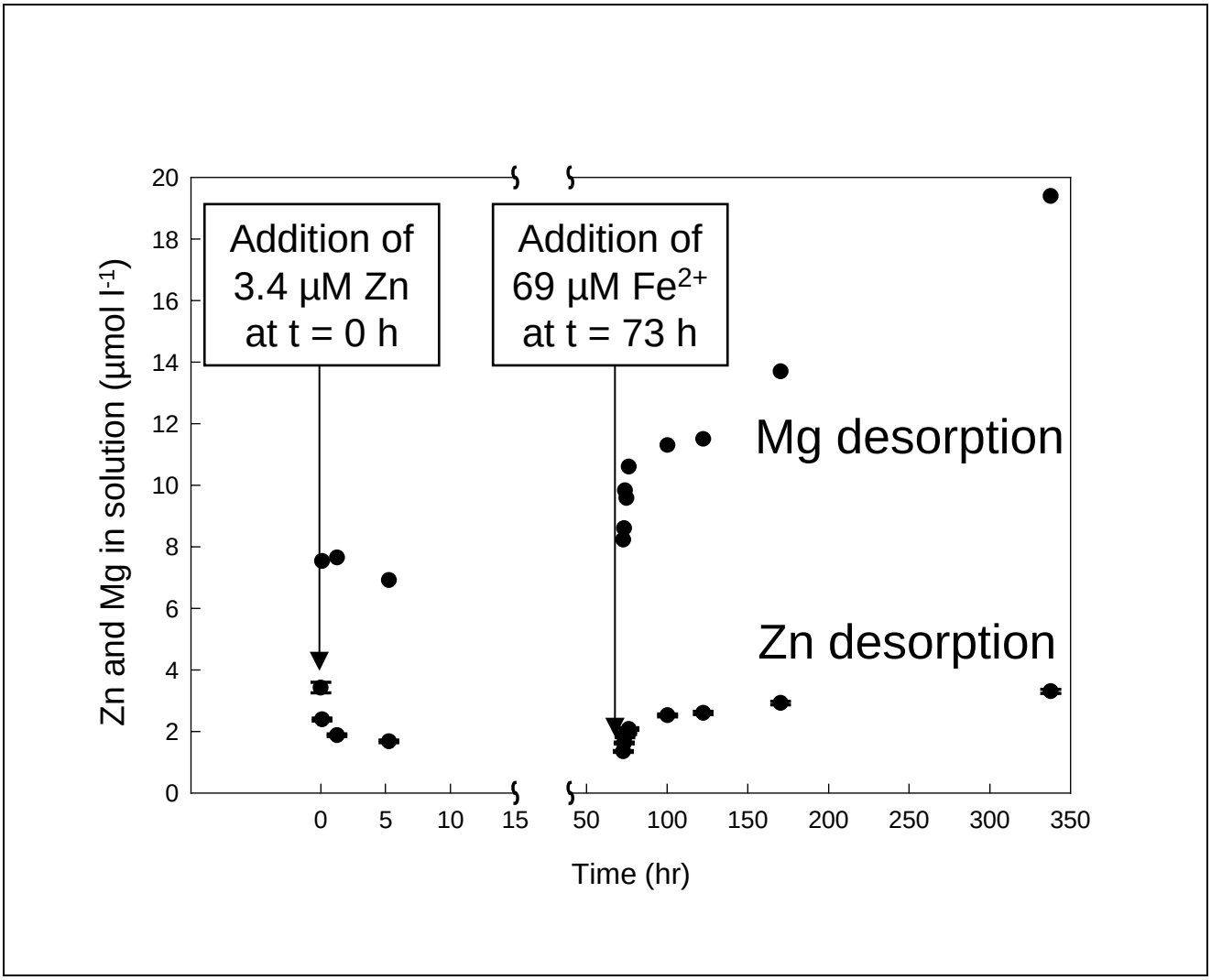


Figure 3.24 : Mg and Zn desorptions as a function of time in a Fe(II)-Zn(II) competition experiments on montmorillonite MX80, at pH 5.82, by adding 3.4 µM Zn(II) at t = 0 hrs and 69 µM Fe(II) at t = 73 hrs to a 4.35 g L^{-1} and 0.05 M $CaCl_2$ clay suspension (Tournassat and Charlet, submitted).

Oxidation of sorbed Fe^{2+}

^{57}Fe Mössbauer spectroscopy results are shown on Figure 3.25, and the associated hyperfine parameters are shown in Tab. 3.13. In addition to the expected quadrupolar doublets of Fe(III) and Fe(II), the MX80_4.4 sample spectrum exhibits a magnetic sextet with broadened lines. This magnetic sextet was already observed on montmorillonite MX80 by Tournassat et al. (Tournassat et al., submitted-c) and was attributed to remaining iron oxides. This magnetic sextet is not retrieved in MX80_2.2 sample spectrum, although MX80_4.4 sample was prepared by (i) adding ^{57}Fe to the same suspension as used for MX80_2.2 sample preparation and (ii) increasing pH to 4.4 value. Nevertheless, the poorly defined baseline of MX80_2.2 sample spectrum may contain this magnetic sextet. In this experiment, we attempted to measure the ^{57}Fe(II) / (^{57}Fe(III) + ^{57}Fe(II)) ratio. The fitting models, consist in two or three main quadrupolar doublets attributed to Fe(II) and Fe(III) surface species. For sample MX80_4.4 a magnetic sextet was attributed to iron oxides. It is clear that other fitting models can be proposed, *e.g.* with additional quadrupolar components but a sensibility analysis on the Fe(II) / Fe(III) + Fe(II) ratio value showed that this value remains almost constant whatever the model. In Tab. 3.14, the percentage of ^{57}Fe(II) in the samples is compared to the expected percentages in case of

total or no oxidation of added $^{57}Fe(II)$. Though all care was taken in the procedure to avoid O_2, it is clear that most of sorbed Fe(II) oxidizes into Fe(III). This oxidation is partial at pH 4.4 and complete at pH 5.9, even in presence of 0.01 mol l^{-1} sodium dithionite. Since the Fe(III) contribution to Mössbauer spectra are quadrupolar peaks, the $^{57}Fe(III)$ atom ions did not polymerize. Otherwise, paramagnetic or magnetic features should have been measured. Then, $^{57}Fe(III)$ atoms are dispersed on the clay surface. This results is in agreement with a sorption of single Fe(II) ions followed by an oxidation step. The nature of the oxidant is unknown. One can imagine that water or structural Fe(III) may oxidize the Fe(II) sorbed on the edges. For instance, Gournis et al. showed that clay edge surfaces can catalyze the formation of hydroxyl radicals, and thus the oxidation of surface iron, and that the yield of hydroxyl radicals depends on the clay lattice iron (Gournis et al., 2002). In the present Mössbauer spectroscopy experiments, the maximum amount of sorbed $^{57}Fe(II)$ was 30.7 mmol kg^{-1}, whereas the clay contains about 350 mmol Fe(III) kg^{-1}. Hence, the electron transfer between structural Fe(III) and Fe(II) atoms sorbed onto clay edges may be responsible for our Mössbauer results.

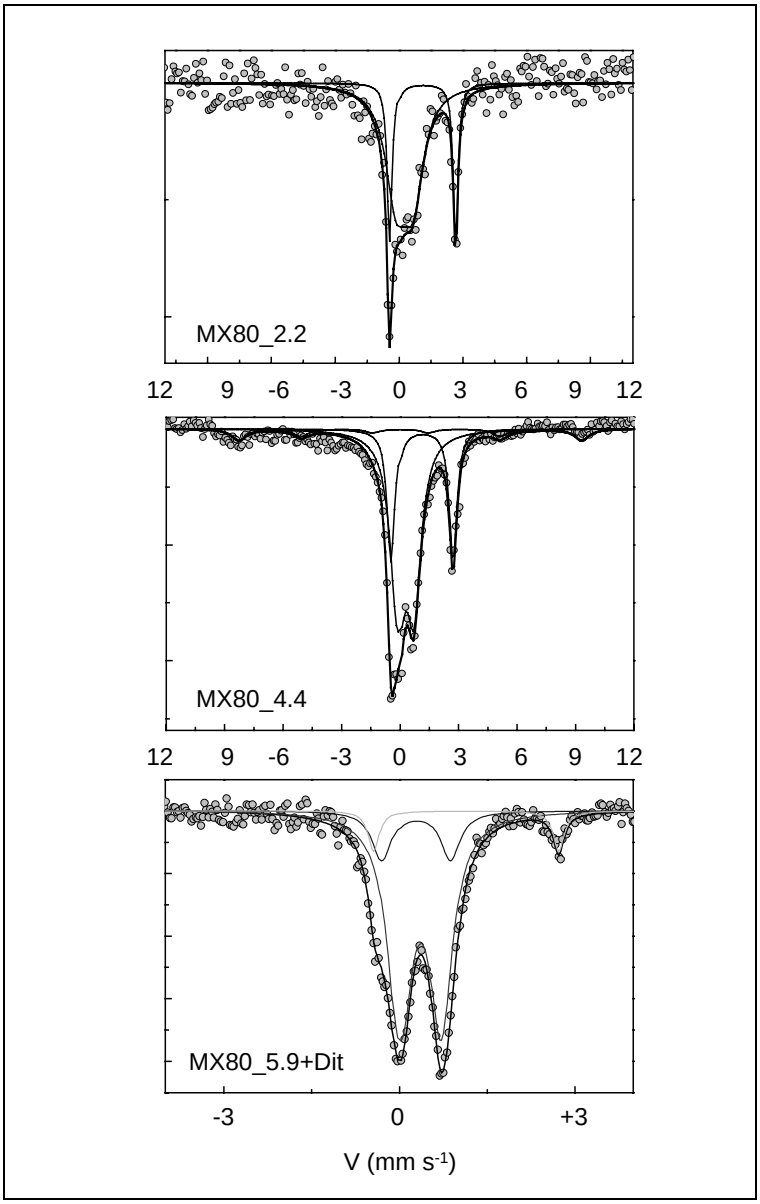


Figure 3.25 : Dots: 77 K Mössbauer spectra of the MX80_2.2 (top), MX80_4.4 (middle) and MX80_5.9Dit (bottom) samples. Thin lines: decomposition of the spectrum. Thick line: sum of all the contributions of the decomposition. The experimental conditions of the sample preparation are given in Tab. 3.12 and the parameters of the decomposition are given in Tab. 3.13.

Sample	*Contribution*	*I.S.* *mm s^{-1}*	*Γ* *mm s^{-1}*	*Q.S. or2ε* *mm s^{-1}*	*H_{hyp}* *T*	*%*
MX80_2.2	Fe(II)	1.27	0.27	3.02		27%
	Fe(III)	0.43	1.20	0.73		73%
MX80_4.4	Fe(II)	1.28	0.47	3.10		28%
	Fe(III)	0.44	0.87	0.76		64%
	Magnetic sextet	0.44	0.90	0.49	54.4	9%
MX80_5.9Dit	Fe(II)	1.27	0.23	3.13		7%
	Fe(III) A	0.48	0.47	0.69		78%
	Fe(III) B	0.41	0.39	1.15		15%

I.S. = isomer shift; *Γ* = linewidth; *Q.S.* = quadrupolar splitting value; *2ε* = quadrupolar shift value, *H_{hyp}* = hyperfine field value, *%* = ratio of each component.

Tab. 3.13 : Mössbauer parameters of the samples listed in Tab. 3.12.

Name of the sample	Measured $\%_{Fe(II)}$	$\%_{Fe(II)}$ in case of total oxidation	$\%_{Fe(II)}$ in case of no oxidation
MX80_2.2	27 %	27 %	27 %
MX80_4.4	28 %	17 %	54 %
MX80_5.9+Dit	7 %	6 %	83 %

Tab. 3.14 : Comparison of measured Fe(II) percentage in Mössbauer samples with predicted percentages based on total or no oxidation of added ^{57}Fe(II).

The Fe(III) sorption isotherm as a function of pH (Figure 3.26) shows that Fe^{3+} can sorb on clay edges with a high affinity, since Fe(III) sorb at almost two pH units below Fe(II). Hence, the high affinity of clay for Fe^{2+} may indeed originate both from the possibility to transform Fe^{2+} into Fe^{3+} by a two steps – sorption + oxidation – process and the Fe^{3+} structural fit and thus high affinity for the structure.

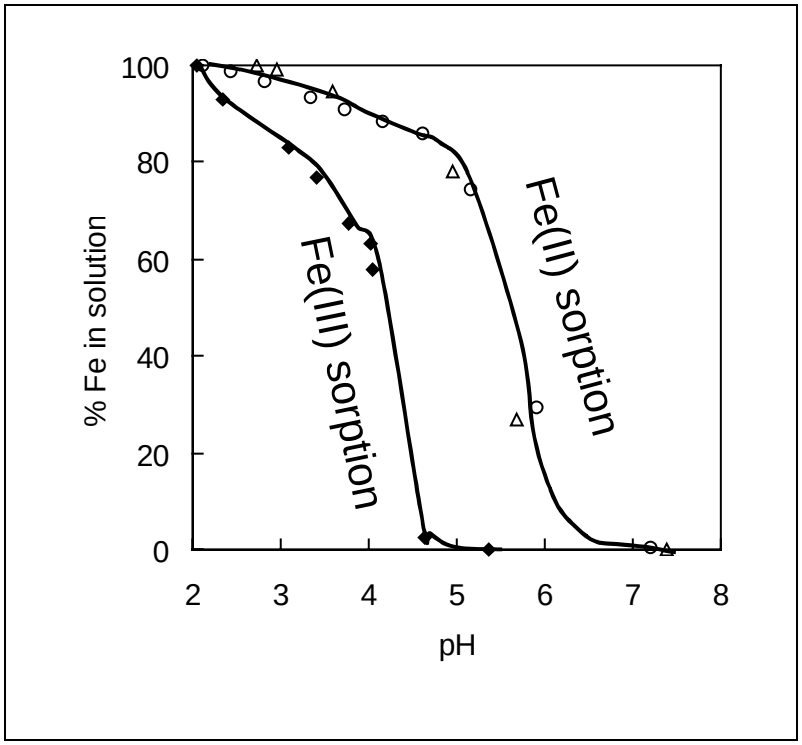


Figure 3.26 : Comparison of Fe(III) sorption isotherms (experiment E, 0.95 g_{clay} l^{-1}, 0.05 mol l^{-1} $CaCl_2$, and $[Fe(III)]_{added}$ = 46 mmol kg^{-1} $_{clay}$ = 44 µmol l^{-1}) and Fe(II) sorption isotherms (experiments A and C). The lines are drawn as eyes guidelines.

Reversibility

Once Fe(II) was sorbed (and transformed into Fe(III)), desorption / dissolution experiments, were performed by decreasing the pH to test the reversibility of the overall sorption process. At variance with what is expected from Mössbauer results, it was possible to retrieve all sorbed iron after less than one day at pH 1.5 – 2 (data not shown). All this iron was retrieved as Fe(II) as shown by both O-phenantrolin (Rodier, 1996) and ferrozin (Viollier et al., 2000) methods. Nevertheless, no data is available to attribute this released Fe(II) to previously adsorbed Fe(II) or to structural Fe(II) / reduced structural Fe(III). Then, we can just say that the Fe(II) sorption plus oxidation process is quantitatively an apparent reversible process.

Clay dissolution and precipitation of Fe-Si new phase

Time-limited dissolution at various pH (experiment A and B)

Figure 3.27 exhibits the effect of added Fe(II) on the solute Si concentration as a function of pH. Results are plotted in mmol kg^{-1} clay. A great discrepancy exists between experiment A (MX80) and B (STx-1). The increase of Si concentration, with increasing pH, starts at pH value equal to approximately 7 for MX80, and approximately 5 for STx-1. We attribute this difference to the presence of large amounts of fine grained silica impurities in STx-1 clay sample. Both quartz and cristobalite are present as impurities in the conditioned clay material. Hence, the solute Si concentrations are compared with quartz and cristobalite(s) equilibrium concentrations. These concentrations are also expressed in mmol kg^{-1}. Two different equilibrium constants for cristobalite, *i.e.* with α- cristobalite and β- cristobalite, are reported in Figure 3.27. At low pH (< 5), the solute Si concentrations are lower than those given by equilibrium with the silica phases and the addition of Fe(II) has no influence. This result denotes that silica dissolves with a too slow kinetics at these pH values to control the concentration in solution and that

montmorillonite dissolution equilibrium constant controls the Si concentration in acid pH range. In the pH range values 5 – 8.5, no effect of added Fe(II) on Si solute concentration is measured but discrepancies exist between experiments A (MX80) and B (STx-1). In case of MX80 clay sample, the solute Si concentration seems to be limited by kinetics and equilibrium with quartz, whereas in cases of STx-1 clay sample, quartz equilibrium does not limit the Si concentration. At pH value 8.5, almost 190 mmol Si per kg of clay dissolved in the STx-1 suspension. It represents 11 g of dissolved SiO_2 per kg of clay. Above pH 8.5, discrepancies exist between experiments A and B and within these experiments as a function of added Fe(II). From pH 8.5 to 10, in experiment A, without added Fe(II), solute Si concentration is limited by the equilibrium with quartz. Beyond, and in both cases, Si concentration is controlled by the precipitation of a Ca-Si phase (Tournassat et al., submitted-c). In presence of added Fe(II), the solute Si concentrations decrease. By applying the same method than shown on Figure 3.19 for potentiometric titration curves, we restore the Fe(II) free Si concentration curve, by adding once (or twice) the amount of sorbed Fe(II) to the amount of Si in solution (arrows in Figure 3.27, left). In experiment B run in presence of added Fe(II), the solute Si concentrations is lower, between pH 8.5 and pH 10.5, compared to Fe(II) free experiment B. We can restore the Si concentration curve, obtained without Fe(II), by adding twice the amount of sorbed Fe(II) to the amount of Si in solution (arrows in Figure 3.27, right). The Si concentration of the last point of experiment B, considered together with the increase of Ca- CEC (Figure 3.21) is clearly influenced by the precipitation of a Ca-Si phase (Tournassat et al., submitted-c).

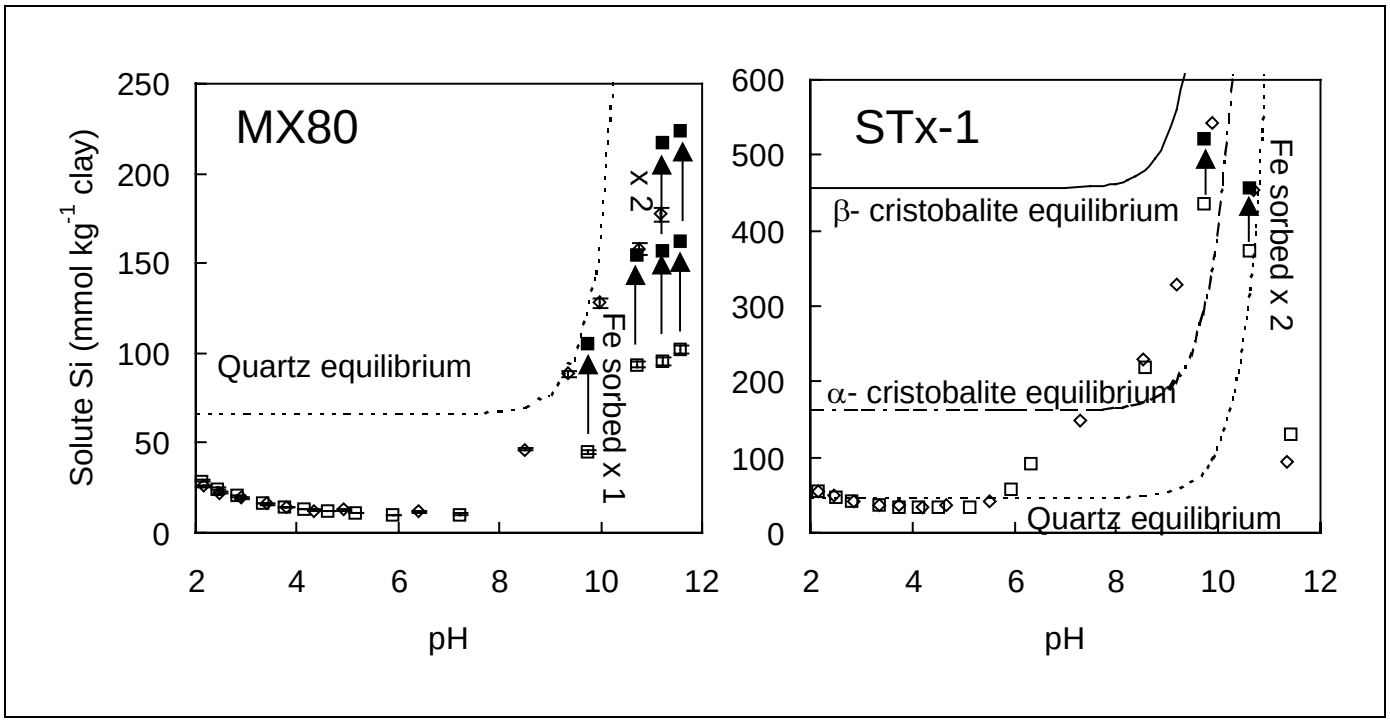


Figure 3.27 : Si concentrations in solution as a function of pH in experiments A (left) and B (right), presented in mmol kg^{-1} clay. Experimental conditions: 0.05 mol l^{-1} $CaCl_2$, clay content: 1.41 g l^{-1} (experiment A) and 2.03 g l^{-1} (experiment B), added [Fe(II)] = 86 µmol l^{-1} (experiments A and B). Open diamonds: experiments without added Fe(II); Open squares: experiments with added Fe(II). The black square and arrows indicate a correction of once (× 1) the value of sorbed Fe(II) (left) or twice (× 2) this amount (right) as explained for Figure 3.19. Equilibrium concentration of Quartz and cristobalite phases are plotted as mmol kg^{-1} clay as a function of pH. α- and β- cristobalite refers to two equilibria listed in the LInl.dat thermodynamic database.

As a conclusion, at even higher pH than the Ca – Si tobermorite like phase precipitates, a Fe – Si containing phase should precipitate, with Si/Fe molar ration varying between 1 and 2 . At low pH, there is no or little influence of the presence of sorbed Fe(II) on the Si concentration. The results, exhibited on Figure 3.28, show that there is no influence of added Fe(II) on Al and Mg concentrations. Hence the addition of Fe(II) has no influence on the montmorillonite dissolution at low pH. This results is at variance with the effect of Zn or Co on the dissolution rate of hectorite, a trioctahedral smectite (Schlegel et al., 1999; Schlegel, 2000; Schlegel et al., 2001a; Schlegel et al., 2001b). Hectorite dissolution starts to be significant below pH 7 (Schlegel, 2000), while the montmorillonite dissolution is significant only below pH 4 (Figure 3.27 and Figure 3.28). For instance, Zn can sorb specifically on hectorite edge surface at high surface coverage (~45 mmol kg^{-1}, Schlegel, 2000) at pH 6.5, i.e. in pH condition where it can affect hectorite dissolution. With montmorillonite, below pH 4, the amount of sorbed Fe(II) is too low to have a sufficient surface coverage (Figure 3.19) and thus to have a significant effect on the dissolution kinetics. At pH higher than 4, Fe(II) sorbs significantly onto montmorillonite edges but the montmorillonite dissolution kinetics is so slow that no effect of added Fe(II) can be measured.

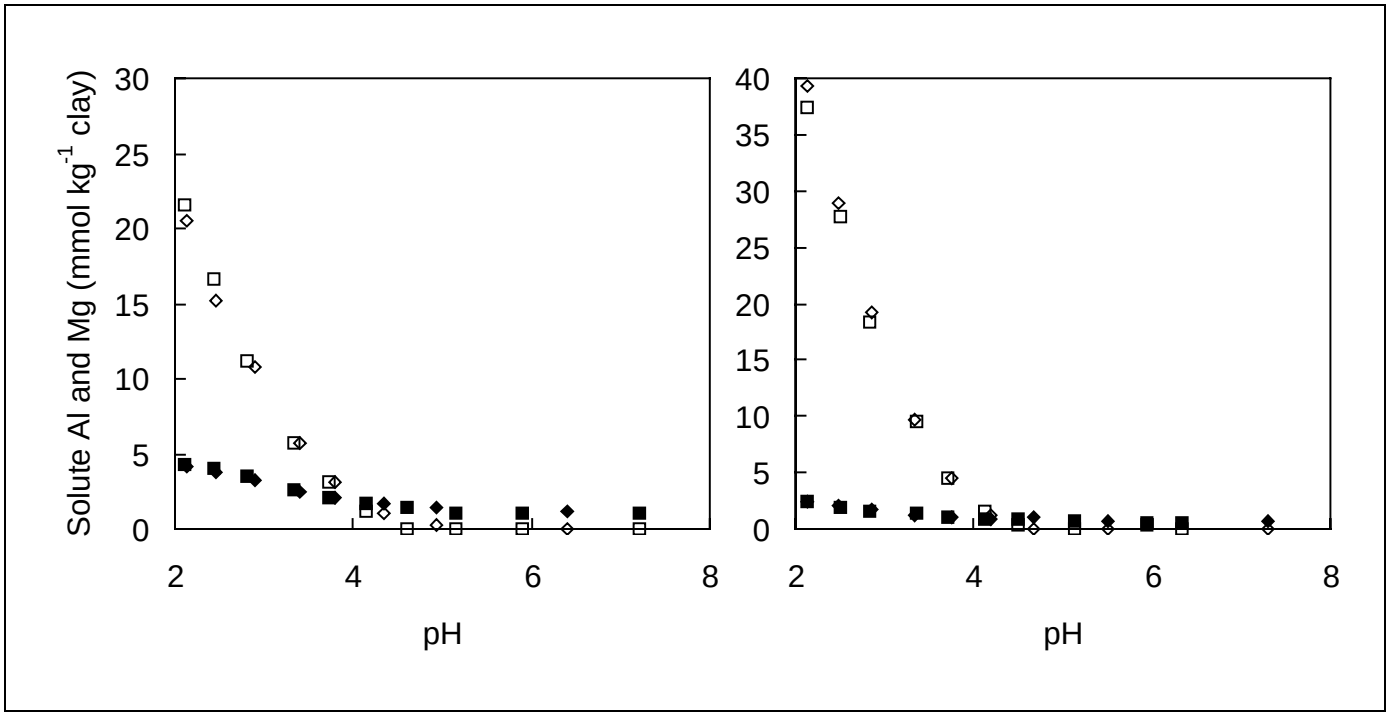


Figure 3.28 : Al (open symbols) and Mg (filled symbols) concentrations in solution as a function of pH in experiments A (left) and B (right), presented in mmol kg^{-1} clay. Experimental conditions: 0.05 mol l^{-1} $CaCl_2$, clay content: 1.41 g l^{-1} (experiment A) and 2.03 g l^{-1} (experiment B), added [Fe(II)] = 86 µmol l^{-1} (experiments A and B)Diamonds: experiments without added Fe(II); Squares: experiments with added Fe(II).

Dissolution at fixed acid pH (experiment C)

Figure 3.29A presents the results of the MX80 montmorillonite dissolution experiment performed at pH 2.1 for Si, Al, Fe and Mg in µmol l^{-1} as a function of time. After a rapid initial

dissolution, the clay seems to dissolve afterwards with an almost constant dissolution rate, *i.e.* steady state is reached after ~5 days. Figure 3.29B was build by applying the following formula:

$$Corrected\ concentration = (C^{Me} - C^{Me}{}_{init}) \times r^{Si/Me} \qquad \text{in µmol l}^{-1} \qquad [2]$$

where C^{Me} is the concentration of element Me, $C^{Me}{}_{init}$ is the concentration of element Me at the first experimental point and $r^{Si/Me}$ is the structural Si to Me ratio. For Si, $r^{Si/Si}$ is equal to 1, for Al $r^{Si/Al}$ is equal to 3.98/1.63 = 2.44, and so on… This Figure 3.29B is built to see if the clay dissolves congruently or not. In case of congruent dissolution, all experimental points should be on the same curve. Figure 3.29B shows that Si and Al dissolve congruently. This result is in agreement with the dissolution mechanism of hectorite and nontronite at low pH, which was found to take place on the edge surfaces (Bosbach et al., 2000; Bickmore et al., 2001). Mg(II) and Fe(II) concentrations are not congruent with the structural formula. This result may be explained by (i) the dissolution of iron oxide remaining phases as shown in Mössbauer spectrum (see above section) and (ii) the subsequent replacement of Mg^{2+} by Fe^{2+} (eventually oxidized, see section above) on clay edges. This result confirms also that Fe^{2+} can sorb on clay edges at very low pH, the increase of Fe^{2+} concentration being controlled by the kinetics of the Fe^{2+} adsorption and the kinetics of iron oxide phase dissolution.

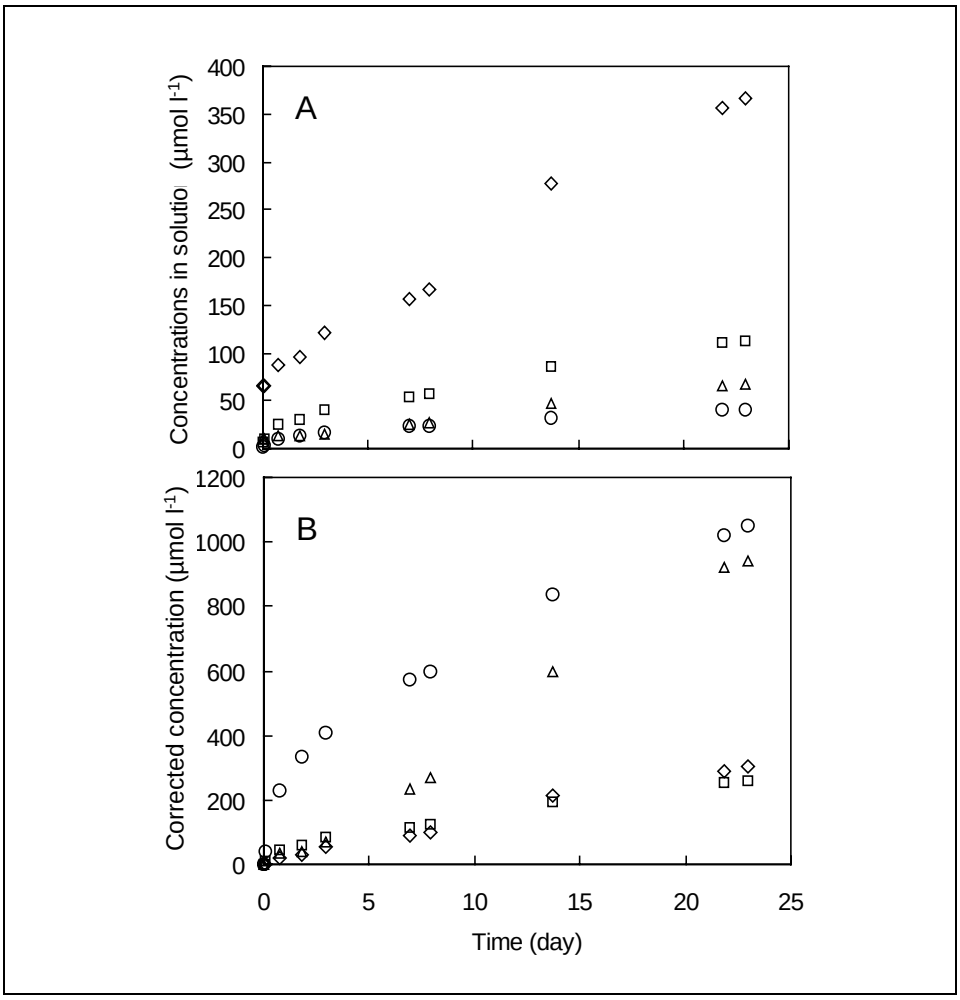


Figure 3.29 : Dissolution experiment as a function of time at fixed low pH of a MX80 clay suspension: 3.6 g clay l^{-1}, 0.05 mol l^{-1} $CaCl_2$ + 1.5 mmol l^{-1} sodium dithionite, pH = 2.1. A: original data. Si (diamonds), Al (squares) Fe (circles) and Mg (triangles) concentrations in solution . B: Si (diamonds), Al (squares) Fe (circles) and Mg (triangles) corrected concentrations in solution as a function of time in dissolution experiment C. The correction corresponds to the

multiplication of the metal concentration by the Si/Metal ratio of the clay structural formula (see text for details).

Si, Al, Mg and Fe titration after etching (experiment C)

Once completed the pH 2.1 dissolution step, aliquots of suspension were titrated up to pH 11 and the readsorption of various solutes was followed. The results are presented in Figure 3.30, in term of "sorbed" amounts in mmol kg^{-1}_{clay}, calculated as follows:

$$Sorbed\ amount(Me) = \frac{C^{Me}{}_0 - C^{Me}}{\rho} \qquad [3]$$

where $C^{Me}{}_0$ is the total initial amount of element Me given by the last point of the pH 2.1 dissolution experiment (t = 0 for the present experiment) and the subsequent dilution (5 ml diluted in 10 or 11 ml). Positive values indicate that a given element has sorbed or precipitated during the 24-hrs experiment, whereas negative values indicate that the given element dissolved.

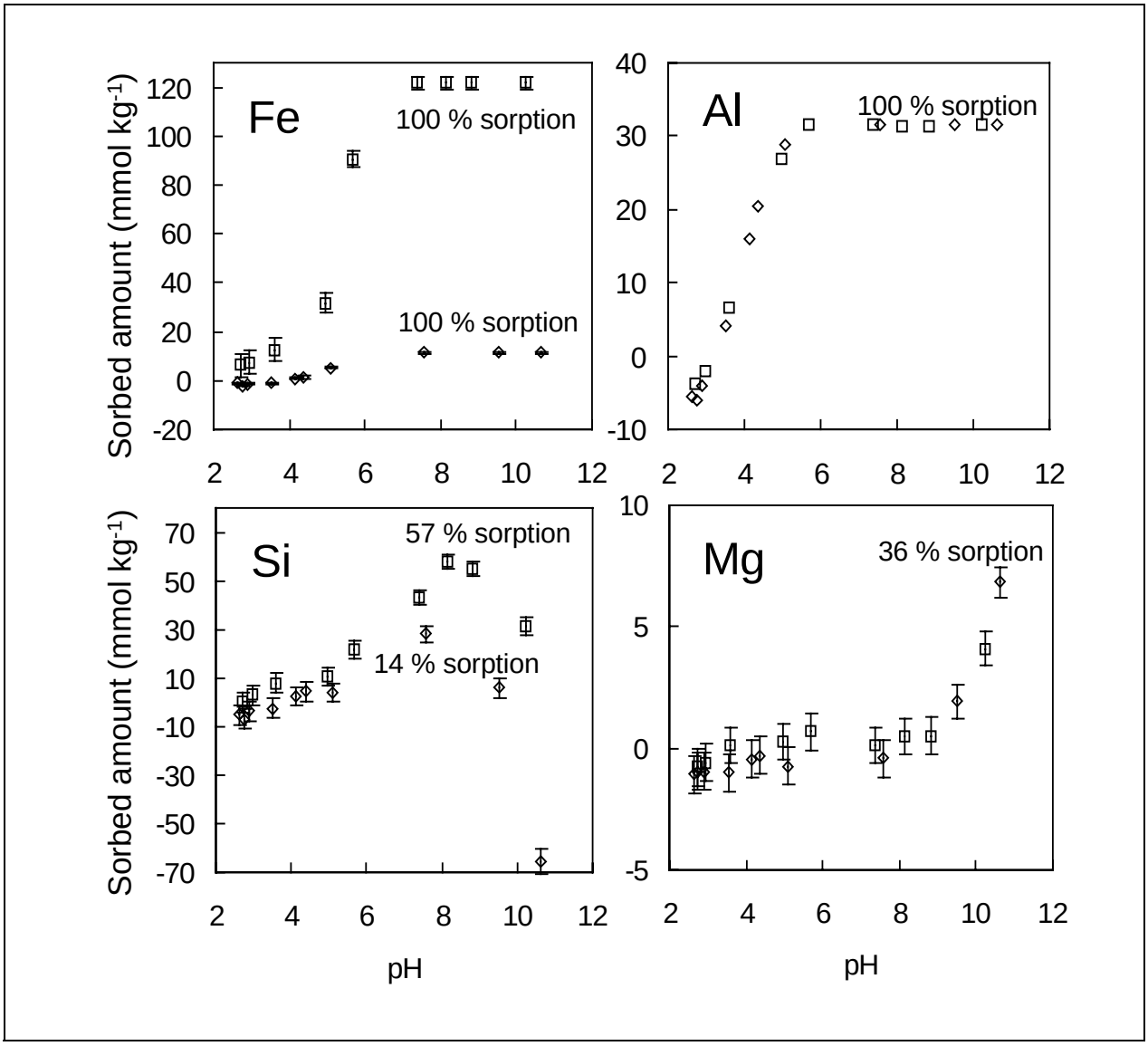


Figure 3.30 : Readsorption experiment in tubes as a function of pH. Experimental conditions: 0.05 mol l^{-1} $CaCl_2$, 1.75 (without added Fe(II)) or 1.52 (with added Fe(II)) g_{clay} l^{-1}, added [Fe(II)] = 175 µmol l^{-1}. Si, Al, Fe and Mg sorbed amounts are plotted as a function of pH. Diamonds: experiment without added Fe(II). Squares: experiment with added Fe(II). The percentages correspond to the maximum sorption data points.

Without added Fe(II) and below pH value of 3.5, Si, Al, Fe and Mg depict a net negative surface excess via desorption or dissolution. Above a pH value of 3.5, Al is adsorbed onto the montmorillonite as previously observed by Charlet et al. (Charlet et al., 1993) and is not influenced by the addition of Fe(II) and its adsorption. Since the sorption of Al occurs in the same pH range than the sorption of Fe(II), this result shows that there is no competitive sorption effect between Fe(II) and Al(III). Then, either sorption site are present in sufficient amount in order not to have competition between the two sorbing species, or Fe(II) and Al(III) do not sorb on the same sites.

Mg is weakly adsorbed above pH 9.5 and is not influenced by the presence of added Fe(II). Since Fe(II) has been shown to be able to displace Mg(II) from the clay, this result indicates that Mg(II) should be readsorbed on a site different from one it desorbed from.

The Si case is different. On the one hand, one should expect Si concentration to increase with pH because equilibrium is not attained with respect to the various silica phases. On the other hand, spectroscopic results showed that the sorption of metal on clay minerals can lead to the neoformation of a clay-like phase, i.e. to the coadsorption of aqueous silica and metal ion (Manceau et al., 1999; Schlegel, 2000; Schlegel et al., 2001b; Dähn et al., 2002b). Silica acid adsorption is typical of a species which deprotonates at high pH (pK_{a1} = 9.83): adsorption increase up to the pK and then decreases, as observed previously in silicic acid adsorption on goethite (Stumm et al., 1980). Indeed, in absence of added Fe(II), Si adsorption increases from pH 5 to 9.5, to decrease afterwards, i.e. when pH gets close to pK_{a1}. We also note that, at pH 8, the sorbed amount of Si is equal to the sorbed amount of Al, i.e. equal to ~30 mmol kg^{-1} clay (14 % of the initial Si in solution) and that the Si and Fe adsorption curves match each other quite well (Figure 3.31, top). In presence of Fe(II), the sorption of Si at low pH is enhanced and at pH ~8.5, 56 % initial Si is sorbed. Figure 3.31 shows that the readsorption of Si at low pH seems to be correlated to the sorption of Fe(II). The presence of Fe(II) prevents also net desorption/dissolution processes up to pH 10.2.

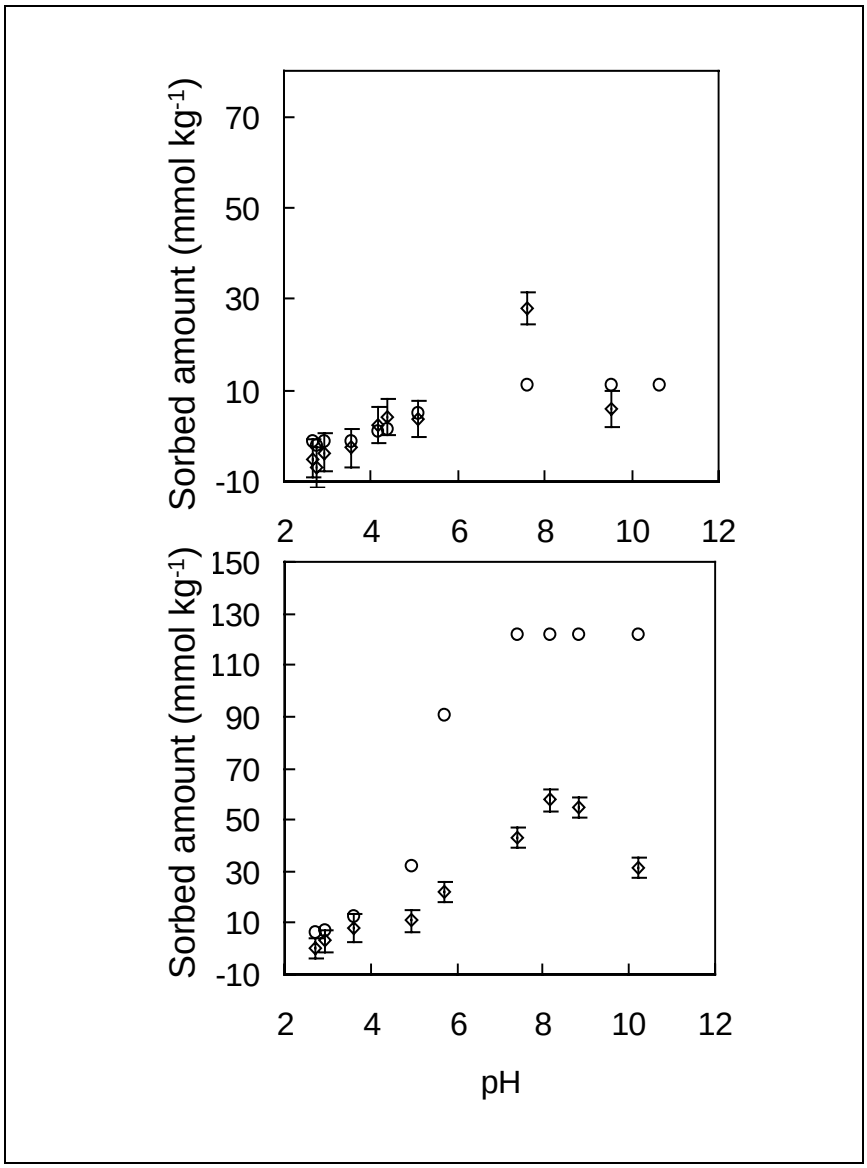


Figure 3.31 : Comparisons of Si (diamonds) and Fe(II) (circles) sorption curves as a function of pH in readsorption experiments. Experimental conditions: 0.05 mol l^{-1} $CaCl_2$, 1.75 (without added Fe(II)) or 1.52 (with added Fe(II)) g_{clay} l^{-1}, added [Fe(II)] = 175 µmol l^{-1}. Top: experiment without added Fe(II). Bottom: experiment with added Fe(II).

These result stand in apparent contradiction with the results of experiments A and B that showed that there is no effect of the presence of Fe(II) on the Si concentration below pH 8.5, when no preliminary dissolution reaction step at low pH was imposed. The simplest way to explain these results is to consider that at low pH, the Si concentration is controlled by the clay phase dissolution equilibrium. In experiment C, after a dissolution step at low pH, the increase of pH leads either to the precipitation of an Al-Fe-Si clay-like phase, or to the sorption of these elements to the clay present in suspension and reconstruction of the clay phase, *i.e.* surface precipitation. We think that the second mechanism is more probable in our experiment, since Al and Fe "sorb" prior to Si, as a function of pH. Since Fe was shown to displace Mg(II) from the clay structure and therefore to be adsorbed on the clay edges, this analytical chemistry experiment could be considered as an evidence of surface precipitation. In experiment A and B, the Si concentration was at equilibrium with the clay at near neutral pH and the added concentration of Fe(II) was not sufficient to increase sufficiently the ion activity product corresponding to the precipitation of the clay, and then to lead to the "sorption" of Si. In experiment C, after increasing pH, the Si concentration was too high with regards to the equilibrium with clay and the added Fe(II) concentration enhanced the precipitation by increasing the ion activity product.

In experiment C, the amount of "sorbed" Si together with Fe(II) represents only 20 % of the total amount of sorbed Fe(II). Then, only part of Fe(II) must sorb on clay surfaces together with Si (cooperative sorption) and the other part must sorb without Si (replacement of Mg^{2+} in the lattice or adsorption plus oxidation mechanism). Then, this experiment shows that the sorption of Fe(II) can not be related to only one phenomena at low pH, as well as at high pH.

ACKNOWLEDGEMENT

This research was funded by the French National radioactive waste management agency (ANDRA).

4. MODELISATION MORPHOLOGICO - STRUCTURALE DE LA REACTIVITE DES ARGILES

4.1. QUANTIFICATION DES AIRES DES DIFFERENTES SURFACES DE L'ARGILE

L'article qui suit présente la détermination des surfaces de la montmorillonite MX80 par deux approches indépendantes : la microscopie à force atomique (AFM) et l'absorption de gaz à très basse pression. Les deux méthodes aboutissent au même résultat pour la valeur des surfaces de côté (ou latérale) de l'argile, à savoir environ 8 m^2 g^{-1} (Figure 4.1). Cette correspondance confirme la justesse des interprétations des isothermes d'adsorption de gaz à très basse pression. Cependant il n'existe pas de correspondance entre les deux expériences pour les autres surfaces. Cette différence provient de la différence d'état d'hydratation et de compaction de l'argile dans les deux types d'expérience. Dans les expériences d'AFM, les particules observées proviennent d'une suspension diluée. Les feuillets sont presque totalement dispersés et les particules sont formées par un ou deux feuillets. La surface mesurée est alors la surface totale des feuillets. Dans les expériences d'absorption de gaz, l'argile est sèche et souvent sous une forme compactée. Les particules sont constituées d'un empilement de feuillets TOT séparés par des espaces interfoliaires. Ces espaces interfoliaires ne sont pas accessibles à la mesure. La surface totale mesurée correspond à la surface totale des feuillets moins les surfaces interfoliaires.

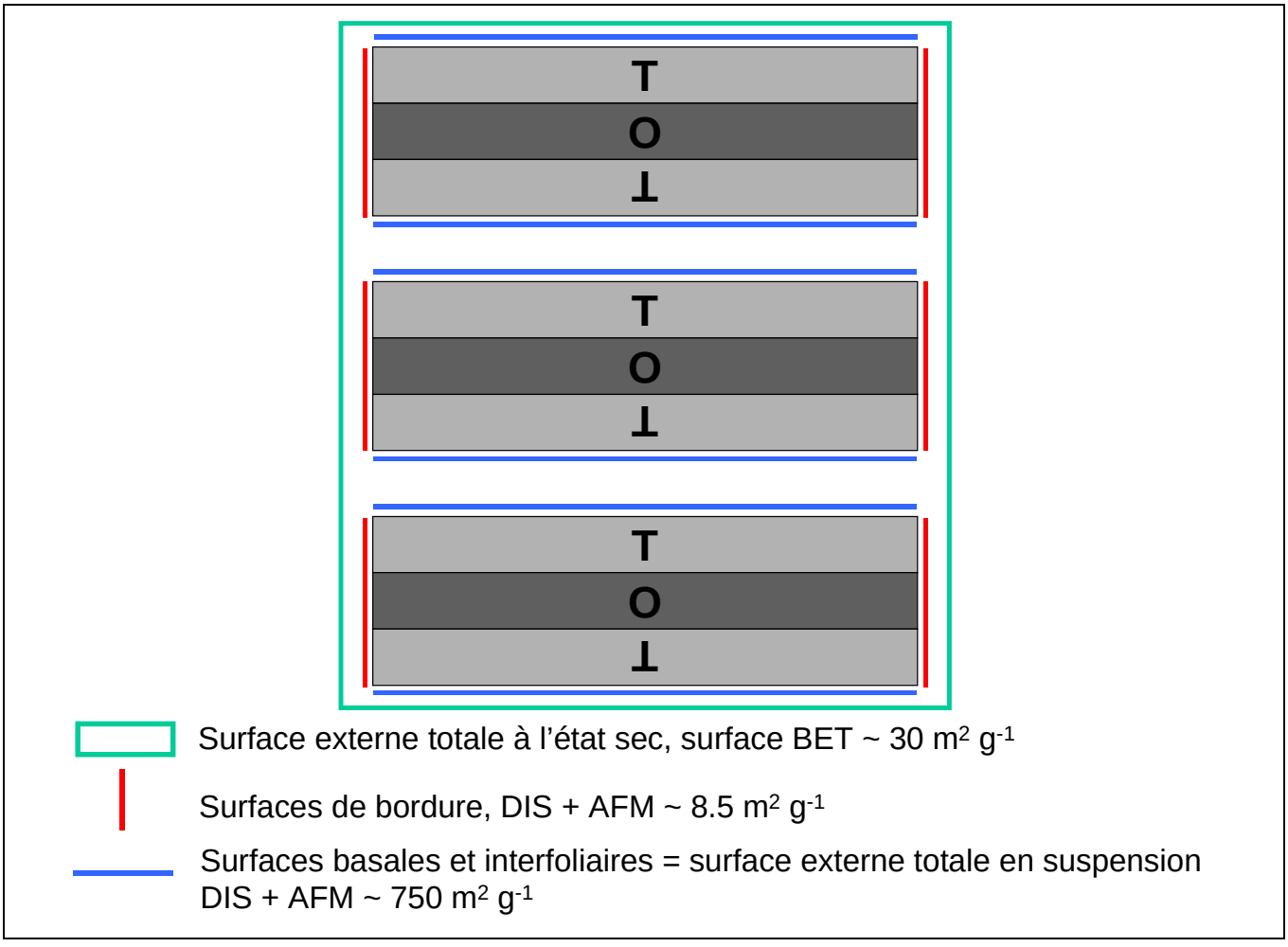


Figure 4.1 : Les différentes surfaces des argiles et leurs aires mesurées par différentes méthodes.

Dans la plupart des études portant sur les argiles, la surface spécifique des particules est mesurée par une méthode d'absorption de gaz, la méthode BET (ex : Wanner et al., 1994; Baeyens and Bradbury, 1997; Cama et al., 2000). Cependant, la valeur donnée par cette mesure est de peu d'utilité pour contraindre les modèles de sorption sur les argiles. En effet la surface BET correspond à la surface externe exprimée par les argiles (Figure 4.1) et ne correspond donc, ni à la surface totale (latérale + basale + interfoliaire), ni à la surface des côtés de l'argile. Les méthodes présentées dans l'article qui suit permettent, elles, de contraindre précisément les surfaces réactives de la montmorillonite MX80, données qui seront utilisées, par la suite, comme un paramètre fixe et non plus comme une variable ajustée.

NANOMORPHOLOGY OF MONTMORILLONITE PARTICLES: ESTIMATION OF THE CLAY EDGE SORPTION SITE DENSITY BY LOW-PRESSURE GAS ADSORPTION AND AFM OBSERVATIONS.

Christophe Tournassat[1, 2], Alexander Neaman[3], Frédéric Villiéras[3], Dirk Bosbach[4], Laurent Charlet[1]

[1] LGIT - CNRS/UJF, Université Joseph Fourier (Grenoble), P.O. Box 53, F 38041 Grenoble, France

2 ANDRA, Parc de la Croix Blanche, 1/7 rue Jean Monnet, F-92298 Châtenay-Malabry CEDEX, France

[3] Laboratoire Environnement et Minéralurgie, UMR 7569 CNRS&INPL, ENSG, P.O. Box 40, F 54 501 Vandoeuvre – lès – Nancy Cedex, France

[4] Institut für Nukleare Entsorgung (INE), Forschungszentrum Karlsruhe, P.O. Box 3640, 76021 Karlsruhe, Germany

ABSTRACT

Dry and *in situ* (fluid cell) Atomic Force Microscopy (AFM) and Low-Pressure Gas Adsorption experiments were used to investigate the surfaces of pure Na-smectite particles. These two techniques permit the identification of different surfaces of the platelets (lateral, basal and interlayer surfaces) and to quantify their surface area. Calculation of the surface area was done for AFM, by measuring directly the dimensions of the clay particles on AFM images, and for gas adsorption experiments, by applying the Derivative Isotherm Summation (DIS) procedure designed by Villiéras et al. (Villiéras et al., 1992; Villiéras et al., 1997a; Villiéras et al., 1997b).

In the present study, we find a discrepancy between the two measurements of the basal and interlayer surface area. This difference is due to the stacking of platelets in dry conditions compared to their dispersion in aqueous suspension. A particle is estimated to be formed of nearly 20 stacked layers in the dehydrated state used in the gas adsorption experiment, whereas it is estimated to be formed of only 1 or 2 layers in aqueous suspension, on the basis of AFM measurements. However, the two techniques give similar results for the lateral surface area of the platelets (i.e., about 8 m^2 g^{-1}) and the *perimeter to area* ratio value of the particles because the stacking of platelets does not alter these values. This correlation confirms the effectiveness of the interpretation of the gas adsorption experiments at the lowest pressure domains as the adsorption on lateral surfaces.

The lateral surface area has important implications in the calculation of specific sorption site density on clay material. The relevance of the lateral surface area value (8 m^2 g^{-1}) was tested subsequently with sorption data found in the literature. Based on these results we show that one essential parameter for the calculation of particle edge site density is the *mean perimeter to area ratio* value. This parameter can be obtained by microscopic techniques but the measurement is tedious. The good correlation between the AFM results and the DIS – method results for the measurement of the lateral surface area confirms that the DIS – method offers a quick and reliable alternative method to measure it. AFM experiments can be further conducted to constrain the dispersion around the DIS value and the anisotropy of suspended particles.

INTRODUCTION

Sorption mechanisms on clay surfaces have been studied for decades: inorganic cation exchange on the interlayer and basal surfaces (e.g., Sposito, 1981), specific pH dependant sorption of inorganic cations and anions on the edges (e.g., Sposito, 1984), sorption of organic hydrophobic molecules on the interlayer and basal surfaces (e.g., Schwarzenbach et al., 1993; Titiloye and Skipper, 2000) and binding of organic matter on the edges (e.g., Claret et al., 2002). Edge sorption mechanisms are related to the acid-basic properties of the clay edges, whereas sorption on the interlayer and basal planes are related to the permanent charge generated by the clay structure (cation exchange) or to the presence of hydrophobic patches on these planes (hydrophobic adsorption).

It appeared in the past twenty years that two types of reaction are necessary to explain ion adsorption on clay surfaces. The first one is a cation exchange mechanism which occurs on the interlayer and basal planes (Figure 4.2), as described by Sposito (Sposito, 1981). It originates from the presence of a permanent negative structural charge in the alumino-silicate layer created by isomorphic substitutions in the lattice. The quantity of exchange sites (σ_0) can be derived from structural formula, and is compensated by “exchangeable cations” which generally form outer sphere complexes with siloxane cavities (Sposito, 1981, 1984). The second type of reaction is the pH-dependent specific sorption on the clay edges (e.g., Fletcher

and Sposito, 1989; Avena et al., 1990; Charlet et al., 1993; Wanner et al., 1994; Zachara and Smith, 1994; Baeyens and Bradbury, 1997; Bradbury and Baeyens, 1997). On these clay edges, the proton surface charge (σ_H) depends on physico-chemical solution parameters (pH, ionic strength) which control the protonation state of the surface (e.g., Fletcher and Sposito, 1989; Avena et al., 1990; Charlet et al., 1993; Wanner et al., 1994; Zachara and Smith, 1994; Baeyens and Bradbury, 1997; Bradbury and Baeyens, 1997). It depends also naturally from the amount of available sites for protonation (*n*):

$$n = N_i \times A \qquad \text{Eq. 4.1}$$

where N_i is the edge site density in mol m^{-2}, and A is the surface area in $m^2\ g^{-1}$. Hence, in the absence of values for these last two parameters, it is not possible to calculate a theoretical value for σ_H. N_i can be obtained by theoretical structural information (White and Zelazny, 1988), but A remains unknown. This information is therefore critical to model the proton and cation sorption on edge surfaces. Furthermore, reactive transport models also need information about the relative amount of basal and interlayer surfaces when applied to a clay medium, *e.g.*, to predict diffusion of radionuclides through a geotechnical bentonite backfill as well as geological clay barrier, or the diffusion of organics out of a waste disposal site. The ion exchange must occur faster between the solution and the basal planes than between the solution and the interlayer planes because, in the latter case, ions must diffuse in (and out) the interlayer space prior to any sorption process (*e.g.* Ochs et al., 1998; Ochs et al., 2001).

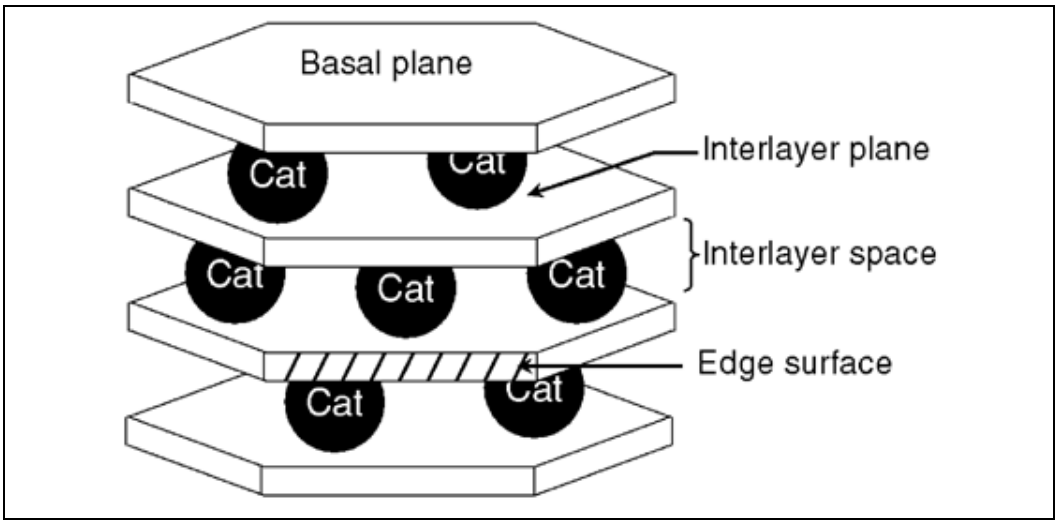


Figure 4.2 : Cartoon of stacked phyllosilicate layers. Cat = exchangeable cation.

The aim of this investigation was to estimate experimentally the area of the different surfaces of swelling clay particles in dry and wet conditions by using two techniques: low pressure argon adsorption and atomic force microscopy. The mean edge surface area derived from these two techniques is then used with literature data to demonstrate the relevance of this result. A synthetic table of clay surface properties is then proposed to model clay systems.

MATERIALS AND METHODS

Solid Preparation and Characterization.

The MX-80 bentonite (Wyoming) sample material was obtained from the French national radioactive waste management agency (ANDRA). The fine fraction of the MX80 montmorillonite has the following structural formula (Sauzéat et al., 2000):

$(Si_{3.98}Al_{0.02})(Al_{1.55}Fe^{3+}_{0.09}Fe^{2+}_{0.08}Mg_{0.28})O_{10}(OH)_2Na_{0.18}Ca_{0.10}$

Clay purification.

For AFM experiments, the sample material was dispersed in deionized water and the fine fraction (< 2 μm) was isolated by sedimentation techniques. A high concentration of NaCl (from 0.5 to 1 M) was maintained during the preparation stages. After saturating the suspension for a minimum of one week with sodium (0.5 M NaCl) it was treated with acidic solution (acetic acid 0.1 M), then with dithionate-citrate-bicarbonate (DCB) and finally with 3% H_2O_2 solutions to remove mineral impurities and organic matter.

For low-pressure gas adsorption analysis, the bentonite was dispersed in water and the fine fraction was separated by sedimentation under gravity. The purified sample was then saturated with Na. It was treated three times as follows: the suspension was saturated with a 1 M NaCl solution, washed with distilled water, and centrifuged until the electrical conductivity of the equilibrium solution was <10 dS/m. The samples were then freeze-dried.

Clay Immobilization for AFM imaging.

AFM experiments were performed on both dry samples and in *situ* samples (*i.e.*, in water). The montmorillonite particles were deposited on a freshly cleaved graphite sample holder by putting on the holder a droplet of a montmorillonite-NaCl suspension and by drying it at 40°C. For *in situ* AFM analysis, the montmorillonite particles were immobilized using variations of the technique described by Bickmore et al. (Bickmore et al., 1999) and Bosbach et al. (Bosbach et al., 2000). A small square of freshly cleaved muscovite is dipped into a 1:1000 (volume:volume) Polyethyleneimine solution (PEI, $(C_2H_5N)_n$ (M.W. 1800, Polysciences, Warrington, Pennsylvania), then rinsed with deionized water, placed at the bottom of a centrifugation tube and immersed in a ~0.05 M NaCl ~0.05 g clay/L suspension. The tube was centrifuged at 2000 rpm (~900 g) for 25 min. The clay-coated muscovite sample was then rinsed one time with deionized water and immersed in pure deionized water in an AFM fluid cell.

AFM Imaging.

A Topometrix TMX2000 Explorer AFM operating in tapping mode was used for imaging clay particles under ambient conditions in air (after drying). High aspect ratio silicon single crystal AFM tips (Topometrix, product #1660) were used. The cantilever nominal oscillation resonance frequency was 190 kHz. The maximum scan rate was 2 Hz. While they were exposed to an aqueous solution, images were taken in contact mode. V-shaped Si_3N_4 cantilevers with integrated pyramidal tips were used. Features in the AFM images were analyzed using the Image WSxM 2.0 software. The areas and perimeters were measured with the Image Tool 2.0 software.

Low pressure argon adsorption at 77K.

High-resolution, low-pressure isotherms of argon and nitrogen were recorded on a custom-built automatic quasi-equilibrium volumetric set-up (Michot et al., 1990; Villiéras et al., 1992; Villiéras et al., 1997a; Villiéras et al., 1997b). The experimental procedure has been discussed by Rouquerol et al. (Rouquerol et al., 1988) and Michot et al. (Michot et al., 1990). Michot et al.(1990) showed that using low pressure quasi equilibrium volumetry proposed by Grillet et al. (Grillet et al., 1977) and Rouquerol et al. (1988), the resolution of adsorption isotherms can be enhanced in the low relative pressure domain, *i.e.* when the first layer of gas is adsorbed. Then, this method equipped with pressure sensors that work at low pressures allows to study in satisfactory conditions the surface heterogeneity of solids. In the case of phyllosilicates, it has been demonstrated that such adsorption experiments coupled to a careful

analysis of experimental adsorption isotherms enable to derive shape factor, *i.e.* lateral and basal surface areas (Bardot et al. 1998; Cases et al. 1986; 2000; Michot et al. 1994; 2002; Villiéras et al. 1992; 1997a; 1997b; Villiéras et al., 2002).

A slow, constant and continuous flow of the adsorbate is introduced into the adsorption system through a microleak. The flowrate is constant, at least up to the BET domain, and can be adjusted by the pressure imposed before the leak. If the introduction rate is low enough, the measured pressures can be considered as quasi equilibrium pressures. Then, from the recording of the quasi equilibrium pressure (in the range of 10^{-3}, 3.10^{4} Pa) as a function of time, the adsorption isotherm is derived. In the most recent apparatus, three high accuracy MKS differential pressure transducers were used for pressure measurements: 1) 0-1.3 Pa, 2) 0-$1.3x10^{2}$ Pa and 3) 0-$1.3x10^{5}$ Pa (698 type Bartron Pressure transducers). The minimal sensitivities were $1.3x10^{-4}$, $1.3x10^{-2}$ and 1.3 Pa for gauges 1) to 3), respectively. Pressure accuracy was 0.05% of read pressure. A dynamic vacuum of 10^{-7} Pa is ensured on the reference side by the use of a turbomolecular vacuum pump. An accurate constant level of liquid nitrogen is maintained by using a home made electronic controlled device. The frequency of pressure recording is adjusted after each measurement to record 100 - 200 experimental points per unit log of relative pressure. Thus, 2000 to 3000 experimental points were collected every time for relative pressures lower than 0.15 (Villiéras et al. 1992, 1997b).

The data were then treated using the Derivative Isotherm Summation (DIS) procedure designed by Villiéras et al. (Villiéras et al., 1992; Villiéras et al., 1997a; Villiéras et al., 1997b) to examine the surface energetic heterogeneity of the samples. Due to the large number of experimental data points acquired by the quasi-equilibrium procedure, the experimental derivative of the adsorbed quantity as a function of the logarithm of relative pressure can be calculated accurately. The total derivative adsorption isotherm on a heterogeneous surface is simulated by the sum of *i* local theoretical derivative adsorption isotherms. The adsorption isotherm on a heterogeneous surface formed with *i* different energetic domains can be written as:

$$\theta_t = \sum_i X_i \theta_{it} = \sum_i X_i \int_{\Omega} \theta_i(\varepsilon).\chi_i(\varepsilon).d\varepsilon \qquad \text{Eq. 4.2}$$

where θ_t is the total adsorption isotherm, θ_{it}, the adsorption isotherms on the different energetic domains of the surface, X_i is its contribution to θ_t, ε is the adsorption energy, Ω is the physical domain of ε, $\theta_i(\varepsilon)$ a "local" theoretical adsorption isotherm and $\chi_i(\varepsilon)$ is the dispersion of ε on the i^{th} domain. The experimental curve is then fitted with theoretical local isotherms derived from BET formalism by using a derivative isotherm summation (DIS) procedure designed for that purpose (Villiéras et al., 1992). For each local isotherm, the following parameters are then obtained:

- the position of the peak (ln P/Po), which depends on solid-gas and gas-gas interaction energies;

- an apparent gas-gas interaction parameter (ω), which depends on real gas-gas interaction energy and the spreading of solid-gas interaction energies;

- a monolayer capacity, which can be converted to surface area by taking into account the cross sectional area of adsorbed argon (*i.e*. 13.8 $Å^2$).

The experimental conditions were a sample mass of ~0.6 g, outgassing at 0.001 Pa at a temperature of 120°C. The gas used was Argon N56 (purity>99.9996), supplied by Alphagaz (France).

AFM RESULTS

Montmorillonite particles have irregular morphologies like “cornflakes” (Figure 4.3). Some of their edges appear to be aligned in a straight line but their direction can not be attributed to any particular crystallographic direction.

Thin isolated montmorillonite particles are identified both in the *in situ* experiment and in the dry experiment. Some particles present several lateral domains with different heights. These differences of height can be attributed either to precipitates, or to platelet stacking. In the dry experiments, many high circular peaks are observed (from 5 to 23 nm high, Figure 4.3, white arrows). These peaks are not observed in the in situ experiments and are attributed to the precipitation of NaCl salt during the drying step. In both experiments, some particles appear to be constituted by several layers (Figure 4.3, circled area). The height of the lowest layer was measured for each particle on several transects. 102 measurements (30 particles) for the dry experiment and 90 measurements (24 particles) for the in situ experiment were recorded. Results are shown in Figure 4.4. Particles do not have the same mean height in dry (12.4 Å $\pm$ 1.4) and hydrated (15.9 Å $\pm$ 2.1) conditions, nor the same height distribution.

Hence, for the same platelet number, the volume of a particle depends on hydration conditions. To avoid this problem in the following calculation, we calculated a theoretical volume for each particle. We determined the number of platelets in each particle, and the volume of one particle is calculated by multiplying its measured basal area by a theoretical height. This theoretical height is equal to the measured number of layers multiplying a constant theoretical height of one layer. The theoretical volume of a particle is then given by the formula:

$$V = area \times H_t = area \times n \times h \qquad \text{Eq. 4.3}$$

where V is the theoretical volume of the considered particle, H_t its theoretical height, n its measured number of platelets and h the theoretical height of one platelet. We consider a 9.5 Å theoretical height in order to be consistent with gas adsorption experiments. This value corresponds to a completely dehydrated layer whose density can be estimated to be 2.7 kg/dm^3 on the basis of the smectite structural formula and cell volume.

The mass of each particle was calculated by the formula: $m_i = V_i \times d$, where m_i and V_i are the mass and the volume of the particle i, and d is the above density. In the case of particles constituted by several layers, the layers were considered individually and summed to obtain the particle mass and volume values. The lateral surface (in m^2/g) of one particle (or layer) was calculated as follows:

$$S = \frac{perimeter \times height}{m_i} = \frac{perimeter \times height}{area \times height \times density} = \frac{perimeter}{area \times density} \qquad \text{Eq. 4.4}$$

In this formula it is clear that the parameter S does not depend on the height of one layer but on the chosen density, *i.e.*, the chosen hydration of the system (see discussion below). In the following text and tables, the results can be applied to dehydrated particles only. In other cases, a correction factor equal to the ratio between density of dehydrated and hydrated clay must be used.

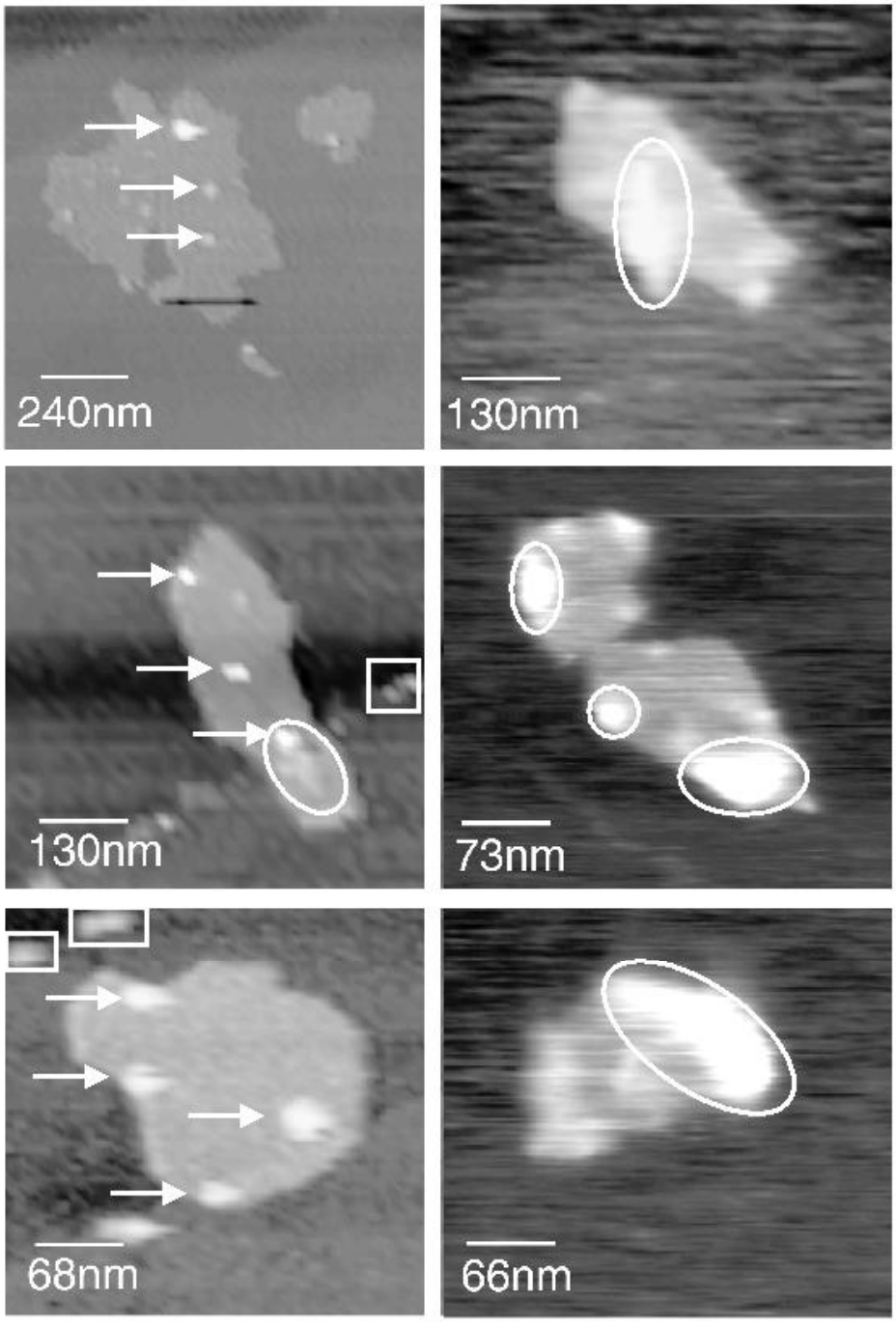


Figure 4.3 : AFM images of MX-80 particles. Left: dry AFM experiment. Right: *in situ* AFM experiment. White arrows indicate NaCl salt precipitates. White rounded areas indicate the possible stacking of platelets. Note the good correlation between the lateral dimensions of the platelets and the lateral dimension derived from low-pressure gas measurements (~170 nm).

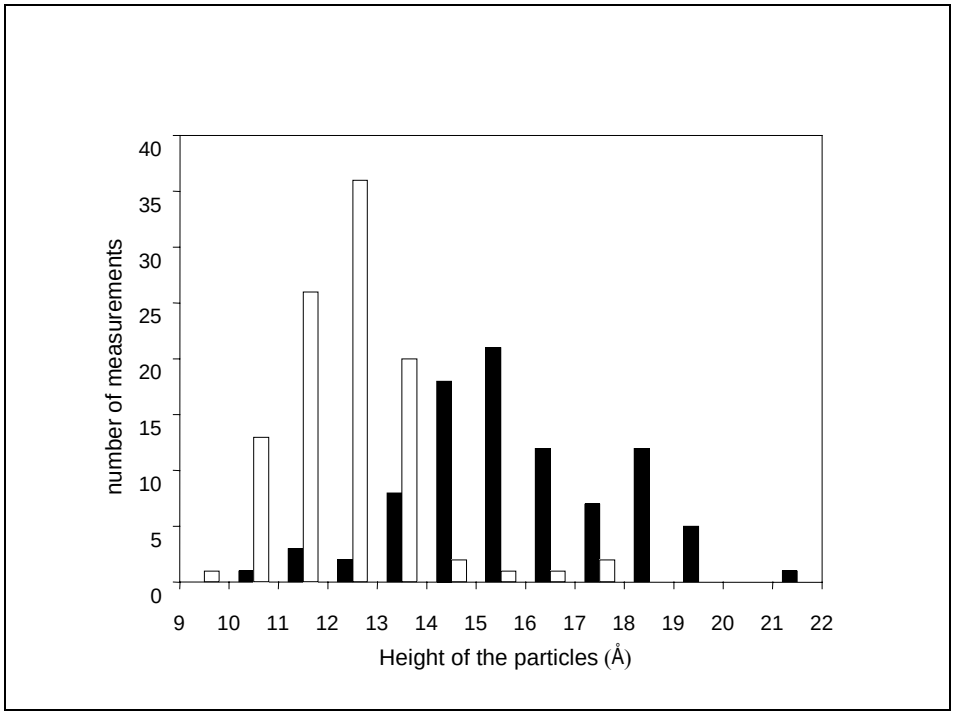


Figure 4.4 : Distribution of the height of the layers as measured with AFM. White bars: distribution within dry samples. Black bars: distribution within in situ samples. The data are grouped in 1 Å intervals.

The weighed mean values for volume, height and lateral surface were calculated as following:

$$\bar{x} = \sum_i x_i \times \frac{V_i}{V_T} \qquad \text{Eq. 4.5}$$

where x is the recorded parameter (volume, height or lateral surface) of particle i, V_i its volume, and V_T the total volume of the measured samples. Results are summarized in the Tab. 4.1. By repeating the measurements 5 times, we estimate the error to be approximately 10%.

	Height of one layer (Å)	Mean height of particles (number of platelets)	Lateral surface area (m^2/g)	lateral surface area / volume ratio = perimeter to area ratio (nm^{-1})
Dry AFM samples	12.5 ± 1.4	1.32	7.4 ± 0.7	0.0199
In situ AFM samples	15.9 ± 2.1	1.82	8.7 ± 0.9	0.0235
Weighed mean	–	1.51	7.9 ± 0.8	0.0212
DIS measurements	9.5*	~29	8.5	0.0230

* Theoretical value

Tab. 4.1 : Morphological parameters of the clay platelets obtained by AFM and low pressure gas adsorption.

LOW-PRESSURE ARGON ADSORPTION RESULTS

An experimental argon derivative isotherm is presented in Figure 4.5 together with the results of the DIS fitting procedure. Fitting parameters are collected in Tab. 4.2. The curve is typical of phyllosilicates (Villiéras et al., 1992; Villiéras et al., 1997a; Villiéras et al., 1997b; Bardot et al., 1998) with a main peak around P/P_0=1.7 10^{-2} and a shoulder around 8.3 10^{-4}. The main peak corresponds to the adsorption on basal faces, whereas the shoulder is assigned to the adsorption on lateral faces. The broad high-energy peak centered on 4.5 10^{-5} is also assigned to lateral faces of the particles, which are considered to be very heterogeneous. As for other phyllosilicates, it is then possible to derive the lateral and basal surface areas to 8.5 and 26.6 m^2/g, respectively (Villiéras et al., 1997b).

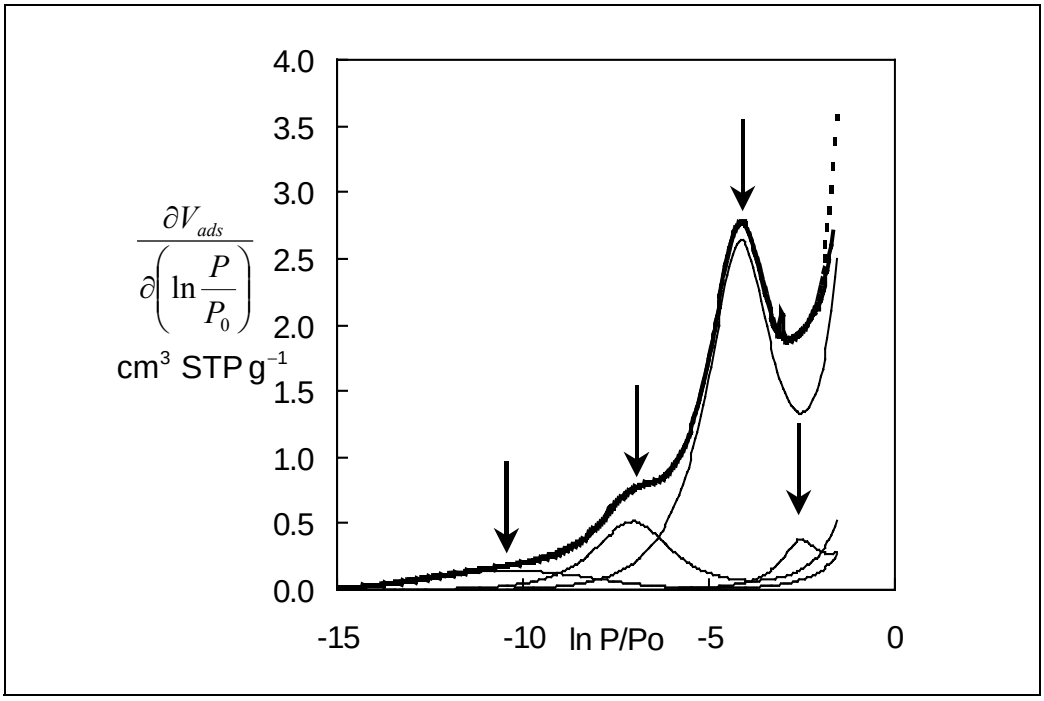


Figure 4.5 : Experimental argon derivative isotherm for the sample MX80 (dotted line) and fitted curve (thin lines: contribution of elementary surfaces; thick line = sum of the contributions). The fitting parameters are presented in Tab. 4.2. Arrows indicate the peaks at P/P_0 values of 8.0 10^{-2}, 1.6 10^{-2}, 8.7 10^{-4} and 3.4 10^{-5}.

As a rough approximation, the smectite particles can be modeled as perfect monodisperse regular plates with square basal faces. In this case, surface areas of basal and lateral faces can be used simply to derive the thickness (*t*) and length (*l*) of the particles:

$l = 4 / d.S_l$ and $t = 2 / d.S_b$ Eq. 4.6

where *d* is the density (2.7 kg/dm^3) and S_l and S_b the lateral and basal surface areas, respectively. Computations give 1743 Å and 278 Å for *t* and *h*, respectively. By taking into account the theoretical thickness of one dry smectite unit layer (taken to be equal to 9.5 Å), the amount of 2:1 layers is around 29 in the modeled particles.

	Peak Position		Vmonolayer	ω	SSA
	ln P/P_0	P/P_0	(cm^3/g)	(kT)	(m^2/g)
Domain 1	-2.52	8.0 10^{-2}	0.55	1.9	2.0

Domain 2	-4.14	$1.6\ 10^{-2}$	6.63	1.3	24.6
Domain 3	-7.05	$8.7\ 10^{-4}$	1.51	1.1	5.6
Domain 4	-10.29	$3.4\ 10^{-5}$	0.78	-1.4	2.9
				Total	35.1

Tab. 4.2 : Parameters adjusted to the experimental argon derivative isotherm presented in Figure 4.5.

DISCUSSION

The AFM observation of Na-montmorillonite particles confirms several properties already demonstrated by other authors with other techniques. First, the AFM observation of the height of the particles confirms that Na-montmorillonite particles are well dispersed (*e.g.* Hight et al., 1960; Hight et al., 1962; Cebula et al., 1978), constituted of single or double platelets. This behavior was suggested by Schramm and Kwak (Schramm and Kwak, 1982) based on viscosity and light-transmission measurements of dilute suspensions of montmorillonite having different exchangeable cations. They reported that the mean number of layers for a Na-montmorillonite is between 1.2 and 1.7 times the value for a Li-montmorillonite. These values are in good agreement with those presented in Tab. 4.1. Complementary experiments are needed to state positively that Li-montmorillonite particles are about one layer thick. Second, the comparison between *in-situ* and dry-state AFM observations confirms that the height value of one layer depends on the hydration conditions (*e.g.*, Mooney et al., 1952; Keren and Shainberg, 1975; Sato et al., 1992; Tamura et al., 2000). The peaks distribution is centered on a ~12.5 Å value for the dry experiment (atmospheric humidity) and on ~15.5 and ~18.5 Å values for the *in situ* experiment (Figure 4.4). This difference could be due to two factors: (i) the presence in the *in situ* experiment of the PEI coating between the particle and the mica substrate as explained in Bosbach et al. (Bosbach et al., 2000), or (ii) a difference of hydration of the particles. This last explanation seems to be in good agreement with previously reported results. Bérend et al. and others (Bérend, 1991; Cases et al., 1992; Bérend et al., 1995) studied the amount of water bound to exchangeable cations as a function of the nature of the cation and the humidity conditions. The unit layer of the Na – montmorillonite presents a 9.55 Å thickness for the zero-layer hydrate montmorillonite, 12.5 Å for the one-layer hydrate, 15.6 Å for the two-layers hydrate and 18.6 Å for the three-layers hydrate. These values are in very good agreement with Figure 4.4 and above cited distribution peaks. In the dry experiment an one-water molecule layer may have formed between the substrate and the clay particle, or between two platelets within a given particle, whereas in the in situ experiment a two- and three-layer hydrates should have formed (Bérend, 1991; Cases et al., 1992).

The observed lateral dimension (*l*) of the platelets (Figure 4.3) are consistent with the mean dimension calculated on the basis of the rectangular plate model (DIS *l* = 174 nm, AFM dry *l* = ~145 nm, AFM in situ *l* = ~190 nm, AFM mean *l* = ~170 nm), although this model shape does not fit real shape of the particles (see Figure 4.3). By considering a rectangular plate model and the measured lateral surface area to calculate the “mean lateral dimension” of the platelets, we underestimate the mean dimension. The particles are, in fact, larger, but have convexities and concavities that increase their lateral surface area.

The important result of this AFM study is that the mean lateral surface area and mean lateral surface area to volume ratio are in good agreement with the value obtained with the DIS method. Hence, the comparison of the AFM and DIS results confirms the reliability of the interpretation of the DIS low-pressure domain as the edge surface contribution. However, the

mean height of the particles is not concordant. No AFM-measured value is in agreement with the BET-surface area reported for the MX-80 montmorillonite (31.5 m^2/g, Wanner et al., 1994). This BET value is close to the sum of the lateral and basal surface areas measured with the DIS method but, in fact, has no significance for montmorillonite in suspension due to layer expansion and dispersion in water (Norrish, 1954). The difference of height values of the particles is due to the stacking of the platelets in dehydrated conditions. This stacking does not change the accessibility of the lateral surfaces, but the stacking of layer creates interlayer surfaces, which are not accessible like all basal surfaces as observed with water vapor. Consequently, basal surface area derived from argon adsorption is meaningless when phenomena at solid/water interface are considered, and should not be used to model edge surface phenomena, as previously done by several authors (e.g. Wanner et al., 1994; Bradbury and Baeyens, 1997; Boult et al., 1998; Cama et al., 2000; Avena, 2002). Instead, we propose that the edge surface value given in this article should be used.

APPLICATION

The models of clay titrations and sorption isotherms on clay minerals involve the knowledge of the amount of sites available for such processes. The site density is sometimes fixed arbitrarily, for example at 10-15 % of the total cation exchange capacity value (CEC) (Fletcher and Sposito, 1989), or is fitted concomitantly with the pK of the edge sites (Bradbury and Baeyens, 1997). In fact, the edge site density does not differ a lot from one study to one another and 10-15 % of the CEC value can be considered as a good empirical value. The aim of this paragraph is to demonstrate, with previously published data, that a reliable estimate of the edge site can be derived from the *perimeter to area ratio* value and some structural information. This result makes sense to the empirical 10-15 % CEC value usually used to model sorption data.

In the following, the reference studies were carried out on the fine fraction of smectites. Then the size of the particles and the *perimeter to area ratio* value measured in the present paper are similar to those of the published data clay material. The number of edge sites is calculated after the results of White and Zelazny (White and Zelazny, 1988) and the *perimeter to area ratio* of the clay ($R_{P/A}$ in m^{-1}), according to the equation:

$$n_{Al} = \frac{N_{Oc} \times R_{P/A}}{d} \qquad \text{Eq. 4.7}$$

$$n_{Si} = \frac{N_{T} \times R_{P/A}}{d} \qquad \text{Eq. 4.8}$$

where n_{Si} and n_{Al} are the site densities of silanol and aluminol edge sites respectively (in mol/kg), N_T and N_{Oc} are the site densities given by White and Zelazny (White and Zelazny, 1988) (in mol/m^2), d is the density of the clay material (in kg/m3). N_T and N_{Oc} depend on the structural formula of the clay. With the following general structural formula of a montmorillonite, $M_{0.33}(Al_{2-x}Mg_x)(Si_{4-y}Al_yO_{1O}(OH)_2$, N_T and N_{Oc} can be estimated to:

$$N_T = 6.39 \times 10^{-6} \times \frac{4-y}{4} \text{ mol/m}^2 \qquad \text{Eq. 4.9}$$

$$N_{Oc} = 6.39 \times 10^{-6} \times \frac{2-x}{2} \text{ mol/m}^2 \qquad \text{Eq. 4.10}$$

Tab. 4.3 summarizes the comparison results. There is a very good agreement between published values and the value calculated with the present method. Then the empirical value for edge sites density can be retrieved with structural and morphological information.

Study + Smectite name	Method for edge site density evaluation	n_{Al} (mmol/kg)	n_{Si} (mmol/kg)	$n_{Al} + n_{Si}$ or total amount of formal sites (>SOH) (mmol/kg)
This study	AFM + DIS*	39.4 ± 1.8‡	51.1 ± 2.3‡	90.5 ± 4.1‡
Stadler and Schindler (Stadler and Schindler, 1993) Swy-1 †	Fitted value	59.8 ± 0.5	35.5 ± 0.4	95.3 ± 0.9
Charlet et al. (Charlet et al., 1993) Swy-1†	Fixed value §	-	-	86.4
Zachara and Smith (Zachara and Smith, 1994) Swy-1	Fitted value	39.5	47.4	86.9
Bradbury and Baeyens (Bradbury and Baeyens, 1997, 1998) Swy-1	Fitted value	-	-	82.0

† Swy-1 structural formula (Zachara et al., 1993):
$M_{0.359}(Al_{1.515}Fe(III)_{0.205}Mg_{0.266})(Si_{3.925}Al_{0.075})O_{10}(OH)_2$
* Calculation assuming d = 2.7 g/cm^3, and a *perimeter to area ratio* value of 0.022 ± 0.001 nm^{-1}.
‡ The standard deviation interval corresponds to the standard deviation between AFM and DIS measurements
§ See reference article for details

Tab. 4.3 : comparison between the number of sites published in the literature and the number of sites calculated by the present method.

This result shows that the *perimeter to area ratio* is the key parameter that must be measured and used for edge-site density calculation. It confirms that a simple BET-measurement is not a reliable measurement for the calculation of clay reactive surface area in electrolyte suspensions as previously suggested by other authors. The *perimeter to area ratio* can be obtained by microscopic techniques but this work is tedious. We have demonstrated that the low-pressure domain of the DIS curve can be interpreted as the contribution of the edge surfaces. Hence, we propose the DIS method as an alternative way to quickly determine the lateral surface area of pure clay minerals. The Tab. 4.4 summarizes our results for the Na-MX80 clay fraction, both in dilute suspension and in a compacted state. The tabulated surface values should be used as fixed parameter in clay models. On going studies of clay titration will confirm the relevance of this approach.

	Basal Surface Area (m^2 g^{-1})	Interlayer Surface Area (m^2 g^{-1})	Edge Surface Area (m^2 g^{-1})	Total Surface Area (m^2 g^{-1})
Compacted clay	26.6	753	8.5	788
Clay in dilute suspension	780*	N.A*	8.5	788

* The platelets are one layer thick

Tab. 4.4 : Surface area values for the Na-MX80 clay fraction in suspension and in compacted state.

ACKNOWLEDGMENTS

This research was partly funded by the French National radioactive waste management agency (ANDRA, Agence Nationale de gestion des Déchets RAdioactifs) and by EGIDE Procope (Project 99151). AFM facilities at the Institut für Nukleare Entsorgung of the Forschungszentrum Karlsruhe were used. Special thanks to M. Plaschke and Ms. Pieper (INE) for their help with the AFM.

4.2. CARACTERISATION DES PROPRIETES ACIDO-BASIQUES DE L'ARGILE ET DES SITES D'ADSORPTION

Les modélisations de sorption des métaux se font en référence à des réactions entre sites réactionnels, métaux et protons selon des réactions du type :

$\equiv SOH + Me^{z+} \Leftrightarrow \equiv SOMe^{(z-1)+} + H^+$ $\qquad K = \frac{(\equiv SOMe^{(z-1)+})(H^+)}{(\equiv SOH)(Me^{z+})}$ $\qquad$ Eq. 4.11

où $\equiv SO^-$ représente un site de surface et Me^{z+} un cation de charge *z*. La constante de complexation du métal, *K*, est donc calculée par rapport à la constante d'affinité des sites pour les protons. Pour construire un modèle de complexation des métaux à la surface des argiles, il est donc nécessaire de modéliser également les propriétés de l'argile vis-à-vis des protons.

La revue des articles consacrés aux titrages potentiométriques d'argile et à leur modélisation montrent une grande hétérogénéité de résultats (Gilbert and Laudelout, 1965; Avena et al., 1990; Stadler and Schindler, 1993; Wanner et al., 1994; Baeyens and Bradbury, 1997; Bradbury and Baeyens, 1997; Avena and De Pauli, 1998; Avena, 2002). L'analyse des données montre que cette hétérogénéité est due davantage aux conditions expérimentales qu'aux différences de matériaux. En effet, lors des expériences de titrage des argiles, des phénomènes cinétiques ainsi que des réactions "parasites" compliquent l'interprétation du signal chimique. La première partie de l'article qui suit présente une méthode de titrage permettant de s'affranchir de ces difficultés et de quantifier les phénomènes qui en sont à l'origine. La deuxième partie présente la modélisation des résultats selon deux types d'approche : une approche empirique publiée par Baeyens et Bradbury (Bradbury and Baeyens, 1997), et une approche théorique basée sur le modèle MUSIC de Hiemstra et Van Riemsdijk (Hiemstra et al., 1996). Cette dernière démarche est résumée sur la Figure 4.6. La justesse de la simulation par rapport aux points expérimentaux, montrée sur le haut de la Figure 4.6 montre que cette approche est valable. Le nombre de variables ajustées est beaucoup moins grand dans ce modèle que dans les modèles empiriques classiques tout en permettant de construire un modèle plus complexe, décrivant plus finement l'interface particule solution. Dans les approches empiriques, 2 ou 3 sites réactionnels de bordure sont utilisés dans la modélisation, tandis que dans le modèle présenté, au moins 27 sites potentiels différents ont pu être identifiés. Sur ces 27 sites, 5 sont absolument indispensables à la simulation des données expérimentales.

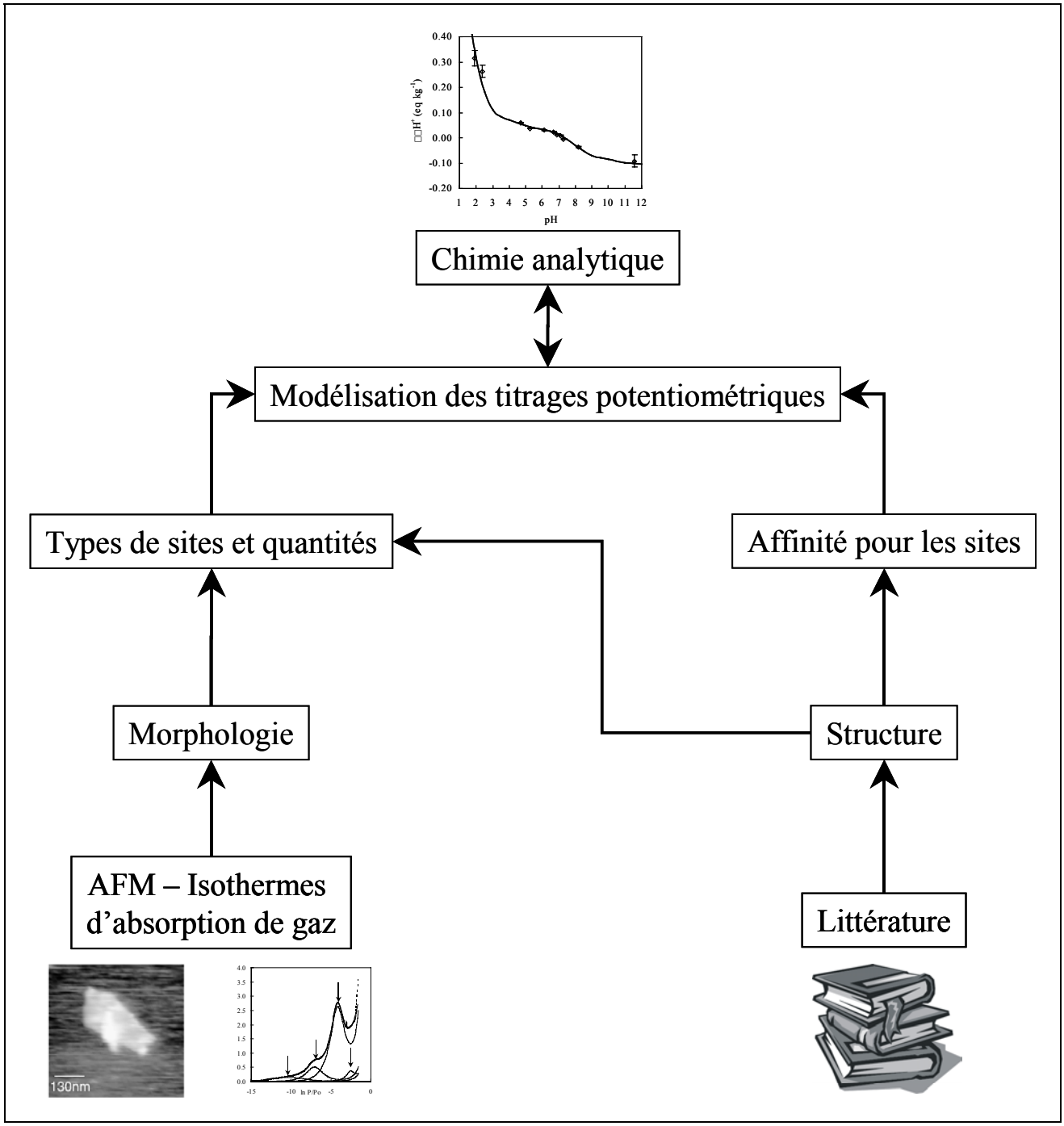


Figure 4.6 : Démarche adoptée pour la construction d'un modèle morphologico-structural de la réactivité des surfaces des argiles.

THE TITRATION OF CLAY MINERALS. PART I. DISCONTINUOUS BACKTITRATION TECHNIQUE COMBINED TO CEC MEASUREMENTS

Christophe Tournassat[1,2], Jean-Marc Greneche[3], Delphine Tisserand[1], Laurent Charlet[1]

To be submitted to Journal of Colloid and Interface Sciences

[1] LGIT - CNRS/UJF, University of Grenoble-I, P.O. Box 53, F 38041 Grenoble, France

[2] ANDRA, Parc de la Croix Blanche, 1/7 rue Jean Monnet, F-92298 Châtenay-Malabry CEDEX, France

[3] Laboratoire de Physique de l'Etat Condensé, UMR CNRS 6087, University du Maine, F-72085 Le Mans, CEDEX 9, France

ABSTRACT

In this paper, a critical review of previous works on clay potentiometric titration is made to point out the difficulties encountered to interpret such data. To avoid these difficulties, a refined titration technique is proposed, combining discontinuous backtitration and CEC measurement techniques. This technique was applied to the potentiometric titration of Na- and Ca-conditioned montmorillonites. Each of the following contributions can be discriminated and precisely estimated: cation exchange, edge surface proton charge, dissolution of clay, and precipitation of new phases.

Thanks to these results, we have shown that a precise measurement of the variations of net proton surface charge is possible. This result has important implications in clay surface modeling (see part II of this article) and in processes that are dependent on the clay surface charge, *e.g.*, alteration, rheological processes, or contamination retention applications. As secondary results, this study confirms the adsorption of ionic pairs such as $CaCl^+$ in exchange site position and shows that $CaOH^+$ can behave like $CaCl^+$. This result, together with the evidence of precipitation of a Ca-Si phase in a short time scale (one week) at high pH and low temperature, could be used to constrain the understanding of the concrete / clays interactions. At low pH, we confirm and quantify the H^+/Na^+ exchange reaction. We demonstrate finally that both the edge surface charge and the permanent structural charge are compensated by the non-specific sorption of cations from the solution in the whole pH range. Therefore, the surface potential is fully screened and does not need to be invoked to model the sorption processes on clay particles in dilute suspensions.

Key words: clay, potentiometric titration, backtitration, CEC

INTRODUCTION

Sorption mechanisms on clay surfaces have been studied for decades and one distinguishes: (i) inorganic cation exchange in the interlayer and on basal plane surfaces (*e.g.* Sposito, 1981) and (ii) specific pH dependant sorption of cations and anions on the edges (*e.g.* Sposito, 1984). Edge sorption mechanism is related to the acid-basic properties of the clay edges (Fletcher and Sposito, 1989; Charlet et al., 1993; Stadler and Schindler, 1993; Zachara and Smith, 1994; Bradbury and Baeyens, 1997; Avena, 2002 and others) whereas cation exchange on basal planes is related to the permanent charge generated by the clay structure (Sposito, 1981). The former mechanism is a pH dependant specific sorption on the clay edges. It has already been well established that the proton surface charge density (σ_H) on the clay edges depends on physico-chemical solution parameters (pH, ionic strength) which control the protonation state of the surface (Fletcher and Sposito, 1989; Charlet et al., 1993; Zachara et al., 1993; Wanner et al., 1994; Baeyens and Bradbury, 1997; Bradbury and Baeyens, 1997; Avena, 2002 and others). The latter mechanism originates from the presence of a permanent negative structural charge in the alumino-silicate layer created by isomorphic substitutions in the lattice. The density of exchange sites (σ_o) can be derived from structural formula, and is compensated by “exchangeable cations”, which generally form outer sphere complexes with siloxane cavities (Sposito, 1981, 1984).

In the literature, these two mechanisms are often analyzed separately. In this study we first show the limitations of such experimental approaches and then we try to develop experimental tools to study of the two mechanisms concomitantly. This approach is used to constrain clay potentiometric titration data.

EXPERIMENTAL AND THEORETICAL BACKGROUND ON TITRATIONS TECHNIQUES

The first attempts to titrate the sorption sites on clay mineral edges were conducted with the same method as for oxides, *i.e.* by continuous titrations in reactor (Charlet et al., 1993; Wanner et al., 1994; Avena and De Pauli, 1998). The amount of H^+ bound to the surface is calculated according to formula (Wanner et al., 1994)

$$\Delta[H^+] = \frac{1}{a}\left([H^+]t - [H^+] + \frac{^cKw}{[H^+]} - C\right) \qquad \text{Eq. 4.12}$$

in which $\Delta[H^+]$ is the proton surface charge expressed in mol kg^{-1} clay, *a* is the clay content of the suspension in kg clay l^{-1}, $[H^+]t$ is the total amount of H^+ in the system in mol l^{-1}, $[H^+]$ is the concentration of proton measured in the suspension in mol l^{-1}, ^cK_w is the dissociation constant of water at the temperature of the experiment and at a given ionic strength, and *C* is a correction factor used to consider side-reactions like clay dissolution. In this approach, some problems are difficult to resolve, *e.g.*, the definition of $[H^+]_t$ absolute value and the definition of *C*. $[H^+]_t$ must be considered as the sum of an initial unknown total concentration of H^+; present in the suspension at the start of the experiment, $[H^+]_{init}$, plus the measured concentration of H^+ added (or removed) during the titration, $[H^+]_{added}$. One titration curve does not give any information on $\Delta[H^+]$ and then does not permit to give an absolute measurement of the proton edge surface charge. In case of oxides, the titration curves recorded at different ionic strengths cross each other at a single point, the point of zero salt effect (PZSE), which is assigned to be equal to the point of zero net proton charge (PZNPC) (*e.g.* Jolivet, 1994 and references therein). Hence, $[H^+]_{init}$ can be calculated and the recalculated $\Delta[H^+]$ values can be considered as absolute values. In the case of clay minerals, the titration experiments conducted at different ionic strengths failed to find a unique cross point of the curves (Wanner et al., 1994; Baeyens and Bradbury, 1997; Avena, 2002). Thus, $[H^+]_{init}$ can not be determined and the $\Delta[H^+]$ values are only relative values as stated by Avena (Avena, 2002). Hence, the results should be expressed as relative values and should be noted $\Delta(\Delta[H^+])$. The *C* factor, when present, is not clearly described (Wanner et al., 1994) and since the dissolution rate of clay minerals as a function of pH is not well known, it is difficult to estimate the relevance of this correction factor. The increase of uncertainty linked to the measurement at low and high pH gives some additional difficulties (Wanner et al., 1994). In previous studies, pH drift lower than of 1 mV h^{-1} (Charlet et al., 1993), 1 mV/5 min (Wanner et al., 1994), 1mV min^{-1} (Avena and De Pauli, 1998) were considered as sufficient criteria to assess the equilibrium of the protonation reaction. 1 mV corresponds to 0.02 pH unit, which can be considered as the standard error on the pH measurement. Then, according to equation 4.12, the error on $\Delta[H^+]$ due to the error on the pH measurement is equal to

$$error = -\frac{1}{a}\left(1 + \frac{Kw}{10^{-2pH}}\right) \times \left(10^{-pH} - 10^{-pH+0.02}\right) \qquad \text{Eq. 4.13}$$

Considering *a* = 5 g l^{-1}, the error is negligible between pH 4.5 to 9.5 (*i.e.* error < 0.5 mmol kg^{-1}) but becomes greater and greater outside of this pH range. At pH 2 or 12 the error value has the same order of magnitude as the total amount of edge sites assumed to be present (100 mmol kg^{-1}, after Charlet et al., 1993; Zachara and Smith, 1994; Bradbury and Baeyens, 1997). Last but not least, a fourth problem arises when the reversibility of the protonation reaction is tested. Baeyens and Bradbury observed a hysteresis phenomena when they tried to titrate a clay suspension by increasing the pH and then by decreasing the pH (Baeyens and Bradbury, 1995, 1997). This behavior was verified as preliminary experiment in the present study. This hysteresis can originate from several processes: dissolution of the solid phase, or carbonate effect, as pointed out by Gaboriaud and Ehrhardt in the case of goethite titration (Gaboriaud and

Ehrhardt, 2003). It could originate also from a kinetics effect. In continuous experiments with a short equilibrium time, no true equilibrium may be attained. An enhancement of H^+ sorption can be measured by increasing the reaction time (Wanner et al., 1994).

The backtitration technique permits to prevent some of these effects. Schultess and Sparks (Schultess and Sparks, 1986) presented this technique for oxide surfaces titrations and Baeyens and Bradbury adapted it for clay surfaces titration (Baeyens and Bradbury, 1997). In this method, centrifugation tubes are filled with a known amount of clay suspension together with acid or alkali solutions. Once equilibrium has been reached (time scale depending on the system), and pH has been measured, all samples are individually centrifuged and filtered. Each supernatant solution is weighed; its pH measured, and is then backtitrated to pH 7, chosen as the titration end point. The difference between the amount of acid or base added at the start of the experiment and the amount of acid or base used in the backtitration yields the amount of H^+ adsorbed or desorbed from the surface:

$$\Delta\left[H^+\right] = \frac{1}{a}\left[\left(V_A C_A - V_B C_B\right) + \left(V_{BT_A} C_{BT_A} - V_{BT_B} C_{BT_B}\right)\frac{V_{tot}}{V_{back}}\right] \qquad \text{Eq. 4.14}$$

where

a = the clay content of the suspension in kg l^{-1};
V_{tot} = the whole volume of solution in one tube in l;
V_{back} = the volume of filtrated suspension used in the backtitration in l;
V_A = the volume of acid solution added to the clay suspension in l;
V_B = the volume of alkali solution added to the clay suspension in l;
C_A = the concentration of the acid solution in mol l^{-1};
C_B = the concentration of the acid solution in mol l^{-1};
V_{BT_A} = the volume of acid solution used in backtitration in l;
V_{BT_B} = the volume of alkali solution used in backtitration in l;
C_{BT_A} = the concentration of acid solution used in backtitration in mol l^{-1};
C_{BT_B} = the concentration of alkali solution used in backtitration in mol l^{-1}.

The end point of the backtitration must be fixed at pH 7 (or at a near neutral value) to prevent any dilution effect and to minimize the error on the volume of base or acid added. This technique, like the continuous titration technique, does not give an absolute position of the titration curve and data previously obtained with this method (Baeyens and Bradbury, 1997) must be considered as relative titration curves as well (Avena, 2002). Nevertheless, the present technique minimizes many problems of the continuous titration technique. First, no kinetics effect is expected. Second, the analytical error is low even at low or high pH. Third, the effect of side reactions is minimized because the pH dependent reactions of solute compounds and the dissolution of minerals are taken into account during the backtitration. But, it is false to consider that the dissolution of clay or other phases is completely counter-balanced during the backtitration: the re-precipitation of clay during the backtitration is not a realistic mechanism. Instead Al oxides or amorphous silica may precipitate. Nevertheless, a significant correction is obtained. Let us consider a congruent dissolution of the MX80 clay in acidic condition (pH = 4, structural formula from Sauzéat et al. (Sauzéat et al., 2001)):

$(Si_{7.96}Al_{0.04})(Al_{3.10}Fe^{3+}_{0.18}Fe^{2+}_{0.16}Mg_{0.56})O_{20}(OH)_4Na_{0.76} + 8.38\ H_2O + 11.62\ H^+$

$\rightarrow$

$7.96\ H_4SiO_4^0 + 3.14\ Al^{+3} + 0.16\ Fe^{2+} + 0.18\ Fe(OH)_{3(s)} + 0.56\ Mg^{2+} + 0.76\ Na^+$

The backtitration to pH 7 leads to the formation of the following solute species:

$7.96\ H_4SiO_4^0 \rightarrow 7.96\ H_4SiO_4^0$

$3.14\ Al^{+3} + 9.42\ OH^- \rightarrow 3.14\ Al(OH)_{3(s)}$

$0.16\ Fe^{2+} \rightarrow 0.16\ Fe^{2+}$

$0.18\ Fe(OH)_{3(s)} \rightarrow 0.18\ Fe(OH)_{3(s)}$

$0.56\ Mg^{2+} \rightarrow 0.56\ Mg^{2+}$

$0.76\ Na^+ \rightarrow 0.76\ Na^+$

Thus, 11.62 H^+ are consumed by the dissolution reaction and 9.42 OH^- are consumed during the backtitration. The global H^+ balance (+ 2.2 H^+) is the same in case of alkali dissolution:

$(Si_{7.96}Al_{0.04})(Al_{3.10}Fe^{3+}_{0.18}Fe^{2+}_{0.16}Mg_{0.56})O_{20}(OH)_4Na_{0.76} + 12.04\ H_2O + 5.92\ OH^-$

$\rightarrow$

$7.96\ H_3SiO_4^- + 3.14\ Al(OH)_{3(s)} + 0.16\ FeOH^+ + 0.18\ Fe(OH)_{3(s)} + 0.56\ Mg^{2+} + 0.76\ Na^+$

$7.96\ H_3SiO_4^- + 7.96\ H^+ \rightarrow 7.96\ H_4SiO_4^0$ or $7.96\ (SiO_{2(s)} + 2\ H_2O)$

$3.14\ Al(OH)_{3(s)} \rightarrow 3.14\ Al(OH)_{3(s)}$

$0.16\ FeOH^+ + 0.16\ H^+ \rightarrow 0.16\ Fe^{2+}$

$0.18\ Fe(OH)_{3(s)} \rightarrow 0.18\ Fe(OH)_{3(s)}$

$0.56\ Mg^{2+} \rightarrow 0.56\ Mg^{2+}$

$0.76\ Na^+ \rightarrow 0.76\ Na^+$

5.92 OH^- are consumed by the dissolution reaction and 8.12 H^+ are consumed during the backtitration. Furthermore, the precipitation of $Al(OH)_{3(s)}$, or $Fe(OH)_{3(s)}$ in the centrifugation tube does not change the final balance. The dissolution of silica phases is also fully taken into account with this technique. Thus the proton release or sink issued from a non-congruent dissolution is also well taken into account with this method. Nevertheless, since trivalent cations generated by dissolution processes are partially removed from solution by cation exchange, they may not be backtitrated and the relative proton charge is underestimated as stated by Baeyens and Bradbury (Baeyens and Bradbury, 1997). This effect can be minimized and or avoided by choosing a high Na^+ or a Ca^{2+} background salt concentration. In other case, a correction must be applied, or the pH-domain, in which the dissolution occurs, cannot be analyzed.

In this study we propose a refinement of the technique by combining the backtitration technique with the cation exchange capacity (CEC) measurement method described by Sposito et al. (Sposito et al., 1981; Sposito et al., 1983a). The combination of the two methods permits to evaluate the relative proton charge variations together with the CEC variations as a function of pH. It allows to distinguish protons sorbed on the basal plane and protons sorbed on clay edges, and to evaluate the effect of proton uptake by clay edges on the overall CEC.

MATERIAL AND METHOD

Chemicals.

All solutions and suspensions were prepared with boiled, argon-degassed Millipore Milli-Q 18 MΩ water. NaOH and HCl stock solutions were made from Titrisol ampoules. NaCl and $CaCl_2$ solutions were prepared from analytical grade salts.

Clay material preparation.

MX80 clay sample (commercial Wyoming bentonite, reference BF100, CETCO France) material was obtained after a homogenization treatment from ANDRA (the French National Radioactive Waste Management Agency) and was dispersed in deionized water. The fine fraction (< 2 μm) was isolated by sedimentation. After saturating the suspension with NaCl (0.5 M), it was successively treated with a 0.1 M acetic acid, 0.5 M NaCl solution to remove carbonates, then with a dithionate-citrate-bicarbonate solution (DCB + 0.5 M NaCl), and finally with 3% H_2O_2, 0.5 M NaCl to remove mineral impurities and organic matter (Schlegel, 2000). The final suspensions were washed with either 0.5 M NaCl or 0.05 M $CaCl_2$ solutions and then argon-degassed.

Clay material characterization.

XRD data

The raw material and the Na- and Ca-conditioned clay material were characterized with a Siemens D501 X-ray diffractometer equipped with a scintillation detector and diffracted-beam monochromated Co Kα radiation. Stepping rotor drive and data collection were performed with a Socabim DACO system. Oriented slides were prepared by pipetting slurry of the clay suspensions on a glass side and drying it at 40°C for a few hours to obtain an air-dried preparation. Results are exhibited in Figure 4.7. The diffraction patterns of the conditioned material were found to be in agreement with Na- and Ca-saturated smectites and showed that few impurities (mostly quartz and cristobalite) were present after preparation. These impurities cannot be removed completely from natural clay, because they are as fine as clay particles and they can not be dissolved by chemical treatment, without dissolving clay particles.

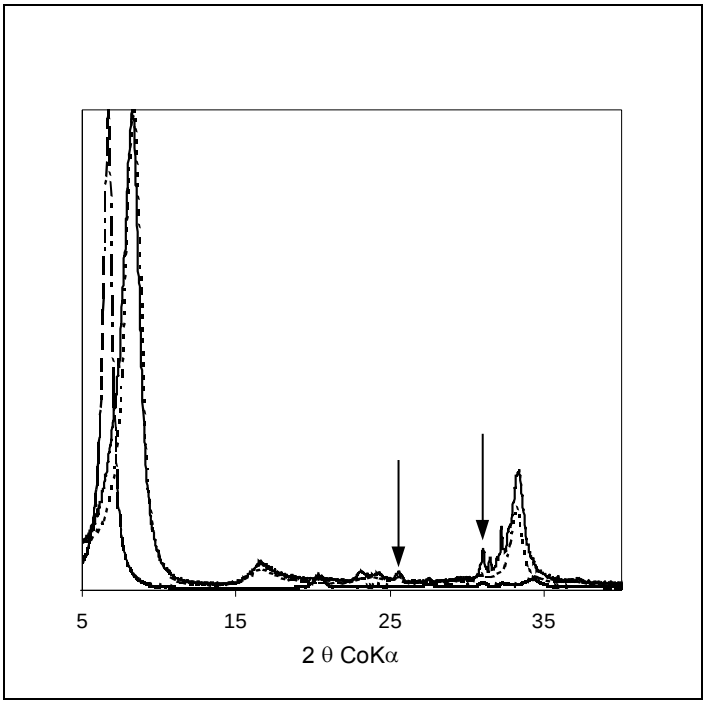


Figure 4.7: Oriented XRD patterns of the fine fraction of the MX80 (full thin line), treated Na-MX80 (dotted line), and treated Ca-MX80 (dotted-dashed line). The arrows indicate the remaining presence of cristobalite (4.03 Å) and quartz (3.34 Å) after treatment.

Mössbauer data and chemical analysis

The Mössbauer spectrum of the Na-conditioned smectite was recorded at 77 K using a constant acceleration spectrometer and a ^{57}Co source diffused into a rhodium matrix. Velocity calibrations were made using α-Fe foil at 300 K. The hyperfine parameters were refined using a least-squared fitting procedure (program MOSFIT, Teillet and Varret,). Results are shown on Figure 4.8, and the associated hyperfine parameters are shown in Tab. 4.5. In addition to the expected quadrupolar doublets of Fe(III) and Fe(II), the spectrum exhibits two unexpected features: a magnetic sextet with broadened lines, and, a strongly distorted base line as it is indicated at about ~ - 2 mm s-1 by the arrow in Figure 4.8. The fitting model consists thus in three quadrupolar doublets (two attributed to Fe(III) sites and one to Fe(II) site), and a single line and a magnetic sextet, both with broad lines. It is clear that other fitting models can be proposed but after different assumptions, we conclude that the present one is rather reasonable. One criterion of goodness was the proportion of each iron type, taken as the absorption area of each component. Let us emphasize that the scattering of results is given by the error bars that are listed in Tab. 4.5. The magnetic sextet is attributed to the presence of remaining iron oxides while the single line is probably due to the presence of superparamagnetic Fe(III) containing particles, resulting from uncompleted chemical reaction. The amount of oxides is too low to be characterized by XRD (~18 % of the total iron). Heron et al. (Heron et al., 1994) have demonstrated that the DCB-treatment does not remove all the oxyhydroxides present in sediments, but, that some large particles (*e.g.* goethite or hematite) are not completely dissolved. This result points out the difficulty in obtaining a pure smectite from a natural bentonite. In absence of other information, the contribution of the singlet is attributed to Fe^{3+} present in the smectite structure. Based on this assumption, the clay structural Fe(II)/Fe(III) balance has been calculated at Fe^{2+}/Fe_{tot} = 11/82 = 13 %. According to Sauzéat et al. (Sauzéat et al., 2001), the fine fraction of the MX80 montmorillonite has the following structural formula in the Na-saturated form:

$(Si_{3.98}Al_{0.02})(Al_{1.55}Fe^{3+}_{0.09}Fe^{2+}_{0.08}Mg_{0.28})O_{10}(OH)_2Na_{0.38}$

with the formula in the Ca-saturated expected to be:

$(Si_{3.98}Al_{0.02})(Al_{1.55}Fe^{3+}_{0.09}Fe^{2+}_{0.08}Mg_{0.28})O_{10}(OH)_2Ca_{0.19}$

	I.S. mm s^{-1}	Γ mm s^{-1}	Q.S. or2ε mm s^{-1}	Bhf T	%
Fe(III) A	0.45 (0.01)	0.47 (0.04)	0.50 (0.05)		20 (2)
Fe(III) B	0.45 (0.01)	0.47 (0.04)	1.12 (0.05)		10 (2)
Singlet	0.45 (0.01)	4.2	0		41 (5)
Fe(II)	1.26 (0.02)	0.27 (0.02)	3.07 (0.05)		11 (2)
Magnetic sextet	0.45 (0.01)	1.65	0.14 (0.05)	50 (2)	18 (5)

I.S. = isomer shift; Γ = linewidth; Q.S. = quadrupolar splitting value ; 2ε = quadrupolar shift value, Bhf = hyperfine field value, % = ratio of each component.

Tab. 4.5 : Mössbauer parameters of the Na-conditioned smectite. Error bars are indicated in parenthesis.

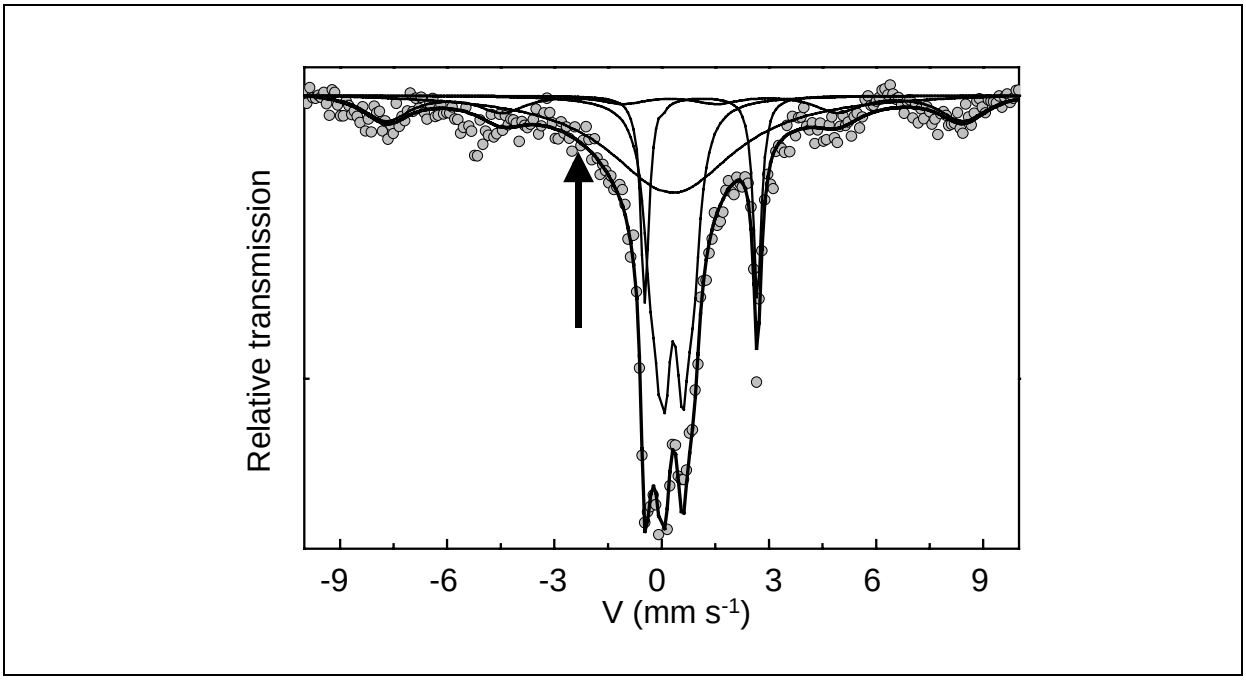


Figure 4.8 : Dots: 77 K Mössbauer spectrum of the Na-conditioned clay. Thin lines: decomposition of the spectrum. Thick line: sum of all the contributions of the decomposition. The parameters of the decomposition are given in Tab. 4.5. Contributions of Fe(III) A and Fe(III) B are shown together.

The Mössbauer results show clearly a discrepancy between their clay and our sample for the Fe^{3+}/Fe^{2+} balance. The above-described pretreatment and the natural heterogeneity of clay material may lead to this discrepancy. In particular the DCB and the following H_2O_2 treatments could have changed the Fe^{3+}/Fe^{2+} ratio compared to the original one. Then, we decided to

complete our clay characterization by a total digestion and chemical analysis by ICP-AES. The results of the chemical analysis are shown in Tab. 4.6. The measured Fe_{tot}/Al and Mg/Al ratio are compared to the ratio issued from the above-mentioned structural formula. The chemical results were corrected in agreement with Mössbauer results (Tab. 4.6): (i) the 18% of the total iron, present as magnetic iron, were subtracted from the total iron in order to take into account only the clay structural iron and (ii), the Fe^{2+}/Fe_{tot} balance was readjusted to the 13 % value. By considering the same tetrahedral Al content, the structural formula was calculated again in order to be in agreement with the values given in Tab. 4.6. It is

$(Si_{3.98}Al_{0.02})(Al_{1.61}Fe^{3+}_{0.13}Fe^{2+}_{0.02}Mg_{0.24})O_{10}(OH)_2Na_{0.28}$ for the Na-saturated form and $(Si_{3.98}Al_{0.02})(Al_{1.61}Fe^{3+}_{0.13}Fe^{2+}_{0.02}Mg_{0.24})O_{10}(OH)_2Ca_{0.14}$ for the Ca-saturated form.

	Chemical analysis	Mössbauer corrected Chemical analysis *	Structural formula
Fe/Al molar ratio	0.116 ± 0.002	0.095	0.108 ± 0.025
Mg/Al molar ratio	0.141 ± 0.002	-	0.178 ± 0.032

* Based on the presence of 18 % magnetic iron, attributed to residual iron oxides.

Tab. 4.6 : Fe/Al and Mg/Al ratios obtained by total digestion and chemical analysis, before and after oxide content correction based on 77 K Mössbauer analysis. Comparison with Fe/Al and Mg/Al ratios obtained with the structural formula given by Sauzéat et al. (Sauzéat et al., 2001).

Surfaces characterization

Various MX80 clay surface areas were well characterized in the work of Tournassat et al. (Tournassat et al., submitted-d) on the basis of derivative gas adsorption and AFM (Atomic Force Microscopy) experiments. The results are summarized in Tab. 4.7.

	Basal Surface Area ($m^2\ g^{-1}$)	Interlayer Surface Area ($m^2\ g^{-1}$)	Edge Surface Area ($m^2\ g^{-1}$)	Total Surface Area ($m^2\ g^{-1}$)
Compacted clay	26.6	753	8.5	788
Clay in dilute suspension	780*	N.A*	8.5	788

* The platelets are between one and two layers thick (Tournassat et al., submitted-d)

Tab. 4.7 : Surface area values for the Na-MX80 clay fraction in suspension and in compacted state (after Tournassat et al., submitted-d).

Clay content in suspension

Titration results are most commonly given as a plot of surface proton density in mol kg^{-1} versus pH (Eq. 4.13, $\Delta[H^+]$), or as a plot of the surface charge, in C m^{-2}, versus pH:

$$\sigma_H = \frac{F}{A}\Delta\left[H^+\right] \qquad \text{Eq. 4.15}$$

where

F = Faraday's constant (96480 C mol^{-1} charge)

A = specific surface area in $m^2\ g^{-1}$.

Both representations need a well-constrained clay content value (see term *a* in Eq. 4.12) to be modeled on a structural interpretation basis. The measurement of the clay content in a suspension is not always easy. One of classical methods is a weighing technique described by Sposito et al. (Sposito et al., 1981). In this method, an aliquot of the suspension is dried, cooled under a vacuum dessicator and weighed. The measurement of salt concentration permits to obtain the amount of clay in suspension (= total weight – salts weight). However this technique has some limits: some water is still attached to the clay platelets after drying (hydration water, Sauzéat et al., 2001), and worse, during the transfer from the dessicator to the balance, the clay can reabsorb some water. This can lead to an overestimation of the clay content in the suspension. We compare here three methods to determine the amount of solid in our suspensions. The first one is the method described by Sposito et al. (Sposito et al., 1981). The second one is derived from the total chemical analysis by dissolution of the solid (Besnus and Rouault, 1973; Samuel et al., 1985). In this technique, a known volume of suspension containing approximately 100 mg of clay is put in a Pt-Au crucible. The suspension is dried at 110°C in an oven. Then, 750 mg of $Li_2B_4O_7$ are added. The crucible is shacked and heated at 1000°C by an induction coil in a Philips Perl'X-2, and then is quickly cooled by pressurized air. The resulting glass is dissolved at 80°C in 20 ml of a 19% glycerin, 6% HNO_3 solution and then diluted in 100 ml of water. The concentrations of Si, Al, Mg, Fe are measured by ICP-AES, and the amount of clay in the suspension is calculated based on the following formula:

$$m_{clay} = \frac{C_{Al} \times M_{clay}}{n_{Al}} \qquad \text{Eq. 4.16}$$

where m_{clay} is the amount of clay in suspension (g l^{-1}), C_{Al} the total measured concentration of Al in the suspension (mol l^{-1}), n_{Al} the amount of Al in one clay structural formula unit, and M_{clay} the molar weight of one clay structural formula unit (733.3 g mol^{-1} on the basis of the structural formula for our MX80 sample). In the third method, the clay suspension is diluted and then is injected directly through the ICP-AES. Its Al content is measured. The Eq. 4.16 is then used to calculate the amount of clay in suspension. The second method (complete digestion) is used as the reference method. It was found that the third method underestimates the amount of solid in an order of approximately 20% and depended on the dilution factor. We do not understand this result. Hence, this method was discarded for a precise estimation of the clay content. Nevertheless, it was used for an other purpose described in the "titration experiments" section. The first method overestimates the amount of solid in an order of 18 %. This difference is very near from the total hydration water in the clay at room temperature (12 % of the total mass, i.e. 14% of the dehydrated mass, Sauzéat et al., 2001). Furthermore the presence of silica impurities must be taken into account. Hence the amount of solid in the suspension has been determined either by dissolution method or by the Sposito weighing method. In this last case 15 % were subtracted, from the total mass, in order to consider only the mass represented by the atoms present in the structural formula of the smectite.

TITRATION EXPERIMENTS

Centrifugation tubes were numbered and precisely weighed (m_{tube} in g) with a Mettler Toledo AG285 balance. A known volume of clay suspension was added in each 17-ml centrifuge tube with a calibrated micropipette (V_{susp}, clay content ρ). Volumes of NaOH and HCl were then added (V_b and V_a, concentration C_b and C_a). Volumes of NaCl or $CaCl_2$ solutions (V_c, $[H^+] = C_c$) solution were used to complete at 15 ml (V_{tot}). The concentrations of NaCl and $CaCl_2$,

and the clay contents are shown in Tab. 4.8 for each experiment. Care was taken to minimize the variations of salt ionic background concentrations from one tube to one another in a given experiment. Nevertheless, these variations cannot be completely avoided because of cation exchange reactions between Na^+, Ca^{2+}, H^+ and ionic pairs (see results and discussion section). The tubes were shaken for one week. One experiment (0.05 M $CaCl_2$ ionic background, experiment 3) was conducted in an O_2-free atmosphere glove box (Jacomex, pO_2 < 0.5 ppm). After one week the tubes were centrifuged. An aliquot of each supernatant tube was filtrated (0.20 µm) and used for backtitration (V_{back}). The backtitrations were performed with a dosimeter (Metrohm 665 Dosimat, volume resolution = 0.005 mL) with pH 7 chosen as the titration end point. The pH was measured with a microelectrode (Mettler Toledo, inlab 423). An other aliquot was filtrated for Na, Ca, Si, Al, Mg and Fe measurement on a Perkin-Elmer Optima 3300 DV inductively coupled plasma atomic emission spectrometer (ICP-AES). The Si, Al, Mg, Fe concentrations of a third supernatant aliquot was measured without filtration to give an estimation of the mass of particles still present in the supernatant ($m_{correction}$, obtained with Eq. 4.15; see second method in clay content determination section). The centrifuged reaction tubes, containing the clay slurry, were weighed ($m_{centrif}$) and 10 ml of 1 M ammonium acetate were added to each. They were shaken for one week. Na- and Ca-CEC were then measured as described by Sposito et al. (Sposito et al., 1983a). The relative proton surface charge $\Delta[H^+]$ is given by Eq. 4.13. The Na- and Ca-CEC, in eq kg^{-1}, are given by:

$$Na - CEC = \frac{C_{Amm}^{Na} \times 10 - C_{sol}^{Na} \times \left(m_{centrif} - m_{tube} - \left(V_{susp} \times \rho\right)\right)}{\left(V_{susp} \times \rho\right) - m_{correction}} \qquad \text{Eq. 4.17}$$

$$Ca - CEC = 2 \times \frac{C_{Amm}^{Ca} \times 10 - C_{sol}^{Ca} \times \left(m_{centrif} - m_{tube} - \left(V_{susp} \times \rho\right)\right)}{\left(V_{susp} \times \rho\right) - m_{correction}} \qquad \text{Eq. 4.18}$$

where volumes are given in ml, concentration in mol l^{-1}, clay content in g l^{-1} and masses in g. The density of all solutions are taken equal to 1.0. Experimental conditions are summarized in Tab. 4.8.

	Experiment 1	Experiment 2	Experiment 3
Ionic background	NaCl 0.02 mol l^{-1}	$CaCl_2$ 0.0068 mol l^{-1}	$CaCl_2$ 0.05 mol l^{-1}
Clay content	4.69 g l^{-1}	3.03 g l^{-1}	1.53 g l^{-1}

Tab. 4.8 : Experimental conditions of the three titrations

RESULTS AND DISCUSSION

Figure 4.9 presents the results of the surface proton charge titrations together with the CEC measurements.

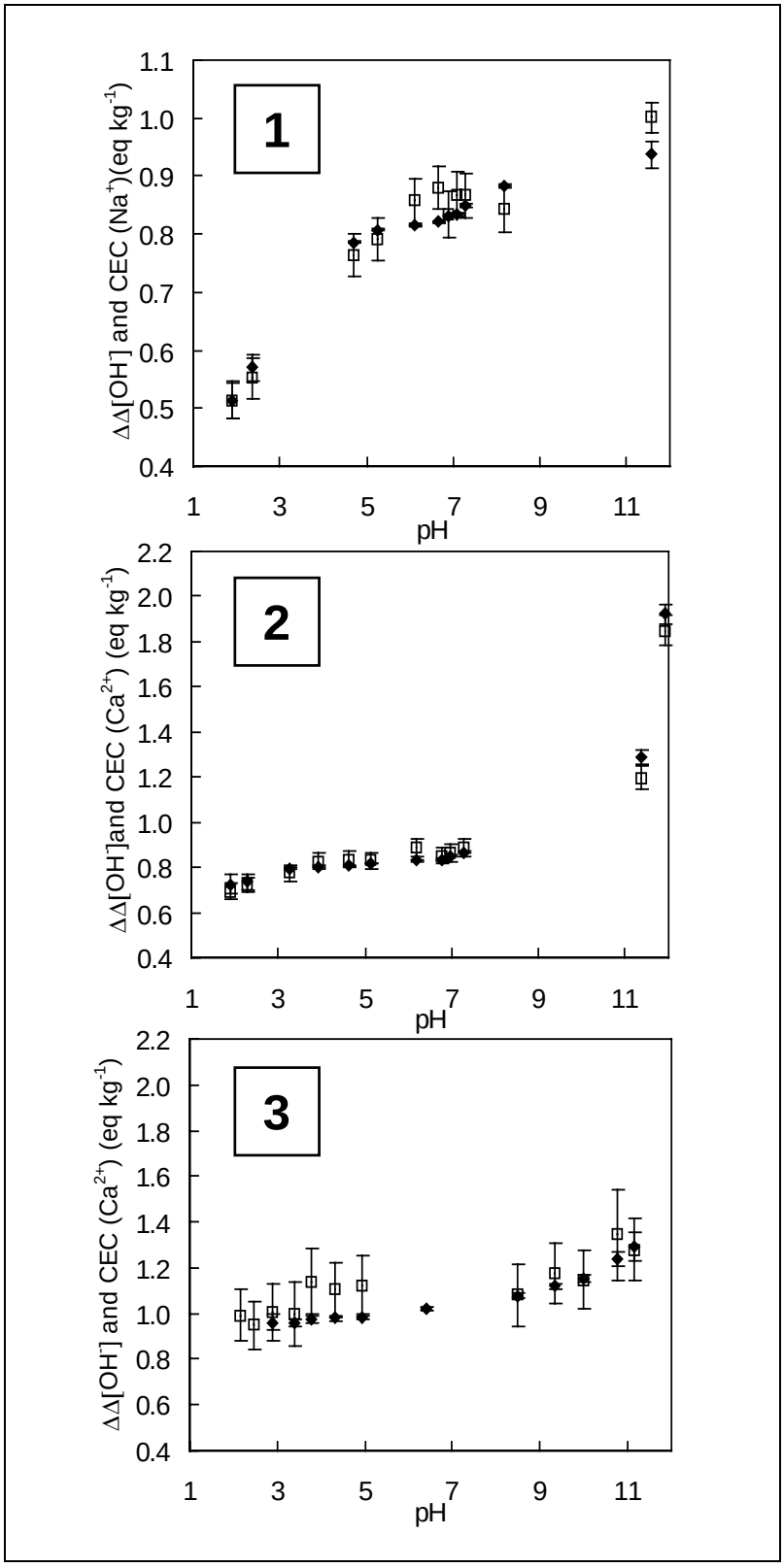


Figure 4.9 : Titration measurements ($\Delta\Delta[OH^-]$ black diamonds) presented concomitantly with the CEC measurements (open squares) as a function of pH. (1) Experiment 1, 0.02 mol l^{-1} NaCl, (2) experiment 2, 0.0068 mol l^{-1} $CaCl_2$, (3) experiment 3, 0.05 mol l^{-1} $CaCl_2$.

$\Delta\Delta[OH^-]$ is plotted as a function of pH to compare easily the variations of surface charge together with those of CEC. $\Delta\Delta[OH^-]$ is the sum of $-\Delta[H^+]$, whose value is given by Eq. 4.13, plus an arbitrary constant Δ_c chosen for a given experiment to match $\Delta\Delta[OH^-]$ and CEC values as close as possible. The constant value is different for experiments 1, 2 and 3. The absolute value

of $\Delta\Delta[OH^-]$ was not sought after, since, in the absence of ZPSE, the experiments did not permit to obtain a true surface charge value. Thus, only $\Delta\Delta[OH^-]$ variations are analyzed. Error bars were calculated on the basis of a standard error of 0.05 ml on volumes V_{BT_A} and V_{BT_B}, on a standard error of 1% on other volumes, and on a standard error of 2% on ICP-AES concentration measurements. Due to the extent of the error bars on the CEC measurement, it is not possible to infer a relation between the constant Δ_c and σ_o. We can only note that the constant value, Δ_c, is slightly higher than the structural CEC value for experiment 1 (constant = 0.82 eq kg^{-1}, structural CEC = 0.76 eq kg^{-1}). Experiments 1 and 2 exhibit both experimental points at pH value 7.3. This pH value was used as a reference point to build Figure 4.10, and we set $\Delta\Delta[OH^-] = \Delta CEC = 0$ at this point. $\Delta\Delta[OH^-]$ and ΔCEC are well correlated: the straight line represents a one to one relationship and the experimental points lie on this line.

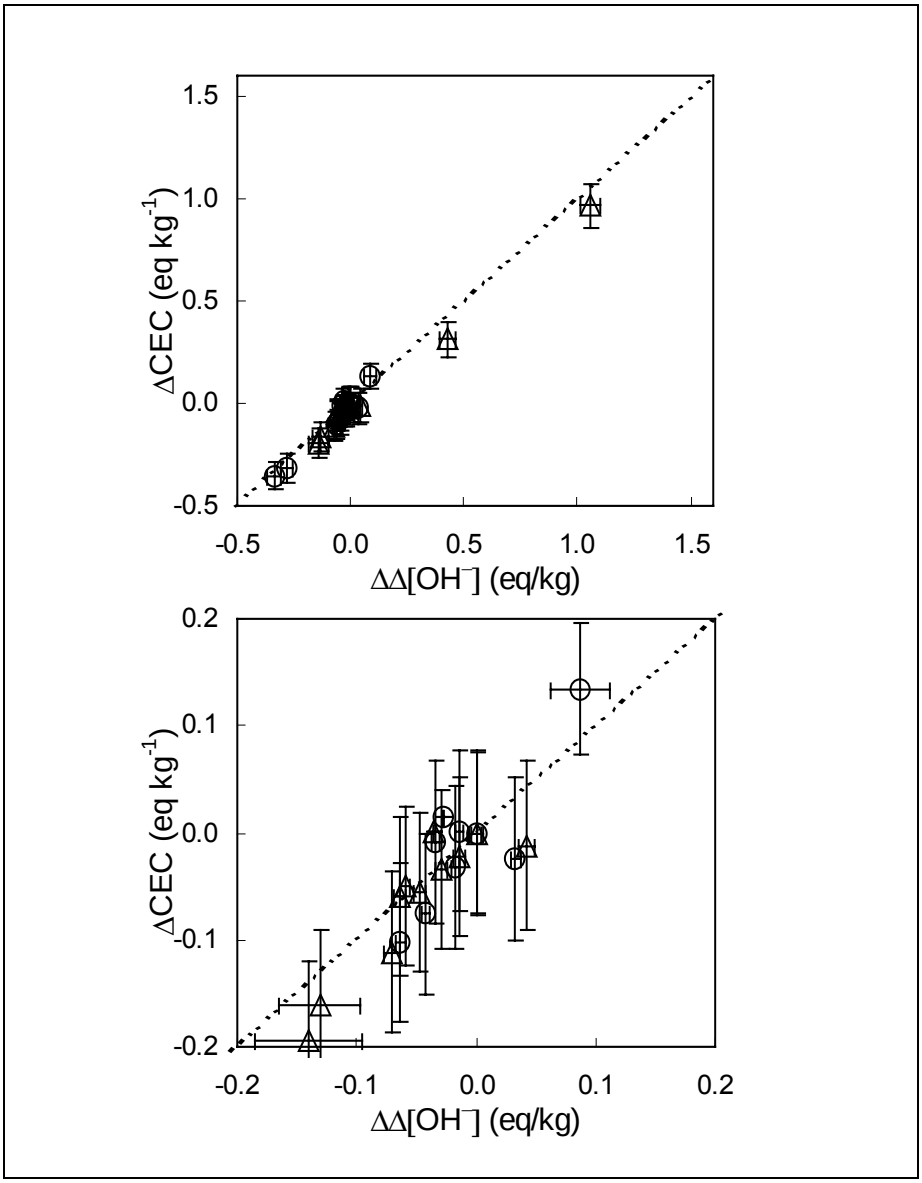


Figure 4.10 : Relationship between the variation of proton surface charge (presented as $\Delta\Delta[OH^-]$) and the variation of CEC (ΔCEC). The reference point ($\Delta CEC = \Delta\Delta OH^- = 0$) is at pH = 7.3. Open circles: experiment 1. Open triangles: experiment 2. Experiment 3 is not represented because the associated error bars are too large to infer any relationship. The dotted line represents a 1:1 relationship.

This result means that a decrease in surface proton charge is counterbalanced by an equivalent increase in Na^+ or Ca^{2+} charge. Thus protonated and deprotonated sites are not present as free charged species but are rather neutralized by the ions present in the neighboring of the surface. This behavior was already suggested by Charlet et al. (Charlet et al., 1993) on the basis of the K-saturated montmorillonite continuous titration, where proton charge was almost independent of ionic strength. As stated by these authors, this result is in agreement with electroacoustic measurements performed on kaolinite indicating that most of the surface charge is balanced by monovalent ions (Hunter and James, 1992). Hence, the surface complexes must contribute nothing to the electrokinetic charge. This could explain why Bradbury and Baeyens needed to suppress the electrostatic term in order to fit their H^+ sorption curves concomitantly with their Zn^{2+}, Ni^{2+}, and Eu^{3+} sorption curves (Bradbury and Baeyens, 1997, 1998, 2002). Figure 4.11 shows the titration data of experiment 1 (NaCl 0.02 M), concomitantly with the 7 days, 0.5 M $NaClO_4$ titration curve of Baeyens and Bradbury (Baeyens and Bradbury, 1995, 1997). There is little difference between the two titration curves. Hence, we can consider that our results can be applied to their system and that the background anion (Cl^- vs. ClO_4^-) has little impact on the titration data. Figure 4.11 shows also the titration data of experiments 1, 2 and 3 from pH 4 to pH 9 on the same graph. Between pH 4 and pH 9, there is no significant difference between the results of the two Ca-clay titration data, and between the results of Na- and Ca-clay titration data. This result is in agreement with the previous statement: there is no effect of the ionic background salt concentration and identity on the titration data.

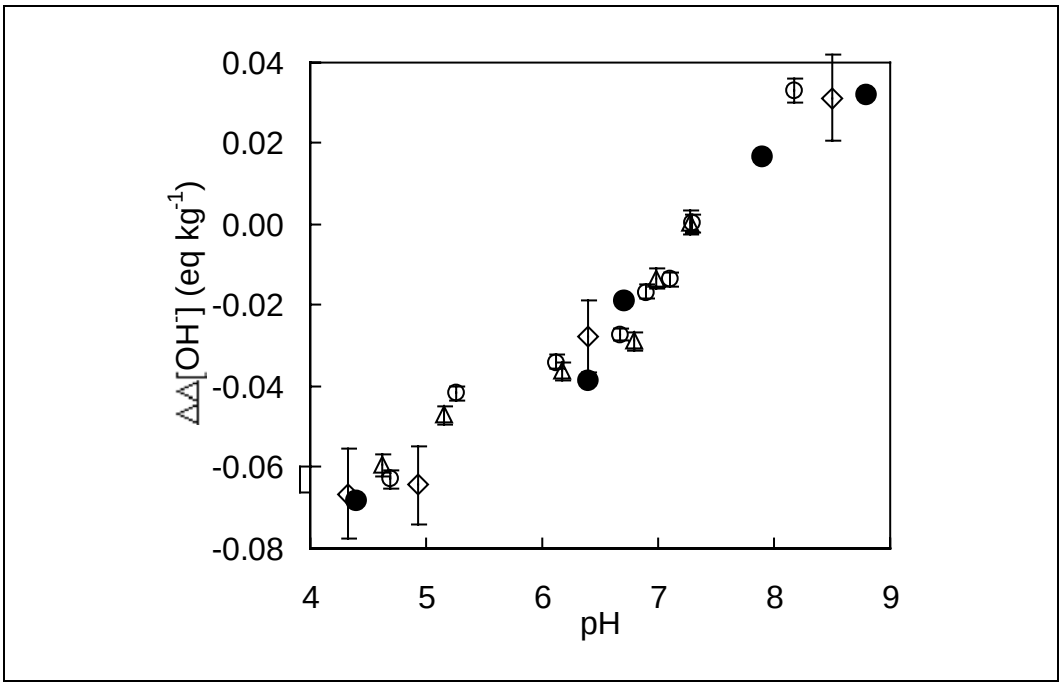


Figure 4.11 : Variation of the proton surface charge (presented as $\Delta\Delta[OH^-]$) as a function of pH for experiments 1 (open circles), 2 (open triangles), 3 (open diamonds) and the 7 days experiments of Baeyens and Bradbury (Baeyens and Bradbury, 1997, black circles). The reference point ($\Delta\Delta[OH^-] \sim 0$) is at pH = 7.3.

Nevertheless, some pronounced differences among experiments appear below pH 4 and above pH 9 (see Figure 4.9). Cation exchange and dissolution likely explain these differences. At pH > 9 and with Ca^{2+} as cationic background, the large increase in $\Delta\Delta[OH^-]$ is correlated to the same increase in apparent Ca-CEC (Figure 4.9). This increase is particularly pronounced between pH 11 and pH 12, *i.e.* around the first hydrolysis constant of Ca^{2+} (pK_a = 12.85, Llnl.dat database). Thus it is likely due to the sorption of $CaOH^+$ cations. In the calculation of the Ca-

CEC (Eq. 4.18), each Ca^{2+} ions is assumed to balance two negative charge of the exchanger. Instead, the reaction $Ca^{2+} + H_2O \rightarrow CaOH^+ + H^+$ leads to (i) a net consumption of one OH^- per $CaOH^+$ in exchange position and thus, to the increase of $\Delta\Delta OH^-$, and (ii) to an overestimation of the CEC, each Ca balancing only one charge of the exchanger. Nevertheless, the amount of $CaOH^+$ in exchange position can not exceed the CEC value. In the extreme case, where all the exchange sites are occupied by $CaOH^+$, the apparent CEC value should be twice the structural CEC value (~1.52 eq/kg based on the structural formula). In experiment 2, the amount of sorbed Ca(II) is equal to 1.85 eq/kg at pH 11.93. Thus an additional mechanism must be invoked, to explain this excess of apparent surface charge. Since this excess of charge is observed in a pH range, where a decrease in aqueous Si is observed (Figure 4.12), the additional mechanism is attributed to the precipitation of a Ca-Si hydrate solid phase, *e.g.* a tobermorite-like phase ($Ca_5Si_6H_6O_{20}$) (Claret et al., 2002). The ion activity product observed in the experimental conditions of the last point of experiment 2 is equal to $10^{72.46}$, and indicates a net oversaturation with respect to tobermorite ($Ca_5Si_6H_6O_{20} + 10\ H^+ \Leftrightarrow 5\ Ca^{2+} + 6\ SiO_2 + 8\ H_2O$ $pK_s = -69.08$).

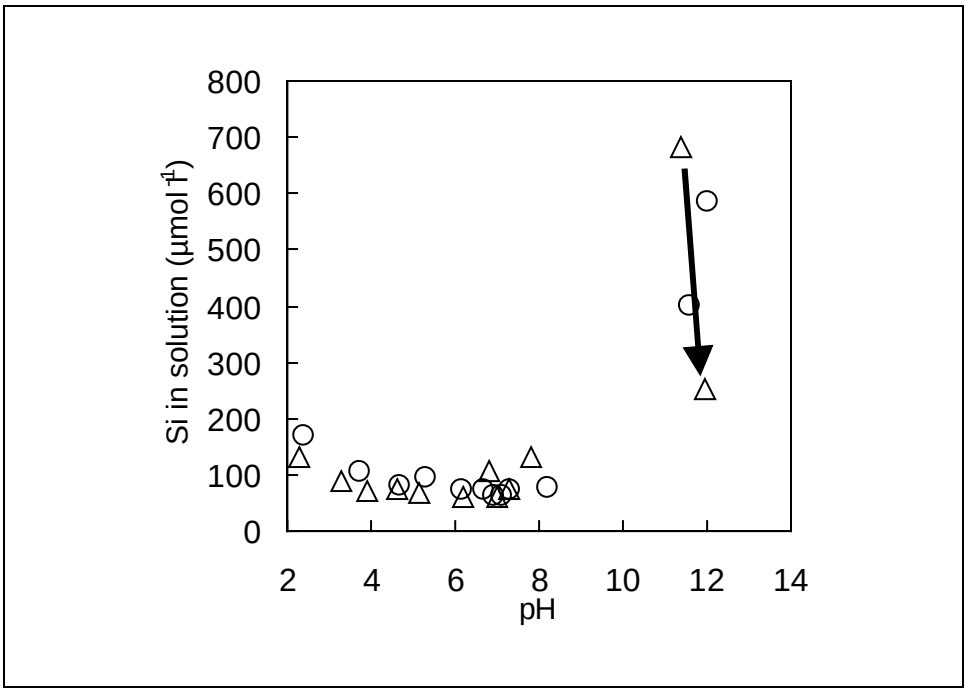


Figure 4.12 : Concentration of Si in solution as a function of pH for experiments 1 (open circles) and 2 (open triangles). The arrow indicates the decrease of the Si concentration at high pH in experiment 2 ($CaCl_2$ ionic background) and the probable precipitation of a Ca-Si hydrated phase.

At pH < 4, the pronounced decrease in $\Delta\Delta[OH^-]$ concomitant to a Na-CEC decrease (Figure 4.9) can be attributed to two distinct phenomena. The first one is a H^+/Na^+ exchange reaction (Gilbert and Laudelout, 1965). The second one is the dissolution of the clay and the exchange of Na^+ by Al^{3+} (Baeyens and Bradbury, 1997). Figure 4.13 shows the concentration of Al, Mg, and Fe between pH 2 and pH 4.5 in experiment 3. Al is significantly released in solution in this experiment (up to 2.9×10^{-5} mol l^{-1} at pH 2.14).

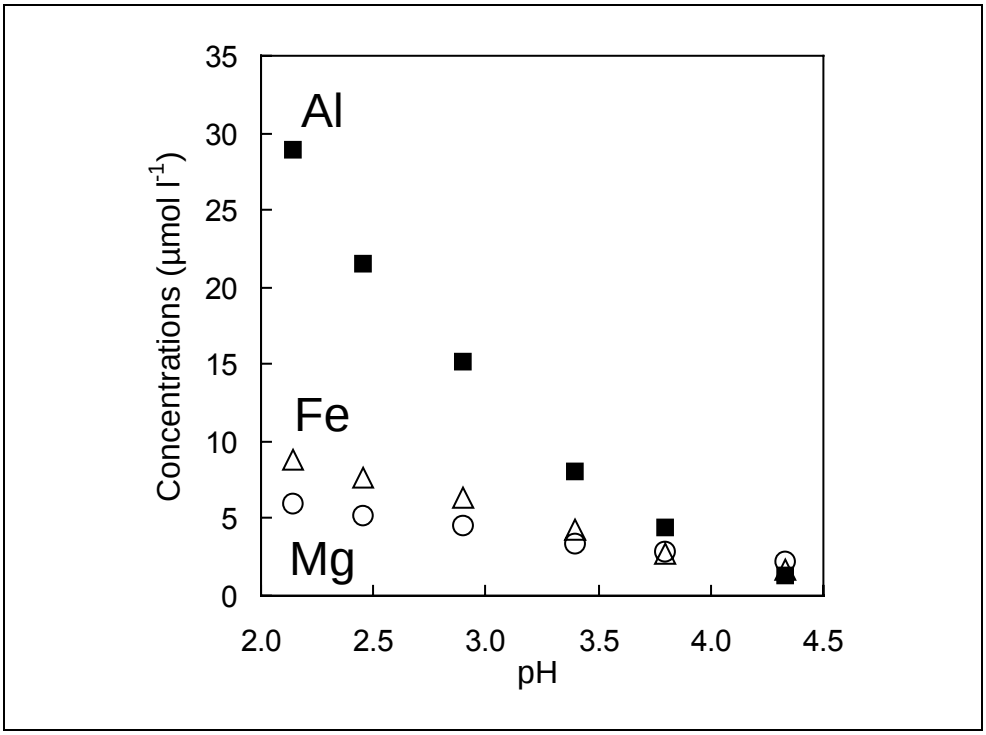


Figure 4.13 : Concentrations of Al (black squares), Fe (open triangles), Mg (open circles) as a function of pH in experiment 3.

The Al concentrations are compared in Figure 4.14 for experiments 1, 2 and 3. It appears that significant and equivalent concentrations of Al are measured in case of experiments 2 and 3, i.e., experiments in $CaCl_2$ ionic background.

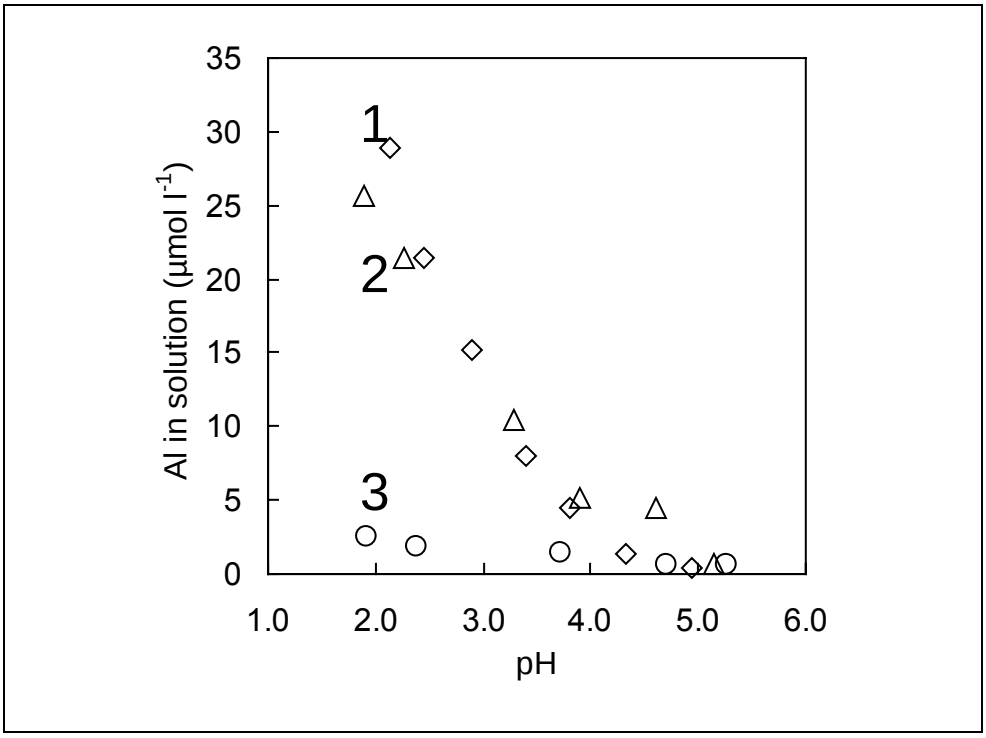


Figure 4.14 : Concentration of Al as a function of pH in experiments 1 (open circles), 2 (open triangles), and 3 (open diamonds).

In case of experiment 1, *i.e.* in NaCl ionic background, the observed Al concentrations are close to the detection limit (d.l. = 0.5 µmol l^{-1}). These low Al concentrations are attributed to the adsorption of Al^{3+} at basal plane cation exchange position, due to the high Al/Na selectivity

coefficient of the montmorillonite (see Charlet et al., 1993, and the tabulation of selectivity coefficients in Llnl.dat, Wateq4f or Phreeqc databases; log $K^{Al/Na}$ values range from 0.41 to 0.67). As a first approximation, we consider that the selectivity coefficient of the Al/Ca exchange can be calculated by combining the Al/Na selectivity coefficient with the Na/Ca selectivity coefficient. This approximation is true if the exchange processes on clay minerals can be considered as ideal processes. In the 80's, Sposito et al. (e.g. Sposito, 1981; Sposito et al., 1981; Sposito et al., 1983a; Fletcher and Sposito, 1989) showed already the ideal behavior of Na^+-divalent cations exchange reactions. This ideality is here assumed for a Na^+-Al^{3+} exchange at low pH. Since the selectivity of the Ca/Na exchange is high (log $K^{Ca/Na}$ = 0.8 after Llnl.dat, Wateq4f and Phreeqc databases), the selectivity coefficient for the Al/Ca exchange must be low (log $K^{Al/Ca}$ value from –1.58 to –1.06 according to the combination of above cited values). Then, Al^{3+} shall not displace Ca^{2+} from the exchange sites. This phenomenon explains the differences of Al^{3+} concentrations measured in the acid pH range, between experiment 1, and, experiments 2 and 3. It is then possible to correct the apparent CEC and $\Delta\Delta[OH^-]$ values from this effect. We consider that the amount of Al^{3+} released in solution by dissolution is equal to the amount released in experiments 2 and 3 at equivalent pH. The CEC and $\Delta\Delta[OH^-]$ values of experiments 1 (0.02 mol l^{-1} NaCl) are then corrected between pH 1 and 4 by the difference of aqueous Al^{3+} moles of charge in solution (in mol kg^{-1}) between experiment 1 and experiment 2 or 3 (0.0068 and 0.05 mol l^{-1} $CaCl_2$ respectively). The correction does not exceed 0.02 mole kg^{-1}. Despite of this correction, the apparent CEC differences remain significant between the experiment 1, and the experiments 2 and 3 (Figure 4.15). Then, by considering the $\Delta\Delta[OH^-]$ and apparent CEC measured in experiments 1, 2 and 3, it appears that H^+ may replace Na^+ in experiment 1, whereas the H^+-Ca^{2+} exchange reaction is very limited in experiment 2 and 3. We may also note that the Ca-CEC is ever greater than the Na-CEC even within the pH range 4 to 7, where neither H^+ nor $CaOH^+$ sorption in exchange site position occurs (Figure 4.15). This difference between Na-CEC and Ca-CEC has been ascribed to the adsorption of $CaCl^+$ ionic pairs (Sposito et al., 1983a).

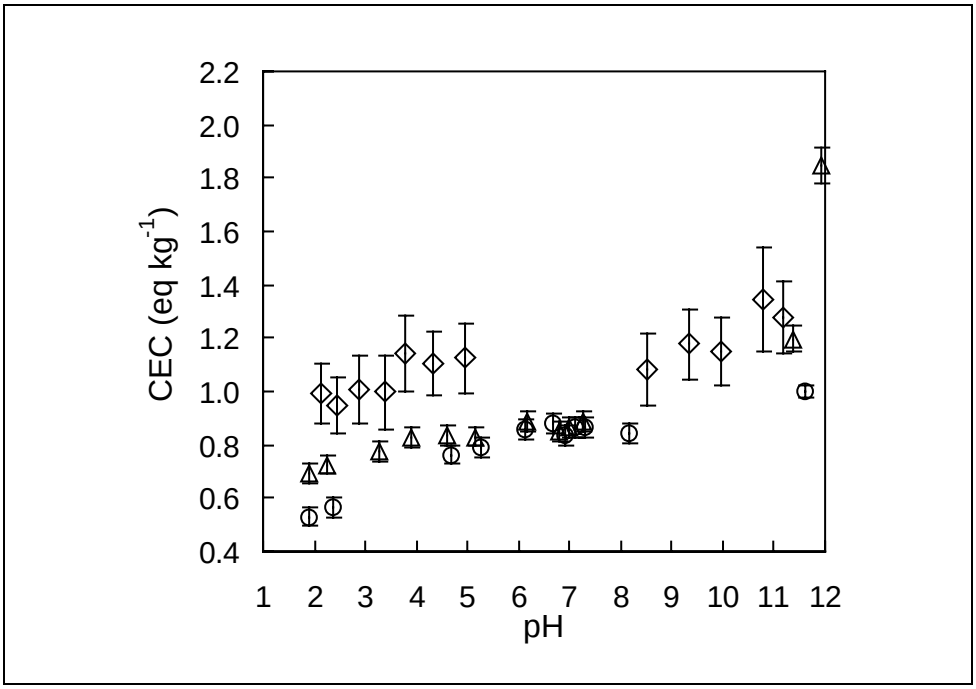


Figure 4.15 : Comparison of the CEC as a function of pH for experiments 1 (open circles), 2 (open triangles), and 3 (open diamonds).

Based on exchange reactions involving Na^+, K^+, or Cs^+, it has been demonstrated already that the CEC of clay minerals vary as a function of pH (e.g. Gilbert and Laudelout, 1965; Maes et al., 1976; Fletcher and Sposito, 1989; Gaucher, 1998). In this article, we demonstrate that these

variations are correlated with protonation/deprotonation reactions attributed to the reactivity of clay platelet edges, for pH value between 4 and 9. The CEC is measured often at near neutral pH (*e.g.* Metson, 1956). In such conditions, the measured CEC must be attributed to two contributions: the contribution of the structural charge (σ_O) given by the structural formula and the contribution of the edge charge (σ_H).

CONCLUSION

The combination of titration plus backtitration technique, for net proton surface excess measurement, with ammonium acetate extraction, for Na- and Ca-CEC measurements, is powerful. It permits to identify the main mechanisms responsible for changes in titration curves: dissolution processes, variations in edge net proton surface charge, exchange mechanisms, adsorption of ionic pairs and precipitation of new phases. As a summary, we have shown that:

- between pH 4 and pH 9, the titration data do depend on neither the ionic background salt (NaCl or $CaCl_2$) nor its concentration;
- below pH 4, dissolution and Na^+/H^+ exchange affects the titration data;
- above pH 9, the sorption in exchange site position of $CaOH^+$ ionic pairs can lead to an overestimation of both Ca^{2+} adsorbed or H^+ desorbed amounts, *i.e.* an overestimate of both the CEC and the net proton surface charge;
- above pH 11, the dissolution of clay together with the presence of calcium in the solution leads to the formation of a tobermorite-like phase; and
- on the whole pH range, the negative charge created by the deprotonation reactions is compensated by an equivalent sorption of Na^+ or Ca^{2+}. Then, the electrostatic term can be ignored in clay complexation models

The whole results can be used to test existing models and/or to construct a coherent H^+ sorption model. This work is presented in part II of the present article.

ACKNOWLEDGEMENT

This research was funded by the French National radioactive waste management agency (ANDRA).

THE TITRATION OF CLAY MINERALS. PART II. STRUCTURAL BASED MODEL AND IMPLICATIONS ON CLAY REACTIVITY.

Christophe Tournassat[1,2], Eric Ferrage[1,2], Christiane Poinsignon[3], Laurent Charlet[1]

To be submitted to Journal of Colloid and Interface Sciences

[1] LGIT - CNRS/UJF, University of Grenoble-I, P.O. Box 53, F 38041 Grenoble, France

[2] ANDRA, Parc de la Croix Blanche, 1/7 rue Jean Monnet, F-92298 Châtenay-Malabry CEDEX, France

[3] LEPMI-ENSEEG, University of Grenoble-I, P.O. Box 75, F 38041 Grenoble, France

ABSTRACT

The potentiometric titration and CEC data, presented in part I, are modeled in the present part II. Two models are compared. The first one is the 2 pK, 3 complexation sites plus exchange sites non-electrostatic model developed by Baeyens and Bradbury. The second one is a model based on the Hiemstra and Van Riemsdijk MUSIC approach. Morphological and structural information is used to develop this model. Morphological information is taken from the literature, whereas structural information is taken from literature and constrained by supporting FTIR experiments.

The Baeyens and Bradbury model is found to respect the whole tendency of the titration curve, whereas the model based on Hiemstra and Van Riemsdijk MUSIC approach permits to better adjust the experimental data. The former uses only 3 edge reaction sites, whereas the later uses at least 27 edge reaction sites. 5 main reactive sites are sufficient to fit the curve, but the model allows us to derivate the properties of 22 other reactive sites. Logically, the greater the amount of sites, the better the adjustment. Nevertheless, a lower amount of adjustable parameters is necessary to build the model based on the Hiemstra and Van Riemsdijk MUSIC approach, than to build the Baeyens and Bradbury model, thanks to structural and morphological constraints. The precision of the potentiometric titration curve is not sufficient to verify that the properties of the 27 sites, given by the model, are effective. Thus, we linked some properties of clay minerals, like dissolution, to the modeled acid – base properties of these sites, to assess our model. Then, we question the ability of oversimplified models to predict the interactions, between clay minerals and solutions, in natural environments.

As secondary results, we have derived, from our CEC data, the cation exchange selectivity coefficients for $CaCl^+$ and $CaOH^+$ ionic pairs, and H^+.

INTRODUCTION

Sorption mechanisms on clay surfaces have been studied for decades and one distinguishes: (i) inorganic cation exchange in the interlayer and on basal plane surfaces (e.g. Sposito, 1981) and (ii) specific pH dependent sorption of cations and anions on the edges (e.g. Sposito, 1984). Edge sorption mechanism is related to the acido-basic properties of the clay edges (Fletcher and Sposito, 1989; Charlet et al., 1993; Stadler and Schindler, 1993; Zachara and Smith, 1994; Bradbury and Baeyens, 1997; Avena, 2002 and others) whereas cation exchange on basal planes is related to the permanent charge generated by the clay structure (Sposito, 1981). The former mechanism is a pH dependant specific sorption on the clay edges. It has already been well established that the proton surface charge density (σ_H) on the clay edges depends on physico-chemical solution parameters (pH, ionic strength) which control the protonation state of the surface (Fletcher and Sposito, 1989; Charlet et al., 1993; Zachara et al., 1993; Wanner et al., 1994; Baeyens and Bradbury, 1997; Bradbury and Baeyens, 1997; Avena, 2002 and others). The latter mechanism originates from the presence of a permanent negative structural charge in the alumino-silicate layer created by isomorphic substitutions in the lattice. The density of exchange sites (σ_o) can be derived from structural formula, and is compensated by “exchangeable cations”, which generally form outer sphere complexes in siloxane cavities (Sposito, 1981, 1984).

In part I (Tournassat et al., submitted-c), Na- and Ca-MX80 montmorillonite surface charge data were presented. They were obtained by the combination of (i) potentiometric backtitration technique (Schultess and Sparks, 1986; Baeyens and Bradbury, 1997) and (ii) CEC measurements technique (Sposito et al., 1983a). This combination is shown to be powerful as it permits to identify each phenomena which concurs to the whole surface charge phenomenon: dissolution processes, variations of the net proton edge surface charge, cation and proton exchange mechanisms, adsorption of ionic pairs and precipitation of new phases. In the present paper (part II), models of the surface charge data are proposed. The first approach is a macroscopic surface complexation model (Bradbury and Baeyens, 1997). The second one is based on the bond valence principle (MUSIC, Hiemstra et al., 1996). The first model is an empirical model, developed by fitting together titration and metal sorption data, the quality criterion being the best agreement between model and experimental data. In the MUSIC model, morphological and structural data are used to derivate chemical properties of the solid. However, even with this more sophisticated approach, assumptions (*e.g.* on cations distributions) are necessary to build the surface clay chemical model. Supporting information, obtained with Fourier Transform Infra Red (FTIR) spectoscopy experiments, is used to constrain these assumptions.

STRUCTURAL INPUT FROM FTIR MEASUREMENTS

Theoretical background

Some sites present within the structure are *a priori* able to present acid-base properties as shall be shown below, based on their affinity for proton. However, diffusion of H^+ through the siloxane plane is doubtful. Hence, the first goal of FTIR experiments was to refute the possible fast proton sorption within the clay structure, and thus to show that fast proton sorption occurs only on edge surfaces. Deuterium atoms (D, = hydrogen isotope of mass value equal to two) have the same chemical properties than hydrogen atoms. Use of D_2O for hydrothermal synthesis is a common method for identifying the IR absorption bands in clay minerals like talc, because of the conversion of some, or of all, of the OH groups to OD groups (Stubican and Roy, 1961; Farmer et al., 1968; Russel et al., 1970; Shirozu and Ishida, 1982; Ishida, 1990; Grauby et al., 1991; Martin et al., 1999). When D replaces H, the difference in atomic mass induces a shift of all vibrations due to OH groups towards lower wavenumbers by a factor *R*

close to 1.37 (Langer and Lattard, 1980). Then deuterated OD stretching bands are present in the 2800-2500 cm^{-1} region. Since this region of the spectrum is free of other structural vibrations in case of clay minerals, it allows the degree of H-D exchange to be easily determined. In the present work, we apply the same technique to smectite, in order to see the possible diffusion of D^+ (and hence H^+) inside of the structure at 25°C.

Gaining knowledge on the cation distribution inside the octahedral layer was the second goal of FTIR experiments. The 950-750 cm^{-1} wavenumbers range OH-bending region gives information on the cation distribution occurring in the octahedral layer (Vantelon et al., 2001). By quantifying the area of the bands corresponding to the substitution of Al by Mg or Fe, it is possible to know if the cation distribution is ordered, random, or clustered. The procedure of Besson and Drits (Schultess and Sparks, 1988; Besson and Drits, 1997a) was here applied to fit the OH-bending bands: the components were extracted, as pure Lorentzian curve, from the total curve together with the background. The bands decomposition program uses a conjugated-gradient fitting procedure taking into account Gaussian and/or Lorentzian shapes functions.

Preparation of the sample and measurement

A Na-conditioned smectite has been equilibrated during 90 days with a 40% D_2O 60% H_2O 0.01 mol l^{-1} NaCl solution, at 25 °C. A 1 ml aliquot of suspension was deposited on a circular silicon support (25 × 2 mm, Eurolabo reference 1840) and was allowed to dry at room temperature. FTIR spectra of the clay film on support and support alone were recorded using a Nicolet 710 FTIR spectrometer (128 scans in the 4000-400 cm^{-1} domain, with a 4 cm^{-1} resolution). Spectra of the clay film were obtained by subtracting the support signal from the total signal.

Results

Figure 4.16 shows the results of the FT-IR experiment. Characteristic deformation bands for montmorillonite are well designed in the region 1100-800 cm^{-1} (Madejova and Komadel, 2001). Impurities of quartz are also visible (arrow on Figure 4.16). The 3800-3200 cm^{-1} wavenumber region exhibits a single band relative to $(Me_1Me_2)OH$ stretching vibration, where Me_1 and Me_2 denote octahedral cations (Al^{3+}, Mg^{2+}, Fe^{3+} and Fe^{2+}). This region is almost free from OH vibration of interlayer water, meaning that most of the water has evaporated. Therefore, OD vibration bands of interlayer deuterated water can not overlap with the OD stretching bands characteristics of inner surface hydroxyl groups. While the $(Me_1Me_2)OH$ stretching bands are usually observed at 3633 cm^{-1}, we do not observe any peak corresponding to the deuteration of the $(Me_1Me_2)OD$ stretching bands in the 2800-2500 cm^{-1} region. Hence, we can conclude that little H^+/D^+ diffusion occurs in the bulk of the smectite structure at 25°C and thus, that clay protonation does not involve – within 90 days reaction time – the structural smectite protons. This is in agreement with previous studies; on talc for instance, H^+ do not diffuse perpendicularly to the basal planes (e.g. Ferrage et al., 2003). Based on these results we shall use only surface reactions to explain the smectite titration data detailed in part I.

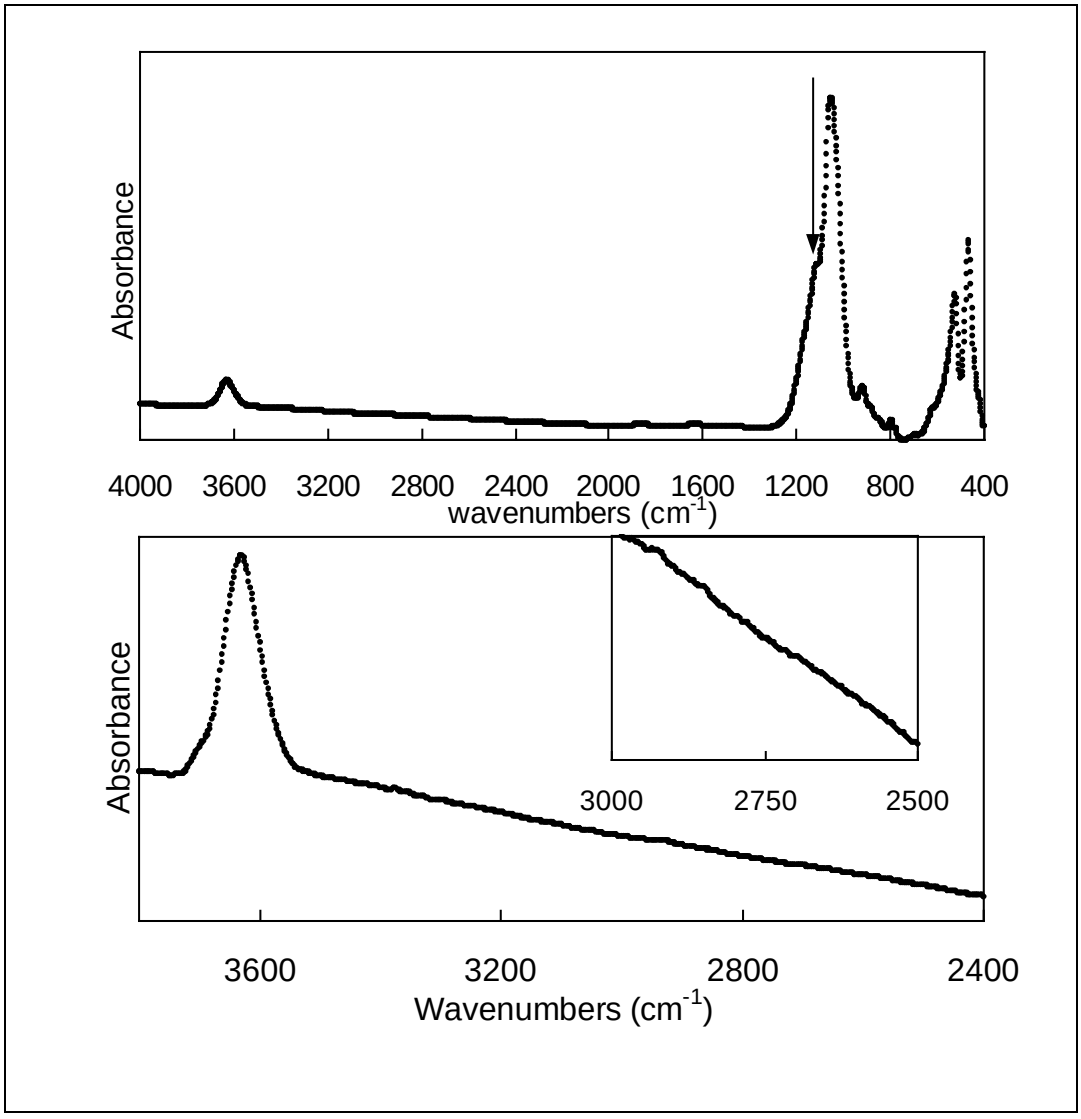


Figure 4.16 : Transmission IR spectra of Na- D_2O-conditioned MX80 montmorillonite at 25°C using a silicon support (see text for details). Top: spectrum in the 4000 to 400 cm^{-1} range. Bottom: zoom on the OH stretching region (3700-3500 cm^{-1}) and on the OD stretching region (3000-2500 cm^{-1}).

Figure 4.17 shows the decomposition of the 950-750 cm^{-1} wavenumbers region. Three main bending bands are expected to be present (δ_{AlAlOH}, δ_{AlFeOH} and δ_{AlMgOH}) based on the structural formula of MX80 smectite clay (Tournassat et al., submitted-c):

$(Si_{3.98}Al_{0.02})(Al_{1.61}Fe^{3+}_{0.13}Fe^{2+}_{0.02}Mg_{0.24})O_{10}(OH)_2Na_{0.28}$

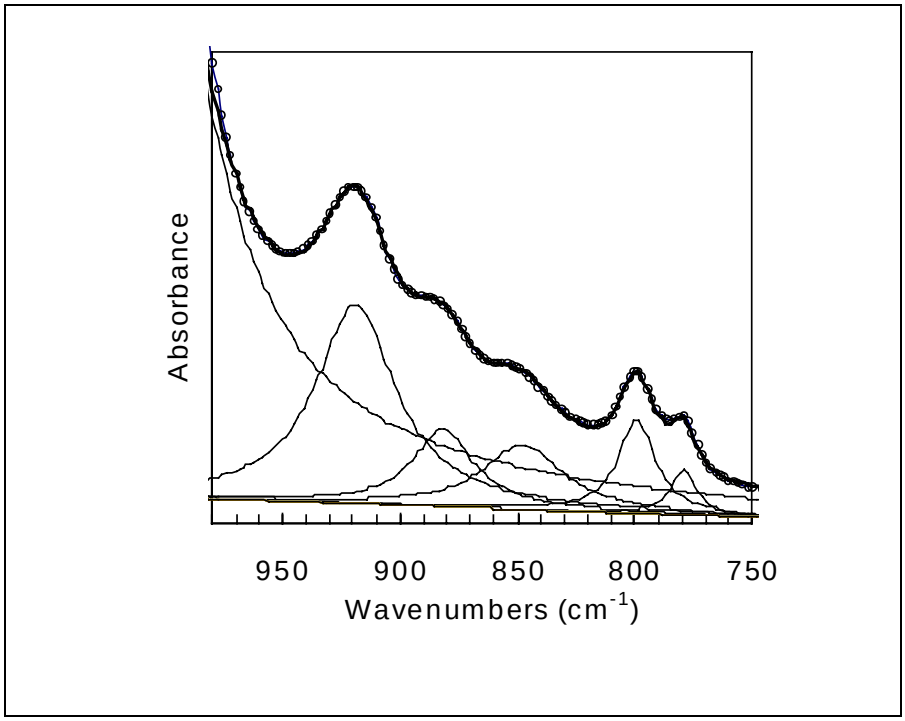


Figure 4.17 : Thick line: transmission IR spectrum of Na-conditioned MX80 montmorillonite in the OH-bending range (980-750 cm^{-1}). Thin line: decomposition of the spectrum (see text for details).

After removal of the background, the spectrum can be fitted with three bending bands in the 820-950 cm^{-1} region corresponding to δ_{AlAlOH} (~919 cm^{-1}), δ_{AlFeOH} (~882 cm^{-1}) and δ_{AlMgOH} (~848 cm^{-1}). These vibration positions are in good agreement with those given by Vantelon et al. (Vantelon et al., 2001) for similar smectites. The position of the δ_{AlFeOH} band fits well with band position given for montmorillonite by Craciun (Craciun, 1984) as a function of Fe content (calculated value at 883 cm^{-1}). Bands at 799 and 780 cm^{-1} are attributed to quartz (Madejova and Komadel, 2001). Other bending bands, such as $\delta_{AlFeIIOH}$ and δ_{MgMgOH} bands, are not detected here, due to low Fe(II) and Mg(II) content in the MX80 smectite octahedral layer.

The area under the δ_{AlAlOH}, δ_{AlFeOH} and δ_{AlMgOH} bands are compared in Figure 4.18 to theoretical areas, calculated on the basis of (i) the above structural formula, (ii) the assumed cation random distribution in the octahedral layer and (iii), an assumed invariant absorption coefficient for the different OH groups (Slonimskaya et al., 1986; Besson and Drits, 1997b, a; Madejova and Komadel, 2001; Vantelon et al., 2001). For example, the δ_{AlAlOH} band should represent $\frac{1.61}{2}\times\frac{1.61}{2}\times 100 = 64.8\,\%$ of the total absorbance area. Figure 4.18 shows that the experimental points lie on the line corresponding to a random distribution. According to this result, the distribution of Al, Fe and Mg cations within the octahedral layer is a near-random distribution. In the following, this information will be used to calculate the proportion of each edge surface functional group.

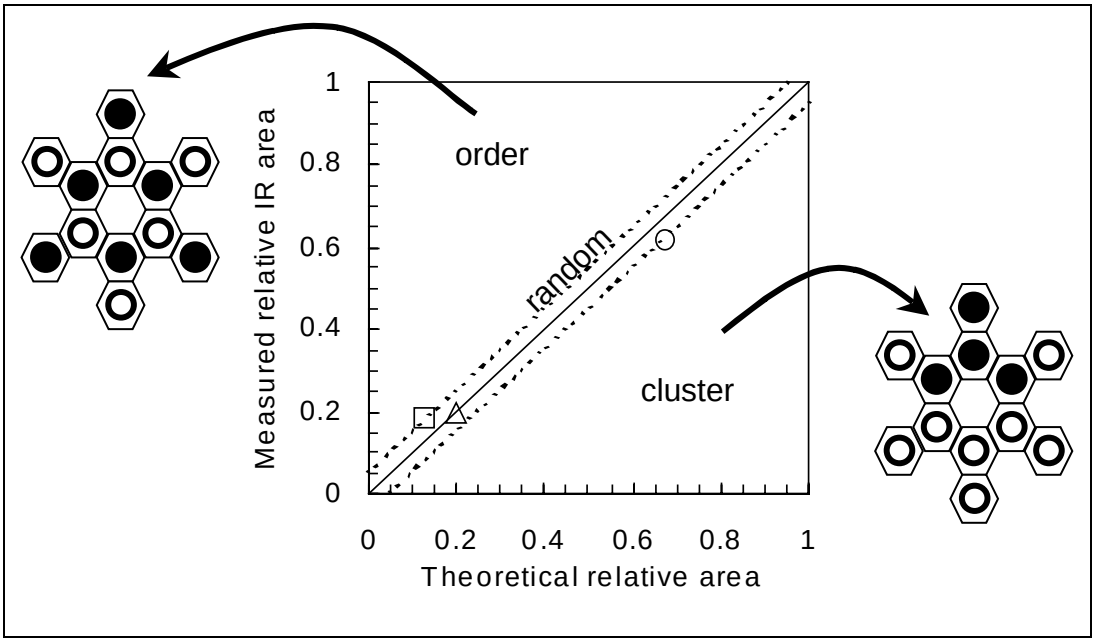


Figure 4.18 : Relative areas of the various OH-bending bands contribution as a function of the theoretical areas derived from assuming a fully random distribution and schematic representation of cation distribution in the octahedral sheet (after Vantelon et al., 2001). Circle: δ_{AlAlOH}. Square: δ_{AlFeOH}. Triangle: δ_{AlMgOH}.

MODELING THE TITRATION DATA

Common mechanisms and code

Two modeling approaches are compared in the present section. The first one is the macroscopic surface complexation model from Bradbury and Baeyens (Bradbury and Baeyens, 1997). The second one is a model based on mineral structure and bond valence principle, according to the MUSIC approach (Hiemstra et al., 1996). Since we have shown that protons uptake within the clay structure is not occurring in a 90 days reaction time, we shall consider only two proton sorption mechanisms: cation exchange on the basal / interlayer planes and specific sorption on clay edges. The electrostatic term is neglected based on the results presented in part I, *i.e.* on the independence of the proton surface charge density with background ionic strength. One should remember that the absolute position of the titration curves is not known (Tournassat et al., submitted-c). The titration data are therefore presented as $\Delta\Delta H^+$ as a function of pH, where

$$\Delta\Delta H^+ = \Delta H^+ + A \qquad \text{Eq. 4.19}$$

ΔH^+ is the surface proton excess given by the Eq. 4.13, and A is a constant. In the following, we simulate ΔH^+. Then, A must be considered as an adjustable parameter and A is chosen in order that the simulation matches as well as possible the experimental results. The Phreeqc2 code (Parkhurst and Appelo, 1999) is used for both approaches, as this versatile computer code is amenable to the various conventions used to describe cation exchange and surface complexation. The Llnl.dat database is used for the calculation of speciation in solution.

Bradbury and Baeyens model

Simulation parameters used in the present study are closed to those used in the original study to describe titration data of saturated Na-montmorillonite (Bradbury and Baeyens, 1997). Few parameters were changed with respect to cation exchange. We have adjusted the CEC

value to our theoretical value (Tournassat et al., submitted-c), which takes into account the stoichiometry of the clay and the dehydrated suspended clay concentration (0.76 eq kg^{-1}). Tab. 4.9 summarizes these parameters. Vanselow's convention was used to model cation exchange (Vanselow, 1932; Sposito et al., 1981). Cation exchange selectivity coefficients were fitted with our Na- and Ca-CEC data and with the CEC data previously published by Sposito et al. (Sposito et al., 1983a). The cation exchange of ion pairs (like $CaCl^+$ and $CaOH^+$) was considered in agreement with Sposito et al. results (Sposito et al., 1983a) and with the results presented in part I (Tournassat et al., submitted-c).

Site types	Site capacities
Strong sites ($\equiv S^sOH$)	2×10^{-3} mol kg^{-1} †
Weak sites 1 ($\equiv S^{w1}OH$)	4×10^{-2} mol kg^{-1} †
Weak sites 2 ($\equiv S^{w2}OH$)	4×10^{-2} mol kg^{-1} †
Cation exchange sites (X^-)	0.76 eq kg^{-1} ‡

† Fixed
‡ Adjusted to the theoretical structural CEC value (Tournassat et al., submitted-c)

Tab. 4.9 : Site types and sites capacities used in the simulation, based on Bradbury and Baeyens model (Bradbury and Baeyens, 1997).

Hiemstra and Van Riemsdijk MUSIC model

In the MUSIC model, the proton affinity of a surface group is calculated from the fractional charge of a surface oxygen and from the bond valence of all its ligands (Hiemstra et al., 1996; Venema et al., 1998). Initially created to model simple oxides like quartz, alumina, titanium oxides or iron (hydr)oxides (Hiemstra et al., 1989a; Hiemstra et al., 1989b), it has been refined several times (Hiemstra et al., 1989b; Hiemstra and Van Riemsdijk, 1996; Hiemstra et al., 1996; Venema et al., 1998). In the present article, we first attempt to apply its updated version (Hiemstra et al., 1996; Venema et al., 1998) to complex oxides, namely clay minerals. Proton affinity were computed with the following formula (Hiemstra et al., 1996):

$$\log K = -A\left(\sum_j s_j + V\right) \qquad \text{Eq. 4.20}$$

where A is a constant set to +19.8 (Hiemstra et al., 1996), V is the valence of the involved oxygen (V= -2), and $\sum_j s_j$ is the sum of all bond valences of the surrounding cations (j) and H bonds:

$$\sum_j s_j = \sum_i s_{Me_i} + m \times s_H + n \times (1 - s_H). \qquad \text{Eq. 4.21}$$

where $\sum_j s_{Me_i}$ is the contribution of the i surrounding Me_i ions, s_H the bond valence of the H donating bond (s_H = 0.8), (1 - s_H) the bond valence of the H accepting bond and m and n respectively the number of donating and accepting H bridges built with adsorbed water. The

contribution of the surrounding *Me* ions (s_{Me}) are calculated according to Brown and Altermatt (Brown and Altermatt, 1985) with :

$$s_{Me} = e^{\frac{(R_0 - R)}{b}} \qquad \text{Eq. 4.22}$$

where R is the Me-O distance, R_0 is the element specific distance (Brown and Altermatt, 1985) and b is a constant (set equal to 0.37 Å). Tab. 4.10 summarizes the calculated s_{Me} values for MX80 montmorillonite. In Eq. 4.21, m and n remain the only free parameters to calculate the proton affinity of surface groups. Thus, these parameters were chosen, based on steric considerations after the Hiemstra et al. criteria (Hiemstra et al., 1996). Singly coordinated surface groups interact with two donating or accepting hydrogen bonds ($m + n = 2$), except the singly coordinated tetrahedral Si-O surface groups, which interact with three hydrogen bonds ($m + n = 3$). Doubly coordinated surface groups interact with only one or two hydrogen bonds ($m + n = 1$ or 2). No criterion was given to choose between these two possibilities (Hiemstra et al., 1996). We chose a $m + n$ value of 1, to better adjust our data. Triply coordinated surface groups interact with only one hydrogen bond.

	d_{Me-O} (Å)	R_0 (Å)	s_{Me}
Si-O	1.646[§]	1.624	0.942
Al_{Oh}-O	1.93[§]	1.651	0.470
Mg-O	2.07[‡]	1.693	0.361
Fe^{III}-O	1.98[‡]	1.759	0.550
Fe^{II}-O	2.12[‡]	1.734	0.352

[§] Based on the muscovite structure (Guggenheim et al., 1987)
[‡] Based on Drits et al. (Drits et al., 1997)

Tab. 4.10 : Distances between the oxygen atom of the surface groups and their nearest metal neighbors (d_{Me-O}), specific distance relative to the ligand (R_0) after Brown and Altermatt (Brown and Altermatt, 1985) and calculated actual bond valence (s_{Me}).

Eq. 4.19 allows therefore to derivate the proton affinity constant of the surface groups from structural information. Nevertheless, others parameters are needed to model the titration data, namely the amounts of each surface functional group types. This can be calculated by multiplying the edge surface area (in $m^2\ kg^{-1}$) by the surface density of edge sites (in mol m^{-2}). The different surface areas of the Na-montmorillonite MX80 in suspension (Tournassat et al., submitted-d) are summarized in Tab. 4.11. Since morphology of the montmorillonite platelets does not exhibit any kind of preferential crystallographic direction (Tournassat et al., submitted-d), it may be assumed that the amount of sites can be determined on the basis of the mean of the amount of sites present in three different crystallographic directions, *i.e.* (100), (010) and (110). The calculation of site densities can be achieved by considering a muscovite structure (Guggenheim et al., 1987), whose TOT layer has the same structure than the montmorillonite one. As stated before by White and Zelazny (White and Zelazny, 1988), the edges can exhibit two types of terminations that these authors called AC type chains and B type chains. In case of AC type chains, the termination of the platelet, constituted by a Si tetrahedron, a Al octahedron and a Si tetrahedron, is oblique compared to the crystallographic *c* axis. In case of B type chains, this termination is parallel to the crystallographic *c* axis. This difference of termination

leads to differences in site types densities. The structure of the montmorillonite is presented in the AC and B type chain configuration in Figure 4.19 (top and bottom respectively).

Basal and Interlayer Surface Area ($m^2\ g^{-1}$)	Edge Surface Area ($m^2\ g^{-1}$)	Total Surface Area ($m^2\ g^{-1}$)
780	8.5	788

Tab. 4.11 : Surface area values for the Na-MX80 clay fraction in suspension (after Tournassat et al., submitted-d).

The calculated sites densities for these two types of configuration are summarized in Tab. 4.12. Since we have no information about the dominant configuration, we considered the mean value of the densities present on the AC and B chains. Tab. 4.12 shows that there is little variations of the total amount of sites between the two types of edge chains. Thus, on the basis of the structural formula and assuming a cation random distribution in the octahedral layer (see structural input from FTIR Section), it is possible to calculate the amounts of each type of surface functional groups. Results are presented in Tab. 4.13, together with the proton affinity constant calculated according to Eq. 4.20. Considering that $\equiv SOH^z$ represents one type of edge surface functional group with a *z* formal charge, then the first protonation constant listed in Tab. 4.13 corresponds to reaction:

$$\equiv SO^{(z-1)} + H^+ \Leftrightarrow \equiv SOH^z \qquad \text{Eq. 4.23}$$

and the second protonation corresponds to reaction:

$$\equiv SOH^z + H^+ \Leftrightarrow \equiv SOH_2^{(z+1)}. \qquad \text{Eq. 4.24}$$

	Site density (sites nm^{-2})				
direction	Me_{Td}-O	Me_{Oh}-O	Me_{Oh}-O-Me_T	Me_{Oh}-O-Me_{Oh}	$(Me_{Oh})_2$-O-Me_T
AC type chains					
(100)	4.05	2.02	2.02	4.04	4.05
(010)	4.67	3.50	1.17	2.34	4.67
(110)	4.67	2.34	2.34	4.66	4.67
Mean	4.46	2.62	1.84	3.68	4.46
B type chains					
(100)	6.07	0	4.05	4.04	4.05
(010)	4.67	2.33	2.33	2.34	4.67
(110)	4.67	0	4.67	4.66	4.67
Mean	5.14	0.78	3.69	3.68	4.46
Mean of AC + B types chains					
	Me_{Td}O	Me_{Oh}O	Me_{Oh}-O-Me_T	Me_{Oh}-O-Me_{Oh}	$(Me_{Oh})_2$-O-Me_T
Sites nm^{-2}	4.80	1.70	2.77	3.68	4.46
mmol kg^{-1}	67.8	24.0	39.0	52.0	63.0

Tab. 4.12 : Density (sites nm^{-2}) of different sites present on the lateral surfaces of clay particles. Td indicates a tetrahedral position whereas Oh indicates an octahedral position of the metal ion (Me). The calculation of the densities is based on the parameters shown on Figure 4.19, on the edge surface area given in Tab. 4.4, and on a TOT layer thickness of 9.5 Å.

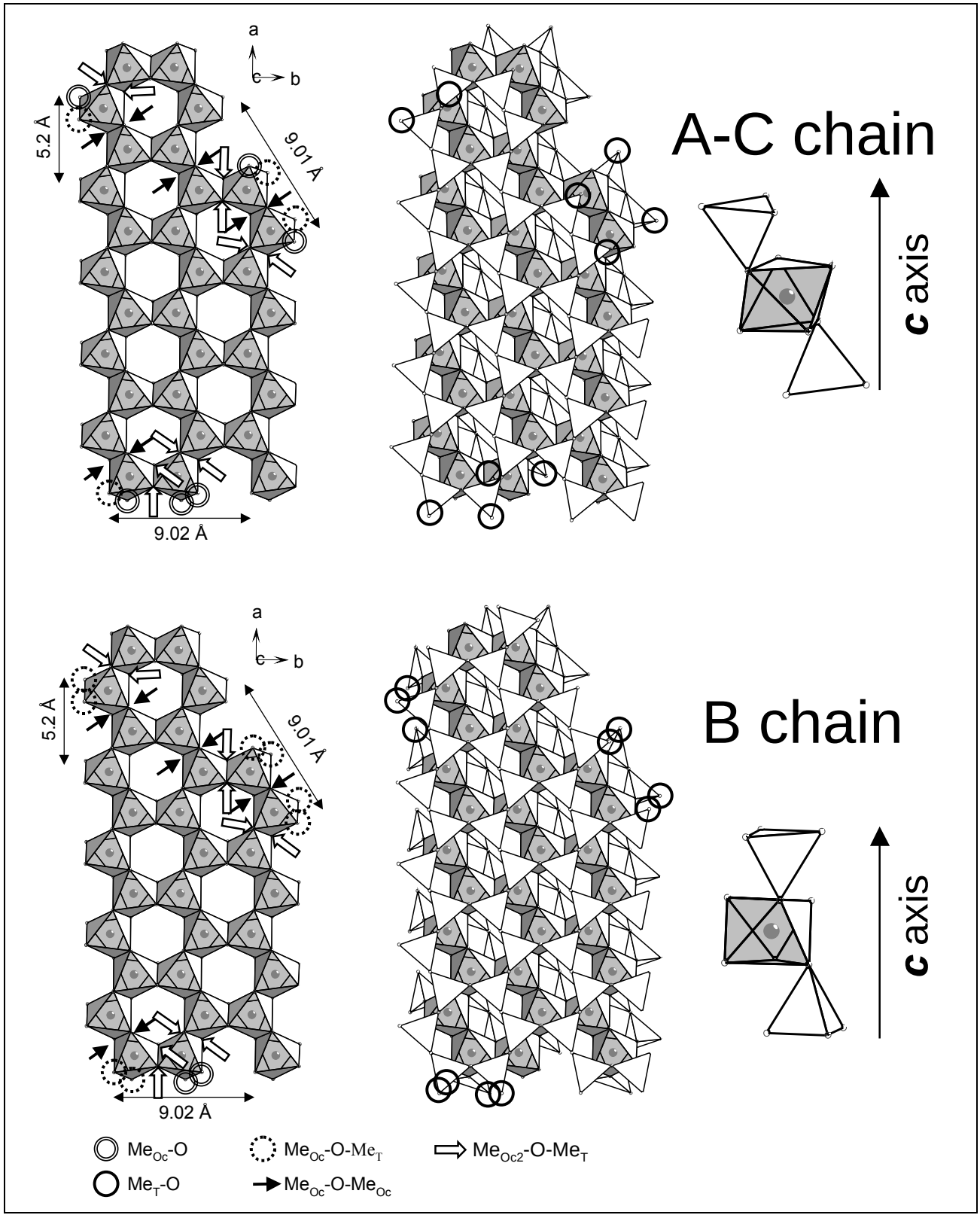


Figure 4.19 : Representation of the clay TOT layer structure. The figures on the left represent the octahedral layer. The figures in the middle represent the whole TOT layer structure seen from above basal plane. The figures on the right represent the two different layer termination types (A-C and B type chains, see text). Arrows and circles, as indicated by the inner caption, show different sites.

Site	m + n	log *K* 1st protonation	log *K* 2nd protonation	Amount of sites (mmol kg^{-1})
Si_{Td}-O	3	9.1 → **8.2**	-2.8	67.5
Al_{Oh}-O	2	22.4	**10.5**	19.3
Mg_{Oh}-O	2	24.5	**12.7**	2.9
Fe^{II}_{Oh}-O	2	24.7	12.8	0.2
Fe^{III}_{Oh}-O	2	20.8	**8.9**	1.6
Al_{Oh}-O -Al_{Oh}	1	17.0	5.1 → **4.8**	33.7
Al_{Oh}-O -Mg_{Oh}	1	19.2	**7.3**	10.0
Al_{Oh}-O -Fe^{II}_{Oh}	1	19.3	7.5	0.8
Al_{Oh}-O -Fe^{III}_{Oh}	1	15.4	**3.5**	5.4
Mg_{Oh}-O -Mg_{Oh}	1	21.3	9.5	0.7
Mg_{Oh}-O-Fe^{III}_{Oh}	1	17.6	5.7	0.8
Mg_{Oh}-O -Fe^{II}_{Oh}	1	21.5	9.6	0.1
Fe^{III}_{Oh}-O-Fe^{III}_{Oh}	1	13.8	2.0	0.2
Fe^{III}_{Oh}-O-Fe^{II}_{Oh}	1	17.8	5.9	0.1
Fe^{II}_{Oh}-O-Fe^{II}_{Oh}	1	21.7	9.8	0.0
Al_{Oh}-O-Si_{Td}	1	7.7 → **7.2**	-4.2	31.3
Mg_{Oh}-O-Si_{Td}	1	**9.8**	-2.0	4.7
Fe^{II}_{Oh}O -Si_{Td}	1	10.0	-1.9	0.4
Fe^{III}_{Oh}-O-Si_{Td}	1	**6.1**	-5.8	2.5
Al_{Oh2}-O-Si_{Td}	1	-2.7	-14.5	40.8
$AlMg_{Oh}$-O-Si_{Td}	1	-0.4	-12.3	12.7
$AlFe^{III}_{Oh}$-O-Si_{Td}	1	-4.3	-16.2	6.6
$AlFe^{II}_{Oh}$-O-Si_{Td}	1	-0.3	-12.1	1.0
Mg_{Oh2}-O-Si_{Td}	1	1.8	-10.1	0.9
$MgFe^{III}_{Oh}$-O-Si_{Td}	1	-2.1	-13.9	1.0
$MgFe^{II}_{Oh}$-O-Si_{Td}	1	2.0	-13.9	0.2
Fe^{III}_{Oh2}-O-Si_{Td}	1	-5.9	-17.8	0.3

Tab. 4.13 : List of the sites present on the lateral surface of the clay platelets with their m+n parameter, the site densities in mmol kg^{-1} and the proton affinity constants given by equation 4.20. Bold values are those used for the simulation. Brackets indicate that several sites were grouped because of their similar proton affinity constants. The shaded sites are not taken into account in the simulation due to their low amount. Example of log *K* calculation is available upon request.

RESULTS AND DISCUSSION

In the present part, potentiometric titration data, given in part I, are simulated according to two models described above, *i.e.* an empirical cation exchange plus 3 sites 2 pK model based on the Bradbury and Baeyens model (Bradbury and Baeyens, 1997), and a 27 sites structural based model using the MUSIC approach (Hiemstra et al., 1996). The apparent CEC, which should match the measured CEC (based on ammonium acetate extraction), is simulated

by setting it equal to the Na- or Ca- calculated adsorbed amount in exchange position, plus the amount of H^+ desorbed from the edges of the clay platelets as a function of pH.

Bradbury and Baeyens model

The simulations together with the experimental potentiometric data are shown on Figure 4.20.

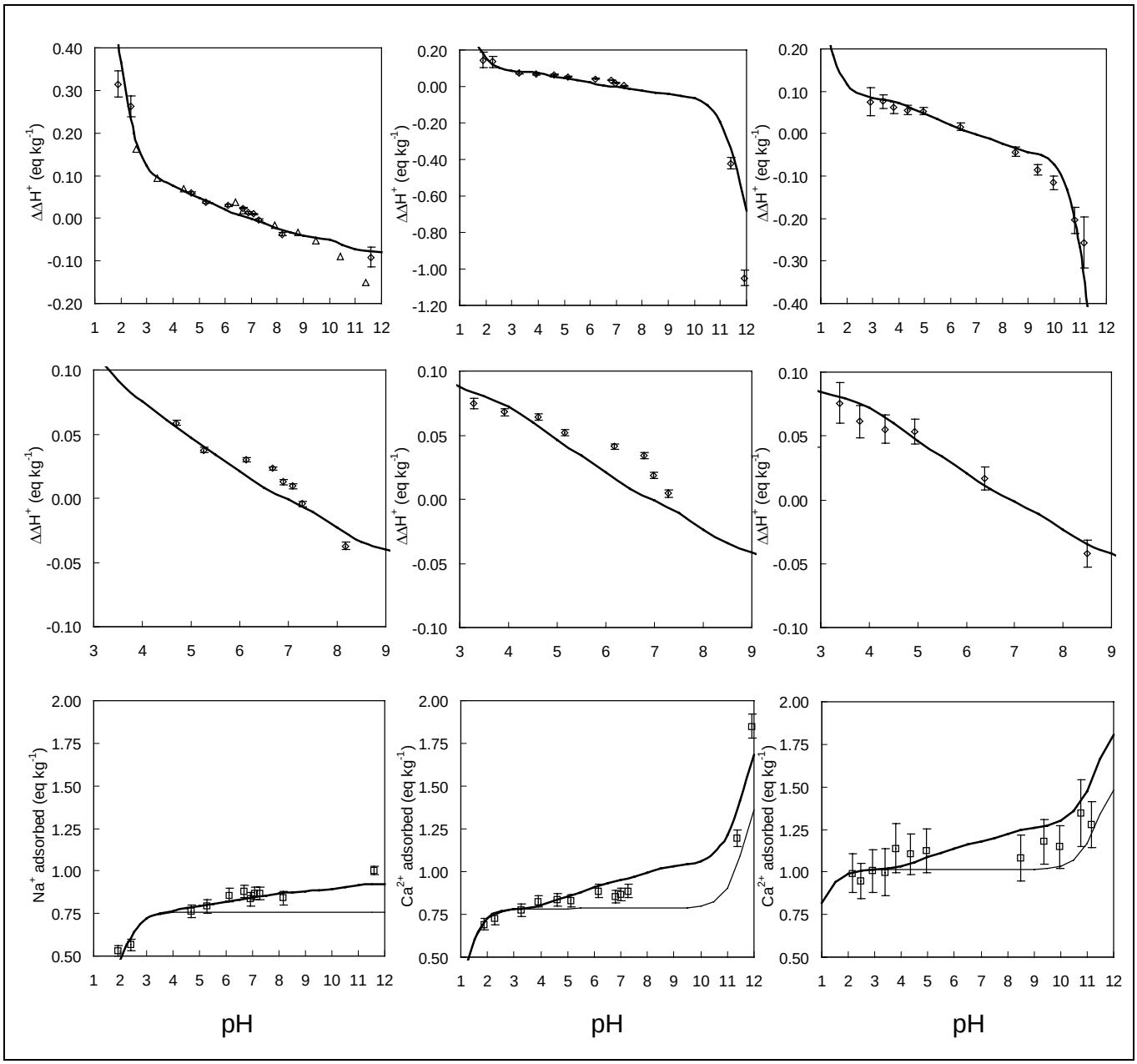


Figure 4.20 : Experimental potentiometric titration data ($\Delta\Delta[H^+]$, top and middle) and CEC data (bottom) of three experiments, described in part I, simulated by the 3 sites, 2 pK Bradbury and Baeyens' model (Bradbury and Baeyens, 1997). From left to right, experiments 1 to 3 respectively (see part I for experimental conditions). Experiment 1, 0.02 mol l^{-1} NaCl, 4.69 g l^{-1}; experiment 2, 0.0068 mol l^{-1} $CaCl_2$, 3.03 g l^{-1}; experiment 3, 0.05 mol l^{-1} $CaCl_2$, 1.53 g l^{-1}.

The parameters of the simulation are given in Tab. 4.14 for edge surface complexation reactions. The only fitted parameters in these simulations are the cation exchange selectivity coefficients. Fletcher and Sposito have already published a synthesis of exchange selectivity

coefficient for montmorillonite (Fletcher and Sposito, 1989). We had some difficulties to fit our data with these coefficients, in particular concerning the $CaCl^+$ ionic pair, whose selectivity coefficient is dependent on the equilibrium constant of the reaction $Ca^{2+} + Cl^- \Leftrightarrow CaCl^+$ and then, on the thermodynamic database used for the simulation. Then, we decided to fit the initial data set (Na/Ca isotherms in ClO_4^- and Cl^- ionic background) to model the binary and ternary $Ca^{2+}/CaCl^+/Na^+$ exchange reactions (Sposito et al., 1983a). The Figure 4.21 shows the results of these simulations. A sensitivity analysis shows that, for Ca^{2+}/Na^+ exchange isotherm obtained in ClO_4^- ionic background, a Ca^{2+}/Na^+ selectivity coefficient value of $10^{0.1}$ to $10^{0.6}$ permits to fit as well the data within the limit of the error bars ($K_v^{Ca/Na} = 10^{0.17}$ in Fletcher and Sposito review Fletcher and Sposito, 1989). We chose a Ca^{2+}/Na^+ exchange selectivity coefficient of $10^{0.4}$. Then, the $Ca^{2+}/CaCl^+/Na^+$ system can be described with a $CaCl^+/Na^+$ exchange selectivity coefficient, which value lies between $10^{2.2}$ and $10^{2.8}$. In agreement with these results and our results (Figure 4.20 and Figure 4.21), the exchange selectivity coefficients were fixed to the values indicated in Tab. 4.15. The 0.0 log *K* value for H^+/Na^+ exchange selectivity coefficient is very near the 0.1 log *K* value tabulated by Fletcher and Sposito (Fletcher and Sposito, 1989) and denotes an equal affinity of the exchanger for the two cations. Furthermore, it should be noted that the experimental data at high pH are well simulated with a $CaOH^+/Na^+$ exchange selectivity coefficient value equal to the $CaCl^+/Na^+$ one. Hence, we suppose that ionic pairs may react with the clay surface with the same affinity, either in the case of Me^{2+}-Cl^-, or in the case of Me^{2+}-OH^-.

Surface complexation reactions	log K_{int}
$S^SOH + H^+ = S^SOH_2$	4.5
$S^SOH = S^SO^- + H^+$	-7.9
$S^{W1}OH + H^+ = S^{W1}OH_2^+$	4.5
$S^{W1}OH = S^{W1}O^- + H^+$	-7.9
$S^{W2}OH + H^+ = S^{W2}OH_2^+$	6.0
$S^{W2}OH = S^{W2}O^- + H^+$	-10.5

Tab. 4.14 : Surface complexation reactions and associated protolysis constants (K_{int}) of the simulation based on the Bradbury and Baeyens model (Bradbury and Baeyens, 1997).

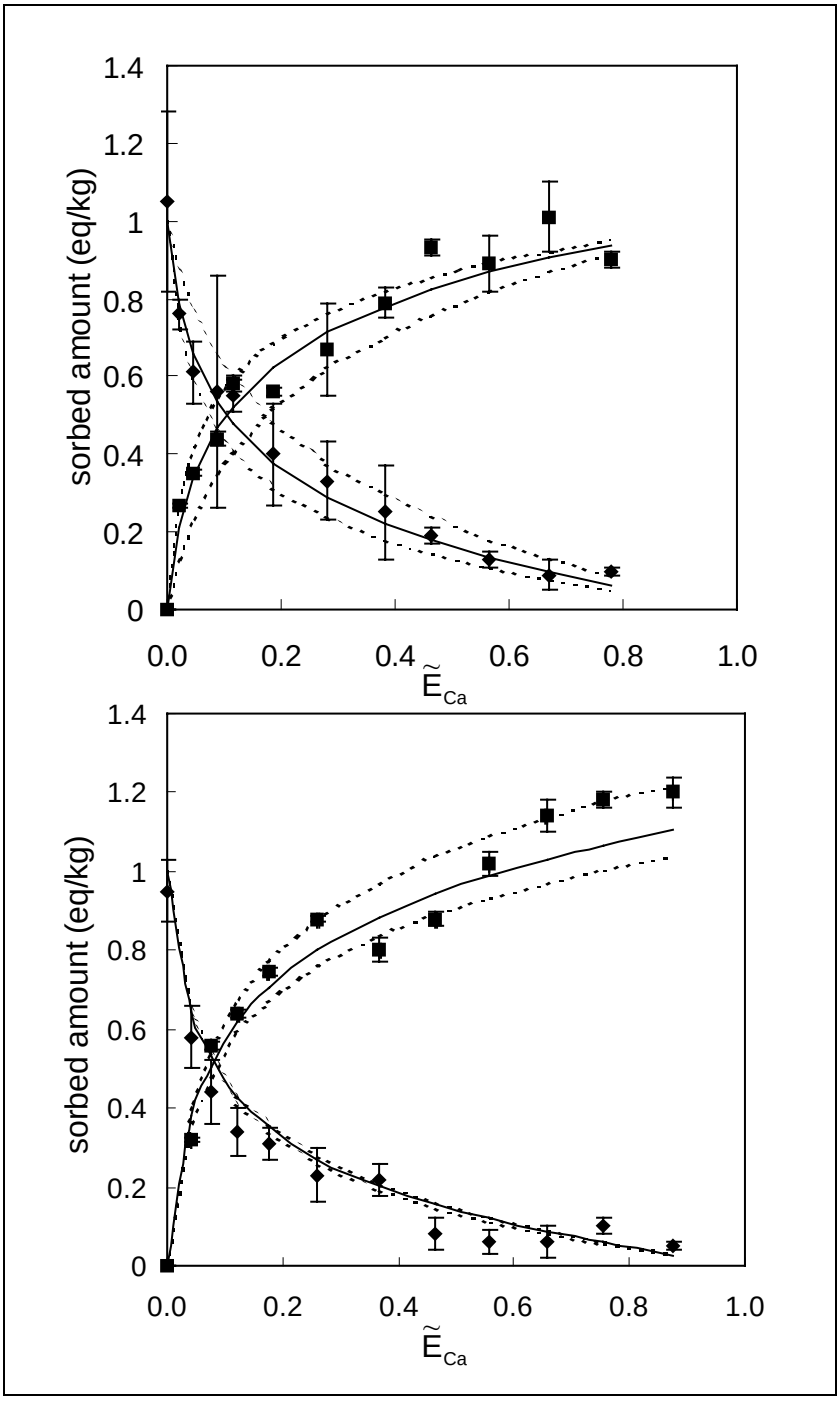


Figure 4.21 : Fit of the Ca^{2+}/Na^{+} exchange data of Sposito and al. (Sposito et al., 1983a) in perchlorate (top) and chloride ionic background (bottom). Perchlorate ionic background: thick line, log $K_v^{Ca2+/Na+}$ = 0.4; thin dotted lines log $K_v^{Ca2+/Na+}$ varied from 0.1 to 0.6. Chloride background: thick line, log $K_v^{Ca2+/Na+}$ = 0.4 and log $K_v^{CaCl+/Na+}$ = 2.5; thin dotted lines, log $K_v^{Ca2+/Na+}$ = 0.4 and log $K_v^{CaCl+/Na+}$ varied from 2.2 to 2.8.

Based on the Bradbury and Baeyens model (Bradbury and Baeyens, 1997), the simulation respects the whole tendency of the proton surface charge titrations and of the apparent CEC increase. Nevertheless, it fails to respect the details of the measurements.

Hiemstra and Van Riemsdijk MUSIC model

In the MUSIC based model we consider both edge sites listed in Tab. 4.13 and cation exchange site used in the previous model. Furthermore, the cation exchange selectivity coefficients are the same as those listed in Tab. 4.15. Some edge sites were grouped together

in the model (brackets in Tab. 4.13) and some sites were neglected due to their low amount present at the edges of the particles (shaded lines). The pK of the sites used in the simulation are marked in bold. Only three log *K* parameters were adjusted (Tab. 4.13, horizontal arrows columns 3 and 4). The slight adjustments correspond to a maximal $d_{Me\text{-}O}$ shortening of less than 0.01 Å and we do not allow the bonds to elongate. The shortening of the Me-O distances at the border of the layers is an expected phenomenon based on the Pauling bond valence approach (Pauling, 1929; Brown, 1981; Brown and Altermatt, 1985; Brown, 1992, Schlegel, 2000).

Exchange reactions	log K_{int}
$2\ NaX + Ca^{2+} \Leftrightarrow CaX_2 + 2\ Na^+$	0.4 §
$NaX + H^+ \Leftrightarrow HX + Na^+$	0.0 §
$NaX + CaCl^+ \Leftrightarrow CaClX + Na^+$	2.5 §
$NaX + CaOH^+ \Leftrightarrow CaOHX + Na^+$	2.5 ¶

§ Adjusted (data from this study and Sposito et al., 1983a)
¶ Set equal to $K_v^{CaCl+/Na+}$

Tab. 4.15 : Cation exchange reaction selectivity coefficients (K_v) used in both simulations.

This model describes very well both the titration data and the apparent CEC variations as a function of pH (Figure 4.22). Despite the numerous approximations done relative to the different edge faces contribution and thus, to the different edge surface groups populations, the MUSIC approach is successful to model the surface proton charge of montmorillonite. Nevertheless, some criticisms can be made on the choice of the $m + n$ values (Gaboriaud and Ehrhardt, 2003). We hope that studies like molecular dynamic studies could help to constrain these last parameters. In order to confirm the effectiveness of our approach, and, of our choices for these questionable parameters, we tried to link some clay properties (surface potential; dissolution kinetics) to the protonation state of the edge sites, as given by our model.

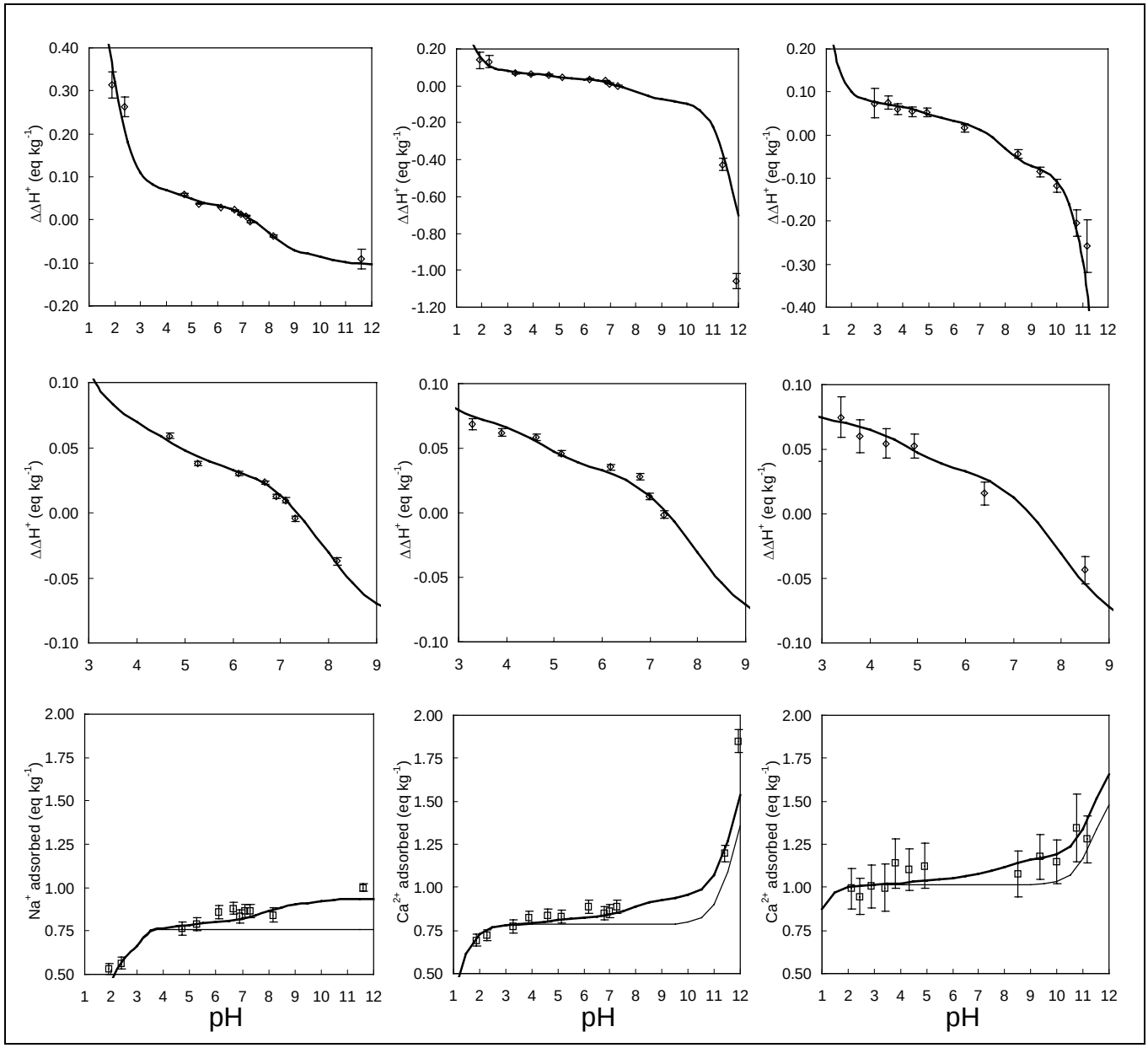


Figure 4.22 : Experimental potentiometric titration data (top and middle) and CEC data (bottom) of part I simulated by the Hiemstra and Van Riemsdijk MUSIC model (this study and Hiemstra et al., 1996). From left to right, experiments 1 to 3 respectively. Experiment 1, 0.02 mol l^{-1} NaCl, 4.69 g l^{-1}; experiment 2, 0.0068 mol l^{-1} $CaCl_2$, 3.03 g l^{-1}; experiment 3, 0.05 mol l^{-1} $CaCl_2$, 1.53 g l^{-1}.

Surface potential of clay minerals

According to the model it is possible to calculate the pH at which the global edge surface charge is zero (Point of Zero Charge, PZC). By setting the edge groups formal charge to the values given in Tab. 4.16, we found a pH_{PZC} value of 7.45 (Figure 4.23). At this pH, the edge contribution to the total charge of the clay should be 0, and then, the apparent CEC should be equal to the structural one. The Figure 4.22 shows that it is not the case: a positive difference of approximately 10% of the structural CEC is observed for experiment 1. The experiments 2 and 3 cannot be considered in this analysis, because of the adsorption of $CaCl^+$ ionic pairs. We estimate that a 10% error in the measurement/calculation of the structural CEC is reasonable since many parameters, such as the Al content in the tetrahedral layer, are difficult to estimate and can significantly influence the theoretical structural CEC value. The clay edges PZC found

value justifies also, *a-posteriori*, the habit of measuring the CEC at near neutral pH (e.g. Metson, 1956).

	Approximated formal charge		
Types of sites	Deprotonation	First protonation	Second protonation
Si_{Td}-O	-1	0	N.A
$Me(III)_{Oh}$-O	N.A.	-1/2	+1/2
$Me(II)_{Oh}$ -O	N.A.	-2/3	+1/3
$Me(III)_{Oh}$-O –$Me(III)_{Oh}$	N.A.	0	+1
$Me(III)_{Oh}$-O –$Me(II)_{Oh}$	N.A.	-1/6	+5/6
$Me(II)_{Oh}$-O –$Me(II)_{Oh}$	N.A.	-1/3	+2/3
$Me(III)_{Oh}$-O-Si_{Td}	-1/2	+1/2	N.A.
$Me(II)_{Oh}$-O-Si_{Td}	-2/3	+1/3	N.A.
$Me(II)_{Oh2}$-O-Si_{Td}	-1/3	+2/3	N.A.
Al_{Oh2}-O-Si_{Td}	0	N.A.	N.A.
$AlMg_{Oh}$-O-Si_{Td}	-1/6	N.A.	N.A.
$AlFe^{III}_{Oh}$-O-Si_{Td}	0	N.A.	N.A.

Tab. 4.16 : Approximated formal charge of the edge surface groups of the clay. Surface sites are grouped into categories, where Me(III) indicates a trivalent cation and Me(II) a divalent cation.

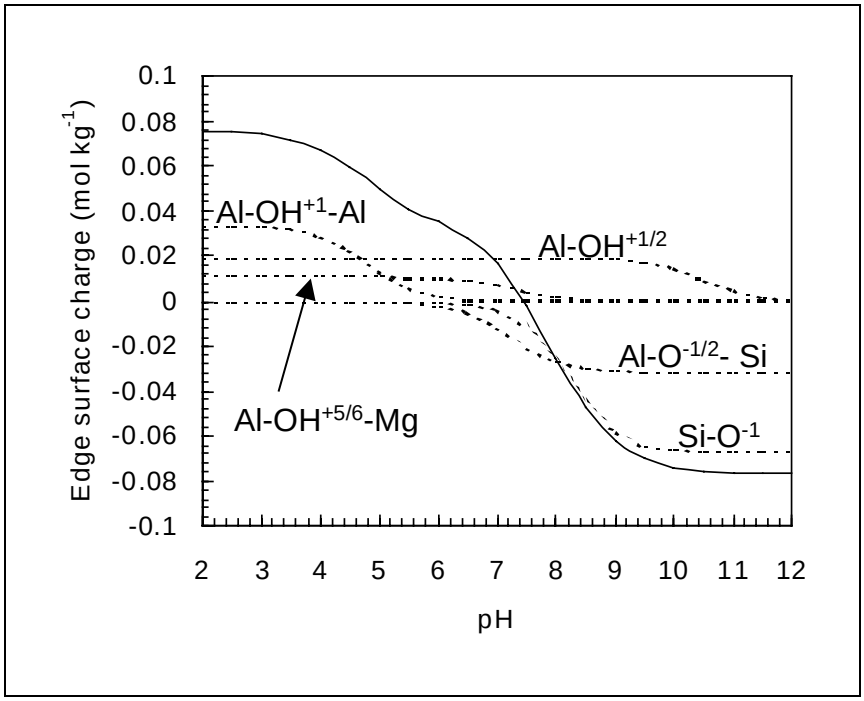


Figure 4.23 : Calculation of the edge surface charge after the parameters given in Tab. 4.14. Thick line: whole surface edge charge. Thin lines: individual contributions of the five main components, Si_{Td}-OH (deprotonation, pK = 8.2, 67.5 mmol kg^{-1}), Al_{Oh}-OH (double protonation, pK = 10.5, 19.3 mmol kg^{-1}), Al_{Oh}-OH-Al_{Oh} (double protonation, pK = 4.8, 33.7 mmol kg^{-1}), Al_{Oh}-OH-Mg_{Oh} (double protonation, pK = 7.3, 10.0 mmol kg^{-1}), and Al_{Oh}-OH-Si_{Td} (double protonation, pK = 7.2, 31.3 mmol kg^{-1}). The Point of Zero Charge pH value is equal to pH = 7.5.

We can note that the maximum variation of the edge surface charge value is smaller than 20% of the structural CEC. Since the charges created at the surface are also compensated by cations present in the solution, such as Na^+ or Ca^{2+}, the effect of pH on the measured surface potential must be negligible. Many studies (*e.g.* Delgado et al., 1986; Delgado et al., 1988; Avena et al., 1990; Avena and De Pauli, 1998; Avena, 2002) have shown already that the zeta potential of montmorillonite is weakly negative and invariant as a function of pH, supporting the presented results and their interpretations. We could also argue that the clay in dilute suspension is almost completely dispersed (e.g. Schramm and Kwak, 1982; Tournassat et al., submitted-d). Hence, the edge surface charge is expressed in only one dimension (the line represented by the perimeter of the platelet), decreasing the capability of the charges to create an electrostatic potential. This supports our assumption, following Bradbury and Baeyens (Bradbury and Baeyens, 1997), of a lack of surface potential.

Edge sites protonation and clay particle dissolution.

Recent Atomic Force Microscopy studies showed clearly, that the dissolution of clay such as nontronite or hectorite occurs by edge retreat rather than by pit formation (Bickmore et al., 2001). Dissolution rates have been shown on various oxides and silicates to be controlled by the protonation state of surface functional groups (Furrer and Stumm, 1986; Stumm and Wollast, 1990).

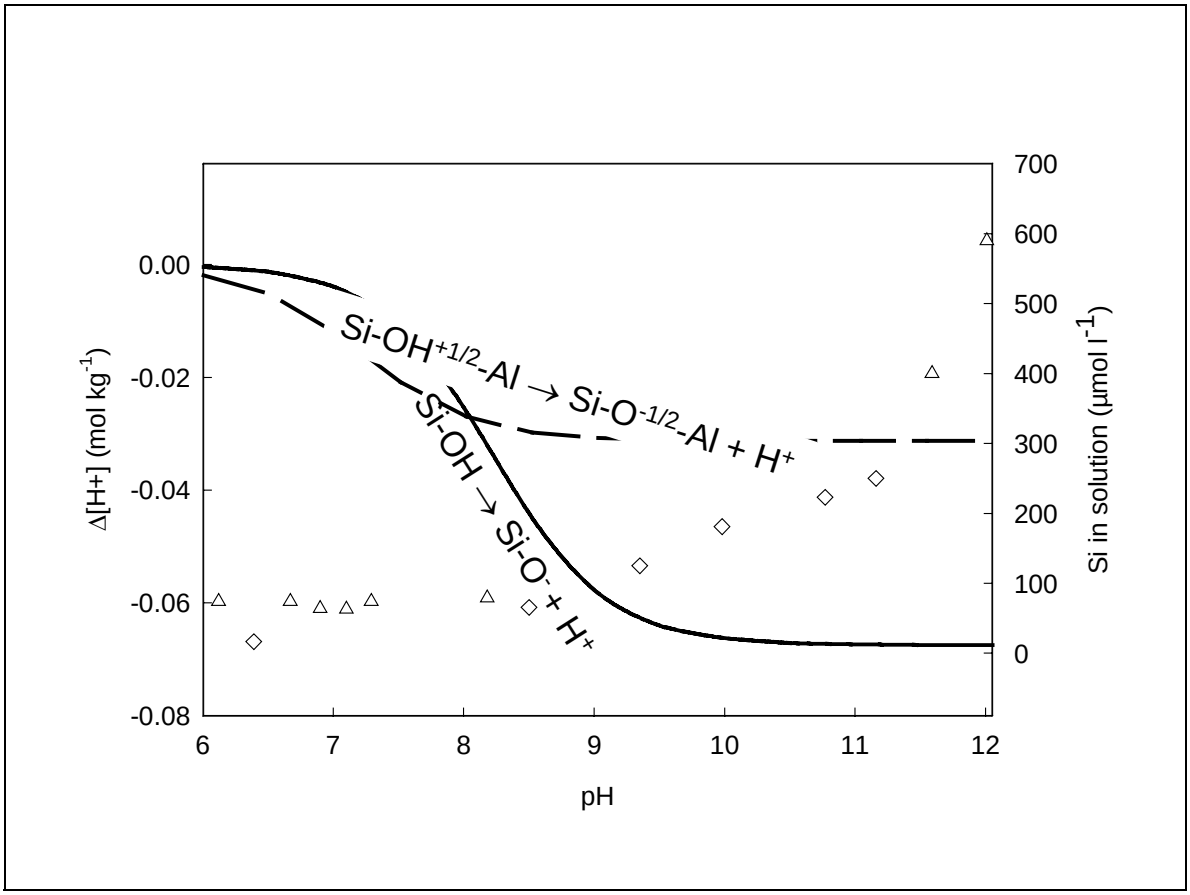


Figure 4.24 : Correlation between the deprotonation of tetrahedral and octahedral-tetrahedral surface sites and the dissolution of clay at high pH, for experiments 1 (open triangles) and 3 (diamonds).

In Figure 4.24, the aqueous Si concentration is reported as a function of pH together with the protonation state of reactive edge sites which involve a bond with Si atom present in tetrahedral position. It appears that the high dissolution of the clay in the alkaline pH range is correlated to the deprotonation of the OH groups bond to at least one Si_{Td}. This apparent clay dissolution could be attributed also to the presence of microcrystalline quartz or cristobalite in the clay suspension. Nevertheless, Cama et al. (Cama et al., 2000) showed that smectite dissolves congruently at pH 8.8 and at T = 80°C. Then, we think that part of the increased Si concentration observed at high pH can be attributed to clay dissolution. Conversely, aqueous Al concentration as a function of pH, is shown on Figure 4.25, together with the protonation state of reactive edge sites involving a bond with an Al atom in octahedral position. It shows that the dissolution of the clay in the acidic pH range is correlated to a double protonation of Al surface groups. We can also note that the stability of the clay towards dissolution is linked to the PZC position of the edge surface groups. Then, the edge sites protonation state given by the model is coherent with the dissolution pH range of the smectite.

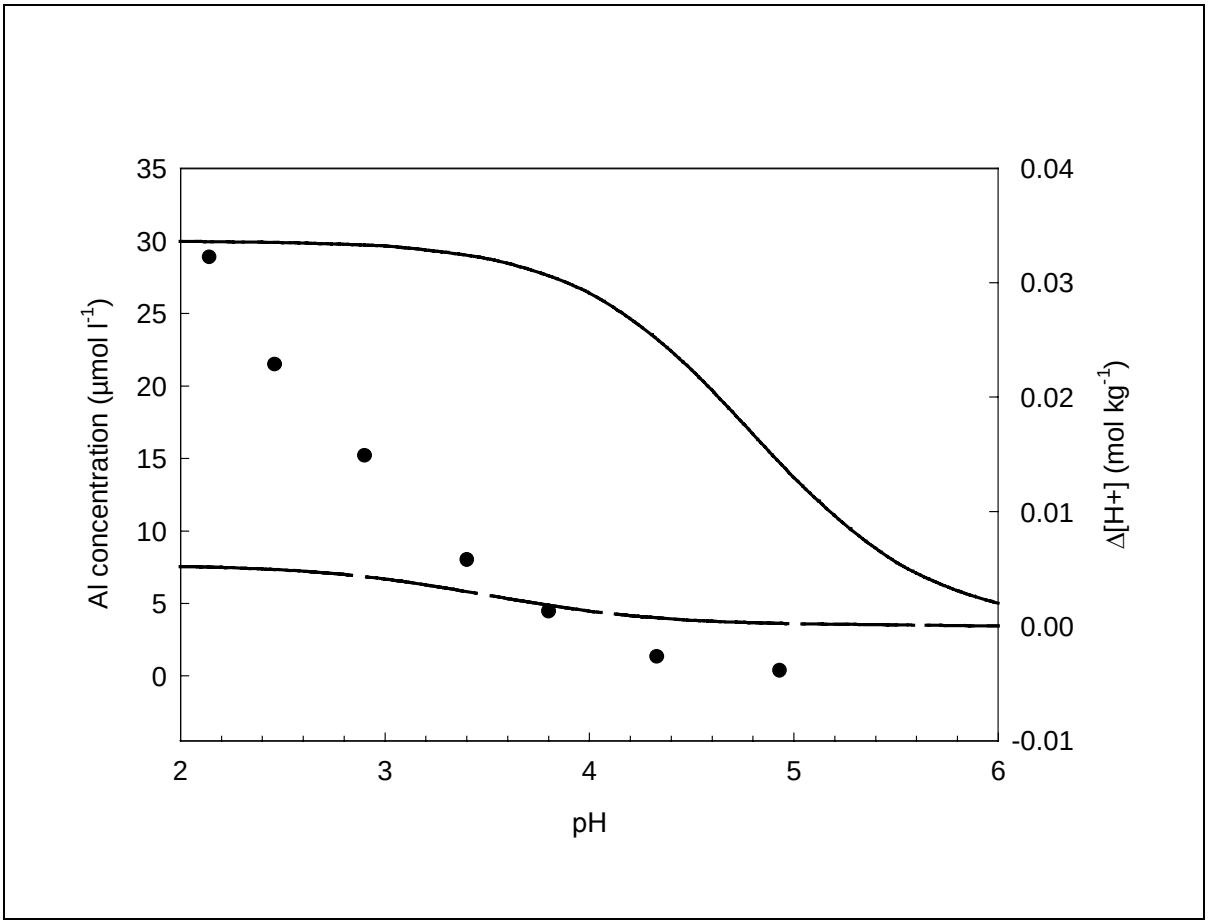


Figure 4.25 : Correlation between the double protonation of dioctahedral surface sites and the dissolution of clay at low pH, for experiment 3 (black points).

The pH conditions for dissolving clay minerals are dependent on clay type, which is considered. Hectorite, a Mg^{2+}, Li^{+} trioctahedral smectite, is less stable at low pH but more stable at high pH than montmorillonite (e.g. Schlegel, 2000). In this structure, the main octahedral surface sites for proton adsorption should be the Mg_2-O-Si, the Mg-O and the Mg-O-Mg sites. The approximate formal charges of these sites are represented as a function of pH in Figure 4.26. Structurally, the presence of two Mg_2-O-Si sites should correspond to the presence of a Mg-O-Mg site. The Mg-O sites should be present at a less extent than the others. Thus the global charge of the edges should be mainly controlled by the charge of the Mg-O-Mg site, since the Mg_2-O-Si site has the same charge over the whole usual pH range. Hence, the PZC should be shifted towards a basic pH value of approximately 10, in agreement with the observed differences of stability pH range for montmorillonite and hectorite.

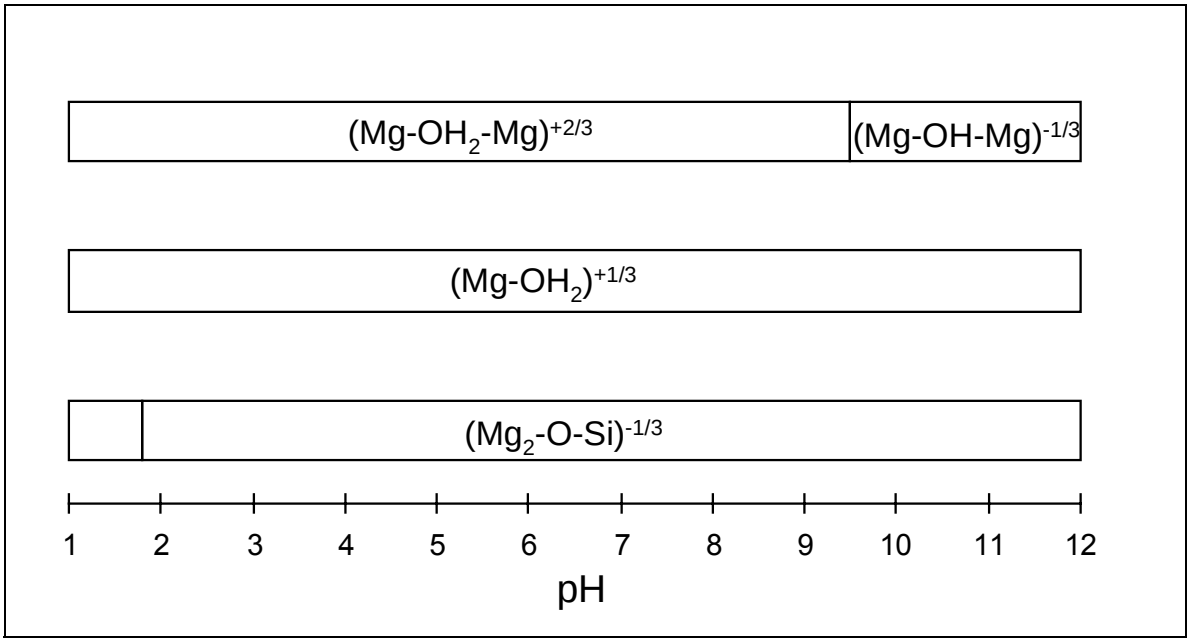


Figure 4.26 : Scheme of the protonation state of the hectorite main octahedral surface sites as a function of pH.

Implications

The edge surfaces of smectite (and by extension, of other clays) are very heterogeneous, and then, complicated systems. Nevertheless, the present structural and morphological model permits to predict their reactivity towards protons. In Tab. 4.13, it can be noted that only 5 main sites are necessary to model the titration data, because the relative amounts of other sites are too low to really affect the goodness of the adjustment. These main sites are: Si_{Td}-OH (deprotonation, pK = 8.2, 67.5 mmol kg^{-1}), Al_{Oh}-OH (double protonation, pK = 10.5, 19.3 mmol kg^{-1}), Al_{Oh}-OH-Al_{Oh} (double protonation, pK = 4.8, 33.7 mmol kg^{-1}), Al_{Oh}-OH-Mg_{Oh} (double protonation, pK = 7.3, 10.0 mmol kg^{-1}), and Al_{Oh}-OH-Si_{Td} (double protonation, pK = 7.2, 31.3 mmol kg^{-1}). The decomposition of the total edge surface charge is shown on Figure 4.23. Only four adjusted parameters were necessary to quantify the amounts of these sites and their affinity for proton, namely three *m+n* values and the ratio between A-C and B type chains. Three pK values were further slightly adjusted to better fit the data, but cannot be considered as freely adjusted parameters. This low amount of adjustable parameters for a 27 (or more) sites model, should be compared to the amount of adjustable parameters for the 3 sites model of Bradbury and Baeyens (Bradbury and Baeyens, 1997): three different amounts of sites and six affinity constants for protonation reactions were necessary to fit their data. This comparison shows the efficiency of a structurally and morphologically based model to predict clay surface reactivity with a maximal precision and a minimal amount of adjustable parameters.

The clay proton affinity constants are often used to derivate clay metal complexation constants (Stadler and Schindler, 1993; Zachara and Smith, 1994; Bradbury and Baeyens, 1997, 1998; Turner et al., 1998). But, by considering the heterogeneity of the clay edges and the chemical properties of H^+ and metallic cations, it becomes doubtful to consider that metallic cations do sorb on the same sites than protons. Schlegel et al. (Schlegel et al., 1999) showed that Co^{2+} can form inner sphere complex onto hectorite edge surfaces and that Co^{2+} shares edges rather than corners with octahedral layer sites, yielding to the link of Co^{2+} to, at least, two oxygen surface groups. Since protons are linked to only one oxygen surface group, the classical empirical modeling approaches for metal complexation on clay minerals should be questioned. For example, Zachara et al. (Zachara et al., 1993; Zachara and Smith, 1994) or Turner et al (Turner, 1995; Turner et al., 1998) consider that the reactivity of clay edges can be modeled by

considering the reactivity of alumina and silica, and by using a triple layer model, as an electrostatic model. In their studies, they fitted the amount of edge sites concomitantly with their metal adsorption data, but without titration data, or, they calculated the amount of sites on the basis of morphological information and on structural information given by White and Zelazny (White and Zelazny, 1988). In this model, only Si-OH and Al-OH amphoteric sites are considered (2-pK model), according to White and Zelazny suggestion (White and Zelazny, 1988). This approach is successful to fit the sorption data, but many hypotheses are not really justified. In the present study, we show for instance that Al_{Oh}-OH-Si_{Td} sites could react in the near neutral pH range towards protons, standing in contradiction with White and Zelazny suggestion. Furthermore, the sites described in this study do not have an amphoteric behavior in the pH range usually considered for sorption experiments (*i.e.* pH value between 2 and 10).

CONCLUSION

Natural clay systems are far more complex than the systems studied in the laboratories. In natural or engineered systems, competition effects for sorption are expected (Tournassat and Charlet, submitted). If the density and affinities of sites available for competitive sorption were not well constrained, these competition effects could not be precisely modeled. Hence, the oversimplification of the clay edge reactivity towards cations could lead to an impossibility to model the interactions between multi-solute system and clay particles. Whereas surface complexation models such as Bradbury and Baeyens models are an improvement compared to *Kd* approach, we question their "mechanistic model" attribute and their effectiveness to model natural systems since:

- cations complexation pK values are fitted relatively to an "arbitrary" surface protonation pK value;

- a given complexation reaction is attributed arbitrarily to a single type of site, and a very limited set of sites is considered in this type of simulation, whereas the structural heterogeneity of surface groups allows a huge amount of site configurations and available coordinations, due to the morphology of the clay platelets, and, due to the chemical composition of the clay (especially the heterogeneous octahedral layer); and

- the complexation reactions involve only one site (*e.g.* via single corner sharing) and the authors do not consider the possible interactions between two or more protonated sites and the cations (*e.g.* via double corner or edge sharing) as shown for Ni^{2+} by polarized EXAFS spectroscopy (Schlegel et al., 1999; Dähn et al., 2003), or the nucleation processes of new phases as shown for Zn and Co on hectorite and montmorillonite (Schlegel et al., 2001b; Dähn et al., 2002b).

With the present study, we have shown that a model, based on sound morphological and structural information, is able to predict the reactivity of clay edge surfaces towards protons with a better accuracy and with fewer free parameters than empirical 3 (or 2) sites 2 pK models. This approach can be combined to the prediction of the variations of the CEC as a function of pH. We hope that such an approach could be extended to other cation complexation reactions.

As secondary results, we have derived the cation exchange selectivity coefficient for $CaCl^+$ and $CaOH^+$ ionic pairs. These ionic pairs have similar and high affinity constants values ($\log K_v = 2.5$). We refer the reader to the article from Sposito et al. (Sposito et al., 1983a) to explain the high $CaCl^+$ exchange constant. The adsorption of $CaOH^+$ and the high affinity of clays for these ion pair is of importance in alkaline medium such a cement alkaline solution. Finally, we have confirmed the non-preference of the clay exchanger for H^+ and Na^+ ($\log K_v = 0$), and clearly distinguished this cation exchange from the (simultaneously occurring) mineral dissolution reaction.

ACKNOWLEDGEMENT

This research was funded by the French National radioactive waste management agency (ANDRA).

5. CONCLUSION GENERALE

5.1. DEMARCHE SCIENTIFIQUE APPLIQUEE LORS DE CES TROIS ANNEES DE RECHERCHE

L'enchaînement des chapitres de cette thèse vise à montrer le plus simplement et logiquement possible l'ensemble des résultats collectés pendant ces trois années de thèse. L'enchaînement des expériences et des résultats fut en fait très différent. La première difficulté fut d'abord de résoudre le problème de l'oxydation en solution du Fe(II) en Fe(III). Cette difficulté nous a amené à définir les protocoles de purification des solutions décrites en annexe 6.3 et à utiliser systématiquement la boîte à gants comme milieu d'expérience. La première boîte à gants utilisée (marque Coy) ne nous donnant pas entière satisfaction (problème de porosité de l'enceinte, fuites à répétition…), nous avons du acquérir un modèle plus performant chez un autre fournisseur (marque Jacomex). L'utilisation de la boîte à gants apporte des restrictions expérimentales. En particulier, il est très difficile de contrôler en début d'expérience les concentrations des solutions et les teneurs des suspensions (problème de l'évaporation de l'eau dans le sas sous vide ou lors de l'équilibrage avec l'atmosphère de la boîte à gants). Cette difficulté explique les valeurs des concentrations et des teneurs qui ne tombent jamais sur des valeurs "rondes". Cette difficulté surmontée, les expériences de sorption ont pu commencer. Nous nous sommes rapidement aperçus que l'adsorption spécifique du Fe(II) se faisait à très bas pH. Ce résultat étonnant fut confirmé pour une gamme de conditions expérimentales assez étendue. Les conséquences de cette forte affinité de l'argile furent envisagées à savoir des phénomènes de saturation des sites et de compétition avec d'autres cations. Les phénomènes de compétition furent confirmés expérimentalement et la forte affinité du Fe(II) pour certains sites de surface était ainsi démontrée. Entre autres conséquences, les expériences d'échange cationique durent être programmées à bas pH. Elles montrèrent un comportement du Fe(II) en accord avec le comportement attendu pour un cation divalent vis-à-vis de l'échange cationique. Toutefois, la quantité équivalente maximum de cations échangés (Ca^{2+}, Na^{+} ou Fe^{2+}) n'était pas en accord avec la capacité d'échange cationique de l'argile MX80 telle qu'elle est donnée dans la littérature. Plusieurs paramètres expérimentaux pouvaient être responsables de cette différence et chacun fut testé par des expériences différentes : la détermination de la teneur en argile des suspensions mère, l'effet du pH, la justesse de la formule structurale de l'argile et le rapport Fe(II)/Fe(III) dans cette formule. Chacune de ces expériences apporta son lot de résultats dont le plus marquant fut la variation de la CEC avec le pH sur toute la gamme de pH. Ce résultat était déjà partiellement disponible dans la littérature mais n'avait jamais été montré sur autant de points expérimentaux et n'était jamais expliqué ou modélisé. Cette expérience fut le point de départ des expériences de titrages potentiométriques des argiles couplés à la mesure de la CEC. Entre-temps, la surface spécifique des bordures de l'argile avait été déterminée par AFM. Au départ l'AFM devait nous permettre de montrer le fort pouvoir réducteur du Fe(II) adsorbé. Il était prévu d'étudier la réduction de composés oxydants (inorganiques du type As(V), ou organiques du type TCE) par le Fe(II) adsorbé sur les bordures. Ces expériences devraient être bientôt possibles grâce à l'introduction d'un AFM en boîte à gants à l'INE Karlsruhe (équipe de Dirk Bosbach) mais ne l'étaient pas encore lors de mon séjour en Allemagne. Nous avons tout de même regardé la morphologie des particules de montmorillonite, travail qui n'avait pas été effectué jusqu'alors. C'est en montrant les images des particules lors d'une séance de travail du groupe Fe - argile à l'ANDRA qu'un des membres du groupe, Frédéric Villiéras, nous fit remarquer que la taille de nos particules correspondait à la taille qu'il calculait à partir d'une méthode totalement différente: l'adsorption de gaz à très basse pression. En faisant l'étude statistique de la taille des particules et de leurs surfaces par AFM et en les comparant aux résultats d'adsorption de gaz, nous montrions alors un excellent accord sur les valeurs trouvées de surface spécifique. Ce résultat me permit alors de me lancer dans la modélisation morphologique et structurale de la réactivité des bordures des particules d'argiles. L'utilisation de la spectroscopie FTIR fut rendue nécessaire par la nécessité de contraindre le lieu de réaction des protons avec l'argile sur les bordures des particules et non

pas dans l'ensemble de la structure, et de contraindre la distribution des cations dans la structure de l'argile (ordre des cations aléatoire dans le feuillet octaédrique). Restait à expliquer la forte affinité des bordures de l'argile pour l'ion Fe(II) comparativement à d'autres ions comme le Zn(II). Des expériences complémentaires de chimie permirent de connaître la stœchiométrie de la réaction et de décrire le phénomène de complexation de surface par la somme de plusieurs phénomènes : précipitation (de surface ?), sorption compétitive et oxydation. Des expériences de spectroscopie Mössbauer furent programmées grâce à l'aide de Jean-Pierre Jollivet et se firent avec Jean-Marc Greneche au Laboratoire de Physique de L'Etat Condensé du Mans (université du Maine). Celles-ci montrèrent que tout le fer adsorbé était sous forme oxydée Fe(III). Aujourd'hui encore, une question persiste : l'oxydation s'est-elle faite pendant l'expérience de sorption (oxydation par l'argile, par l'eau ?) ou pendant le transport de Grenoble jusqu'au Mans malgré toute les précautions prises ? De nouvelles expériences sont programmées avec un renforcement des précautions (en particulier, l'utilisation de l'azote liquide pour le stockage pendant le transport). Si l'oxydation par l'argile ou par l'eau est confirmée, celle-ci pourrait être invoquée comme étant la "driving force" de la réaction d'adsorption du Fe(II).

5.2. RETOUR SUR LA PROBLEMATIQUE DU STOCKAGE DES DECHETS RADIOACTIFS EN PROFONDEUR

Cette thèse montre un certain nombre d'effets du Fe(II) ou d'autres cations sur les propriétés de l'argiles, pouvant avoir une influence positif ou negatif sur la performance de la barrière ouvragée.

5.2.1. Adsorption des paires ioniques en sites d'échange cationique et conductivité hydraulique

Les résultats des expériences d'échanges montrent qu'en fond chloré, des paires ioniques du type $CaCl^+$ ont une forte affinité pour les sites d'échange. A haut pH, le phénomène semble être le même pour les paires ioniques $CaOH^+$. Les cations monovalents (dont font partie ces paires ioniques) favorisent la dispersion des plaquettes d'argiles et devraient donc avoir un effet contrecarrant la coagulation et dans un sédiment la formation de gros agrégats. La présence d'agrégats favorisant la conductivité hydraulique, la présence de ces paires ioniques devrait diminuer cette conductivité et donc avoir un effet positif sur la performance de la barrière. Toutefois, des expériences de mesures de porosité ou de conductivités comparées en milieu sodique et chloro – calcique sont nécessaires pour confirmer cet effet et surtout pour connaître son importance.

5.2.2. Effet tampon-pH de l'argile

A bas pH, les résultats de titration et leur modélisation permettent de prédire avec plus de précision l'effet tampon de l'argile (environ 0.1 mol H^+ par kg d'argile entre pH 5 et 8). A haut pH, la présence de $CaOH^+$ en site d'échange cationique procure à l'argile un pouvoir tampon fort en milieu calcique (fond géologique et solutions issues de l'altération des ciments). Ce pouvoir tampon peut-être facilement estimé à partir de la CEC. Entre pH 10 et 12, ce pouvoir tampon est égal à la valeur de la CEC. Cette propriété pourrait avoir un effet important sur la modélisation de l'évolution du pH dans la barrière.

5.2.3. Effet de précipitation à haut pH

A haut pH, des phases de type CSH (tobermorite ?) précipitent rapidement en présence de Ca(II) en solution. En présence de Fe(II), une phase Fe-Si précipite. Ces précipitations peuvent avoir des effets soit positifs soit négatifs sur les performances des barrières : elles peuvent contribuer à limiter la porosité du matériau (effet positif sur la performance liée à la conductivité hydraulique) mais également contribuer à la perte de plasticité de la barrière en transformant des argiles gonflantes en matériau rigide.

5.2.4. Effet compétiteur du Fe(II)

Nous avons montré que le Fe(II) peut entrer en concurrence avec d'autres éléments sur certains sites de l'argile. Ces sites peuvent être des sites d'adsorption ou de des sites structuraux. Des expériences futures devraient permettre d'affirmer ou d'infirmer cet effet compétiteur avec les radionucléides, la question étant : le Fe(II) s'adsorbe-t-il sur les mêmes sites que les radionucléides ? En cas de réponse positive, ce phénomène aurait un effet négatif sur la performance de la barrière, celle-ci perdant une partie de son efficacité chimique vis-à-vis de la diffusion des polluants une fois la corrosion du containeur assez avancée. Un front de radionucléides adsorbés sur les argiles de la barrière en avant d'un front de Fe(II) adsorbé serait alors à prévoir. Toutefois ce résultat est à nuancer en fonction de la solubilité du Fe(II) à haut pH. En effet cet effet compétiteur a été montré à pH 6 environ, où la solubilité du Fe(II) est bonne. A haut pH le Fe(II) peut précipiter (sidérite, berthiérine, chlorite…) ou s'incorporer dans des phases minérales le rendant moins disponible pour la compétition. Ceci a été vérifié lors de nos expériences, puisque à haut pH et en présence d'argile le Fe(II) précipite avec la silice en solution. Toutefois, l'épisode à haut pH de la barrière devrait être limité dans le temps pour progressivement revenir à un épisode avec un pH proche de la neutralité correspondant à l'eau de site. Ce pH favoriserait alors la dissolution du Fe(II) et son adsorption compétitive plus loin en avant du front, là ou seraient localisés les radionucléides.

5.3. BACK TO THE PROBLEMATIC OF THE NUCLEAR WASTES DEEP REPOSITORY FIELD

This thesis shows various effects of the presence of Fe(II) and other cations on the clay properties. These effects can be positive or negative on the performance of the engineered barrier.

5.3.1. Ions pairs adsorption in cation exchange position and hydraulic conductivity

In a chloride medium, ionic pairs, like $CaCl^+$, have a high affinity for cation exchange sites. At high pH, $CaOH^+$ seems to have the same behavior. The presence of monovalent cations (including ionic pairs) leads to the dispersion of clay platelets and then, big clay aggregates are not expected to appear. The disappearance of clay aggregates should decrease the clay hydraulic conductivity and hence should increase the performance of the barrier. Porosity and conductivity experiments are necessary to assess and quantify this effect.

5.3.2. Clays as pH-Buffer

At low pH, titration results should permit to enhance the precision of the model of pH evolution in the barrier. At high pH, the $CaOH^+$ sorption in cation exchange position should give a high pH-buffer capacity to clay material. This capacity is estimated to be equal to the CEC between pH 10 and 12.

5.3.3. High pH precipitation

At high pH, CSH like phase (tobermorite) precipitates rapidly in presence of clay and Ca(II). If Fe(II) is present, a Fe-Si phase precipitates. Precipitation could have both positive and negative effect on the barrier performance. It can limit the porosity of the material and then can enhance the effectiveness of the barrier, since hydraulic conductivity decreases. It can decrease also the plasticity of the barrier.

5.3.4. Fe(II) Competition effect

Fe(II) can compete with other elements on clay specific sorption sites. Experiments in the future should allow us to assess (or not) the competition effect between Fe(II) and radionuclides. If Fe(II) did compete for sorption with these elements, the performance of the barrier would decrease. The front of sorbed radionuclides would be ahead from the front of sorbed Fe(II). The competition effect was shown for pH ~6. Fe(II) is soluble at this pH. In a repository field, the pH should be very higher in a first time and will limit the solubility of Fe(II), decreasing its capacity of competition. Nevertheless, thereafter, the system should equilibrate with the composition of “site” water and the pH should drop to near neutral pH, releasing Fe(II) in solution which will be available for competition with radionuclides.

5.4. SYNOPSIS DES RESULTATS

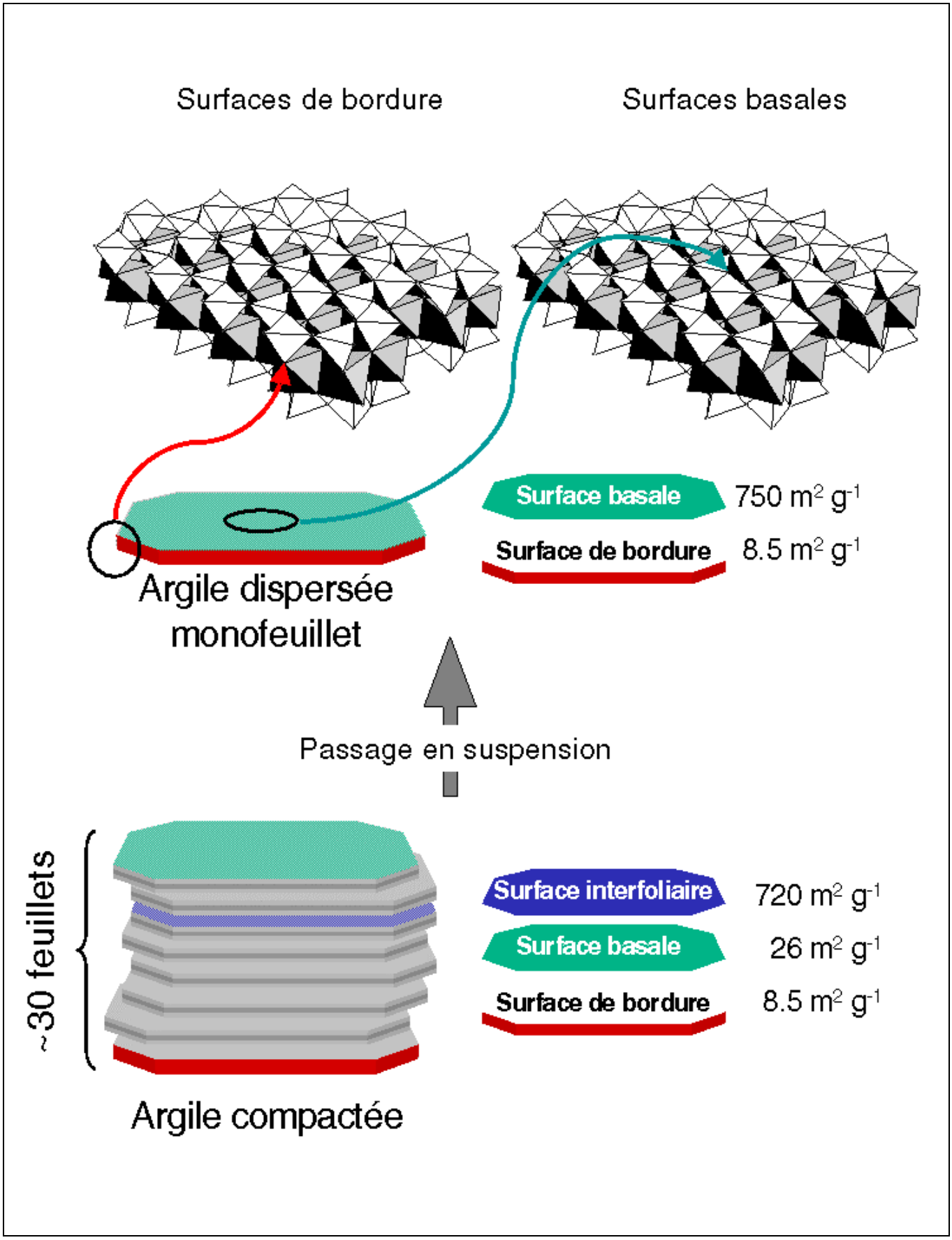


Figure 5.1 : Caractérisation des surfaces des argiles.

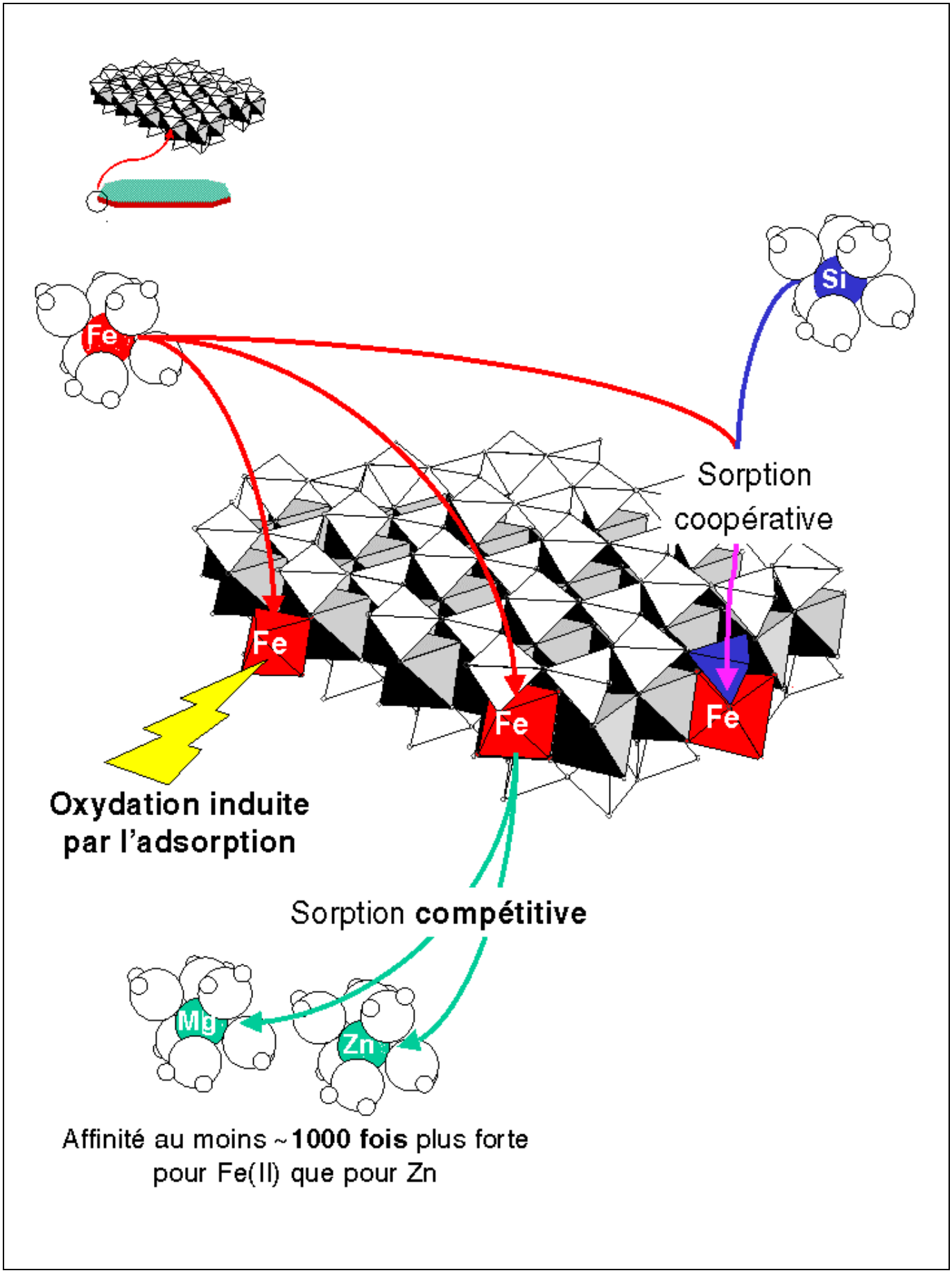


Figure 5.2 : Schématisation des interactions Fe(II)–montmorillonite sur les surfaces de bordure.

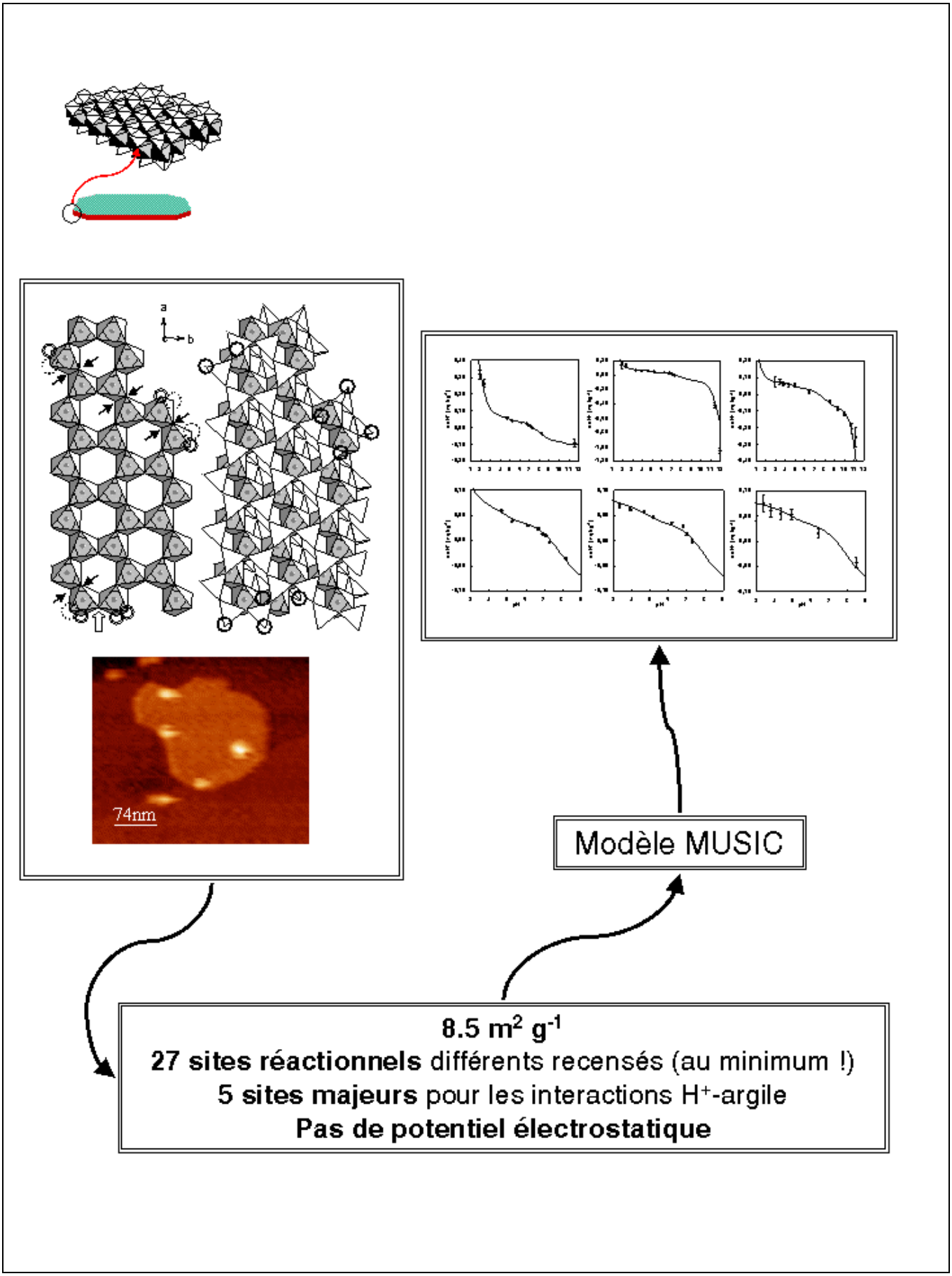
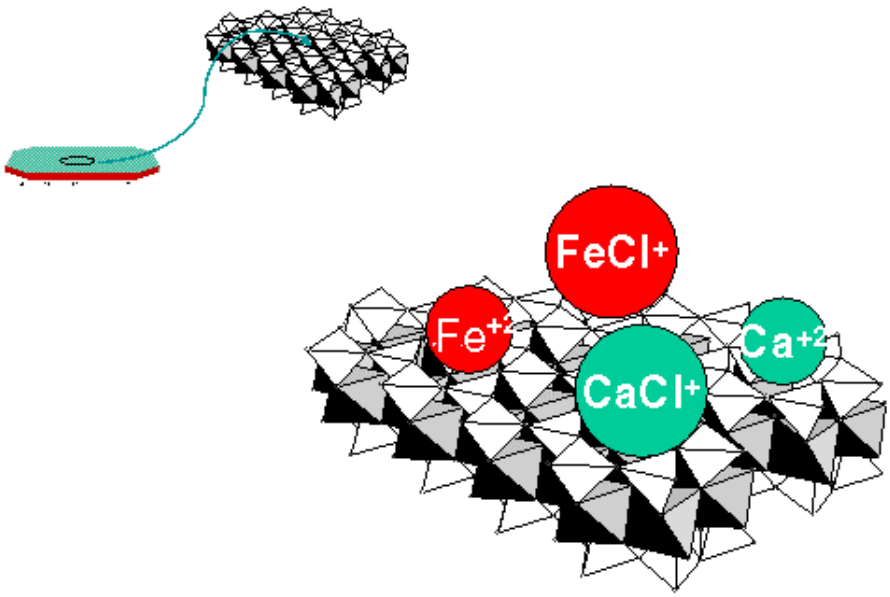


Figure 5.3 : Vers une modélisation morphologico – structurale des interactions argiles – solutés sur les bordures des argiles.



Sorption de deux espèces de Fe(II) : Fe^{2+} et $FeCl^{+}$ avec des affinités proches de celles de Ca^{2+} et $CaCl^{+}$

Sorption préférentielle des paires ioniques chlorées

Réactions d'échange	Log K_v
≡XNa + H^+ ⇔ ≡XH + Na^+	0.0
≡XNa + K^+ ⇔ ≡XK + Na^+	0.6
≡XNa + $CaCl^+$ ⇔ ≡XCaCl + Na^+	2.5
≡XNa + $CaOH^+$ ⇔ ≡XCaOH + Na^+	2.5
≡XNa + $MgCl^+$ ⇔ ≡XMgCl + Na^+	1.9
≡XNa + $FeCl^+$ ⇔ ≡XFeCl + Na^+	2.3
2 ≡XNa + Ca^{2+} ⇔ $≡X_2Ca$ + 2 Na^+	0.5
2 ≡XNa + Mg^{2+} ⇔ $≡X_2Mg$ + 2 Na^+	0.5
2 ≡XNa + Fe^{2+} ⇔ $≡X_2Fe$ + 2 Na^+	0.4

Figure 5.4 : résumés des réactions d'échanges cationiques sur les surfaces basales des particules de montmorillonite.

5.5. CHAMPS D'APPLICATIONS DES RESULTATS DE CETTE THESE

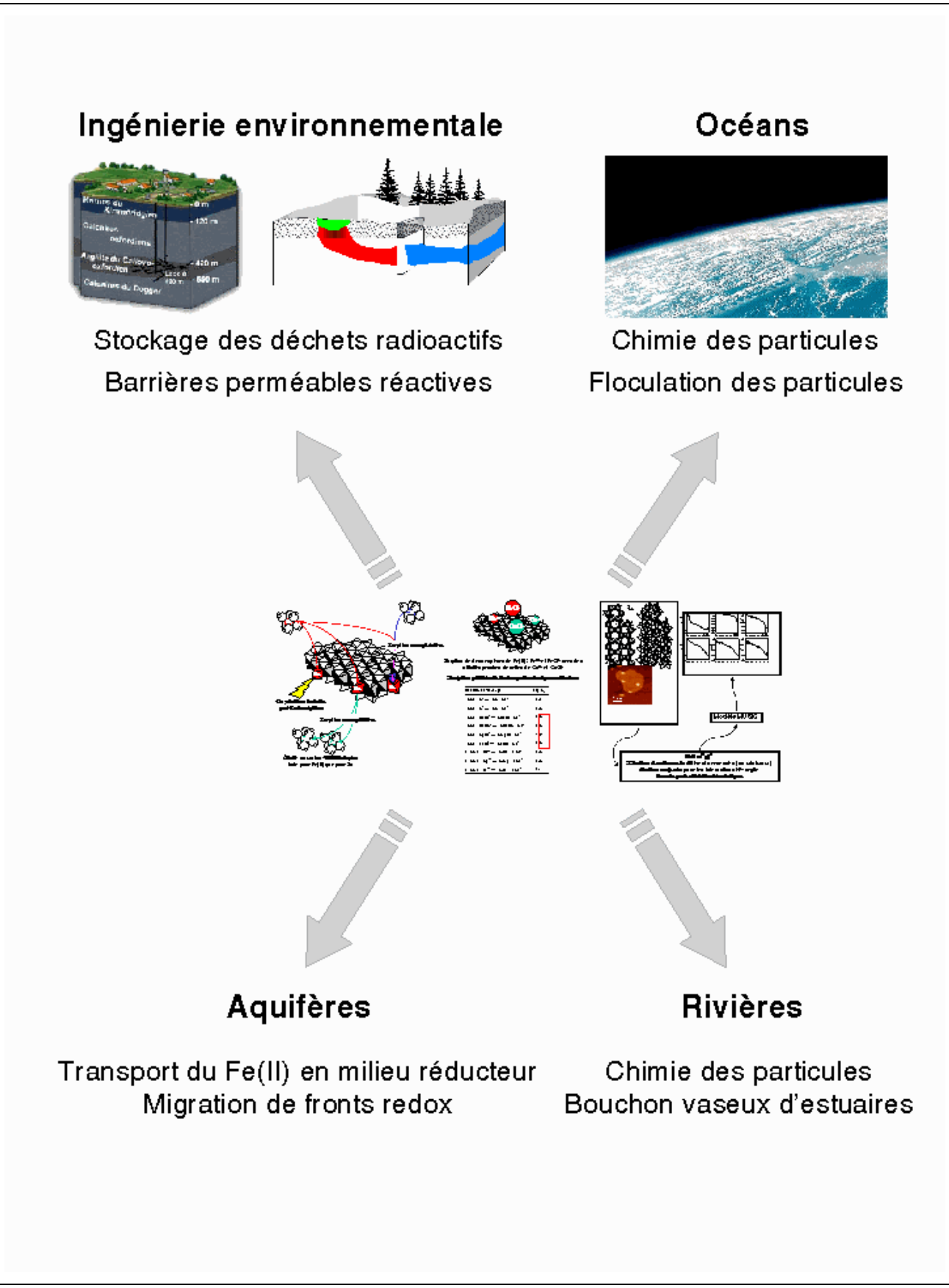


Figure 5.5 : Champs d'application explorés ou en cours d'exploration des résultats présentés dans cette thèse.

5.6. PERSPECTIVES

Le thème de cette thèse, initialement axée sur les interactions entre le Fe(II) en solution et les argiles, a été rapidement étendu aux interactions solutés – argiles en général. En effet, devant la multiplicité et la complexité des phénomènes engendrés par la présence de Fe(II) dans des suspensions argileuses en système anoxique, les modèles empiriques d'interactions solutés – argile déjà présents dans la littérature montrent leurs limites. La modélisation individuelle des phénomènes englobés sous le terme générique de "sorption" représente un premier grand chantier à explorer (Figure 5.6).

Dans cette thèse, une approche morphologico – structurale des interactions solutés–argiles a été ébauchée. Son efficacité à modéliser les interactions argile – H^+ est encourageante. L'étape de modélisation suivante est l'établissement de constantes de complexation des métaux sur des critères autres que l'ajustement des isothermes d'adsorption (Figure 5.7), c'est à dire sur des critères structuraux pour les ions dont le complexe de surface ou le précipité de surface, a une structure connue.

Ces données pourront alors servir à la modélisation de la dynamique des fronts redox liés au déplacement du Fe(II) dans des aquifères, des sédiments marins ou encore dans des systèmes d'ingénierie. Elles permettront également de mieux interpréter et prédire l'effet d'atténuation naturelle du Fe^{2+} adsorbé vis – à – vis de polluants tels que les solvants chlorés, les explosifs ou encore les pesticides.

Le nombre d'oxydation des espèces adsorbées est, comme nous l'avons vu pour le Fe(II), pas forcément celui de l'absorbat. L'argile – voir l'eau à l'interface – peut jouer le rôle d'oxydant, et ce, même quand le potentiel d'oxydo – réduction est imposé en solution à un niveau très bas. Ce phénomène, *a priori*, pas limité au Fe^{2+} a souvent été reporté pour le cérium (source de l'anomalie du cérium dans la série des lanthanides) et pourrait affecter nombre de radionucléides présents sous divers degrés d'oxydation.

Les effets de compétition pour les sites d'adsorption spécifique sont également un sujet à explorer plus profondément et sur davantage de minéraux naturels (Figure 5.6). Les expériences de compétition doivent permettre de différencier des phénomènes de sorption pure pour lesquels cette compétition existe, de phénomène de précipitation de surface pour lesquels cette compétition est moins probable mais où la précipitation de nouvelles surfaces entraîneraient plutôt la création de nouveaux sites d'adsorption. Il est tout à fait envisageable que ces expériences montrent que les phénomènes de complexation de surfaces sont en fait limités aux domaines de pH acide et neutre voir faiblement basique et que les phénomènes de précipitation de surface prennent le relais à plus haut pH. La thermodynamique de ces précipités de surface est un domaine encore presque vierge.

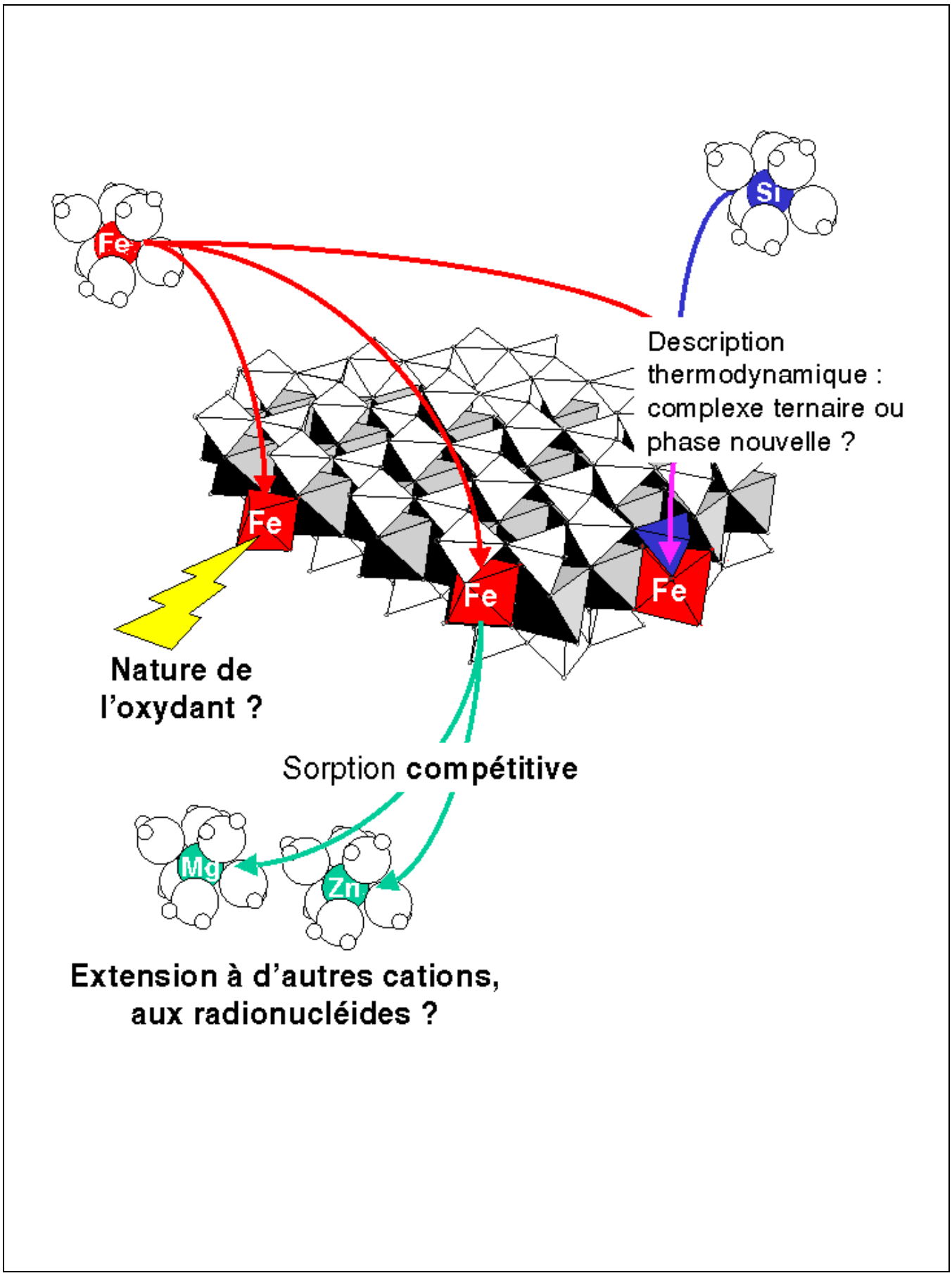


Figure 5.6 : Résumé des perspectives liées aux interactions Fe(II)–montmorillonite.

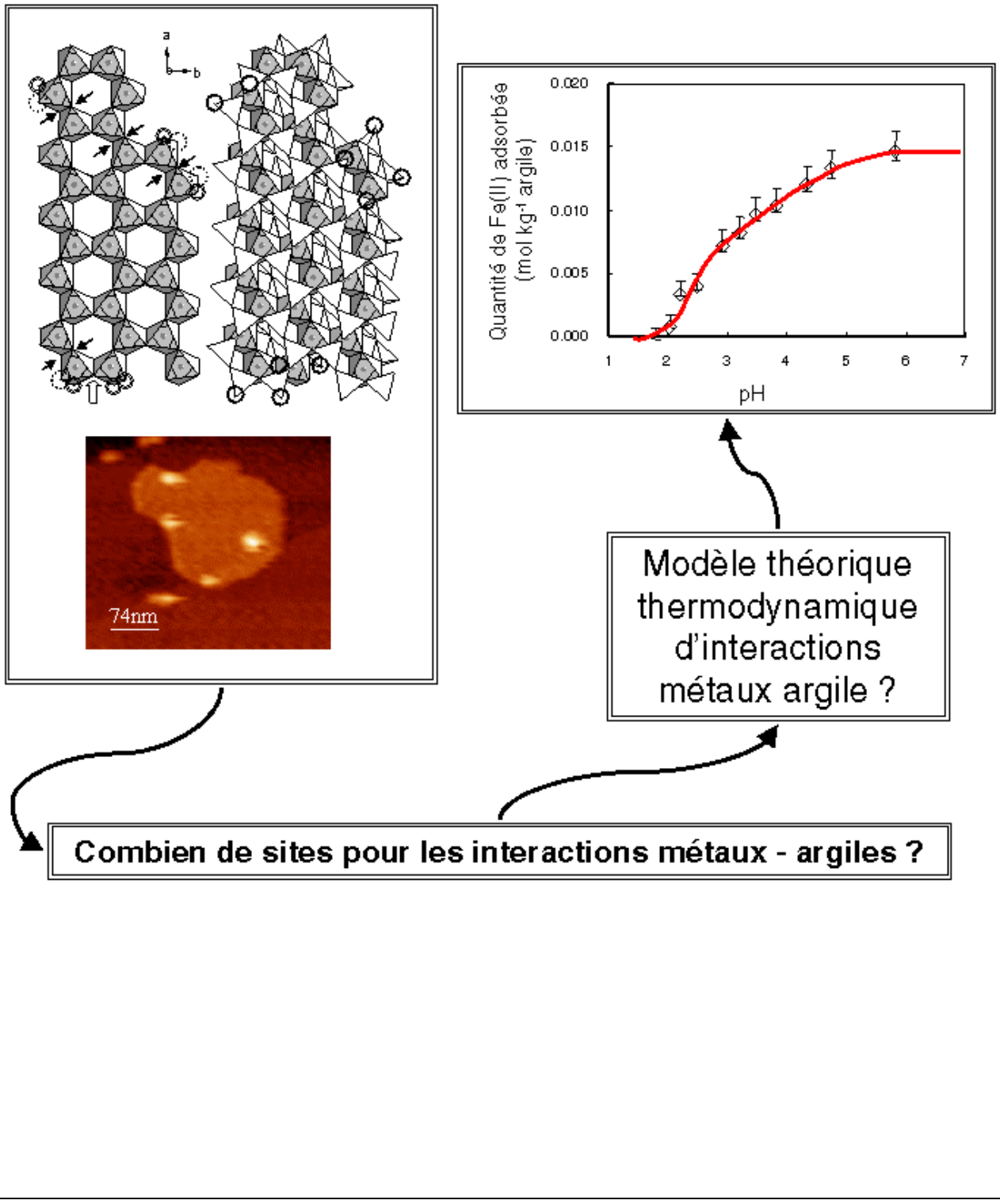


Figure 5.7 : Résumé des perspectives liées aux interactions ions–argile en général.

6. ANNEXES

6.1. PREPARATION DES ARGILES

6.1.1. Mise en suspension de l'argile :

Peser l'argile sèche (30 g/L max.) dans les pots à centrifugeuse.

Compléter les pots avec une solution NaCl 0,2 M.

Agiter sur table d'agitation pendant 2 jours au moins, à 100 tours par minute (tpm).

6.1.2. Fractionnement granulométrique par centrifugation à plat, pour avoir les particules inférieures à 2 µm :

6.1.2.1. Méthode utilisée

La centrifugation dure 6 minutes à 700 tours par minute pour obtenir la fraction inférieure à 2 µm.

Le surnageant est récupéré sur 5 cm par aspiration à l'aide d'une pipette pasteur au bout incurvé et d'une pompe à eau. Puis le mettre dans des grands Becher.

Le reliquat est à nouveau dilué par de l'eau bidistillée. Les pots sont agités à la main pour décoller le culot du dépôt et homogénéiser la suspension. L'argile est à nouveau centrifugée.

Environ 8 ou plus cycles sont nécessaires pour récupérer la majorité des particules.

Les suspensions d'argiles sont floculées en ajoutant du NaCl pour obtenir une concentration de 0,5 M puis sont centrifugées à 4300 tpm pendant 15 minutes.

Le surnageant est éliminé, seule l'argile compactée (le dépôt) est conservée. Cette opération peut être réitérée plusieurs fois pour augmenter la teneur en argile de la suspension finale.

6.1.2.2. Principe du fractionnement granulométrique par centrifugation à plat

La centrifugation à plat permet une ségrégation des particules en fonction de leur taille. Cette technique est plus rapide qu'une simple décantation. La centrifugation est effectuée dans une centrifugeuse Beckmann Avanti J-20 avec une croix de centrifugation à berceaux pivotants (Beckman JS 4-3). La durée de centrifugation nécessaire à la récupération des particules de taille inférieure à « r » dans le surnageant est donné par la formule suivante (Jackson, 1975) :

$$t = \frac{\eta \log_{10} \frac{R}{S}}{3{,}81 \times N^2 r^2 \Delta S}$$

où :
η est la viscosité en poise de la solution ;
R la distance de la surface du dépôt à l'axe du rotor ;
S la distance de la surface de la suspension à l'axe du rotor ;
N est la vitesse de rotation en tours par seconde ;
r le rayon maximal en cm des particules désirées ;
ΔS la différence de gravité spécifique entre la particule et la suspension liquide i.e. la différence de densité.

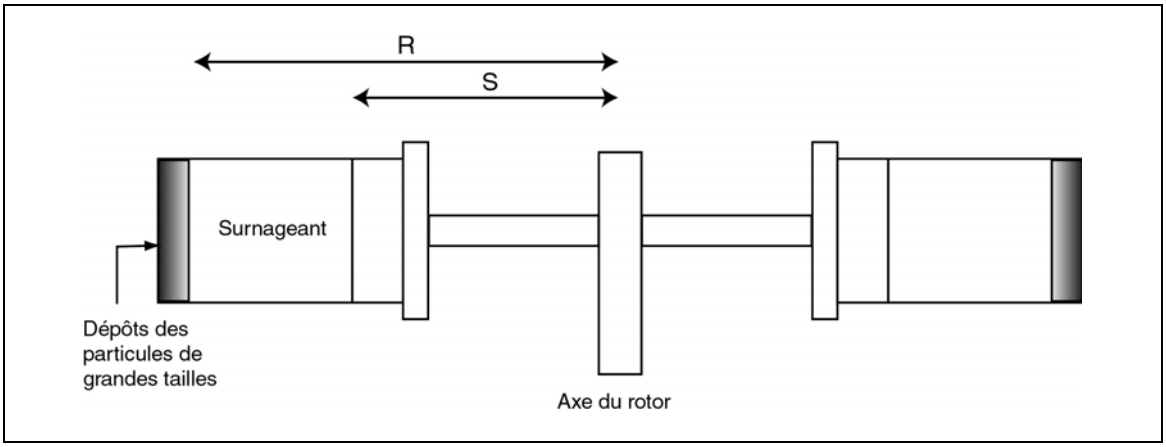


Figure 6.1 : Schéma de la centrifugation sur axe à berceau rotatif et variables associées

Dans cette étude R = 13 cm, S = 6,5 cm, η = 0,00894 p à 20°C, et la centrifugation dure 6 minutes à 700 tours par minute pour obtenir la fraction inférieure à 2 µm. Le surnageant est récupéré sur 5 cm (pour prévenir toute pollution par des particules trop grosses) par aspiration à l'aide d'une pipette pasteur au bout incurvé et d'une pompe à eau. Le reliquat qui contient encore des particules de diamètre inférieur à 2 µm du fait de leur entraînement par les autres particules est à nouveau dilué par de l'eau bidistillée. Les pots sont agités à la main pour décoller le culot du dépôt et homogénéiser la suspension. L'argile est à nouveau centrifugée.

6.1.3. Purification minéralogique

6.1.3.1. Attaque acide (élimine les carbonates)

Chaque pot à centrifuger est complété avec une solution d'acide acétique 0,1 M (5.6 ml dans 1L) et de NaCl 0,5 M. (29.22 g dans 1 L).

Les pots sont agités à la main quelques dizaines de secondes,

Puis ouverts pour laisser s'échapper les gaz produits (CO_2), sous la hotte.

Ils sont ensuite fermés et mis sur table d'agitation pendant 1 heure.

Les suspensions sont ensuite centrifugées pendant 30 min à 4300 tpm. Le surnageant est éliminé et une deuxième attaque acide est effectuée.

Les pots à centrifuger sont complétés avec une solution NaCl 0,5 M, agités pendant 1 heure et centrifugés 30 min à 4300 tpm. Ce lavage est répété trois fois.

6.1.3.2. Attaque DCB (élimine les hydroxydes de fer et de manganèse par dissolution en conditions réductrices)

Chaque pot est complété avec une solution de citrate 0,2 M (52.62 g dans 1L), NaCl 0,5 M (29.22 g dans 1 L) et bicarbonate 0,1 M ou NaOH 6 $g.L^{-1}$ approximativement (pour tamponner le pH autour de 6).

Une petite spatule de dithionite de sodium ($Na_2S_2O_4$) est ajoutée dans chaque pot.

Les pots sont mis au bain-marie dans un évier d'eau chaude (40°C) pendant 5 minutes, puis sont ouverts sous hotte pour libérer les gaz produits. Ils sont ensuite agités sur table pendant 1 heure, puis centrifugés pendant 30 min à 4300 tpm. Le surnageant est éliminé. Le cycle est répété 1 fois. Il est suivi de trois cycles de lavage au NaCl 0,5 M.

6.1.3.3. Attaque à l'eau oxygénée (H_2O_2) (élimine la matière organique)

Chaque pot est complété par une solution de H_2O_2 3% (100 ml de H_2O_2 30 % dans 1 L) et NaCl 0,5 M.

Agités à la main et sur table pendant ½ heure.

Le contenu de tous les pots est transféré dans un grand bêcher préalablement rincé avec la solution de H_2O_2.

La suspension est chauffée à 55-60°C et agité par un barreau aimanté pendant 1 heure.

La suspension refroidie est ensuite versée dans des pots et centrifugés pendant 30 min à 4300 tpm.

Le surnageant est éliminé. 3 cycles de lavages sont alors effectués avec du $NaNO_3$ 0.5 M

L'argile purifiée peut alors être stockée au réfrigérateur ou être mise à l'équilibre avec une solution adéquate.

6.1.4. Saturation des argiles au Na^+ et au Ca^{2+}

La saturation de l'argile au sodium ou au calcium est obtenue par des cycles de lavages avec la solution d'intérêt ($NaNO_3$ ou $CaCl_2$,$2H_20$), centrifugation et élimination du surnageant. Les 3 premiers cycles se font avec des solutions concentrées (1 M) puis au minimum 3 autres cycles sont effectués avec la solution de molarité souhaitée.

6.2. METHODE DE DOSAGE DU FE(II) ET DU FE(III) PAR SPECTROPHOTOMETRIE D'ABSORPTION : METHODE FERROZINE

Cette méthode permet de descendre vers des valeurs de concentrations assez basses (autour du micromolaire – 0.05 ppm – jusqu'environ 100 micromolaire sans dilution préalable). La publication d'origine est celle de Viollier et al., 2000.

6.2.1. Réactifs et standards :

Réactif A
Ferrozine 10^{-2} mol.L^{-1} ($C_{20}H_{14}N_4O_6S_2$, ALDRICH 16,060-1) dans acétate d'ammonium 10^{-1} mol.L^{-1} (ALDRICH 37,233-1). Soit pour 20 mL de réactif : 0,1542 g d'acétate d'ammonium et 0,09849 g de Ferrozine.

Réactif B
Hydroxylamine hydrochloride 1,4 mol.L^{-1} (ALDRICH 37,992-1, pureté > 99,9999%) dans une solution d'HCl analytique à 2 mol.L^{-1}. Soit pour 20 mL de réactif 1,9457 g d'hydroxylamine hydrochloride.

Réactif C = Buffer
Acétate d'ammonium 10 mol.L^{-1} ajusté à pH 9,5 avec une solution d'hydroxyde d'ammonium. Soit pour 10 mL de réactif 7,708 g d'acétate d'ammonium.

Standards de Fer
Préparation à partir d'une solution 1000 µg.mL^{-1} de Fe(III) (standard ICP) diluée dans une solution à la force ionique de l'expérience.

6.2.2. Protocole :

$$C_{Fe(II)} = \frac{A_1 * (pente2) - A_2 * pente1}{(pente2) * (\frac{pente2}{\alpha} - pente1)}$$

$$C_{Fe(III)} = \frac{A_2 - A_1 * \alpha}{\alpha * (\frac{pente2}{\alpha} - pente1)}$$

1. Mesurer l'absorbance A_1 à 562 nm de 5 mL d'échantillon filtré + 0,5 mL de réactif A. Tracer la courbe concentration en fonction de l'absorbance $A_1 \rightarrow$ *pente1* ;

2. Ajouter 0,5 mL de réactif B $\rightarrow$ réduction du Fe(III) en Fe(II) et attendre 10 min (réduire l'attente si la solution contient peu de Fe(III)) ;

3. Ajouter 0,17 mL de réactif C et mesurer l'absorbance A_2 à 562 nm. Tracer la courbe concentration en fonction de l'absorbance $A_2 \rightarrow$ *pente2*.

Pour quelques standards, les étapes 2 et 3 sont répétées une fois ($\rightarrow A_2'$) pour obtenir le facteur de dilution α entre les mesures de A_1 et A_2 : $\alpha = A_2'/A_2$. La moyenne des α trouvés donne une bonne estimation du facteur de dilution.

6.3. METHODE POUR LIMITER LA QUANTITE DE O_2 PRESENTE DANS LES SUSPENSIONS ET LES SOLUTIONS

La solution idéale est de préparer le maximum de solutions et suspensions en boîte à gants.

Toutes les solutions sont effectuées à partir d'eau milli-Q bouillie et refroidie ensuite sous argon ou azote (bullage par un fritté). Butler et al. (Butler et al., 1994) ont montré que faire buller de l'azote pendant une heure dans une solution était la méthode la plus simple et la plus efficace pour supprimer le O_2 présent en solution; la phase d'ébullition n'étant pas nécessaire. Cependant, l'ébullition permet également de se débarrasser des traces de carbonates puisque la dissolution des bicarbonates est moins forte à haute température qu'à basse température. Il est possible de purifier le gaz dont on se sert pendant le refroidissement de l'eau, en le faisant passer successivement dans trois bains différents (Figure 6.2)

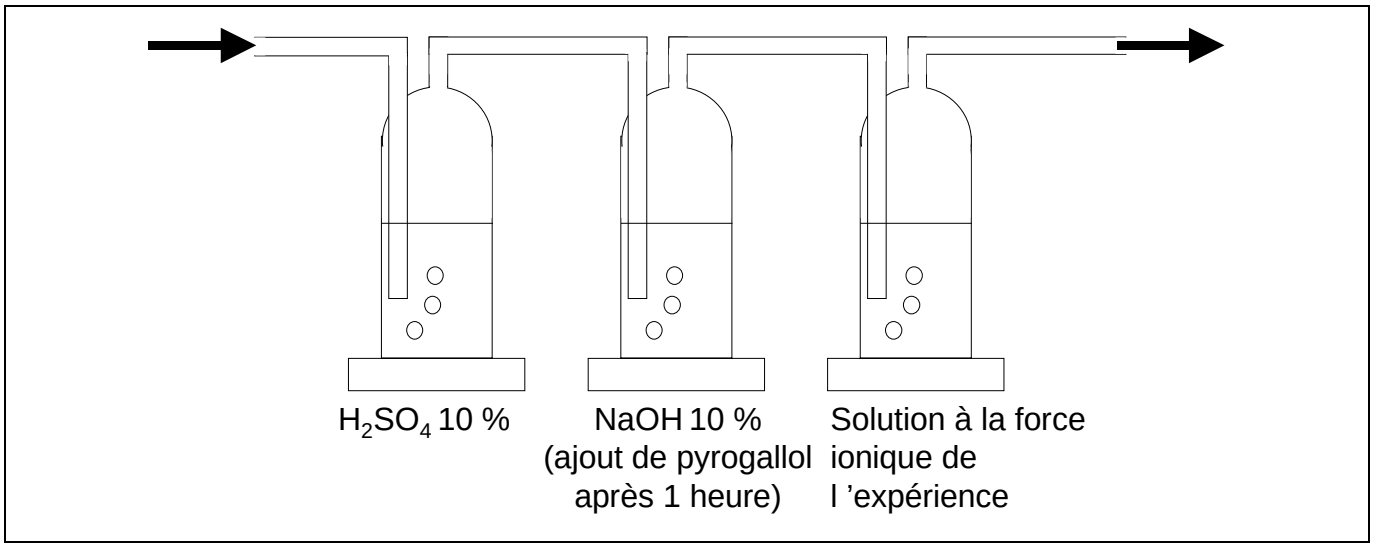


Figure 6.2 : Schéma des 3 bains, purifiant le gaz (argon ou N_2) avant son utilisation. H_2SO_4 permet d'éliminer les impuretés acides, NaOH les impuretés basiques (ex : carbonates) et le pyrogallol l'oxygène (méthode tirée de Liger et al., 1999).

Transférer cette eau immédiatement en boîte à gant permet d'éviter qu'elle se recharge en O_2. La faire équilibrer avec l'atmosphère de la boîte à gant (en ouvrant la bouteille) doit permettre de gagner encore en pureté.

Certaines solutions ou suspensions ne peuvent pas être préparées dans la boîte à gant, voir sont déjà préparées avec de l'eau non dégazée (ex : suspensions d'argile, ampoules titrisol…). Avant de les utiliser, il convient de les faire dégazer une nuit par de l'azote purifié (on veillera à ce que le dernier bain soit à la force ionique de la solution pour éviter une évaporation trop importante). Elles ont alors rentrées en boîte à gants et si possible mises à équilibrer avec son atmosphère (pendant cette phase, il peut y avoir évaporation et donc changement des concentrations).

7. BIBLIOGRAPHIE GENERALE

Akcay, H. Aqueous speciation and pH effect on the sorption behavior of uranium by montmorillonite, *Journal of Radioanalytical and Nuclear Chemistry*, **1998**, *237*, p. 133-137.

ANDRA Référentiel matériaux. ANDRA C.RP.AMAT.01.060, **2001**.

Avena, M. J. Acid-base behavior of clay surfaces in aqueous media, *Encyclopedia of surface and colloid science*, **2002**, p. 37-63.

Avena, M. J., Cabrol, R. and De Pauli, C. Study of some physicochemical properties of pillared montmorillonites: acid-base potentiometric titrations and electrophoretic measurements, *Clays and Clay Minerals*, **1990**, *38*, p. 356-362.

Avena, M. J. and De Pauli, C. Proton adsorption and electrokinetics of an argentinean montmorillonite, *Journal of Colloid and Interface Science*, **1998**, *202*, p. 195-204.

Baeyens, B. and Bradbury, M. H. A quantitative mechanistic description of Ni, Zn and Ca sorption on Na-montmorillonite. Paul Scherrer Institut (PSI) ISSN 1019-0643, **1995**.

Baeyens, B. and Bradbury, M. H. A mechanistic description of Ni and Zn sorption on Na-montmorillonite. Part I: Titration and sorption measurements, *Journal of Contaminant Hydrology*, **1997**, *27*, p. 199-222.

Balzer, W. On the distribution of iron and manganese at the sediment / water interface: thermodynamic versus kinetic control, *Geochimica et Cosmochimica Acta*, **1982**, *46*, p. 1153-1161.

Bardot, F., Villiéras, F., Michot, L. J., François, M., Gérard, G. and Cases, J. M. High resolution gas adsorption study on illites permuted with various cations: assessment of surface energetic properties, *J. Dispersion Science and Technology*, **1998**, *19*, p. 739-759.

Bérend, I. *Les mécanismes d'hydratation de montmorillonites homoioniques pour des pressions relatives inférieures à 0,95*. Thesis defended at INPL Nancy, **1991**.

Bérend, I., Cases, J. M., François, M., Uriot, J.-P., Michot, L., Masion, A. and Thomas, F. Mechanism of adsorption and desorption of water vapor by homoionic montmorillonites: 2. The Li^+, Na^+, K^+, Rb^+ and Cs^+-exchanged forms, *Clays and Clay Minerals*, **1995**, *43*, p. 324-336.

Berner, R. A., Ed. *Principles of Chemical Sedimentology* McGraw-Hill, 1971.

Besnus, Y. and Rouault, R. Une methode d'analyse des roches au spectrometre d'arc à lecture directe par un dispositif d'electrode rotative, *Analusis*, **1973**, *2*, p. 111-116.

Besson, G. and Drits, V. A. Refined relationship between chemical composition of dioctahedral fine-grained micaceous minerals and their infrared spectra within the OH stretching region. Part I: identification of the OH stretching bands, *Clays and Clay Minerals*, **1997a**, *45*, p. 158-169.

Besson, G. and Drits, V. A. Refined relationship between chemical composition of dioctahedral fine-grained micaceous minerals and their infrared spectra within the OH stretching region. Part II: the main factors affecting OH vibrations and quantitative analysis, *Clays and Clay Minerals*, **1997b**, *45*, p. 170-183.

Bickmore, B., Bosbach, D., Hochella, M. F., Charlet, L. and Rufe, E. In situ atomic force microscopy study of hectorite and nontronite dissolution: implications for phyllosilicate edge surface structures and dissolution mechanisms, *American Mineralogist*, **2001**, *86*, p. 411-423.

Bickmore, B., Hochella, M. F., Bosbach, D. and Charlet, L. Methods for performing atomic force microscopy imaging of clay minerals in aqueous solution, *Clays and Clay Minerals*, **1999**, *47*, p. 573-581.

Bosbach, D., Charlet, L., Bickmore, B. and Hochella, M. F. The dissolution of hectorite: in-situ, real-time observations using atomic force microscopy, *American Mineralogist*, **2000**, *85*, p. 1209-1216.

Bosbach, D., Charlet, L., Brandt, F., Pieper, H. and Plaschke, M., The reactivity of clay mineral surfaces: a microscopic perspective of nanoscale geochemical processes. In *Clays in natural and engineered barriers for radioactive waste confinement*, Reims, **2002**.

Bott, M. *Iron sulfides in Baldeggersee during the last 8000 years: formation processes, chemical speciation and mineralogical constrains from EXAFS spectroscopy*. Thesis defended at ETH Zürich, **2002**.

Boult, K. A., Cowper, M. M., Heath, T. G., Sato, H., Shibutani, T. and Yui, M. Towards an understanding of the sorption of U(VI) and Se(VI) on sodium bentonite, *Journal of Contaminant Hydrology*, **1998**, *35*, p. 141-150.

Bradbury, M. H. and Baeyens, B. A mechanistic description of Ni and Zn sorption on Na-montmorillonite. Part II: modeling, *Journal of Contaminant Hydrology*, **1997**, *27*, p. 223-248.

Bradbury, M. H. and Baeyens, B. Modeling the sorption of Zn and Ni on Ca-montmorillonite, *Geochimica et Cosmochimica Acta*, **1998**, *63*, p. 325-336.

Bradbury, M. H. and Baeyens, B. Sorption of Eu on Na- and Ca-Montmorillonites: Experimental Investigations and Modeling with Cation Exchange and Surface Complexation, *Geochimica et Cosmochimica Acta*, **2002**, *66*, p. 2325-2334.

Brown, I. D. On the geometry of O-H...O hydrogen bonds, *Acta Crystallographica*, **1976**, *A32*,

Brown, I. D. *The bond-valence method: an empirical approach to chemical structure and bonding.* London, **1981**.

Brown, I. D. Chemical and steric constrains in inorganic solids, *Acta Crystallographica*, **1992**, *48*, p. 553-572.

Brown, I. D. and Altermatt, D. Bond-valence parameters obtained from a sytematic analysis of the inorganic crystal structure database, *Acta Crystallographica*, **1985**, *41*, p. 244-247.

Butler, I. B., Schoonen, M. A. A. and Rickard, D. T. Removal of dissolved oxygen from water: a comparison of four common techniques, *Talanta*, **1994**, *41*, p. 211-215.

Cama, J., Ganor, J., Ayora, C. and Lasagna, C. A. Smectite dissolution kinetics at 80°C and pH 8.8, *Geochimica et Cosmochimica Acta*, **2000**, *64*, p. 2701-2717.

Cases, J. M., Bérend, I., Besson, G., François, M., Uriot, J.-P., Thomas, F. and Poirier, J. E. Mechanism of adsorption and desorption of water vapor by homoionic montmorillonite. 1. The sodium-exchanged form, *Langmuir*, **1992**, *8*, p. 2730-2739.

Cebula, D. J., Thomas, R. K. and White, J. W., The structure and dynamics of clay-water systems studied by neutron scattering. In *Proc. Int. Clay Conf.*, Oxford, **1978**.

Chang, F. R. C., Skipper, N. T. and Sposito, G. Computer-Simulation of Interlayer Molecular-Structure in Sodium Montmorillonite Hydrates, *Langmuir*, **1995**, *11*, p. 2734-2741.

Chang, F. R. C., Skipper, N. T. and Sposito, G. Monte Carlo and molecular dynamics simulations of electrical double-layer structure in potassium-montmorillonite hydrates, *Langmuir*, **1998**, *14*,

Charlet, L., Bosbach, D. and Peretyashko, T. Natural attenuation of TCE, As, Hg linked to the heterogeneous oxidation of Fe(II): an AFM study, *Chemical Geology*, **2002**, *190*, p. 303-319.

Charlet, L. and Manceau, A. Evidence fot the neoformation of clays upon sorption of Co(II) and Ni(II) on silicates, *Geochimica et Cosmochimica Acta*, **1994**, *58*, p. 2577-2582.

Charlet, L., Schindler, P. W., Spadini, L., Furrer, G. and Zysset, M. Cation adsorption on oxides and clays : The aluminum case, *Aquatic Science*, **1993**, *55/4*, p. 1015-1621.

Claret, F., Bauer, A., Schäfer, T., Griffault, L. and Lanson, B. Experimental investigation of the interaction of clays with high pH solutions: A case study from the Callovo-Oxfordian formation, Meuse - Haute Marne underground laboratory (France), *Clays and Clay Minerals*, **2002**, *50*, p. 632-645.

Craciun, C. Influence of the Fe3+ for Al3+ octahedral substitutions on the IR spectra of montmorillonite minerals, *Spectroscopy Letters*, **1984**, *17*, p. 579-590.

Criaud, A. and Fouillac, C. Etude des eaux thermominérales carbogazeuses du Massif Central français. I. Potentiel d'oxydo-réduction et comportement du fer, *Geochimica et Cosmochimica Acta*, **1986a**, *50*, p. 525-533.

Criaud, A. and Fouillac, C. Etude des eaux thermominérales carbogazeuses du Massif Central français. II. Comportement de quelques métaux en trace, de l'arsenic, de l'antimoine, et du germanium, *Geochimica et Cosmochimica Acta*, **1986b**, *50*, p. 1573-1582.

Dähn, R., Scheidegger, A. M., Manceau, A., Curti, E., Baeyens, B., Bradbury, M. H. and Chateigner, D. L. Th uptake on montmorillonite: A powder and polarized extended X-ray absorption fine structure (EXAFS) study, *Journal of Colloid and Interface Science*, **2002a**, *249*, p. 8-21.

Dähn, R., Scheidegger, A. M., Manceau, A., Schlegel, M., Baeyens, B., Bradbury, M. H. and Chateigner, D. L. Structural evidence for the sorption of Ni(II) atoms on the edges of montmorillonite clay minerals: A polarized X-ray absorption fine structure study, *Geochimica et Cosmochimica Acta*, **2003**, *37*, p. 1-15.

Dähn, R., Scheidegger, A. M., Manceau, A., Schlegel, M., Baeyens, B., Bradbury, M. H. and Morales, M. Neoformation of Ni phyllosilicate upon Ni uptake on montmorillonite: a kinetics study by powder and polarized extended X-ray absorption fine structure spectroscopy, *Geochimica et Cosmochimica Acta*, **2002b**, *66*, p. 2335-2347.

Davison, W., Phillips, N. and Tabner, B. J. Soluble iron sulfide species in natural waters: reappraisal of their stoichiometry and stability constants, *Aquatic Sciences*, **1999**, *61*, p. 23-43.

de Carvalho, R. J. F. L. and Skipper, N. T. Atomistic computer simulation of the clay-fluid interface, *Journal of Chemical Physic*, **2001**, *114*, p. 3727-3733.

Delgado, A., Gonzalez-Caballero, F. and Bruque, J. M. On the zeta potential and surface charge density of montmorillonite in aqueous electrolyte solutions, *Journal of Colloid and Interface Science*, **1986**, *113*, p. 203-211.

Delgado, A., Gonzalez-Caballero, F., Salcedo, J. and Cabrerizo, M. A. A study of the electrophoretic properties of montmorillonite particles in aqueous electrolyte solutions, *Materials Chemical Physics*, **1988**, *19*, p. 327-340.

Drever, J. I. Magnesium-iron replacement in clay minerals in anoxic marine sediments, *Science*, **1971**, *172*, p. 1334-1336.

Drits, V. A., Dainyak, L. G., Muller, F., Besson, G. and Manceau, A. Isomorphous cation distribution in celadonites, glauconites and Fe-illites determined by infrared, Mössbauer and EXAFS spectroscopies, *Clay Minerals*, **1997**, *32*, p. 153-179.

Dzombak, D. A. and Morel, F. M. M. *Surface complexation modeling-Hydrous ferric oxide.* New York, **1990**.

Emerson, S. Early diagenesis in anaerobic lake sediments: chemical equilibria in intersticial waters, *Geochimica et Cosmochimica Acta*, **1976**, *40*, p. 925-934.

Emerson, S., Jahnke, R., Bender, M., Froelich, P., Klinkhammer, G., Bowser, C. and Setlock, G. Early diagenesis in sediments from the eastern equatorial pacific. I. pore water nutrient and carbonate results, *Earth Planete Science Letters*, **1980**, *49*, p. 57-80.

Farmer, V. C., Russel, J. D. and Ahlrichs, J. L., Characterization of clay minerals by infrared spectroscopy. In *9th International Congress of Soil Science*, **1968**.

Ferrage, E., Martin, F., Petit, S., Pejo-Soucaille, S., Micoud, P., Fourty, G., Ferret, J., Salvi, S., De Parseval, P. and Fortuné, J. P. Evaluation of talc morphology using FTIR and H/D substitution, *Clay Minerals*, **2003**, *38*,

Fletcher, P. and Sposito, G. The chemical modeling of clay/electrolyte interactions for montmorillonite., *Clay Minerals*, **1989**, *24*, p. 375-391.

Furrer, G. and Stumm, W. The coordination chemistry of weathering: I. Dissolution kinetics of δ-Al_2O_3 and BeO, *Geochimica et Cosmochimica Acta*, **1986**, *50*, p. 1847-1860.

Gaboriaud, F. and Ehrhardt, J. J. Effects of different crystal faces on the surface charge of colloidal goethite (α-FeOOH) particles: an experimental and modeling study, *Geochimica et Cosmochimica Acta*, **2003**, *67*, p. 967-983.

Gaucher, E. *Interactions eaux-argiles. Etude experimentale*. Thesis defended at Denis Diderot, **1998**.

Gehring, A. U., Fry, I. V., Lloyd, T. and Sposito, G. Residual manganese(II) entrapped in single-layer-hydrate montmorillonite interlayers, *Clays and Clay Minerals*, **1993**, *41*, p. 565-569.

Gehring, A. U. and Sposito, G. Residual manganese(II) speciation in montmorillonite (reply to comment), *Clays and Clay Minerals*, **1995**, *43*, p. 385-386.

Gilbert, M. and Laudelout, H. Exchange properties of hydrogen ions in clays, *Soil Science*, **1965**, *100*, p. 157.

Gournis, D., Karakassides, M. A. and Petridis, D. Formation of hydroxyl radicals catalyzed by clay surfaces, *Physics and Chemistry of Minerals*, **2002**, *29*, p. 155-158.

Grauby, O., Petit, S., Enguehard, F., Martin, F. and Decarreau, A., XRD, EXAFS and FTIR octahedral cation distribution in synthetic Ni-Co kerolites. In *7th Euroclay Conference*, Dresden, **1991**.

Grillet, Y., Rouquerol, F. and Rouquerol, J. Etude de l'adsorption physique des gaz par une procédure continue. I. Application à la détermination des surfaces spécifiques d'adsorbants non poreux et mésoporeux, *Journal of Chemical Physic*, **1977**, *74*, p. 179-182.

Guggenheim, S., Chang, Y. and Koster van Groos, A. F. Muscovite dehydroxylation: high-temperature studies, *American Mineralogist*, **1987**, *72*, p. 537-550.

Heron, G., Crouzet, C., Bourg, A. C. M. and Christensen, T. H. Speciation of Fe(II) and Fe(III) in contaminated aquifer sediments using chemical extraction techniques, *Environmental Science and Technology*, **1994**, *28*, p. 1698-1705.

Hiemstra, T., De Wit, J. C. M. and Van Riemsdijk, W. H. Multisite proton adsorption modelling at the solid/solution interface of (hydr)oxides: a new approach. II. Application to various important (hydr)oxides, *Journal of Colloid and Interface Science*, **1989a**, *133*, p. 105-117.

Hiemstra, T. and Van Riemsdijk, W. H. A surface structural approach to ion adsorption: the charge distribution (CD) model, *Journal of Colloid and Interface Science*, **1996**, *179*, p. 488-508.

Hiemstra, T., Van Riemsdijk, W. H. and Bolt, G. H. Multisite proton adsorption modelling at the solid/solution interface of (hydr)oxides: a new approach. I. Model descritpion and evaluation of intrinsic reaction constants, *Journal of Colloid and Interface Science*, **1989b**, *133*, p. 91-104.

Hiemstra, T., Venema, P. and Van Riemsdijk, W. H. Intrinsic proton affinity of reactive surface groups of metal (hydr)oxides: the bond valence principle, *Journal of Colloid and Interface Science*, **1996**, *184*, p. 680-692.

Hight, R. J., Higdon, W. L., Darley, H. C. H. and Schmidt, P. W. Small angle X-ray scattering from montmorillonite clay suspensions. II, *Journal of Chemical Physic*, **1962**, *37*,

Hight, R. J., Higdon, W. L. and Schmidt, P. W. Small angle scattering study of sodium montmorillonite clay suspensions, *Journal of Chemical Physic*, **1960**, *33*, p. 1656-1661.

Holland, H. D. *The chemistry of the atmosphere and oceans.* New York, **1978**.

Hunter, R. J. and James, M. Charge reversal of kaolinite by hydrolyzable metal ions: an electroacoustic study, *Clays and Clay Minerals*, **1992**, *40*, p. 644-649.

Hyun, S. P., Cho, Y. H., Kim, S. J. and Hahn, P. S. Cu(II) sorption mechanism on montmorillonite: an electron paramagnetic resonance study, *Journal of Colloid and Interface Science*, **2000**, *222*, p. 254-261.

Ishida, K. Identification of infrared OH librational bands of talc-willemseite solid solutions and Al(IV) free amphiboles through deuteration, *Mineralogical Journal*, **1990**, *15*, p. 93-104.

Jackson, M. L. *Soil chemical analysis - advanced course 2nd edition.* University of Wisconsin, Madison, Wisconsin, **1975**.

Jensen, H. E. Potassium - calcium exchange equilibria on a montmorillonite and a kaolinite clay, *Agrochimica*, **1973**, *17*, p. 181-190.

Jolivet, J. P. *De la solution à l'oxyde. Condensation des cations en solution acqueuse. Chimie de surface des oxydes.* Paris, **1994**.

Keren, R. and Shainberg, I. Water vapor isotherms and heat of immersion of Na/Ca-montmorillonite systems. I: homoionic clay, *Clays and Clay Minerals*, **1975**, *23*, p. 193-200.

Langer, K. and Lattard, D. Identification of a low OH valence vibration in zoisite, *American Mineralogist*, **1980**, *50*, p. 779-783.

Liger, E., Charlet, L. and Van Cappellen, P. Surface catalysis of uranium (VI) reduction by iron(II), *Geochimica Cosmochimica Acta*, **1999**, *63*, p. 2939-2955.

Madejova, J. and Komadel, P. Baseline studies of the clay minerals society source clays: infrared method, *Clays and Clay Minerals*, **2001**, *49*, p. 410-432.

Maes, A., Peigneur, P. and Cremers, A., Thermodynamics of transition metal ion exchange in montmorillonite. In *International Clay Conference 1975*, **1976**.

Manceau, A. and Gates, W. P. Surface structural model for ferrihydrite, *Clays and Clay Minerals*, **1997**, *43*, p. 448-460.

Manceau, A., Schlegel, M. L., Nagy, K. L. and Charlet, L. Evidence for the formation of trioctahedral clay upon sorption of Co^{2+} on quartz, *Journal of Colloid and Interface Science*, **1999**, *220*, p. 181-197.

Martin, F., Petit, S., Grauby, O. and Lavie, M. P. Gradual H/D substitution in synthetic germanium bearing talcs: a method for infrared band assignment, *Clay Minerals*, **1999**, *34*, p. 365-374.

McBride, M. B. *Environmental Chemistry of Soils.* New York Oxford, **1994**.

McBride, M. B. On the natural Mn(II) EPR signal of SWy-1 montmorillonite (comment), *Clays and Clay Minerals*, **1995**, *43*, p. 383-384.

McBride, M. B., Fraser, A. R. and McHardy, W. J. Cu2+ interaction with microcrystalline gibbsite. Evidence for oriented chemisorbed copper ions, *Clays and Clay Minerals*, **1984**, *32*, p. 12-18.

McBride, M. B., Pinnavaia, T. J. and Mortland, M. M. Perturbation of structural Fe^{3+} in smectite by exchange ions, *Clays and Clay Minerals*, **1975**, *23*, p. 103-107.

Mermut, A. R. and Cano, A. F. Baseline studies of the clay minerals society source clays: chemical analyses of major elements, *Clays and Clay Minerals*, **2001**, *49*, p. 381-386.

Mermut, A. R. and Lagaly, G. Baseline studies of the clay minerals society source clays: layer-charge determination and characteristics of those minerals containing 2:1 layers, *Clays and Clay Minerals*, **2001**, *49*, p. 393-397.

Metson, A. J. Methods of chemical analysis for soil survey samples, *Neo-Zealand Soil Buro Bulletin*, **1956**, *12*,

Michot, L., François, M. and Cases, J. M. Surface heterogeneity studied by a quasi-equilibrium adsorption procedure, *Langmuir*, **1990**, *6*, p. 637-643.

Millero, F. J. *Chemical Oceanography.* Second Edition ed., Washington D.C., **2002**.

Mooney, R. W., Keenan, A. G. and Wood, L. A. Adsorption of water vapor by montmorillonite. II. Effect of exchangeable ions and lattice swelling as measured by X-ray diffraction, *Journal of American Chemical Society*, **1952**, *74*, p. 1331-1374.

Naftz, D. L., Feltcorn, E. M., Fuller, C. C., Wilhelm, R. G., Davis, J. A., Morrison, S. J., Freethey, G. W., Piana, M. J., Rowland, R. C. and Blue, J. E. Field demonstration of permeable reactive barriers to remove dissolved uranium from groundwater, Fry Canyon, Utah. United State Environmental Protection Agency EPA 402-C-00-001, **2000**.

Norrish, K. The swelling of montmorillonite, *Faraday Discussion Society*, **1954**, *18*, p. 120-134.

Ochs, M., Boonekamp, M., Wanner, H., Sato, H. and Mikazu, Y. A quantitative model for ion diffusion in compacted bentonite, *Radiochimica Acta*, **1998**, *82*, p. 437-443.

Ochs, M., Lothenbach, B., Wanner, H., Sato, H. and Mikazu, Y. An integrated sorption-diffusion model for the calculation of consistent distribution and diffusion coefficients in compacted bentonite, *Journal of Contaminant Hydrology*, **2001**, *47*, p. 283-296.

Pabalan, R. T., Turner, D. R. and Bertetti, F. P. Sorption modeling for HLW performance assesment. NRC high-level radioactive waste research at CNWRA. Center for Nuclear Waste Regulatory Analyses CNWRA 94-01S, **1994**.

Parkhurst, D. L. and Appelo, C. A. J. Phreeqc2 user's manual and program, **1999**, http://www.geo.vu.nl/users/posv/phreeqc.html.

Pauling, L. The principles determining the structure of complex ionic crystals, *Journal of American Chemical Society*, **1929**,

Pitteloud, C., Powell, D. H., Gonzalez, M. A. and Cuello, G. J. Neutron diffraction studies of ion coordination and interlayer water structure in smectite clays: lanthanide(III)-exchanged Wyoming montmorillonite, *Colloids and Surfaces A: Physicochemical Engineering Aspects*, **In press**,

Postma, D. Pyrite and siderite formation in brackish and freshwater swamp sediments, *American Journal of Science*, **1982**, *282*, p. 1151-1183.

Powell, D. H., Fischer, H. E. and Skipper, N. T. The structure of interlayer water in Li-montmorillonite studied by neutron diffraction with isotopic substitution, *Journal of Physical Chemistry B*, **1998**, *102*, p. 10899-10905.

Rodier, J. *L'Analyse de l'eau, eaux naturelles, eaux résiduaires, eau de mer.* 8ème édition ed., Paris, **1996**.

Rouquerol, J., Rouquerol, F., Grillet, Y. and Ward, R. J. In *Characterization of Porous solids*. Hunger, K. K., Ed. **1988**, Vol. 67-76.

Russel, J. D., Farmer, V. C. and Velde, B. Replacement of OH by OD in layer silicates and identification of these groups in infrared spectra, *Mineralogical Magazine*, **1970**, *37*, p. 292.

Samuel, J., Rouault, R. and Besnus, Y. Analyse multielementaire standardisee des materiaux geologiques en spectrometrie d'emission par plasma à couplage inductif, *Analusis*, **1985**, *13*, p. 312-317.

Sato, T., Watanabe, T. and Otsuka, R. Effects of layer charge, charge location, and energy change on expansion properties of dioctahedral smectites, *Clays and Clay Minerals*, **1992**, *40*, p. 103-113.

Sauzéat, E., Guillaume, D., Neaman, A., Peiffert, C., Ruck, R., Dubessy, J., Cathelineau, M., Villiéras, F. and Yvon, J. MX-80 : une argile de référence méthodologique pour l'ANDRA. ANDRA, Agence nationale pour la gestion des déchets radioactifs **2000**.

Sauzéat, E., Guillaume, D., Villiéras, F., Dubessy, J., François, M., Pfeiffert, C., Pelletier, M., Ruck, R., Barrès, O., Yvon, J. and Cathelineau, M. Caractérisation minéralogique, cristallochimique et texturale de l'argile MX-80. ANDRA C RP 0LEM 01-001, **2001**.

Saylest, F. L. and Mangelsdorf, P. C. J. Cation-exchange characteristics of Amazon River suspended sediment and its reaction with seawater, *Geochimica et Cosmochimica Acta*, **1979**, *43*, p. 767-779.

Schindler, P. W., Fürst, B., Dick, R. and Wolf, P. U. Ligand properties of surface silanol groups: I. Surface complex formation with Fe^{2+}, Cu^{2+}, Cd^{2+} and Pb^{2+}, *Journal of Colloid and Interface Science*, **1976**, *55*, p. 469-475.

Schlegel, M. *De l'adsorption du cobalt et du zinc sur l'hectorite et le quartz, à la nucléation hétérogène de phyllosilicates*. Thesis defended at Université Grenoble-I, **2000**.

Schlegel, M., Charlet, L. and Manceau, A. Sorption of metal ions on clay minerals. II. Mechanism of Co sorption on hectorite at high and low ionic strength and impact on the sorbent stability, *Journal of Colloid and Interface Science*, **1999**, *220*, p. 392-405.

Schlegel, M., Manceau, A., Charlet, L. and Hazemann, J. L. Adsorption mechanisms of Zn on hectorite as a function of time, pH, and ionic strength, *American Journal of Science*, **2001a**, *301*, p. 798-830.

Schlegel, M. L., Manceau, A., Charlet, L., Chateigner, D. L. and Hazemann, J. L. Sorption of metal ions on clay minerals. III. Nucleation and epitaxial growth of Zn phyllosilicate on the edges of hectorite, *Geochimica et Cosmochimica Acta*, **2001b**, *65*, p. 4155-4470.

Schramm, L. L. and Kwak, J. C. T. Influence of exchangeable cation composition on the size and shape of montmorillonite particles in dilute suspension, *Clays and Clay Minerals*, **1982**, *30*, p. 40-48.

Schultess, C. P. and Sparks, D. L. Backtitration tecnhique for proton isotherm modeling of oxide surfaces, *Soil Science Society of America*, **1986**, *50*, p. 1406-1411.

Schultess, C. P. and Sparks, D. L. A critical assessment of surface adsorption model, *Soil Science Society of America*, **1988**, *52*, p. 92-97.

Schwarzenbach, R. P., Gschwend, P. M. and Imboden, D. M. *Environmental organic chemistry.* New York, **1993**.

Shannon, R. D. Revised effective ionic radii and systematic studies of interatomic distances in halides and chalcogenides, *Acta Crystallographica*, **1976**, *32*, p. 751-767.

Shirozu, H. and Ishida, K. Infrared study of some 7 Å and 14 Å layer silicates by deuteration, *Mineralogical Journal*, **1982**, *11*, p. 161-171.

Skipper, N. T., Chang, F. R. C. and Sposito, G. Monte Carlo simulation of interlayer molecular structure in swelling clay minerals. 1. Methodology, *Clays and Clay Minerals*, **1995a**, *43*, p. 285-293.

Skipper, N. T., Sposito, G. and Chang, F. R. C. Monte Carlo simulation of interlayer molecular structure in swelling caly minerals. 2. Monolayer hydrates., *Clays and Clay Minerals*, **1995b**, *43*, p. 294-303.

Slonimskaya, M. V., Besson, G., Dainyak, L. G., Tchoubar, C. and Drits, V. A. Interpretation of the IR spectra of celadonites and glauconites int he region of OH stretching frequencies, *Clay Minerals*, **1986**, *21*, p. 377-388.

Sposito, G. *The thermodynamics of soil solution.* New York, **1981**.

Sposito, G. *Surface chemistry of soils.* New York, **1984**.

Sposito, G., Holtzclaw, K. M., Charlet, L., Jouany, C. and Page, A. L. Sodium-calcium and sodium-magnesium exchange on Wyoming bentonite in perchlorate and chloride background ionic media, *Soil Science Society of America*, **1983a**, *47*, p. 51-56.

Sposito, G., Holtzclaw, K. M., Johnston, C. T. and Le Vesque, C. S. Thermodynamics of sodium-copper exchange on Wyoming bentonite at 298 K, *Soil Science Society of America*, **1981**, *45*, p. 1079-1084.

Sposito, G., Holtzclaw, K. M., Jouany, C. and Charlet, L. Cation selectivity in sodium-calcium, sodium-magnesium, and calcium-magnesium exchange on Wyoming bentonite at 298 K, *Soil Science Society of America*, **1983b**, *47*, p. 917-921.

Sposito, G., Skipper, N. T., Sutton, R., Park, S. and Soper, A. K. Surface geochemistry of the clay minerals, *Proceedings of the National Academy of Sciences of the United States of America*, **1999**, *96*, p. 3358-3364.

Stadler, M. and Schindler, P. W. Modeling of H^+ and Cu^{2+} adsorption on calcium-montmorillonite, *Clays and Clay Minerals*, **1993**, *41*, p. 288-296.

Stubican, V. and Roy, R. A new approach to assignment of infrared absorption band in layer-structure silicates, *Zeischrift für Kristallographie*, **1961**, *115*, p. 200-214.

Stumm, W., Kummert, R. and Sigg, L. A ligand exchange model for the adsorption of inorganic and organic ligands at hydrous oxide interfaces, *Croatica Chemica Acta*, **1980**, *53*, p. 291-312.

Stumm, W. and Lee, G. F. Oxygenation of ferrous iron, *Industrial and Engineering Chemistry Research*, **1961**, *53*, p. 143-146.

Stumm, W. and Morgan, J. J. *Aquatic chemistry.* **1996**.

Stumm, W. and Wollast, R. Coordination Chemistry of Weathering: Kinetics of the Surface-Controlled Dissolution of Oxide Minerals, *Reviews of Geophysics*, **1990**, *28*, p. 53-90.

Tamura, K., Yamada, H. and Nakazawa, H. Stepwise hydratation of high-quality synthetic smectite with various cations, *Clays and Clay Minerals*, **2000**, *48*, p. 400-404.

Teillet, J. and Varret, F. Unpublished program MOSFIT, MOSFIT.

Titiloye, J. O. and Skipper, N. T. Computer simulation of the structure and dynamics of methane in hydrated Na-smectites clays, *Chemical Physical Letters*, **2000**, *329*, p. 23-28.

Tournassat, C. and Charlet, L. Competitive specific sorption of Fe(II) on clay minerals in anoxic waters, *Environmental Science and Technology*, **submitted**,

Tournassat, C., Charlet, L. and Greneche, J. M. Fe(II)-Na(I)-Ca(II) cation exchange on montmorillonite in chloride medium; evidence for preferential clay adsorption of chloride – metal ion pairs in seawater., *Aquatic Geochemistry*, **submitted-a**,

Tournassat, C., Ferrage, E., Poinsignon, C. and Charlet, L. The titration of clay minerals. Part II. Insights from infrared spectroscopy, and models using Bradbury and Baeyens or MUSIC approach, *Journal of Colloid and Interface Science*, **submitted-b**,

Tournassat, C., Greneche, J. M., Tisserand, D. and Charlet, L. The titration of clay minerals. Part I. Discontinuous backtitration technique combined to CEC measurements, *Journal of Colloid and Interface Science*, **submitted-c**,

Tournassat, C., Neaman, A., Villiéras, F., Bosbach, D. and Charlet, L. Nanomorphology of montmorillonite particles: Estimation of the clay edge sorption site density by low-pressure gas adsorption and AFM observations, *American Mineralogist*, **submitted-d**,

Turner, D. R. A uniform approach to surface complexation modeling of radionuclide sorption. Center for Nuclear Waste Regulatory Analyses NRC-02-93-005, **1995**.

Turner, D. R., Pabalan, R. T. and Bertetti, F. P. Neptunium(V) sorption on montmorillonite: an experimental and surface complexation modeling study, *Clays and Clay Minerals*, **1998**, *46*, p. 256-269.

Vanselow, A. P. Equilibria of the base-exchange reaction of bentonites, permutites, Soil colloids and zeolites, *Soil Science*, **1932**, *33*, p. 95-113.

Vantelon, D., Pelletier, M., Michot, L., Barrès, O. and Thomas, F. Fe, Mg and Al distribution in the octahedral sheet of montmorillonites. An infrared study in the OH-bending region, *Clay Minerals*, **2001**, *36*, p. 369-379.

Venema, P., Hiemstra, T., Weidler, P. G. and Van Riemsdijk, W. H. Intrinsic proton affinity of reactive surface groups of metal (hydr)oxides: application to iron (hydr)oxides, *Journal of Colloid and Interface Science*, **1998**, *198*, p. 282-295.

Villiéras, F., Cases, J. M., François, M., Michot, L. J. and Thomas, F. Textural properties and surface energetic heterogeneity of solids from modeling of low pressure gas adsorption isotherms, *Langmuir*, **1992**, *8*, p. 1789-1795.

Villiéras, F., Michot, L. J., Bardot, F., Cases, J. M., François, M. and Rudzinski, W. An improved derivative isotherm summation method to study surface heterogeneity of clay minerals, *Langmuir*, **1997a**, *13*, p. 1104-1117.

Villiéras, F., Michot, L. J., Bardot, F., Chamerois, M., Eypert-Blaison, C., Gérard, G. and Cases, J. M. Surface heterogeneity of minerals, *C. R. Geosciences*, **2002**, *334*, p. 597-609.

Villiéras, F., Michot, L. J., Cases, J. M., Berend, I., Bardot, F., François, M., Gérard, G. and Yvon, J., Eds. *Static and dynamic studies of the energetic surface heterogeneity of clay minerals*; Elsevier Sci. Pub. B. V.: Amsterdam, 1997b; Vol. 104.

Viollier, E., Inglett, P. W., Hunter, K., Roychoudhury, A. N. and Van Cappellen, P. The ferrozine method revisited : Fe(II)/Fe(III) determination in natural waters, *Applied Geochemistry*, **2000**, *15*, p. 785-790.

Wanner, H., Albinson, Y., Karnland, O., Wieland, E., Wersin, P. and Charlet, L. The acid/base chemistry of montmorillonite, *Radiochimica Acta*, **1994**, *66/67*, p. 157-162.

White, G. N. and Zelazny, L. W. Analysis and implications of the edge structure of dioctahedral phyllosilicates, *Clays and Clay Minerals*, **1988**, *36*, p. 141-146.

Zachara, J. M. and Smith, S. C. Edge complexation reactions of cadmium on specimen and soil-derived smectite, *Soil Science Society of America*, **1994**, *58*, p. 762-769.

Zachara, J. M., Smith, S. C., McKinley, J. P. and Resch, C. T. Cadmium sorption on specimen and soil smectites in sodium and calcium electrolytes, *Soil Science Society of America*, **1993**, *57*, p. 1491-1501.

RESUME

Les interactions entre du Fe(II) en solution et une montmorillonite sont étudiées dans des conditions anoxiques et à température ambiante, sur une échelle de temps variant de l'heure à la semaine.

Le Fe^{2+} s'adsorbe sur les sites d'échange cationique de l'argile avec la même affinité que le Ca^{2+} ; en présence de chlore, le Fe(II) forme des paires ioniques, $FeCl^+$, qui s'adsorbent avec une affinité comparable à celles de $CaCl^+$ et $MgCl^+$. Les simulations montrent qu'en fond anionique chloré concentré (comme l'eau de mer) les ions monovalents (Na^+ et paires ioniques du type $CaCl^+$ et $MgCl^+$) sont majoritaires sur les sites d'échange cationique.

Le Fe^{2+} s'adsorbe sur les surfaces de bordure de la montmorillonite avec une affinité très forte. Cette adsorption spécifique peut être modélisée convenablement avec des modèles simples de complexation de surface. Le Fe^{2+} s'adsorbe sur l'argile avec une affinité d'environ 1000 fois plus forte que celle du Zn^{2+}. Des expériences couplées d'adsorption, de titrage, de dissolution et de spectroscopie Mössbauer montrent que l'adsorption spécifique du Fe^{2+} est due à plusieurs réactions distinctes :

- une adsorption compétitive avec remplacement de cations présents sur les surfaces de bordure ou dans la structure (ex : Mg^{2+}, Zn^{2+}) ;
- une adsorption coopérative avec H_4SiO_4, ce mécanisme étant compatible avec la précipitation de surface d'une phase Fe – Si ;
- un mécanisme d'adsorption suivi d'une oxydation du Fe^{2+} en Fe^{3+}, cette réaction libérant deux H^+ en solution par Fe^{2+} adsorbé.

Ces phénomènes ne peuvent pas tous être pris en compte dans les modèles classiques de complexation de surface. Une approche nouvelle pour les argiles est donc développée pour modéliser les interactions solutés – argiles, basée sur une approche morphologique et structurale de l'argile. Les surfaces de la montmorillonite sont caractérisées par deux méthodes indépendantes, la microscopie à force atomique (AFM) et l'adsorption de gaz à très basse pression, qui donnent le même résultat pour les surfaces de bordure : 8,5 $m^2\ g^{-1}$. L'étude théorique de la structure de l'interface argiles – solutés montre qu'elle ne porte pas moins de 27 sites réactionnels différents pour les interactions argile – H^+. Le modèle MUSIC est utilisé pour prédire leur réactivité. L'excellent accord entre les données expérimentales de titrage potentiométrique et leur simulation nous encourage à poursuivre dans cette voie et à compléter le modèle pour prédire les interactions surface – cations métalliques.

ABSTRACT

Solute Fe(II) – montmorillonite interactions are studied in anoxic conditions and at room temperature for reaction times from hour to week.

Fe^{2+} is shown to be sorbed on cation exchange site with the same affinity than Ca^{2+}. In chloride anionic medium, Fe(II) form ionic pairs – $FeCl^+$ - which is sorbed with almost the same affinity than $CaCl^+$ and $MgCl^+$ are. The exchange thermodynamics constants derived from this study are used to simulate the change in the exchanger composition as clay river particles enter seawater. In high concentration chloride medium, as seawater, monovalent ions (Na^+ and $CaCl^+$, $MgCl^+$ ionic pairs) are shown to be the major species of the exchanger.

Fe^{2+} is sorbed specifically on the montmorillonite edge surfaces with a very high affinity. Simple complexation model are able to model the sorption data and show that the Fe^{2+} affinity for clay edge surfaces is ~1000 times higher than the Zn^{2+} one. Mössbauer experiments combined to sorption, titration and dissolution experiments show that the Fe^{2+} sorption is due to several different reactions:

- effective competitive sorption with replacement of previously sorbed or structural cations (Zn^{2+}, Mg^{2+});
- cooperative sorption together with H_4SiO_4, in agreement with a possible surface precipitation of a Fe – Si phase;
- a sorption mechanism followed by an oxidation reaction, with a release of two H^+ in solution per Fe(II) sorbed, and a product (Fe(III)) fitting better octahedral surface "sites".

All these phenomena can not be taken into account in a classical surface complexation model. Hence, an innovative model is developed to model clay – solute interactions, based on a morphological and structural approach. Montmorillonite edge surface area was determined using two independent methods, AFM measurement and low-pressure gas adsorption, that give the same value for this area, i.e. 8.5 $m^2\ g^{-1}$. The clay – solute interface was found to be constituted by a mix of, at least, 27 reactive sites. Their reactivity towards H^+ was modeled with the MUSIC model. An excellent agreement is found between potentiometric measurement data and predicted curves. This model should be further developed to predict the clay surfaces – metallic cations interactions.